TAMPEREEN TEKNILLINEN YLIOPISTO
TAMPERE UNIVERSITY OF TECHNOLOGY

Sener Dikmese

Enhanced Spectrum Sensing Techniques for Cognitive Radio Systems

Julkaisu 1280 • Publication 1280

Tampere 2015

Tampereen teknillinen yliopisto. Julkaisu 1280
Tampere University of Technology. Publication 1280

Sener Dikmese

Enhanced Spectrum Sensing Techniques for Cognitive Radio Systems

Thesis for the degree of Doctor of Science in Technology to be presented with due permission for public examination and criticism in Tietotalo Building, Auditorium TB109, at Tampere University of Technology, on the 13th of February 2015, at 12 noon.

Tampereen teknillinen yliopisto - Tampere University of Technology
Tampere 2015

Supervisor
Markku Renfors, Dr. Tech., Professor
Department of Electronics and Communications Engineering
Tampere University of Technology
Tampere, Finland

Pre-examiners
Alexander M. Wyglinski, Ph.D., Associate Professor
Department of Electrical and Computer Engineering
Worcester Polytechnic Institute (WPI)
Worcester, MA, United States of America

Olav Tirkkonen, Ph.D., Associate Professor
Department of Communications and Networking
Aalto University
Helsinki, Finland

Opponents
Jacques Palicot, Ph.D., Professor
Signal Communications and Embedded Electronics (SCEE)
École supérieure d'électricité (Supélec)
Rennes, France

Olav Tirkkonen, Ph.D., Associate Professor
Department of Communications and Networking
Aalto University
Helsinki, Finland

ISBN 978-952-15-3454-6 (printed)
ISBN 978-952-15-3465-2 (PDF)
ISSN 1459-2045

ABSTRACT

Due to the rapid growth of new wireless communication services and applications, much attention has been directed to frequency spectrum resources. Considering the limited radio spectrum, supporting the demand for higher capacity and higher data rates is a challenging task that requires innovative technologies capable of providing new ways of exploiting the available radio spectrum. Cognitive radio (CR), which is among the core prominent technologies for the next generation of wireless communication systems, has received increasing attention and is considered a promising solution to the spectral crowding problem by introducing the notion of opportunistic spectrum usage. Spectrum sensing, which enables CRs to identify spectral holes, is a critical component in CR technology. Furthermore, improving the efficiency of the radio spectrum use through spectrum sensing and dynamic spectrum access (DSA) is one of the emerging trends. In this thesis, we focus on enhanced spectrum sensing techniques that provide performance gains with reduced computational complexity for realistic waveforms considering radio frequency (RF) impairments, such as noise uncertainty and power amplifier (PA) non-linearities.

The first area of study is efficient energy detection (ED) methods for spectrum sensing under non-flat spectral characteristics, which deals with relatively simple methods for improving the detection performance. In realistic communication scenarios, the spectrum of the primary user (PU) is non-flat due to non-ideal frequency responses of the devices and frequency selective channel conditions. Weighting process with fast Fourier transform (FFT) and analysis filter bank (AFB) based multi-band sensing techniques are proposed for overcoming the challenge of non-flat characteristics. Furthermore, a sliding window based spectrum sensing approach is addressed to detect a re-appearing PU that is absent in one time and present in other time. Finally, the area under the receiver operating characteristics curve (AUC) is considered as a single-parameter performance metric and is derived for all the considered scenarios.

The second area of study is reduced complexity energy and eigenvalue based spectrum sensing techniques utilizing frequency selectivity. More specifically, novel spectrum sensing techniques, which have relatively low computational

complexity and are capable of providing accurate and robust performance in low signal-to-noise ratio (SNR) with noise uncertainty, as well as in the presence of frequency selectivity, are proposed. Closed-form expressions are derived for the corresponding probability of false alarm and probability of detection under frequency selectivity due the primary signal spectrum and/or the transmission channel. The offered results indicate that the proposed methods provide quite significant saving in complexity, e.g., 78% reduction in the studied example case, whereas their detection performance is improved both in the low SNR and under noise uncertainty.

Finally, a new combined spectrum sensing and resource allocation approach for multicarrier radio systems is proposed. The main contribution of this study is the evaluation of the CR performance when using wideband spectrum sensing methods in combination with water-filling and power interference (PI) based resource allocation algorithms in realistic CR scenarios. Different waveforms, such as cyclic prefix based orthogonal frequency division multiplexing (CP-OFDM), enhanced orthogonal frequency division multiplexing (E-OFDM) and filter bank based multicarrier (FBMC), are considered with PA nonlinearity type RF impairments to see the effects of spectral leakage on the spectrum sensing and resource allocation performance. It is shown that AFB based spectrum sensing techniques and FBMC waveforms with excellent spectral containment properties have clearly better performance compared to the traditional FFT based spectrum sensing techniques with the CP-OFDM.

Overall, the investigations in this thesis provide novel spectrum sensing techniques for overcoming the challenge of noise uncertainty with reduced computational complexity. The proposed methods are evaluated under realistic signal models.

PREFACE

THIS thesis is based on research work carried out during the years 2009-2014 at the Department of Electronics and Communications Engineering, Tampere University of Technology, Tampere, Finland.

First and foremost, I would like to express my deepest gratitude to my supervisor, Prof. Markku Renfors. His guidance and continuous support based on his vast knowledge has been of a great help for my research to progress smoothly. It has been a great privilege to have the opportunity to study under his guidance. He always was there, when I had any request patiently clarified all my doubts. I have been many times impressed by his way of approach in understanding and solving problems. Throughout these years I tried to learn from him how to ask the right questions that lead to a valuable research. Despite the amazing career that he has already established, his hardworking nature that surpasses anyone I know makes him an excellent role-model for his students and colleagues. I also greatly appreciate his skills and sincerity in developing personal relations. He is the key person in establishing the friendly atmosphere in our department for which I am thankful from the bottom of my heart.

I also would like to thank to Prof. Mikko Valkama who shared his invaluable ideas in many different studies and together with Prof. Markku Renfors, provided an excellent guidance for my research.

I am grateful to Associate Professor Alexander M. Wyglinski and Associate Professor Olav Tirkkonen who agreed to be the thesis pre-examiners and put their valuable efforts in the review process. I also thank to Professor Jacques Palicot and Associate Professor Olav Tirkkonen for aggreeing to act as opponents at my dissertation.

The research work was done partly in international collaboration with other research groups under a number of projects, such as European Union FP7-ICT project Enhanced Multicarrier Techniques for Professional Ad-Hoc and Cell-Based Communications (EMPhAtiC), COST Action IC0902 and the project Enabling Methods for Dynamic Spectrum Access and Cognitive Radio (ENCOR2) funded by the Finnish Funding Agency for Technology and Innovation

(Tekes). The research work was also financially supported by Graduate School in Electronics, Telecommunications and Automation (GETA) and Tekniikan Edistamissaation (TES).

Starting from my academic life Prof. Ismail Erturk, Prof. Yasar Becerikli, Prof. Adnan Kavak, Prof. Hasan Dincer, Prof. Huseyin Arslan who always have my gratitudes, there has been many influential people in my life who got me interested in science and technology. Among those, there are many colleagues that I had the pleasure to work with. I should thank to Dr. Ahmet Gokceoglu with whom I had collaborated a lot and always shared nice time during my stay in Finland. Thanks to Dr. Juha Yli-Kaakinen, AlaaEddin Loulou, Petteri Liikkanen and Aki Hakkarainen, our office was one of the most "friendly and silent" rooms where it was really nice environment to study. Assoc. Prof. Faouzi Bader (co-author), Dr. Tero Ihalainen (co-author), Dr. Paschalis Sofotasios (co-author), Dr. Musbah Shaat (co-author) and Sudharsan Srinivasan (co-author) have my gratitudes for sharing a great deal of time in academic discussions. I had incredible conference and research visits with Assoc. Prof. Simona Lohan, Dr. Ville Syrjala and Aki Hakkarainen and would like to thank them for their friendliness. Hoping that without forgetting any valuable colleague and personnel, I would like to thank to: Adnan Kiayani, Mahmoud Abdelaziz, Janis Werner, Alireza Razavi, Jaakko Marttila, Jukka Talvitie, Markus Allen, Vesa Lehtinen, Toni Levanen, Joonas Sae, Pedro Silva, Dani Korpi, Lauri Anttila, Ari Asp, Yaning Zou, Kai Shao, Diego Menegazzo, Juuso Alhava, Sari Kinnari, Ulla Siltaloppi, Soile Lonnqvist, Heli Ahlfors, Tuija Grek and Marja Leppaharju. I also would like to thank to Mehmet Emin Kurtbogan, Mahmut Yalcin, Fahrettin Caliskan, Osman Sahan, Ozkan Yapar, Selimcan Dede, Tugrul Acikgoz, Umur Caglar, Murat Birinci, Claudia Peltonen and Emrah Senbahceli for their friendship during my stay in Finland.

Finally, I wish to thank the ones dearest to me. My adorable wife Guzin, for her love, patience and understanding. I have been fortunate to have you on my side to share the joys and disappointments, and to provide hope and motivation at times I started to losing them. I would like to give my dearest and warmest gratitudes to my mother and father Sukran and Huseyin.

Tampere, December 2014
Sener Dikmese

CONTENTS

LIST OF PUBLICATIONS

This thesis is a compound thesis based on the following four publications.

[P1] Sener Dikmese, Paschalis C. Sofotasios, Tero Ihalainen, Markku Renfors and Mikko Valkama, "Efficient Energy Detection Methods for Spectrum Sensing under Non-Flat Spectral Characteristics," *IEEE Journal on Selected Areas in Communications (JSAC)*, DOI:10.1109/JSAC.2014.236-1074, Oct. 2014.

[P2] Sener Dikmese and Markku Renfors, "Performance Analysis of Eigenvalue Based Spectrum Sensing under Frequency Selective Channels," in *Proceedings of 7th International Conference on Cognitive Radio Oriented Wireless Networks (CROWNCOM)*, Stockholm, Sweden, June 2012.

[P3] Sener Dikmese, Sudharsan Srinivasan, Musbah Shaat, Faouzi Bader and Markku Renfors, "Spectrum Sensing and Spectrum Allocation for Multicarrier Cognitive Radios under Interference and Power Constraints," *EURASIP Journal on Advances in Signal Processing*, DOI: 10.1186/1687-6180-2014-68, May 2014.

[P4] Sener Dikmese, AlaaEddin Loulou, Sudharsan Srinivasan and Markku Renfors, "Spectrum Sensing and Resource Allocation Models for Enhanced OFDM Based Cognitive Radio," in *Proceedings of 9th International Conference on Cognitive Radio Oriented Wireless Networks (CROWNCOM)*, Oulu, Finland, June 2014.

LIST OF PUBLICATIONS

ABBREVIATIONS

5G	fifth generation
ADC	analog-to-digital converter
AFB	analysis filter bank
AUC	area under the receiver operating characteristics curve
AWGN	additive-white-gaussian-noise
CAF	cyclic autocorrelation function
CP-OFDM	cyclic prefix based orthogonal frequency division multiplexing
CLT	central limit theorem
CR	cognitive radio
CSD	cyclic spectral density
CSI	channel state information
DFT	discrete Fourier transform
DSA	dynamic spectrum access
DSP	digital signal processing
ED	energy detection
EMaxE	maximum eigenvalue and energy detector
E-OFDM	enhanced ortogonal frequency divison dublexing
ESD	energy spectral density
FBMC	filter bank based multicarrier
FCC	Federal Communications Commission
FDM	frequency-division multiplexing
FFT	fast Fourier transform
FH-FSK	frequency hopped frequency shift keying

FIR	finite impulse response
ICI	intercarrier interference
IDFT	inverse discrete Fourier transform
IEEE	Institute of Electrical and Electronics Engineers
IFFT	inverse fast Fourier transform
IQ	inphase-quadrature
ISI	inter-symbol interference
ISM	industrial, scientific and medical
ITU	International Telecommunication Union
KKT	Karush-Kuhn-Tucker
Max-Min ED	maximum - minimum energy detector
OFDM	orthogonal frequency-division multiplexing
OQAM	offset quadrature amplitude modulation
PA	power amplifier
PAPR	peak-to-average power ratio
PI	power interference
PSD	power spectral density
PU	primary user
QAM	quadrature amplitude modulation
QPSK	quadrature phase shift keying
RF	radio frequency
RMS	root mean square
ROC	receiver operater characteristics
RX	receiver
SDR	software defined radio
SFB	synthesis filter bank
SINR	signal-to-interference ratio
SNR	signal-to-noise ratio
SU	secondary user
SW-ED	sliding window energy detection
TDD	time-division duplexing
TDMA/TDD	time-division multiplexing/duplexing
TX	transmitter
WLAN	wireless local-area-networks
WPAN	wireless personal-area-networks

CHAPTER 1

INTRODUCTION

1.1 Background and Motivation

Wireless communications have been growing exponentially, and in spite of intensive research and development efforts for more effective technologies, the scarcity of available radio spectrum is considered as a critical issue for further advancement of the field. Opportunistic dynamic spectrum access (DSA) and cognitive radio (CR) techniques have received increasing attention as potential solutions to the spectrum shortage issue for the next generation of wireless communication systems namely, fifth generation (5G) [2, 32, 33, 106, 124, 125, 136, 170, 185, 191, 198]. A CR is defined by Federal Communications Commission (FCC) as: "*A radio or system that senses its operational electromagnetic environment and can dynamically and autonomously adjust its radio operating parameters to modify system operation, such as maximize throughput, mitigate interference, facilitate interoperability, access secondary markets.*" [54].

Due to global availability, the 2.4 GHz industrial, scientific and medical (ISM) band is a popular frequency band suitable for low cost wireless systems, such as wireless local-area-networks (WLAN) and wireless personal-area-networks (WPAN). One important problem is that users operating in the same radio environment may cause significant interferences to each other. For the multitude of systems operating in the ISM bands, no effective coordination or radio resource management functions exists, which leads to inefficient utilization of these frequency bands. As a solution to these challenges, advanced CR and signal processing techniques have been recently considered [2, 28, 106, 124, 125, 170, 184, 191, 198].

One of the main tasks of a CR is to find non-interfered spectrum for communication. In the current CR developments, the geolocation database based approach is greatly emphasized due to its reliability. In this approach, secondary user (SU) devices obtain spectrum availability information from a database which contains information about the primary user (PU) activity in the geographical area where the SU intends to operate [170, 185, 191]. Nevertheless,

there is great interest on spectrum sensing based techniques, as a possible future evolution path and as a complementary element in database based CR networks, especially in short-range communication. This thesis focuses on the concept where the CR devices sense the local spectrum utilization through the spectrum sensing functionality in order to find spectrum access opportunities. Due to varying channel conditions, repeated monitoring and cooperation with other users is required for robust, high-sensitivity spectrum sensing [2, 32, 33, 106, 118, 136, 170, 185, 191, 198].

Energy detection (ED) is among the most popular spectrum sensing methods thanks to its decent performance and very simple practical realization [69, 191]. Most of the studies on ED based spectrum sensing utilize simple signal models, where the whole frequency band under sensing includes either noise, or noise in addition to a PU signal, both having constant power spectral density (PSD). A Neyman-Pearson type binary hypothesis testing problem is commonly used to formulate ED that is typically modeled by the well-known chi-square, Gaussian or gamma type statistical distributions [19, 69, 132, 165].

The main shortcoming of ED is its sensitivity to the information of the noise variance [158]. Small variations and unpredictability of the noise variance estimation is a critical issue, which is called *noise uncertainty* [158]. In most of the studies, the noise variance is assumed to be exactly known according to previous measurements.

Wideband multichannel based sensing brings various possibilities for calibrating the noise spectral density of the sensing receiver. Hence, we focus on fast Fourier transform (FFT) and analysis filter bank (AFB) based sensing solutions in some parts of this thesis [P1] and [38, 39, 45]. One of the alternative solutions is to consider the spectral slot(s) with the lowest observed PSD as candidate(s) for white space, and use the corresponding PSD level as a reference for noise. It is also possible to generalize this method by searching for time-frequency zones with minimum PSD levels, and then using them as noise reference. A reappearing PU can be observed through an increase in the energy level of the corresponding time-frequency zone [P1]. We focus on refining the analytical tools related to ED methods beyond the simplistic signal models and sensing scenarios that are commonly considered in the literature [2, 106, 170, 191, 198].

Multi-antenna sensing based spectrum sensing techniques can be considered as alternative methods to provide robustness against noise uncertainty by exploiting the spatial correlation properties of the received energy [76, 156, 167, 172–174, 176–180]. However, this solution brings increased hardware complexity and size, which often renders it impractical for several applications. Hence, single-antenna sensing is purely the focus of this thesis [P1]-[P4], but the results can be extended to multi-antenna schemes and/or cooperative sensing, which is an effective way to ensure spectrum sensing robustness in realistic wireless communication scenarios.

Receivers are commonly assumed to have an ideal frequency response due to the consideration of always flat wireless channels. Based on this idea, numerous investigations have been reported in the context of additive-white-gaussian-noise (AWGN), fading channels, diversity techniques and collaborative detection (see [3, 4, 37, 59, 60, 72, 73, 98, 140, 153] and the references therein). Neverthe-

less, the sensing receiver has non-ideal frequency response in realistic communication scenarios in which the transmitted PSD is non-flat and the frequency-selective multipath channel has an effect on the received PU PSD. Motivated by these effects, another direction of this thesis is to propose optimized ED based spectrum sensing solutions for non-flat spectral characteristics [P1] and [38,45].

Several advanced methods such as eigenvalue [97, 196] and autocorrelation [76, 197] based methods, which are robust to noise uncertainty, are also considered as alternative solutions to the noise uncertainty challenge utilizing the frequency selectivity. However, these algorithms have much higher computational complexity and it is not possible to reach the sensing performance of ED under modest noise uncertainty and practical PU signal-to-noise ratio (SNR) levels [97, 196, 197]. Hence, developing reduced complexity eigenvalue based spectrum sensing solutions is an important direction to investigate [117, 130, 131, 175, 176, 195, 199], and it is addressed in this thesis and in [43, 44]. Furthermore, we propose an alternative subband energy based detection scheme utilizing the variability of the energy spectral density (ESD), which can effectively remove the noise floor, resulting in the elimination of the noise uncertainty effects [40, 41]. Additionally, our proposed scheme is conceptually simple compared to the eigenvalue based spectrum sensing methods since it is achieved by the replacement of the calculation of the covariance matrix and its eigenvalues by blockwise FFT or AFB processing [40, 41].

Combining spectrum sensing with resource allocation is the final direction of this thesis [P3], [P4] and [42, 154]. Most spectrum sensing studies have been done without considering any kind of resource allocation algorithms for efficiently using spectral holes [2, 106, 170, 191, 198], whereas resource allocation studies commonly assume ideal information about the spectral holes without considering the limitations of the sensing methods [7–9, 80, 96, 135, 150, 183, 200]. Additionally, cyclic prefix based orthogonal frequency division multiplexing (CP-OFDM) based signal models are considered as the PU and CR signal models for spectrum allocation techniques in [7–9, 80, 96, 135, 150, 183, 200], and filter bank based multicarrier (FBMC) has been considered for the CR only in [146, 147]. Our studies can be applied to any realistic multicarrier PU and CR systems utilizing the receivers' FFT or AFB processing for spectrum sensing purposes. In our case studies, the PU waveform is based on a 802.11g standard CP-OFDM, an enhanced orthogonal frequency division multiplexing (E-OFDM) [P4], or a 802.11g -like FBMC waveform with similar parameterization [P3]. Furthermore, most of the existing spectrum sensing studies assume ideal radio frequency (RF) receiver model, especially when the impact of practical power amplifier (PA) non-linearity and inphase-quadrature (IQ) imbalance have not been considered. In this thesis, a basic RF nonlinearity model, so-called the Rapp PA model [137] is included for the PU in order to obtain a realistic model for the PU spectrum [P3], [P4] and [42, 154]. To the best of our knowledge, this aspect has not been considered in any earlier work. The effects of the PU spectral characteristics on the SU capacity can be quantified in this way. In addition, the effects of IQ imbalance on ED and eigenvalue based spectrum sensing in both single-channel and multi-channel direct-conversion receiver scenarios have also been analyzed in our previous studies [61–63].

The described three issues form the main motivation and focus of this thesis.

1.2 Objectives and Scope of the Thesis

The main objective of this thesis is to study and analyze certain important spectrum sensing techniques and to develop enhanced spectrum sensing algorithms that can enable the design and practical implementation of CR based transceivers. A novel combined spectrum sensing and resource allocation approach is also proposed for multicarrier radio systems. However, the topic of enhanced spectrum sensing techniques is too vast to be covered fully in a single thesis. The scope is thus limited to focus on the efficient non-cooperative, single-antenna spectrum sensing methods which have reduced computational complexity and are robust to noise uncertainty conditions.

1.3 Outline and Main Contributions of the Thesis

In achieving the above objectives, the study of the enhanced spectrum sensing techniques covers both a reliable theoretical analysis and development of novel spectrum sensing methods with reduced computational complexity under noise uncertainty and very low SNR challenges. The structure of the thesis can be summarized as follows:

1. Chapter 2 briefly discusses the spectrum sensing methodology in CR applications at an overview level.

2. Chapter 3 focuses on wideband multichannel spectrum sensing techniques utilizing FFT or AFB based methods for spectrum analysis [P1]. Proposed sensing schemes can be tuned to the spectral characteristics of the target PU signals, allowing simultaneous sensing of multiple target PU signals with low additional complexity. The corresponding false alarm and detection probabilities are derived as novel analytic expressions with weighting process for non-flat spectral characteristic. The overall performance of the proposed spectrum sensing algorithms and scenarios are introduced with the concept of the area under the receiver operating characteristics curve (AUC). Furthermore, the specific scenario of detecting a reappearing PU during secondary transmission is considered. The results are also validated extensively through comparisons with corresponding results from computer simulations and are subsequently employed in the evaluation of each technique, providing meaningful insights that are anticipated to be useful in the future deployment of CR systems.

3. Chapter 4 focuses on the reduced complexity spectrum sensing solutions in the presence of noise uncertainty. The effects of channel frequency selectivity, in combination with noise uncertainty, in case of energy detector and eigenvalue based detection are explained at the beginning of this chapter [P2]. The last part of this chapter proposes a subband energy based approach denoted as Max-Min ED. The proposed sensing techniques have

relatively low computational complexity while they are capable of providing accurate and robust performance under noise uncertainty conditions, as well as in the presence of frequency selectivity. The corresponding false alarm and detection probabilities are derived as novel expressions under different communication scenarios. The validity of the offered expressions is justified extensively through comparisons with results from respective computer simulations and are subsequently employed in evaluating the corresponding sensing performance.

4. Chapter 5 studies the dynamics of spectrum sensing and resource allocation functions within a CR context using very practical signal models for the PU, including the effects of power amplifier nonlinearities. ED based wideband multichannel spectrum sensing algorithm and optimal resource allocation are applied for the spectrum sensing and utilization, respectively. In this chapter, effects of spectral regrowth due to the inevitable power amplifier nonlinearities of the PU transmitters are also studied. Frequency selective block-fading channel models for both secondary and primary transmissions are also considered in the signal models. Filter bank based wideband spectrum sensing techniques are applied for detecting spectral holes, and FBMC modulation is selected for transmission as an alternative multicarrier waveform to avoid the disadvantage of limited spectral containment of orthogonal frequency-division multiplexing (OFDM) based multicarrier systems. The optimization technique used for the resource allocation approach considered in this study utilizes the information obtained through spectrum sensing, as well as knowledge of spectrum leakage effects of the underlying waveforms, including a practical power amplifier model for the PU transmitter. This study utilizes a computationally efficient algorithm to maximize the SU link capacity with power and interference constraints. The contents of this chapter are mainly based on the publications [P3] and [P4] .

5. Chapter 6 summarizes the thesis and draws the conclusions.

1.4 Author's Contribution to the Publications

Altogether, most parts of this thesis are based on the works reported in publications [P1]-[P4] which were all carried out at the Department of Electronics and Communications Engineering, Tampere University of Technology, Finland. The author of the thesis is the first author and main contributor in all these publications and novel contributions reported in Chapter 4. The thesis supervisor Prof. Markku Renfors is a co-author of all publications and made valuable contributions regarding the technical contents and presentation. The part of the research related to efficent ED methods using weighting process [P1] were carried out mostly in collaboration with Prof. Mikko Valkama, Dr. Paschalis C. Sofotasios and Dr. Tero Ihalainen. The idea, analysis, simulations and writing in [P2] were done only with Prof. Markku Renfors. Regarding [P3], the technical contents and presentation were equally contributed by the Author and

M.Sc. Sudharsan Srinivasan, and this publication is likely to be included also in Mr. Srinivasan's thesis. Assoc. Prof. Faouzi C. Bader and Dr. Musbah Shaat shared their expertise and participated in detailed discussions on resource allocation. M.Sc. AlaaEddin Loulou contributed related to E-OFDM issue in [P4]. Prof. Mikko Valkama and Dr. Paschalis C. Sofotasios provided many insightful comments and discussions supporting the work that is reported in Chapter 4 of this thesis and partly also in a journal paper submission [41].

1.5 Basic Mathematical Notations

Throughout the thesis, the following mathematical notations are used extensively. The operators that return the real and imaginary parts of a complex variable are denoted as $\Re\{.\}$ and $\Im\{.\}$, respectively. The vectors and matrices are written in bold and $*$, T, $\dagger$ in the superscript returns the complex-conjugate, transpose and Hermitian (complex conjugate transpose) of the associated variable. The forward Fourier, Discrete Time Fourier and N-point Discrete Fourier transforms are defined and denoted as

$$X(f) = \mathrm{FT}\{x(t)\} := \int x(t)e^{-j2\pi ft}dt$$
$$X(f) = \mathrm{DTFT}\{x(t)\} := \sum_n x(n)e^{-j2\pi fn}$$
$$X(k) = \mathrm{DFT}\{x(t)\} := \sum_n x(n)e^{-j2\pi kn/N}$$

whereas the corresponding inverse transforms are defined and denoted as

$$x(t) = \mathrm{IF}\{X(f)\} := \int X(f)e^{j2\pi ft}df$$
$$x(n) = \mathrm{IDTFT}\{X(f)\} := \int X(f)e^{j2\pi ft}df$$
$$x(n) = \mathrm{IDFT}\{X(k)\} := \sum_k X(k)e^{j2\pi kn/N}$$

CHAPTER 2

SPECTRUM SENSING METHODS FOR COGNITIVE RADIO

2.1 Overview of Spectrum Sensing for Cognitive Radios

Wireless communication systems have been growing exponentially, with more spectrum resources needed due to this rapid growth. Most of the spectrum bands are allocated to specific licensed services in the current spectrum framework. However, a large portion of licensed bands such as TV bands remains underutilized [54]. In recent years, FCC has been considering to open the licensed bands to unlicensed users [1, 69, 83, 113, 114].

On the other hand, an increasing number of companies are making products that use unlicensed bands. Due to its global availability, 2.4 GHz ISM band is a suitable frequency band for low cost radio solutions such as WLAN and WPAN. One important problem is that a large number of non-coordinated users that operate in the same environment may lead to severe interference effects. Increasing traffic rates, limited system capacity, and low coverage range of base stations are other major challenges to reliable communication in such environments. In solving these challenges, the idea of CR and related signal processing techniques have been proposed [69, 113, 114].

CR is the key enabling technology that arises as a tempting solution to the spectral congestion challenge by introducing opportunistic usage of the frequency bands that are not extensively occupied by the PUs [113]. CR is based on the concept of software defined radio (SDR), which provides a flexible radio architecture that allows changing the radio personality in real-time; the same hardware can be used to implement different waveform processing at different times. CR has some additional vital characteristics compared to the SDR such as radio scene analysis, channel identification and transmit power control. While radio scene analysis includes estimation of the interference temperature of the radio environment and detection of spectrum holes, the channel identifi-

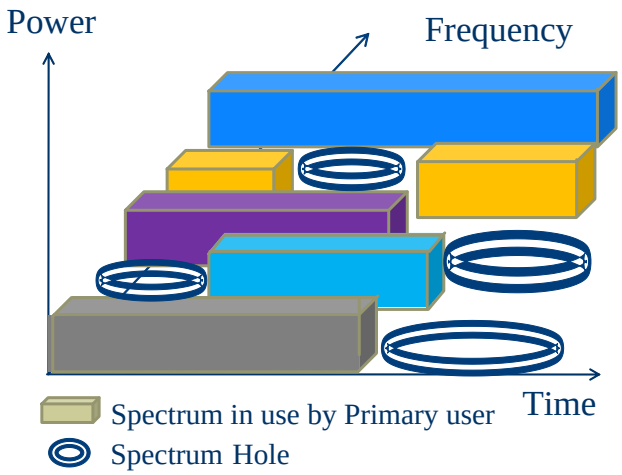

Figure 2.1: Illustration of spectral holes

cation part has tasks such as the estimation of the channel-state and prediction of channel capacity for use by the transmitter. Another task in a CR terminal, after selecting the frequency slot for transmission, is the transmit power control, or more generally the dynamic spectrum management process. While the CR system works in the same band of frequencies with PU networks, significantly high interference between different PUs and CRs is unavoidable.

Spectrum sensing is a critical part of CR applications. CRs may sense the local spectrum utilization either though a dedicated sensor or using a configured SDR receiver channel as shown in Figure 2.1. With this spectrum information, it may find out spectrum access opportunities. Hence, the main task of a CR is to obtain non-interfered spectrum for robust communication of the secondary system. Due to variant channel conditions, repeated monitoring and cooperation with the other users is required for effective spectrum sensing approaches.

Due to the importance of spectrum sensing, several spectrum sensing techniques have been studied in the literature [2,106,170,191,198]. The most useful ones of these spectrum sensing techniques can be chosen according to the sensing performance and implementation complexity. While energy detectors are the most commonly studied spectrum sensing technique due to low implementation complexity [2, 106, 170, 191, 198], the performance of energy detectors is largely vulnerable to noise uncertainty effects [37, 73, 140, 158, 165]. Eigenvalue sensing methods have been proposed to overcome noise uncertainty challenges, but they have substantially higher computational complexity. Furthermore, the performance of these detectors significantly decrease when even small adjacent channel interference is present [97, 196, 197]. Cyclostationary spectrum sensing techniques, which can reject the effects of adjacent channel interference, are robust against noise variance uncertainty [89, 90, 92, 102, 139, 141, 148, 149, 166]. However, these algorithms have high computational complexity and a large number of samples is needed to obtain the cyclostationary behavior of the signal. Furthermore, they are sensitive to cyclic frequency mismatch. Waveform based sensing is more robust than energy detector due to the coherent pro-

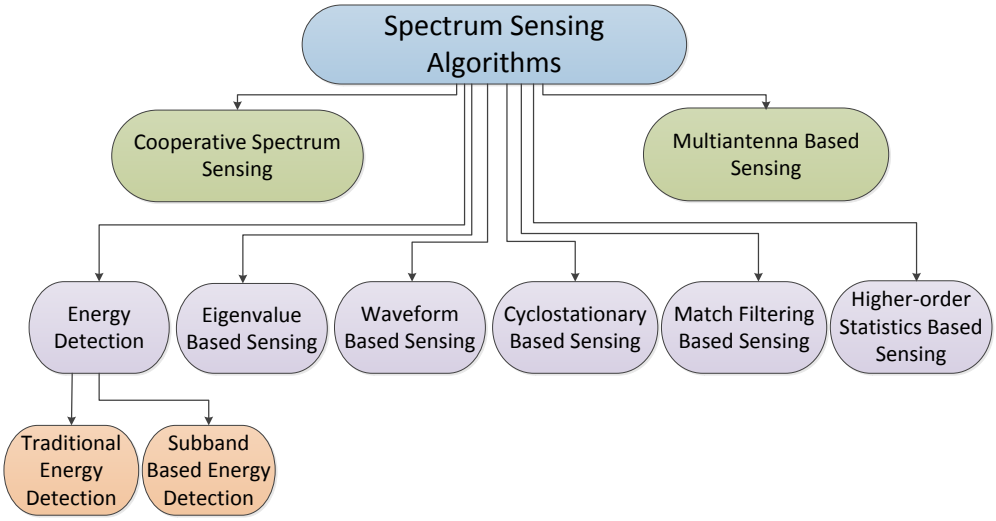

Figure 2.2: Spectrum sensing techniques

cessing that comes from deterministic signal component [78,143,159,167]. The main drawback of the waveform sensing is the requirement of the *a priori* information about the characteristics of the PU. Matched filtering is the optimum technique for detection of primary users when the transmitted signal is known [13,81,87,108,115,133,142,157,201]. Recently, subband based ED methods have been studied as alternative methods to overcome the above challenges [P1], [P3], [P4] and [38,42,45,154].

Most common spectrum sensing techniques, which are listed in Figure 2.2, will be briefly explained in this chapter.

2.2 Energy Detection Based Spectrum Sensing

ED based spectrum sensing techniques can be classified as traditional and subband energy detectors as follows:

2.2.1 Traditional Energy Detection

Traditional ED, also known as radiometry, is commonly used due to its low computational complexity and hardware simplicity [37,73,140,165]. Additionally, ED, which requires no prior information about the PU, is more generic compared to many advanced spectrum sensing techniques. The signal is detected by comparing the measured energy with the threshold value, which is determined according to the assumed noise variance and desired false alarm probability [165].

ED can be formulated as a binary hypothesis testing problem [37, 73, 140, 165],

$$\begin{aligned} \mathcal{H}_0 &: y[n] = w[n] \\ \mathcal{H}_1 &: y[n] = \overbrace{s[n] \otimes h[n]}^{x[n]} + w[n]. \end{aligned} \tag{2.1}$$

Here, $y[n]$ is the signal observed by the sensing receiver with $s[n]$ and $w[n]$ denoting the PU information signal and the zero-mean, complex, circularly symmetric, AWGN, respectively. Furthermore, $h[n]$ denotes the channel impulse response and $x[n]$ is the received PU signal with channel effects. Under hypothesis $\mathcal{H}_0$, $y[n]$ consists only of $w[n]$ in the absence of the PU whereas the PU signal $x[n]$ is present along with $w[n]$ under hypothesis $\mathcal{H}_1$. The corresponding test statistic is obtained as, $T(y) = \frac{1}{N}\sum_{n=0}^{N-1} |y[n]|^2$, where N is the length of the observation sequence.

It has been extensively shown that in practical cases the test statistics can be accurately assumed to follow the Gaussian distribution, $\mathcal{N}(\cdot\,,\cdot)$, since the central limit theorem (CLT) conditions are satisfied by the large number of the involved samples [23, 160, 161]. As a result, the following expressions are obtained,

$$T(y)|_{\mathcal{H}_0} \sim \mathcal{N}\left(\sigma_w^2, \frac{\sigma_w^4}{N}\right) \tag{2.2}$$

and

$$T(y)|_{\mathcal{H}_1} \sim \mathcal{N}\left(\sigma_x^2 + \sigma_w^2, \frac{(\sigma_x^2 + \sigma_w^2)^2}{N}\right), \tag{2.3}$$

where σ_x^2 and σ_w^2 denote the variance of the received PU signal with channel effects and AWGN process, respectively. The hypothesis testing problem is illustrated in Figure 2.3. Based on this, and defining the instantaneous SNR by $\gamma = \sigma_x^2/\sigma_w^2$, the corresponding P_{FA} and P_D can be formulated as follows:

$$P_{FA} = \Pr(T(y) > \lambda|\mathcal{H}_0) = Q\left(\frac{\lambda - \sigma_w^2}{\sigma_w^2/\sqrt{N}}\right) \tag{2.4}$$

$$P_D = \Pr(T(y) > \lambda|\mathcal{H}_1) = Q\left(\frac{\lambda - \sigma_w^2(1+\gamma)}{\sigma_w^2(1+\gamma)/\sqrt{N}}\right), \tag{2.5}$$

where $Q(\cdot)$ is the standard Gaussian complementary cumulative distribution function and λ is the predefined energy threshold.

In practice, the power (variance) of the PU information signal is unknown to the CR, and thus the value of λ is commonly calculated by the assumed noise variance and desired P_{FA}, namely, $\lambda = \sigma_w^2\left(1 + Q^{-1}(P_{FA})/\sqrt{N}\right)$. There is no possibility to know the exact noise variance in practice, hence the P_{FA} and P_D results are highly dependent upon the accuracy of the noise variance estimate. Therefore, small noise power estimation variabilities cause significant loss in the detection performance. In practice, the noise variance can be expected to lie within the range $\sigma_w^2 \in [(1/\rho)\sigma_n^2, \rho\sigma_n^2]$, where $\rho > 1$ is a parameter that

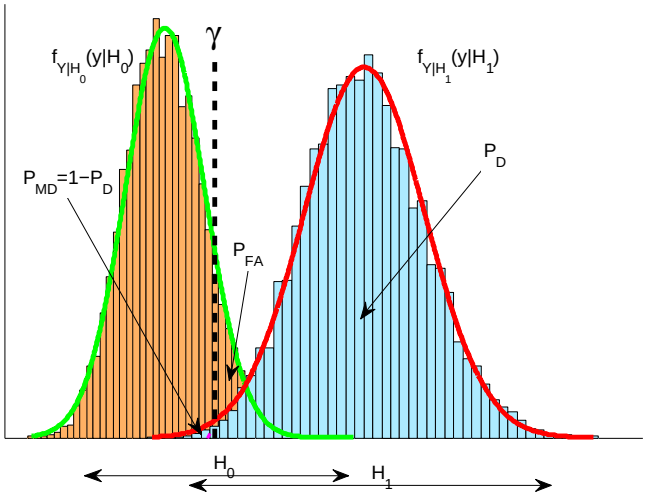

Figure 2.3: Illustration of the binary hypotesis testing of the test statistics and examples of probability distribution with assumed Gaussian approximation.

quantizes the size of the corresponding uncertainty. It is noted that the noise uncertainty is usually expressed in dB as $x = 10\log_{10}\rho$, which is chosen between 0.1 dB and 1 dB values in practice and under its effect P_{FA} and P_D can be straightforwardly formulated as follows [158],

$$P_{FA} = \max_{\sigma_w^2 \in \left[\frac{1}{\rho}\sigma_n^2, \rho\sigma_n^2\right]} Q\left(\frac{\lambda - \sigma_w^2}{\sigma_w^2/\sqrt{N}}\right) = Q\left(\frac{\lambda - \rho\sigma_n^2}{(\rho\sigma_n^2)/\sqrt{N}}\right) \tag{2.6}$$

and

$$P_D = \min_{\sigma_w^2 \in \left[\frac{1}{\rho}\sigma_n^2, \rho\sigma_n^2\right]} Q\left(\frac{\lambda - \sigma_w^2(1+\gamma)}{\sigma_w^2(1+\gamma)/\sqrt{N}}\right) = Q\left(\frac{\lambda - \sigma_n^2((1/\rho)+\gamma)}{(\sigma_n^2((1/\rho)+\gamma))/\sqrt{N}}\right), \tag{2.7}$$

respectively.

2.2.2 Subband Based Energy Detection

Spectrum analysis techniques make it possible to identify rapidly the spectral holes in a wide frequency band and allocate the most feasible parts of the band for CR operation. The most basic and computationally effective approach for spectrum analysis is block-wise FFT processing of the observed signal and measuring the power of each subband [120]. However, due to spectrum leakage effects, FFT has serious limitations in this task. Among various alternative spectrum analysis methods, AFB has been found to be particularly interesting for CRs [30,31,51,52,110]. From the sensing point of view, the main benefits of AFB are found in high-dynamic range scenarios, when performing the sensing in the presence of strong transmissions at nearby frequencies. Our proposed filterbank methods have been reported in [P1], [P3], [P4] and [38, 42, 45, 154], and they will be explained in Chapter 3 and Chapter 5 in details.

2.3 Eigenvalue Based Sensing

Eigenvalue based spectrum sensing techniques, which need no noise variance information, have been reported as potential solutions to the challenging and problematic noise uncertainty conditions [97, 196, 197]. Since the knowledge of the noise variance is not required in the eigenvalue and covariance based spectrum sensing methods, small changes or uncertainty on the noise variance have only a small effect on the sensing performance, as also seen in our studies [P2]. The changes are just due to changes in SNR, if PU signal power is assumed to be constant. The main drawback of the eigenvalue spectrum sensing techniques is their high computational complexity. Largest eigenvalue and trace based approaches have been presented in [117,130,131,195]. Additionally, power iteration algorithms for efficient eigenvalue computation are proposed to obtain less computational complexity in [82,193]. With our modified eigenvalue sensing techniques [41, 43, 44], relatively low computational complexity can be obtained, as will be discussed in Chapter 4. To avoid the calculation of both covariance matrix and eigenvalues, alternative ESD based spectrum sensing techniques were proposed in [40, 41] and will be explained in Chapter 4.

2.4 Waveform-Based Sensing

Known patterns, such as preambles, transmitted pilot patterns, and spreading sequences are commonly used for synchronization in wireless communication devices. Correlation between the received signal and a known copy of the pattern can help to reach better detection performance in spectrum sensing [78, 143, 159, 167]. The main drawback of this approach is that it is only applicable to systems with known signal patterns. Using the same signal model as in (2.1), the waveform sensing metric can be expressed as

$$M = \Re\left[\sum_{n=1}^{N} y(n)s^*(n)\right]. \tag{2.8}$$

In the absence of the primary user, the metric value can be obtained as

$$M = \Re\left[\sum_{n=1}^{N} w(n)s^*(n)\right]. \tag{2.9}$$

Similarly, the sensing metric can be obtained in the presence of the primary signal as

$$M = \sum_{n=1}^{N} |s(n)|^2 + \Re\left[\sum_{n=1}^{N} w(n)s^*(n)\right]. \tag{2.10}$$

The decision can be obtained by comparing the decision metric M against a fixed threshold γ. It should be mentioned that this is an idealized model, e.g., assuming perfect frequency synchronization, and that the channel effect is not included.

Cyclic prefix correlation method, which is a specific case of waveform sensing approach, is introduced as a simple and computationally efficient sensing technique for CP-OFDM signals in [15, 24].

2.5 Cyclostationary Feature Based Sensing

Cyclostationary feature detection is an effective sensing method to detect primary signals by exploiting the cyclostationary features of the received signal [18, 55, 75, 89–92, 99, 102, 121, 122, 134, 139, 141, 148, 149, 166]. Since the noise is wide-sense stationary and modulated signals are cyclostationary with spectral correlation, the PU signal can be differentiated from noise. Additionally, distinguishing among different types of transmissions and primary users can be obtained by cyclostationary feature detection [107].

The cyclic spectral density function of the received signal can be obtained as [56],

$$S(f,\alpha) = \sum_{\tau=-\infty}^{\infty} R_y^{\alpha}(\tau) e^{-j2\pi f\tau}, \tag{2.11}$$

where

$$R_y^{\alpha}(\tau) = \mathbb{E}\left[y(n+\tau)y^*(n-\tau)e^{j2\pi\alpha n}\right]. \tag{2.12}$$

Here, $R_y^{\alpha}(\tau)$ is the cyclic autocorrelation function (CAF) and α is the cyclic frequency. When the cyclic frequency is equal to one of the fundamental frequencies of the transmitted signal $x(n)$, the peak values can be obtained by the cyclic spectral density (CSD) function.

2.6 Matched Filtering Based Detection

Matched filtering, which is also a non-blind spectrum sensing method, is known as the optimum technique when the transmitted signal is known at the receiver [13,81,87,108,115,133,142,157,201]. While the main advantage of matched filter detection is the short sensing time to achieve a desired detection performance, it requires perfect knowledge of the primary signal such as bandwidth, modulation type, etc. The sensing receiver should also be able to synchronize to the received PU signal, which is an unreasonable assumption in typical spectrum sensing scenarios. The sensing receiver should also implement most of the specific waveform processing functions of the corresponding PU receiver, which would lead to high complexity. For these reasons, matched filter based detection is not consider as a relevant choice in CRs.

2.7 Cooperative Spectrum Sensing

Noise uncertainty, multipath fading and shadowing, which are characteristics of practical wireless channels, limit the detection performance in spectrum sensing significantly. As an alternative solution to overcome the challenges of practical environments, cooperative sensing has been widely studied in the literature [6, 29, 36, 49, 66, 67, 94, 112, 116, 127, 151, 161, 169, 172, 175, 194, 202] as a method to improve the sensing performance. *Hidden PU problem*, which appears when the PU is not detectable by the sensing station, e.g., due to shadowing, can be solved, and the sensing time can be considerably reduced by cooperative sensing.

The main challenge of cooperative spectrum sensing is that it requires developing an efficient information sharing network between CRs. This is often referred to as cognitive control channel, and it should not introduce more than a limited amount of delay [17, 128].

Another challenge in the cooperative sensing is the performance degradation due to the correlated shadowing [59, 126]. Hence, the most effective way of the cooperative sensing can be reached when the collaborating radios observe independent fading and shadowing [19, 103]. It is obvious that better sensing performance can be obtained with the same amount of users collaborating over a reasonably large area than a small area.

Cooperation can be performed by CRs equipped with the sensing function or external sensors can be used to establish a cooperative spectrum sensing network [1]. In general, the sensing decisions can be done either in a centralized manner by a fusion center, or the decision making can be distributed among the sensing devices in various alternative ways [181].

2.8 Multiantenna Based Sensing

Multiantenna sensing methods utilizing spatial correlations of PU signals have been widely studied and their efficiencies have been shown in different aspects [76, 156, 167, 172–174, 176–180]. Furthermore, multi-antenna sensing has also been recently studied as an alternative method to provide robustness against the noise uncertainty effects [76, 167, 172–174, 176–180]. However, the main disadvantage of the multiantenna sensing techniques is their increased hardware and computational complexity [76, 156, 167, 172–174, 176–180].

2.9 Other Sensing Techniques

Several other spectrum sensing methods are proposed in literature. Some of them will be briefly introduced in this section.

- **Quickest Detection**

  An agile and robust detection can be obtained by utilizing the theory of quickest detection that makes a statistical test to detect the change of the distribution as quickly as possible [93, 100]. When a PU appears, the unknown parameters can be estimated using the successive refinement, which combines both generalized likelihood ratio and cumulative test.

- **Learning and Reasoning Based Detection**

  The optimal detection idea which is reinforcement based approach for the detection of spectral resources in multi-band CR can be obtained by using a Markov decision process [12]. Hence, with knowledge based reasoning [171], a medium access control (MAC) layer sensing algorithm can perform the detection through proactive fast sensing and channel quality information.

- **Measurement Based Sensing and Modeling**

  Unique statistics of the cellular primary usage can be obtained with huge number of collected data over a long period at many base stations [5,182]. With the long period of measurement, spectrum usage patterns can be found and this helps to find the spectral holes in both time and spatial domains. Hence, dynamic access protocols can be improved based on these results [5, 182].

- **Teager-Kaiser Energy Detector Based Sensing**

  Kaiser has proposed a simple and fast method [85] to estimate the energy of a signal, when the restriction related to the bandwidth of the signal is respected. The Teager-Kaiser sensing is applied to measure the energy activity of the observed sequence in [35, 46, 47, 84] instead of using the conventional energy detector. Teager-Kaiser ED has also been used to detect wireless microphone signals as it's practical application, see [57,58], and the references therein.

- **Compressed Spectrum Sensing**

  Compressed sensing which is also known as the theory of compressive sampling is a novel sensing paradigm that one can recover certain signals from far fewer samples or measurements than the number of samples used in traditional methods. Compressed sensing approach is dependent upon two principles: sparsity, which pertains to the signals of interest, and incoherence, which pertains to the sensing modality. Several studies have investigated this idea so far [20, 50, 53, 86, 89, 91, 95, 101, 109, 111, 119, 186, 187].

- **High-order Statistics Based Sensing**

  Higher-order statistics based spectrum sensing algorithms have been recently studied in the CR context [11, 14, 21, 74]. High-order statistics represent the third and higher order statistics, in which there are two basic statistics as moment and cumulant. While the first-order and second-order statistics are used to detect the signals in most of the CR applications, certain kinds of PU waveforms can be identified, for example through the relations of the second and fourth-order statistics. Therefore, high-order moment based detectors have been considered as alternative solutions to obtain better detection performance compared to the traditional first and second-order statistics based methods [11, 14, 21, 74].

CHAPTER 3

EFFICIENT SUBBAND BASED ENERGY DETECTION METHODS FOR SPECTRUM SENSING

In this chapter, efficient subband based ED methods are proposed for spectrum sensing under non-flat spectral characteristics [P1]. The aim of the study is to investigate the effects of non-flat characteristics and frequency selectivity on the energy detector performance and quantify the corresponding deviations from the ideal model. Specifically, we wish to study:

- Wideband multichannel based spectrum sensing techniques utilizing FFT or AFB based spectrum analyzer are introduced.
- The case of non-flat PU spectrum is analyzed, focusing on a realistic Bluetooth signal model as an indicative example. Analytic expressions of the optimum weights are found for FFT and AFB based sensing where the PU signal band is divided into approximately flat subbands. In this context, simple numerical methods for evaluating the performance of practical and optimum sensing filters are provided.
- Performance analysis for the case where the sensing window in time-frequency domain contains both a zone where the PU signal is present and a zone where the PU signal is absent is presented. The idea of sliding window is an effective method to detect a re-appearing PU, which is an important specific scenario in practical spectrum sensing.
- The effects of a stationary frequency selective channel are quantified.
- Novel analytical expressions of AUC are derived for all considered spectrum sensing scenarios.

The main idea of this chapter is to provide a toolbox of FFT and/or AFB based energy detectors in the form of easy-to-use analytical or semi-analytical

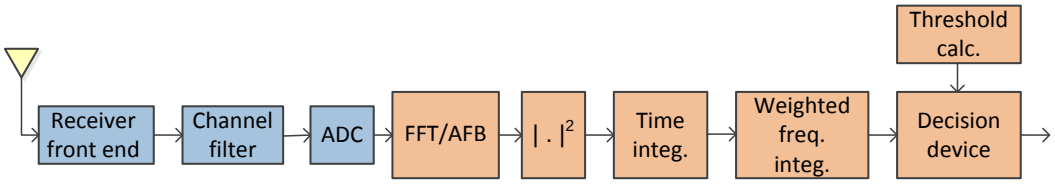

Figure 3.1: Block diagram for energy detection with FFT/AFB based spectrum analysis.

expressions for performance analysis. On the one hand, the presented ideas provide significant gains in terms of sensing performance compared to the existing traditional ED methods, while on the other hand they facilitate the comparison of suboptimal/simplified schemes with respect to the optimal methods.

3.1 FFT and AFB based schemes for multiband sensing

CP-OFDM based multicarrier techniques, which are characterized by the simplicity and robustness of the receiver signal processing techniques, are the dominating multicarrier technology. FBMC based waveforms, which have demonstrated various potential benefits in the field of CR communication [10, 52, 138, 152], are alternative techniques for next generation wireless communications, such as 5G. As a transmission technique, FBMC has been shown to reach higher spectral efficiency compared to CP-OFDM. The concept of FBMC includes synthesis filter bank (SFB) and AFB as it's core elements on the transmitter and receiver sides, respectively [10, 138, 152]. The FFT processing in OFDM or the AFB processing in FBMC on the receiver side can also be used for sensing the spectrum for the CR based transmission. For the spectrum sensing purpose, AFB has significant benefits due to much better spectral containment of the subbands [10, 52, 138, 152]. These properties also assist in improving the interference control in CR transmission links, particularly in scenarios where users are not precisely synchronized to each other. Detailed analysis of OFDM and FBMC based systems in terms of false alarm probability is given in Chapter 5.

A block diagram of FFT or AFB based energy detector is illustrated in Figure 3.1. Wideband multichannel based spectrum sensing, where ED is performed at subband level at the output of an FFT or AFB, is our focus. The output of these blocks is expressed as $y_k[m]$, where $k = 0, \ldots, K-1$ is the subband index and m is the subband sample index. In the context of spectrum sensing the subband signals can be expressed as follows:

$$\begin{aligned} y_k[m] &= w_k[m] && \mathcal{H}_0 \\ y_k[m] &= x_k[m] + w_k[m] && \mathcal{H}_1 \end{aligned} \tag{3.1}$$

where $x_k(m) \cong H_k s_k(m)$ is the PU information signal at the m^{th} FFT or AFB output sample in subband k, H_k is the complex gain of subband k, and $w_k[m]$ is the corresponding noise sample. Furthermore, it is assumed that $w_k[m] \sim$

$\mathcal{N}(0, \sigma_{w,k}^2)$ and $x_k[m] \sim \mathcal{N}(0, \sigma_{x,k}^2)$, with $\sigma_{x,k}^2$ denoting the PU signal variance in subband k. Since a uniform filter bank or FFT is used for spectrum analysis, the subband noise variances can be assumed to be the same, $\sigma_w^2/K \simeq \sigma_{w,k}^2$, while the channel noise is assumed to be white. The integrated test statistics over multiple subbands and certain observation time can be formulated as

$$T(y_{m_0,k_0}) = \frac{1}{N_t N_f} \sum_{k=k_0-\lfloor N_f/2 \rfloor}^{k_0+\lceil N_f/2 \rceil-1} \sum_{m=m_0-N_t+1}^{m_0} |y_k[m]|^2 \tag{3.2}$$

where N_f and N_t are the averaging filter lengths in the frequency and time domain, respectively. Based on Parseval's theorem, FFT/AFB based subband integration and full-band time-domain integration over the same time interval yield the same test statistics when a spectral component is entirely captured by the subband integration range.

When the PU spectrum is assumed to be flat over the sensing band, the probability distribution of the test statistics can be expressed as

$$\begin{aligned} T(y_{m_0,k_0})|\mathcal{H}_0 &\sim \mathcal{N}\left(\sigma_{w,k}^2, \frac{\sigma_{w,k}^4}{N_t N_f}\right) \\ T(y_{m_0,k_0})|\mathcal{H}_1 &\sim \mathcal{N}\left(\sigma_{x,k}^2 + \sigma_{w,k}^2, \frac{(\sigma_{x,k}^2 + \sigma_{w,k}^2)^2}{N_t N_f}\right) \end{aligned} \tag{3.3}$$

which yields,

$$\begin{aligned} P_{FA} &= \Pr(T(y) > \lambda|\mathcal{H}_0) = Q\left(\frac{\lambda - \sigma_{w,k}^2}{\sigma_{w,k}^2/\sqrt{N_f N_t}}\right) \\ P_D &= \Pr(T(y) > \lambda|\mathcal{H}_1) = Q\left(\frac{\lambda - \sigma_{w,k}^2(1+\gamma_k)}{\sigma_{w,k}^2(1+\gamma_k)/\sqrt{N_f N_t}}\right) \end{aligned} \tag{3.4}$$

where

$$\lambda = \sigma_{w,k}^2\left(1 + \frac{Q^{-1}(P_{FA})}{\sqrt{N_f N_t}}\right). \tag{3.5}$$

Here, $\gamma_k = \sigma_{x,k}^2/\sigma_{w,k}^2$ is the subband-wise SNR. FFT/AFB based processing makes it possible to tune the sensing frequency band to the expected band of the PU signal, as well as sensing multiple PU bands simultaneously. The tradeoffs in choosing the integration range in the time-frequency domain are illustrated in Figure 3.2. Several candidate PUs, which can have different spectral characteristics and possibly overlapping spectra, can be sensed simultaneously in the optimized ways.

3.2 Energy Detection in the Presence of Frequency Variability

Spectrum sensing is fundamentally performed to assist opportunistic access for SUs and also for monitoring the spectrum during SU operation for a possible

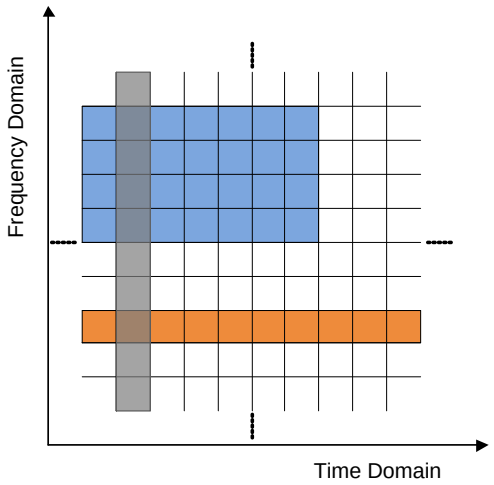

Figure 3.2: Illustration of various integration zones in time-frequency domain.

reappearance of a PU. The aim of this section is to develop tractable models for ED in cases where the PU signal and/or noise are *non-white* within the sensing frequency band or the PU transmission is not constant within the sensing window in time and/or frequency directions, e.g., due to a possible reappearance of a PU [77]. The spectrum of the PU signal is determined by the spectrum of the transmitted waveform, channel frequency response and the sensing receiver filter, whereas the spectrum of the channel noise only depends on the receiver filter frequency response.

3.2.1 Band Edge Detection and Transmission Burst Detection

It is commonly assumed that the PU is either absent or active for accounting of the test statistic during the whole sensing interval. However, in practical communication scenarios, it is often the case that either a PU re-activates during the measurement period or the sensing frequency band fails to match the band of the PU signal [77]. Therefore, only some fraction of the integration window matches the time-frequency zone of the PU activity. This transient scenario in time or frequency direction is illustrated in Figure 3.3 with the associated test statistic distributions.

The distribution of the transient phase test statistics, $T(y)|_{TR}$, can be expressed by virtually splitting the integration window into two distinct subwindows such that the first one contains the observation samples before PU is active, $N - N_1$ samples, whereas the other one contains the remaining N_1 samples. According to this idea, the distributions corresponding to the sample subsets within these virtual sub-windows can be written as[1], $\mathcal{N}\left(\sigma_w^2, \sigma_w^4/(N-N_1)\right)$ and $\mathcal{N}\left(\sigma_x^2+\sigma_w^2, (\sigma_x^2+\sigma_w^2)^2/N_1\right)$, respectively. The distribution of the overall sequence of N samples can be interpreted as a linear combination of these in-

[1]For the sake of notational simplicity, Sections 3.2.1 and 3.2.2 are formulated in a basic single-band ED setting.

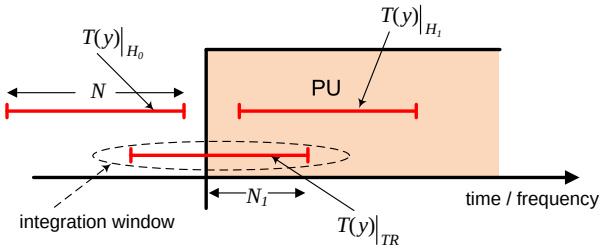

Figure 3.3: Distribution analysis of the transient phase test statistic.

dependent normal random variables using relative weights of $(N - N_1)/N$ and N_1/N. Hence, $X_1 \sim \mathcal{N}(\mu_1, \sigma_1^2)$ and $X_2 \sim \mathcal{N}(\mu_2, \sigma_2^2)$ and with the aid of the standard property of the normal distribution, $aX_1 + bX_2 \sim \mathcal{N}(a\mu_1 + b\mu_2, a^2\sigma_1^2 + b^2\sigma_2^2)$, the following mixture-distribution is deduced,

$$T(y)|_{TR} \sim \mathcal{N}\left(\sigma_w^2 + \frac{N_1}{N}\sigma_x^2, \frac{\sigma_w^4(N - N_1) + N_1(\sigma_x^2 + \sigma_w^2)^2}{N^2}\right). \tag{3.6}$$

The detection probability of the presence of a PU signal during the transient phase is calculated by the tail probability towards $+\infty$ over the mixture distribution in (3.6), namely, $P_{D,TR} = Pr(T(y)|_{TR} > \lambda)$. Hence, the probability of false alarm and probability of detection can be expressed as $P_{FA} = Pr(T(y)|_{\mathcal{H}_0} > \lambda)$ and $P_D = Pr(T(y)|_{\mathcal{H}_1} > \lambda)$, respectively. After algebraic manipulations, the P_{FA} becomes identical to (2.4) whereas the P_D is expressed as,

$$P_D = Q\left(\frac{\lambda N\sigma_w^{-2} - N - N_1\gamma}{\sqrt{N - N_1 + N_1(1+\gamma)^2}}\right) = Q\left(\frac{\sqrt{N}Q^{-1}(P_{FA}) - \gamma N_1}{\sqrt{N - N_1 + N_1(1+\gamma)^2}}\right). \tag{3.7}$$

3.2.2 Sliding Window Based Spectrum Sensing

Sliding window energy detection (SW-ED) is another alternative solution to detect a reappearing PU signal. For simplicity, it is assumed that the sensing receiver is able to monitor the target frequency channel continuously. For instance, when the secondary system leaves a slot of the frequency channel unused for spectrum sensing purposes, this could be reached [77]. The test statistic for a time instant $n + 1$ is obtained effectively with a sliding window of constant length N as follows:

$$T_{n+1}(y) = T_n(y) + \frac{|y[n+1]|^2 - |y[n+1-N]|^2}{N}. \tag{3.8}$$

SW-ED under action is shown in Figure 3.4. It is noted that while the test statistic at any particular time instance follows the statistical model adequately, the probability of exceeding the decision threshold within a time interval grows

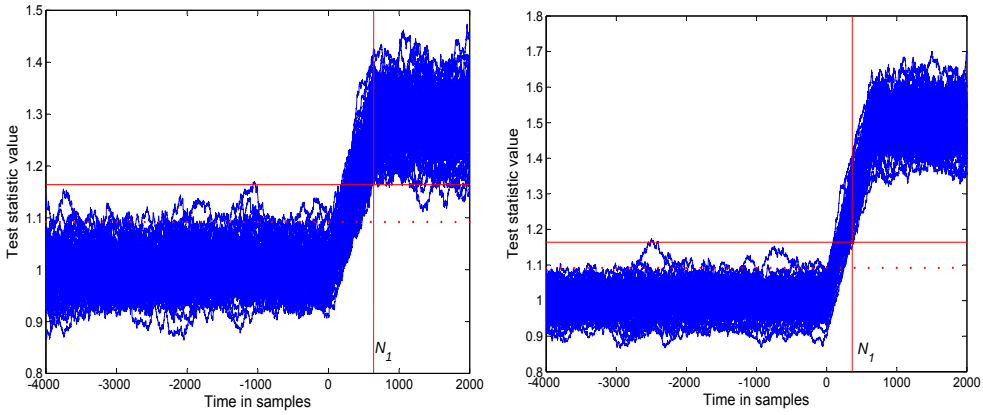

Figure 3.4: Sliding window energy detection in action: 100 instances of SW-ED processing with block length of $N = 640$ for -5.5 dB PU SNR (left) and -3 dB SNR (right). The horizontal lines indicate the thresholds for $P_{FA} = 0.01$ in basic single-shot energy detection (dotted) and in SW-ED with 12800 samples (solid). Time instant 0 corresponds to the beginning of the PU transmission and the vertical line indicates the first time instance (N_1) when $P_D = 0.99$ is reached.

with the length of the interval. Hence, the decision threshold has to be increased, compared to the basic single-window sensing, to reach reasonable P_{FA}. The specific case of multiple (B) non-overlapping ED windows is rather convenient to handle. In this case, the probability of not exceeding the threshold in any of the sensing windows can be expressed as:

$$1 - P_{FA}^{(B)} = \Pr\left(\max_{k=1}^{B} T^k(y) < \lambda\right) = \prod_{k=1}^{B} \Pr\left(T^{(k)}(y) < \lambda\right) = \left(1 - P_{FA}^{(1)}\right)^B. \tag{3.9}$$

However, for the presented SW-ED model, no analytical models that address this scenario exist while consecutive outputs are strongly correlated. Therefore, a numerical approach for analyzing the performance of this idea is proposed [P1].

3.2.3 Effects of non-flat primary user spectrum

As seen in the flexible multiband sensing illustration of Figure 3.1, FFT or AFB is used to split the signal into relatively narrow subbands, after the receiver front-end and analog-to-digital converter (ADC). According to the bandwidth of possible PU, a number of consecutive subbands is combined with an optimized weighting process for enhancing the sensing performance. Two different ideas can be applied to obtain better performance with the weighting process: *a*) If the PU signal is with flat spectrum, constant weights are optimal solution, and they may also provide a good approximation with properly selected number of subbands for non-flat spectral characteristics. When there is no knowledge about the PU signal, this method is naturally the best approach. *b*) If there is prior knowledge about the PU signal, optimized weights can be applied for

optimal solution. When the channel is frequency selective, the spectrum of the received signal is affected, but the channel characteristics can not be assumed to be known. Anyway, the optimized weighting process based on knowledge of the transmitted spectrum may be considered, especially if the channel is not severely frequency selective within the PU bandwidth.

The test statistics are approximated as a sum of independent Gaussian variables with different variances under $\mathcal{H}_0$ and $\mathcal{H}_1$. Hence, the probability distribution of the test statistic T_k for center frequency k and arbitrary weighting coefficients can be expressed as follows,

$$\begin{aligned} f(T_k)|_{\mathcal{H}_0} &\sim \mathcal{N}\left(\sum_{\kappa=k-\overline{N_f}}^{k+\overline{N_f}} g_k\sigma_{w,k}^2, \sum_{\kappa=k-\overline{N_f}}^{k+\overline{N_f}} \frac{g_k^2\sigma_{w,k}^4}{N_tN_f}\right) \\ f(T_k)|_{\mathcal{H}_1} &\sim \mathcal{N}\left(\sum_{\kappa=k-\overline{N_f}}^{k+\overline{N_f}} \frac{\sigma_{x,k}^2+\sigma_{w,k}^2}{g_k^{-1}}, \sum_{\kappa=k-\overline{N_f}}^{k+\overline{N_f}} \frac{(\sigma_{x,k}^2+\sigma_{w,k}^2)^2}{N_tN_fg_k^{-2}}\right) \end{aligned} \tag{3.10}$$

where $N = N_tN_f$ is the overall sample complexity. To simplify the notation, it is assumed that the value of the window size in frequency domain is odd, i.e., $N_f = 2\overline{N_f}+1$. The integration in frequency domain takes the weighted average of the time filter outputs, with g_k denoting the real-valued weight for subband k with PU signal power $\sigma_{x,k}^2$. Next, the problem of optimizing the subband weights is addressed.

For arbitrary weight values, the corresponding P_{FA} and P_D is given by,

$$\begin{aligned} P_{FA} &= Q\left(\left(\lambda - \sum_{\kappa=k-\overline{N_f}}^{k+\overline{N_f}} g_k\sigma_{w,k}^2\right)\Bigg/\sqrt{\sum_{\kappa=k-\overline{N_f}}^{k+\overline{N_f}} \frac{g_k^2\sigma_{w,k}^4}{N}}\right) \\ P_D &= Q\left(\left(\lambda - \sum_{\kappa=k-\overline{N_f}}^{k+\overline{N_f}} g_k\sigma_{w,k}^2\,(1+\gamma_k)\right)\Bigg/\sqrt{\sum_{\kappa=k-\overline{N_f}}^{k+\overline{N_f}} \frac{g_k^2\sigma_{w,k}^4(1+\gamma_k)^2}{N}}\right). \end{aligned} \tag{3.11}$$

Using P_{FA} and P_D expressions, the corresponding energy threshold λ can be expressed,

$$\begin{aligned} \lambda &= Q^{-1}(P_{FA})\sqrt{\sum_{\kappa=k-\overline{N_f}}^{k+\overline{N_f}} \frac{g_k^2\sigma_{w,k}^4}{N}} + \sum_{\kappa=k-\overline{N_f}}^{k+\overline{N_f}} g_k\sigma_{w,k}^2 \\ &= Q^{-1}(P_D)\sqrt{\sum_{\kappa=k-\overline{N_f}}^{k+\overline{N_f}} \frac{g_k^2(1+\gamma_k)^2}{N\sigma_{w,k}^{-4}}} + \sum_{\kappa=k-\overline{N_f}}^{k+\overline{N_f}} \frac{1+\gamma_k}{g_k^{-1}\sigma_{w,k}^{-2}}. \end{aligned} \tag{3.12}$$

The minimum required sample complexity, $N = N_t N_f$, can be calculated as follows,

$$\hat{N} = \left[Q^{-1}(P_{FA}) \sqrt{\frac{\sum_{\kappa=k-\overline{N_f}}^{k+\overline{N_f}} g_k^2}{\left(\sum_{\kappa=k-\overline{N_f}}^{k+\overline{N_f}} g_k \gamma_k\right)^2}} - Q^{-1}(P_D) \sqrt{\frac{\sum_{\kappa=k-\overline{N_f}}^{k+\overline{N_f}} g_k^2 (1+\gamma_k)^2}{\left(\sum_{\kappa=k-\overline{N_f}}^{k+\overline{N_f}} g_k \gamma_k\right)^2}} \right]^2 \tag{3.13}$$

which is expressed as a function of P_{FA}, P_D, g_k and γ_k. The required time record length N_t is determined according to the targeted minimum detectable PU power level in practice. When optimum weighting coefficients are used, the frequency block length N_f should be chosen to include all subbands that essentially contribute to the test statistics.

It is assumed that the weights are normalized for constant noise power level i.e., $\sum_i g_i^2 = 1$, the first term of (3.13) is maximized by choosing:

$$g_k = \frac{\sigma_{x,k}^2}{\sum_{\kappa=k-\overline{N_f}}^{k+\overline{N_f}} \sigma_{x,k}^2} = \frac{\sigma_{x,k}^2}{\sigma_x^2} = \frac{\gamma_k}{\gamma}. \tag{3.14}$$

In any realistic case, with $P_D > 0.5$ also the second term is positive and it is maximized by choosing $g_k = \frac{\gamma_k}{S(1+\gamma_k)^2}$. Here, $S = \sum_{\kappa=k-\overline{N_f}}^{k+\overline{N_f}} \frac{\gamma_k}{(1+\gamma_k)^2}$.

The proofs are provided in [P1] in detail. Also, additional numerical results for the example case of Bluetooth are shown in Section 3.4.

3.2.4 Effects of fading frequency selective channel

A vast majority of the spectrum sensing studies have been focused on the AWGN channel case so far, while the channel is frequency selective and fading in most CR scenarios. Hence, we analyze and discuss the selectivity issue in this sub-section. It is recalled that $\gamma = \sigma_x^2/\sigma_w^2$ and $\gamma_k = \sigma_{x,k}^2/\sigma_{w,k}^2$ denote the overall PU SNR and the subband-wise SNR's, respectively. The channel frequency response, represented by the subband gains F_k, is assumed to satisfy the relationship $\sum_{k=1}^{N_f} F_k^2 = N_f$, which basically indicates that the received PU signal power is assumed to be constant. Naturally, any fading channel would introduce temporal variations of the total received power, but our idea is to analyze the effects of time and frequency selectivity separately. Based on this and given that $\gamma_k = F_k \gamma$, the test statistics in (3.3) can be extended for the case of frequency selective channels as follows,

$$\begin{aligned} T(y)|_{\mathcal{H}_0} &\sim \mathcal{N}\left(\sigma_w^2, \frac{\sigma_w^4}{N_t N_f}\right) \\ T(y)|_{\mathcal{H}_1} &\sim \mathcal{N}\left(\sigma_s^2 + \sigma_w^2, \frac{\beta_{ch}}{N_t N_f}(\sigma_s^2 + \sigma_w^2)^2\right) \end{aligned} \tag{3.15}$$

where,

$$\beta_{ch} = \frac{1}{N_f}\sum_{k=1}^{N_f}\frac{(\sigma_{x,k}^2+\sigma_{w,k}^2)^2}{(\sigma_x^2+\sigma_w^2)^2} = \frac{1}{N_f}\sum_{k=1}^{N_f}\frac{(1+F_k^2\cdot\gamma)^2}{K^2(1+\gamma)^2}. \tag{3.16}$$

The corresponding P_{FA} and P_D are similar to (3.4), and can be straightforwardly deduced by making the necessary change of variables yielding,

$$P_D = Q\left(\frac{\sqrt{N_f N_t}\left[\lambda-\sigma_w^2(1+\gamma)\right]}{\sigma_w^2(1+\gamma)\sqrt{\beta_{ch}}}\right) = Q\left(\frac{Q^{-1}(P_{FA})-\gamma\sqrt{N_t N_f}}{(1+\gamma)\sqrt{\beta_{ch}}}\right). \tag{3.17}$$

It is clear that the variance of the test statistic is affected by the channel frequency response only under H_1. The effect of the frequency selectivity on the ED performance can not be significant under the low PU SNR regime. On the other hand, equations (3.16) and (3.17) can assist in quantifying this and evaluate whether the effect is significant when operating with highly frequency selective channels at relatively high SNR levels. Numerical results that demonstrate this effect are presented in Section 3.4.

3.3 Area Under the Receiver Operating Characteristics Curve

AUC, which is used in different areas of science as a performance metric, is considered here as an alternative measure to assess the performance of ED based spectrum sensing. The performance of a basic ED is commonly analyzed in terms of two parameters, P_{FA} and P_D. Based on this, the most common method to analyze the performance is to fix one of the two measures and vary the other one. On the country with AUC model, there is only one parameter involved, which provides a better insight on the overall performance of the detector. While the AUC approaches ideally the value of 1, in which case $P_D = 1$ for any given value of P_{FA}, the useful values of the AUC are those that are greater than 0.65 with those greater than 0.85 considered acceptable in practice.

In the presence of AWGN, AUC is expressed as [4]:

$$\text{AUC} = A(\gamma) \triangleq -\int_0^\infty P_D(\gamma,\lambda)\frac{\partial P_{FA}(\lambda)}{\partial\lambda}d\lambda. \tag{3.18}$$

Analytic expressions for the AUC of each proposed spectrum sensing scenario are summarized now in the form $\text{AUC} = \mathcal{I}(a,b,c,d) = \frac{c}{\sqrt{2\pi}}\int_0^\infty Q(ax-b)e^{-\frac{(cx-d)^2}{2}}dx$. The AUC for the traditional ED can be expressed as follows,

$$\text{AUC}\,|_{ED} = \mathcal{I}\left(\frac{\sqrt{N}}{\sigma_w^2(1+\gamma)},\sqrt{N},\frac{\sqrt{N}}{\sigma_w^2},\sqrt{N}\right). \tag{3.19}$$

For the specific scenario of re-appearing PU, the AUC can be formulated as,

$$\text{AUC}\,|_{TR} = \mathcal{I}\left(\frac{N}{\sigma_w^2\sqrt{N-N_1+N_1(1+\gamma)^2}},\frac{N+N_1\gamma}{\sqrt{N-N_1+N_1(1+\gamma)^2}},\frac{\sqrt{N}}{\sigma_w^2},\sqrt{N}\right). \tag{3.20}$$

For the case of the weighting process, AUC can be expressed as,

$$\mathrm{AUC}|_{weights} = \mathcal{I}\left(\frac{\sqrt{N}}{\sqrt{\sum_{k=\kappa-\overline{N_f}}^{\kappa+\overline{N_f}} g_k^4 \sigma_{w,k}^4 (1+\gamma_k)^2}}, \frac{\sqrt{N}\sum_{k=\kappa-\overline{N_f}}^{\kappa+\overline{N_f}} g_k^2(1+\gamma_k)}{\sqrt{\sum_{k=\kappa-\overline{N_f}}^{\kappa+\overline{N_f}} g_k^4 (1+\gamma_k)^2}}, \ldots \right. \\ \left. \frac{\sqrt{N}}{\sqrt{\sum_{k=\kappa-\overline{N_f}}^{\kappa+\overline{N_f}} g_k^4 \sigma_{w,k}^4}}, \frac{\sqrt{N}\sum_{k=\kappa-\overline{N_f}}^{\kappa+\overline{N_f}} g_k^2}{\sqrt{\sum_{k=\kappa-\overline{N_f}}^{\kappa+\overline{N_f}} g_k^4}} \right). \quad (3.21)$$

Finally, under the frequency selectivity, AUC can be obtained as

$$\mathrm{AUC}\,|_{sel} = \mathcal{I}\left(\frac{\sqrt{N_t N_f}\sigma_w^{-2}}{\sqrt{\beta_{ch}}(1+\gamma)}, \sqrt{\frac{N_t N_f}{\beta_{ch}}}, \frac{\sqrt{N_t N_f}}{\sigma_w^2}, \sqrt{N_t N_f} \right). \quad (3.22)$$

Detailed derivations of these expressions are given in [P1]. To the best of the authors' knowledge, these expressions are novel.

3.4 Numerical Results

In this section, the main simulation results of our proposed spectrum sensing analysis methods and algorithms are presented. First, the ED performance in the case of a re-appearing PU and AWGN is demonstrated and subsequently the results of our proposed algorithms under frequency selectivity are given with the indicative example of the non-flat spectrum of the Bluetooth signal.

Figure 3.5 shows the overall ED performance for the re-appearing PU case in terms of the corresponding receiver operating characteristics (ROC) and AUC for $N = 1000$. Particularly, the AUC results indicate that ED can achieve

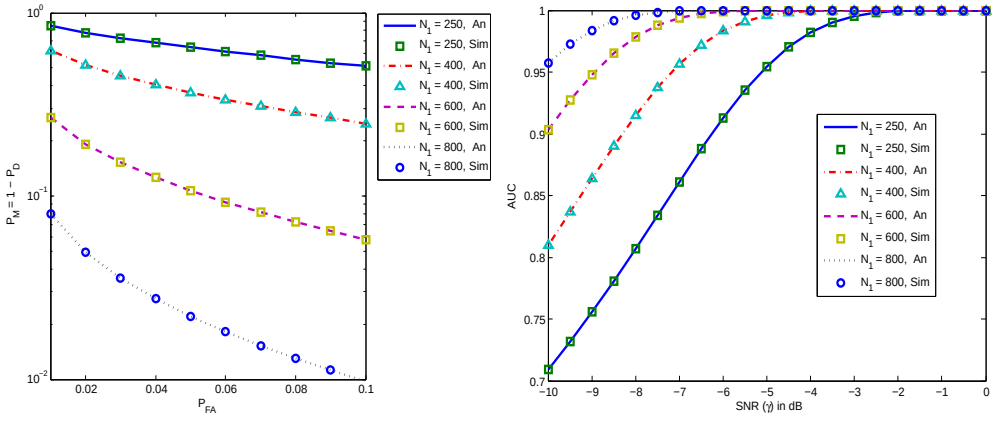

Figure 3.5: AUC and ROC with $\gamma = -8$ dB, $N = 1000$ and different values of N_1 for the transient phase ED.

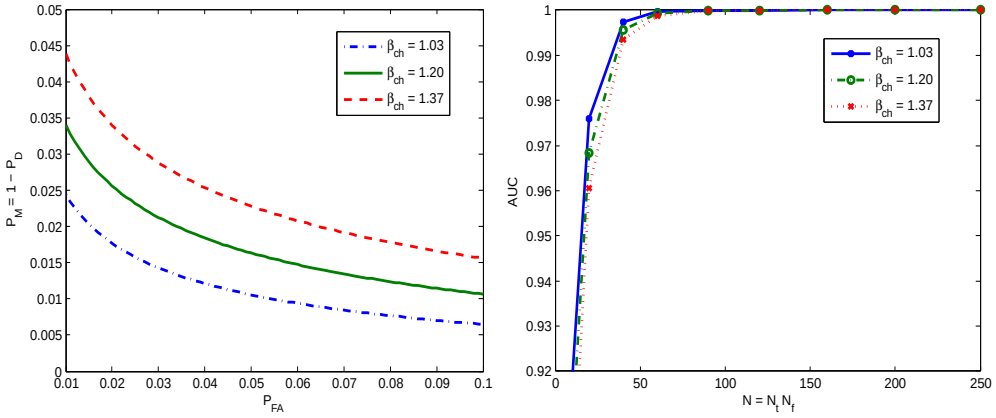

Figure 3.6: ROC and AUC curves for frequency selective channels at $\gamma = 0$ dB, for different values of β_{ch} and $N_t N_f = 20 \times 2$ for the ROC case.

robust performance in the re-appearing PU scenario as its value exceeds 0.95 as N_1 increases. Figure 3.5 provides an indicative connection on the behavior between P_D and AUC. According to this figure, it is evident that such transient situations, i.e., unknown PU channel band edges and/or transmission burst timing, can be handled effectively through the sliding window processing. Sliding window processing can be performed with FFT or AFB based ED in time and/or frequency domain. Hence, the PU transmission can be located in time or frequency direction, respectively.

The theoretical β-values are found with (3.16) to be in the range $[1.13, 2.47]$ for the noise-free case, whereas the corresponding range of β_{ch}-values is $[1.03, 1.37]$ for 0 dB SNR and $[1.01, 1.06]$ for -6 dB SNR for the International Telecommunication Union (ITU)-R Vehicular A channel. Here ITU-R Vehicular A channel with 20 MHz bandwidth is considered and 1024 subbands are used in the analysis. Figure 3.6 shows the ROC and AUC curves for three cases with $\gamma = 0$ dB, i.e., $\beta_{ch} \in \{1.03, 1.20, 1.37\}$. We assume that $N_t = 20$ and $N_f = 2$ for the ROC case, while the AUC is shown as a function of $N = N_t N_f$. Evidently, the effect of frequency selectivity on the performance of the ED is significant at relatively high SNR values, beyond 0 dB. However, our numerical results related β_{ch} values clearly indicate the effects of frequency selectivity on ED performance are practically negligible in the low SNR regime and the performance is determined by the temporal variations of the received PU signal power [37]. It is enough to model the variation of the total received power, while the multipath effects on frequency selectivity are not essential in the low SNR regime [37, 140, 153] in ED based spectrum sensing.

In the majority of wireless communication scenarios in practice, wireless channels are frequency selective and hence, one cannot realistically assume knowledge of the observed PU signal spectrum. However, channel models are commonly assumed to be flat for certain short range applications, such as IEEE 802.15 based Bluetooth wireless technology, which has 1 MHz nominal bandwidth with 1600 hops per second hopping rate [71]. We mostly consider a simplified scheme with continuous Bluetooth signal at the 33$^{\text{rd}}$ channel as seen

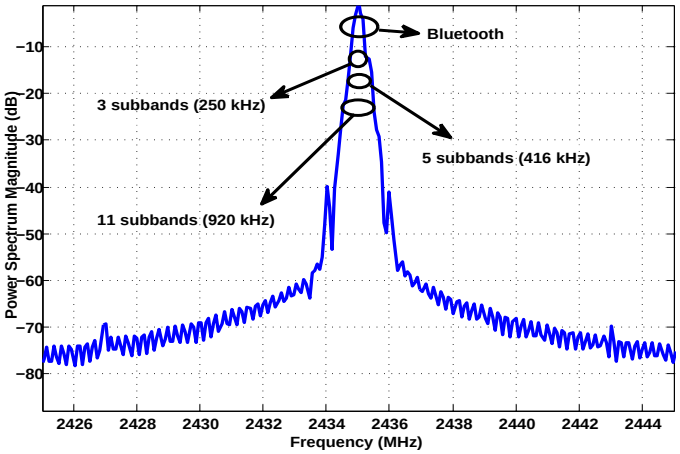

Figure 3.7: Bluetooth signal spectrum in 2.4 GHz ISM band.

in Figure 3.7. The performance of the multiband spectrum sensing scheme with weighting process in sensing a Bluetooth information signal and the corresponding spectral holes is analyzed. The differences between filter bank and FFT based sensing in the absence of strong PUs at adjacent frequencies are insignificant. Hence, the results are shown only for the FFT case. We assume 83.5 MHz sampling rate and that the ISM band consists of 1024 subbands. The sensing window comprises of 11 subbands corresponding to the 1 MHz sensing bandwidth of the Bluetooth signal. In this scenario, we target at $\gamma = -5$ dB in spectrum sensing, $P_{FA} = 0.1$ and $P_D = 0.9$.

The required sample complexity for the target SNR, P_D and P_{FA} is determined with (3.14) as $\hat{N} = 89$ under non-frequency-selective model. If the Bluetooth power was equally distributed among the 11 subbands, 8 samples from each of these subbands would be sufficient for reaching the target requirements. Also, when sensing is performed only by utilizing the center subband, $\hat{N} = 89$ is a lower bound for the time record length. Table 3.1 depicts the number of required subband samples needed with the BT signal for different sensing bandwidths and with optimized and constant weights. When the optimum weight values are used for all 11 subbands of the Bluetooth signal, the required number of subband samples is 45, which corresponds to a lower time record length than the respective 50 samples hoping interval as an example case. It can be also observed that almost the same time recording length can be used when sensing a single subband at the Bluetooth center frequency as when sensing the entire 1 MHz Bluetooth band with constant weights. For the case of constant weights, 3 subbands constitutes the optimum choice for all considered SNR values. On the contrary, using optimum weights reduces the sensing time by about 10%.

Figure 3.8 shows the P_D with constant and optimum weight values as a function of the active Bluetooth SNR with: *a*) AWGN, *b*) ITU-R Vehicular and *c*) Indoor channel. Constant and optimum weight cases use 3 and 11 subbands, respectively. The Vehicular A channel has 6 taps and its maximum delay spread is about 2.5 μs [79]. A 16-tap model with 80 ns root mean square (RMS) delay

Table 3.1: Required time record length in subband samples for different weighting schemes in Bluetooth sensing.

Bluetooth SNR	Weight Factors	11 subbands	5 subbands	3 subbands	1 subband
0 dB	Const.	12	8	8	15
	Opt.	7	7	8	
-3dB	Const.	39	25	23	41
	Opt.	21	21	23	
-4 dB	Const.	60	37	34	60
	Opt.	31	31	33	
-5 dB	Const.	92	56	51	89
	Opt.	45	46	49	
-6 dB	Const.	143	84	77	132
	Opt.	68	69	73	
-7 dB	Const.	223	131	117	200
	Opt.	104	105	111	

spread is also applied as a realistic Indoor channel model [79, 192]. Highest detection probability performance is achieved with optimum weight values using 11 subbands, but the benefit over the constant weight case is relatively small. It is also evident that the P_D is not substantially different between FFT and AFB in this low dynamic range case. It is also clearly seen that the optimum weighting scheme derived for the flat-fading model gives the best results also with frequency-selective channels. The difference is most noticeable with the ITU-R Vehicular A channel.

The previous discussion did not consider the frequency hopping characteristic of the Bluetooth system. A critical issue is that if the time window for calculating the test statistics is not aligned with the received Bluetooth burst, the detection performance degrades significantly, as discussed earlier in this

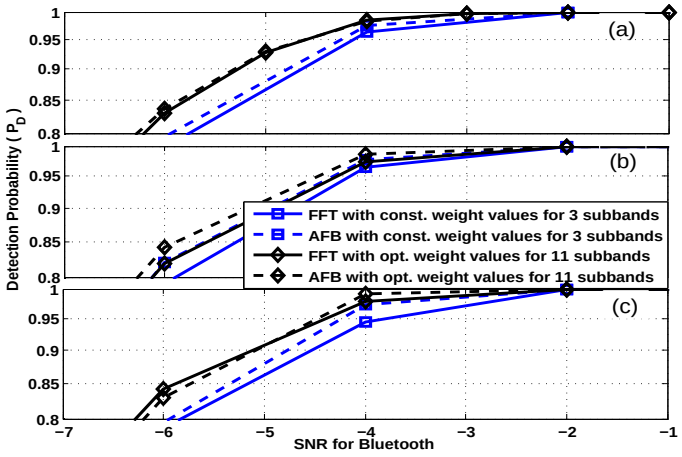

Figure 3.8: Detection probability of Bluetooth signal with $P_{FA} = 0.1$ using time record length of 50 for constant and optimum weight values under (a) AWGN, (b) ITU-R Vehicular A channel, (c) Indoor channel including both FFT and AFB based sensing.

section. Notably, this issue can be ultimately avoided by determining the test statistics with the aid of the sliding window approach.

3.5 Chapter Summary

The effect of misaligned time-frequency window on the test statistics was investigated in a generic way by means of a mixed statistical model based on Gaussian approximation. The effects of the frequency selectivity on ED performance were also analyzed. Sliding window processing for re-appearing PU detection was studied as an extended method to search for the best match in cases where the frequency range or burst timing of the PU signal is unknown to the sensing receiver.

Next, non-flat PU spectral characteristics, considering Bluetooth as an example case was addressed. Optimum weights were derived for FFT or AFB based sensing and an analytical model was developed to quantify the effect of channel frequency selectivity on the sensing performance.

Finally, novel analytic methods with AUC as a single-valued performance metric were developed for the proposed ED scenarios. The offered results were subsequently employed in analyzing extensively the corresponding detectors' performance.

In our discussions, the central tool was splitting a wideband multichannel signal into relatively narrow subbands and then combining subbands samples within a proper time-frequency zone with optimized weighting. This can be regarded as a very useful tool for the next generation CRs. While there is no major difference between FFT and AFB based spectrum sensing in terms of detection performance in low dynamic range scenarios, AFB based algorithms provide clearly better false alarm performance in the presence of strong spectral components in the sensing band due to better control of spectral leakage, as demonstrated in [38] and Chapter 5.

CHAPTER 4

REDUCED COMPLEXITY SPECTRUM SENSING BASED ON ENERGY AND EIGENVALUE DETECTORS

In this chapter, reduced complexity eigenvalue based and subband energy based sensing algorithms are introduced. They are capable of overcoming the noise uncertainty problem with relatively low computational complexity compared to the existing spectrum sensing techniques such as traditional eigenvalue based sensing.

ED is widely used in CR context due to its relatively simple practical realization and low computational complexity [69, 191]. Hence, numerous methods have been reported in the context of AWGN channels, fading channels and cooperative sensing [4, 59, 60, 72, 73]. However, it is well known that performance of ED is largely vulnerable to very low SNR levels and noise uncertainty effects in practical wireless communications scenarios [158]. Since multipath fading and shadowing phenomena cause power fluctuations of the received signal, the need to operate under very low PU SNR is unavoidable in many CR systems [4, 59, 60, 72, 73].

Eigenvalue-based spectrum sensing techniques which have been shown to perform adequately even at the problematic low SNR detection [P2] and [97, 196, 197] are alternative spectrum sensing techniques to overcome the noise uncertainty challenges. However, this type of advanced spectrum sensing techniques have high computational complexity due to calculation of the covariance matrix of the received signal and its corresponding eigenvalues.

Alternative eigenvalue based approaches, which only require the largest eigenvalue and trace of the covariance matrix, have been presented to decrease the computational complexity in [117, 130, 131, 176, 195, 199]. However, the largest eigenvalues are still calculated using the traditional methods in these

studies. Possible solutions to solve complexity issue are reported in [43,82,193], where the power iteration algorithm is proposed to obtain the largest eigenvalue of the covariance matrix with relatively low computational complexity. On the other hand, the most commonly considered eigenvalue based spectrum sensing methods in [43, 82, 193] still require the information of the smallest eigenvalue, leading to higher computational complexity. In fact, to the best of our knowledge, careful analysis and comparison of the computational complexity of different eigenvalue based methods is missing in the literature. Another alternative solution is ESD based spectrum sensing techniques which utilize the order statistics of subband energy differences in frequency domain [25–27]. These methods are able to remove the involved noise floor which results in the elimination of the corresponding uncertainty effects.

Motivated by the above, we investigate here Max-Min ED approaches, which show highly accurate spectrum sensing performance and reduced computational complexity [40, 41, 44]. Specifically, the contributions of this chapter are summarized below:

- We evaluate the performance and complexity of the EMaxE, which uses the maximum eigenvalue over energy as the decision statistic (which is equivalent to the ratio of the largest eigenvalue and trace of the covariance matrix used in [117,130,131,176,195]) and calculates the maximum eigenvalue using the power iteration method. We consider this as the computationally most effective form of eigenvalue based sensing and use it as a reference algorithm in the complexity evaluation of the proposed subband energy based detectors.

- The proposed Max-Min ED algorithm has significantly lower complexity than EMaxE, and in most cases it reaches or exceeds the performance of eigenvalue based methods.

- The proposed techniques are analyzed to see the effects of the transmitted spectral shape and multipath channel. Detection performance and computational complexity are evaluated under different scenarios.

4.1 Traditional Eigenvalue Based Spectrum Sensing

Before starting to explain the reduced complexity based eigenvalue detection methods, the traditional eigenvalue based spectrum sensing approach is briefly explained as a reference model.

The signal model of (2.1) is also valid in this case. We consider L consecutive symbol intervals with each of them consisting of M samples and highly correlated signals. The sequences of the received and primary signals are defined as

$$\hat{\mathbf{y}} = \; [y(n) \;\; y(n-1) \;\; y(n-2) \;\; ... \;\; y(n-ML+1)]^T \tag{4.1}$$

and

$$\hat{\mathbf{s}} = \; [s(n) \;\; s(n-1) \;\; s(n-2) \;\; ... \;\; s(n-ML+1)]^T \tag{4.2}$$

respectively, whereas the sequence of the noise is given by

$$\hat{\mathbf{w}} = [w(n)\ w(n-1)\ w(n-2)\ ...w(n-ML+1)]^T. \tag{4.3}$$

The statistical covariance matrices of the transmitted signal, the received signal and the corresponding noise are defined as: $\mathbf{R}_{yy} = E(\hat{\mathbf{y}}\hat{\mathbf{y}}^\dagger)$, $\mathbf{R}_{ss} = E(\hat{\mathbf{s}}\hat{\mathbf{s}}^\dagger)$ and $\mathbf{R}_{ww} = E(\hat{\mathbf{w}}\hat{\mathbf{w}}^\dagger)$. Furthermore, the covariance matrix of the received signal can be further expressed as, $\mathbf{R}_{yy} = \mathbf{H}\mathbf{R}_{ss}\mathbf{H}^\dagger + \mathbf{R}_{ww}$, where the channel matrix $\mathbf{H}$ and eigenvalues of $\mathbf{R}_{yy}$ and $\mathbf{H}\mathbf{R}_{ss}\mathbf{H}^\dagger$ are defined as $\lambda_1 \geq \lambda_2 \geq ... \geq \lambda_{ML}$ and $\rho_1 \geq \rho_2 \geq ... \geq \rho_{ML}$, respectively [P2].

In practice, the statistical covariance matrix can only be calculated with a limited number of samples. The sample auto-correlations of the received signal are defined as follows:

$$\delta(l) = \frac{1}{NM} \sum_{m=0}^{NM-1} y(m)y(m-l), \quad l = 0, 1, ..., ML-1, \tag{4.4}$$

The statistical covariance matrix can be approximated by the sample covariance matrix defined as

$$\mathbf{R}_{yy} = \begin{bmatrix} \delta(0) & \delta(1)\dots & \delta(ML-1) \\ \delta(1) & \delta(0) & \delta(ML-2) \\ \vdots & \ddots & \vdots \\ \delta(ML-1) & \delta(ML-2) & \delta(0) \end{bmatrix} \tag{4.5}$$

Note that the sample covariance matrix is symmetric and Toeplitz. In the Max/Min eigenvalue based detector, the ratio of λ_{max} and λ_{min} is compared with the threshold which is calculated according to the distribution of the covariance matrix of noise, when the signal is absent. The detailed analytical model is explained in [P2].

4.2 Reduced Complexity Spectrum Sensing Based on Maximum Eigenvalue and Energy Detector

The EMaxE algorithm which requires only the largest eigenvalue and average energy is illustrated in Figure 4.1. Power iteration algorithm is used to approximate the maximum eigenvalue of a matrix by exploiting its Hermitian or Toeplitz structure [168, 193].

Firstly, the average energy of the corresponding received signal which is used in the calculation of the test statistics is computed like in the traditional ED methods as follows:

$$T(N) = \frac{1}{MN} \sum_{n=0}^{NM-1} |y(n)|^2. \tag{4.6}$$

The sample covariance matrix $\mathbf{R}_{yy}$ and its largest eigenvalue $\lambda_{\max}$ are calculated from an observed sequence of MN samples [43,44]. The covariance matrix estimate is calculated using a block length of L symbols, where L is the smooth-

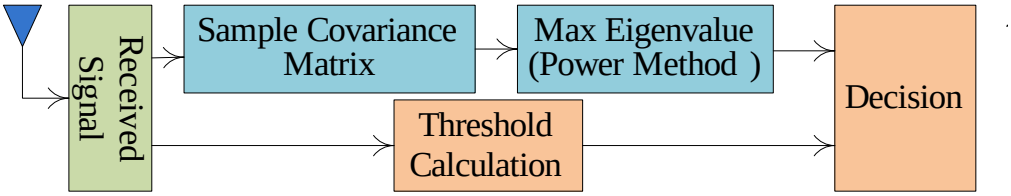

Figure 4.1: Block diagram of the modified maximum eigenvalue / energy based spectrum sensing.

ing factor and its dimension is $ML \times ML$. The largest eigenvalue of a symmetric positive definite matrix is obtained with the power iteration method [82]. The involved computational complexity is of the order of $O(kML)$, with k denoting the number of iterations depending on the error threshold.

In the EMaxE algorithm, the signal is assumed to be present if $(\lambda_{\max}/T(N)) > \gamma$, otherwise it is expected that the band of interest consists only of noise. The threshold value γ can be determined with the aid of the random matrix theorem [196]. While analytical expressions for this algorithm exist in the literature, more straightforward derivations of the threshold, false alarm and detection probabilities are given in the Appendix A.

4.3 Connection between Subband Energy and Eigenvalue Based Spectrum Sensing

While the EMaxE algorithm has lower computationally complexity than commonly used eigenvalue based detection, the complexity is still higher than that of the traditional ED, which is significantly effected by the noise uncertainty. Hence, the connection between PSD and eigenvalue based methods has critical importance to decrease the computational complexity while trying to overcome the noise uncertainty issue.

The eigenvalues of the covariance matrix are bounded by the minimum and maximum values of the PSD [70]. By letting λ_i denote the eigenvalues of the $ML \times ML$ covariance matrix of $\mathbf{R}_{yy}$ of a discrete-time stochastic process $y(n)$ and $\mathbf{q}_i$, $i = 1, 2, ...ML$, present their associated eigenvectors, one obtains

$$\lambda_i = \frac{\mathbf{q}_i^H \mathbf{R}_{yy} \mathbf{q}_i}{\mathbf{q}_i^H \mathbf{q}_i}, \quad i = 1,\ 2,\ ...\ ML \tag{4.7}$$

By expanding the numerator of (4.7), it follows that

$$\mathbf{q}_i^H \mathbf{R}_{yy} \mathbf{q}_i = \sum_{k=1}^{ML} \sum_{l=1}^{ML} q_{ik}^* r(l-k) q_{il} \tag{4.8}$$

where q_{ik}^* is the k^{th} element of the row vector $\mathbf{q}_i^H$, $r(l-k)$ is the kl^{th} element of the matrix $\mathbf{R}_{yy}$, and q_{il} is the l^{th} element of the column vector $\mathbf{q}_i$. With the Einstein-Wiener-Khintchine theorem [70], one obtains

$$r(l-k) = \frac{1}{2\pi} \int_{-\pi}^{\pi} S(w) e^{jw(l-k)} dw. \tag{4.9}$$

Thus, the numerator of (4.7) can be re-written as

$$\mathbf{q}_i^H \mathbf{R}_{yy} \mathbf{q}_i = \frac{1}{2\pi} \sum_{k=1}^{ML} \sum_{l=1}^{ML} q_{ik}^* q_{il} \int_{-\pi}^{\pi} S(w) e^{jw(l-k)} dw. \tag{4.10}$$

Finally, the i^{th} eigenvalue of the covariance matrix $\mathbf{R}_{yy}$ in terms of the PSD $S(w)$ is formulated as

$$\lambda_i = \frac{\mathbf{q}_i^H \mathbf{R}_{yy} \mathbf{q}_i}{\mathbf{q}_i^H \mathbf{q}_i} = \frac{\int_{-\pi}^{\pi} |Q_i'(e^{jw})|^2 S(w) dw}{\int_{-\pi}^{\pi} |Q_i'(e^{jw})|^2 dw} \tag{4.11}$$

where, $Q_i'(e^{jw}) = \sum_{k=1}^{ML} q_{ik}^* e^{-jwk}$. Thus, the λ_i eigenvalues are bounded by the maximum and minimum values of the associated PSD, i.e. $S_{\min}(w) \leq \lambda_i \leq S_{\max}(w)$, $i = 1, 2, ..., ML$. Likewise, the eigenvalue spread is bounded as follows:

$$\chi(\mathbf{R}_{yy}) = \frac{\lambda_{\max}}{\lambda_{\min}} = \frac{\lambda_1}{\lambda_{ML}} \leq \frac{S_{\max}(w)}{S_{\min}(w)}. \tag{4.12}$$

The relation between spectral density and eigenvalue based sensing is also shown in [64, 88, 167].

4.4 Proposed Maximum−Minimum Energy Detection Based Spectrum Sensing

A new Max-Min ED method, which is less complex and robust to noise uncertainty, is proposed as illustrated in Figure 4.2. This is achieved by using the difference of maximum and minimum energies of the subbands as the decision statistic. The proposed method can be summarized with the following main steps:

- Subband energy detector (SED)
- Quantification of the maximum and minimum energy levels
- Threshold calculation and decision device

It is noted that the ordering and differentiation blocks are considered in [25–27] as follows, but they are removed from our simplified method:

∗ Ordering of the determined subband energies

∗ Differentiation of the ordered subband energy sequence

Subband Energy Detector: The N_{FFT} point FFT operation on rectangularly windowed sets of N_{FFT} samples is applied in the first stage. (Alternatively, an AFB with the same number of subbands can be used and is preferred in high dynamic range scenarios.) The subband signals are formulated as

$$Y_m[k] = \begin{cases} W_m[k], & \mathcal{H}_0 \\ S_m[k]H_k + W_m[k], & \mathcal{H}_1 \end{cases} \tag{4.13}$$

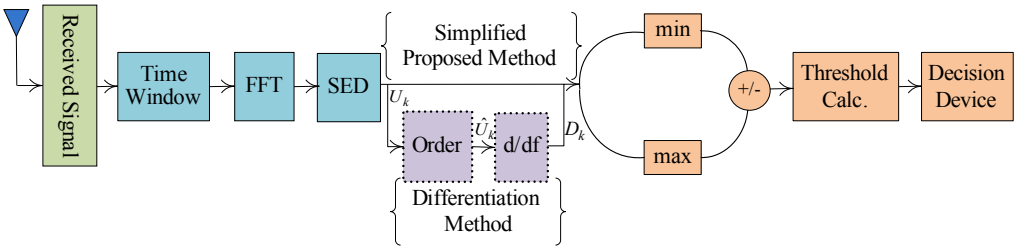

Figure 4.2: Block diagram of the subband energy detection methods.

where $W_m[k]$ is the corresponding channel noise sample under $\mathcal{H}_0$ hypothesis and $S_m[k]H_k$ is the received PU signal in the m^{th} FFT output sample in subband k under $\mathcal{H}_1$ hypothesis. The channel frequency response is modeled through the subband gains H_k. The AWGN can be modeled as a zero-mean Gaussian random variable with variance $\sigma^2_{w,k}$, i.e., $W_m[k] \sim \mathcal{N}(0, \sigma^2_{w,k})$. The subband noise variances are assumed to be equal, such that $\sigma^2_{w,k} = \sigma^2_w / N_{FFT}$. Furthermore, $S_m[k] \sim \mathcal{N}(0, \sigma^2_k)$ with σ^2_k denoting the power at subband k under $\mathcal{H}_1$ hypothesis in the absence of the channel effect. The overall subband ED process can be summarized as $U_k = \frac{1}{L_t}\sum_{m=1}^{L_t} |Y_m[k]|^2$, where $L_t = N/N_{FFT}$. At this point, it is possible to make the following approximations with the aid of the CLT:

$$U_k = \begin{cases} \mathcal{N}\left(\sigma^2_{w,k}, \frac{2}{L_t}\sigma^4_{w,k}\right), & \mathcal{H}_0 \\ \mathcal{N}\left(|H_k|^2\sigma^2_k + \sigma^2_{w,k}, \frac{2}{L_t}\left(|H_k|^2\sigma^2_k + \sigma^2_{w,k}\right)^2\right). & \mathcal{H}_1 \end{cases} \tag{4.14}$$

Finding of Maximum and Minimum Subband Energies: In this stage, maximum and minimum energy values of subbands are determined as seen in Figure 4.2.

Threshold Calculation and Decision Device: The test statistic, which is obtained as the difference between the maximum and minimum energy values, is compared with a predetermined threshold that can be obtained from the target P_{FA} with the aid of Gumbel distribution. If $U_{max-min} = U_{max} - U_{min} > \gamma$, the signal is assumed to be present; otherwise only noise is assumed to be present in the band of interest. Detailed analysis of the threshold calculation will be given later in Section 4.5.1.

Differential Subband Energy based Scheme: The original subband energy based scheme from [25, 27] utilizes the following additional steps after obtaining the subband energies:

* *Ordering* : This step requires placing of the subband energies by the order of magnitude. This has no effect on the statistical properties of the ordered sequence, $\widehat{U}_k$, which follows the distribution in (4.14).

* *Differentiation* : The ordered subband energy sequence is differentiated such that $D_k = \widehat{U}_{k+1} - \widehat{U}_k$. This operation can be interpreted as a subtraction of two normally distributed random variables, as shown in (4.14), yielding

$$D_k \simeq \begin{cases} \mathcal{N}\left(0, \frac{4}{L_t}\sigma_{w,k}^4\right), & \mathcal{H}_0 \\ \mathcal{N}\left(E[\widehat{U}_k] - E[\widehat{U}_{k-1}], \frac{4}{L_t}\left(|H_k|^2\sigma_k^2 + \sigma_{w,k}^2\right)^2\right). & \mathcal{H}_1 \end{cases} \tag{4.15}$$

Under the $\mathcal{H}_0$, the above expression yields a normal distribution with zero mean and twice the corresponding variance in (4.14). It can be noted that when the spectrum of the PU is white, the mean value becomes zero and all subband energies follow zero-mean Gaussian distribution also under $\mathcal{H}_1$ and and the algorithm fails to sense the PU.

The threshold γ is calculated in the same way as in the simplified method. Finally, if $D_{max} - D_{min} > \gamma$, the signal is assumed to be present; otherwise only noise is assumed to be present.

4.5 Analytical Models for Max-Min ED based Sensing

Novel analytic expressions are formulated and derived for the Max-Min ED detector in this section. Our analytical results are much better matching with the simulation results compared to the previous studies in the literature [25,26].

4.5.1 Probability of False Alarm and Energy Threshold

It is recalled that the test statistics depend on the maximum and minimum values of U_k in (4.14). Furthermore, the Von Mises theorem can be used in order to characterize the statistics of both maximum and minimum distribution [22, 34, 65, 68]. Based on this, the extreme values of an arbitrary distribution can be efficiently represented by the Gumbel distribution, namely,

$$f_{\min}(x) = \frac{1}{\beta} e^{\frac{x-\alpha}{\beta}} e^{-e^{\frac{x-\alpha}{\beta}}} \tag{4.16}$$

and

$$f_{\max}(x) = \frac{1}{\beta} e^{-\frac{x-\alpha}{\beta}} e^{-e^{-\frac{x-\alpha}{\beta}}} \tag{4.17}$$

where α and β denote the location and scale parameters of the distribution. With the aid of (4.16) and (4.17), it is primarily essential to derive the expected value and standard deviation of the difference of maximum and minimum values. In what follows, we derive novel closed-form analytic expressions for these important measures which are subsequently used in deriving a comprehensive analytical framework for the proposed detector. It is firstly recalled that the n^{th} moment of a continuous distribution with probability density function $f(x)$ is defined as $E[x^n] = \int_{-\infty}^{\infty} x^n f(x) dx$ and the corresponding mean value is readily obtained for $n = 1$, i.e. $\mu = E[x]$. As a result, the mean value of (4.16) and

(4.17) is given by $E[U_{\min}] = \int_{-\infty}^{\infty} x f_{\min}(x)dx$ and $E[U_{\max}] = \int_{-\infty}^{\infty} x f_{\max}(x)dx$, respectively, which yields $\mu_{min} = E[U_{\min}] = -\alpha + \beta C$ and $\mu_{max} = E[U_{\max}] = \alpha - \beta C$, where $C = 0.577215665$ is the Euler's constant. Consequently, the expected value of the difference of the maximum and minimum values is expressed as,

$$\mu_{max-min} = E[U_{\max-\min}] = 2\alpha - 2\beta C, \tag{4.18}$$

and the location parameter can be determined by

$$\alpha = (E[U_{\max-\min}] + 2C\beta)/2. \tag{4.19}$$

Likewise, the corresponding variances are determined by

$$\sigma^2_{\min} = \mathrm{Var}[U_{\min}] = \frac{1}{\beta}\int_{-\infty}^{\infty} (x - E[U_{\min}])^2 \frac{e^{\frac{x-a}{\beta}}}{e^{e^{\frac{x-a}{\beta}}}} dx \tag{4.20}$$

and

$$\sigma^2_{\max} = \mathrm{Var}[U_{\max}] = \frac{1}{\beta}\int_{-\infty}^{\infty} (x - E[U_{\max}])^2 \frac{e^{-\frac{x-a}{\beta}}}{e^{e^{-\frac{x-a}{\beta}}}} dx \tag{4.21}$$

which, unlike the mean values, are equivalent to each-other, i.e.,

$$\mathrm{Var}[U_{\min}] = \mathrm{Var}[U_{\max}] = \frac{\pi^2\beta^2}{6}. \tag{4.22}$$

By recalling that $\mathrm{Var}(X \pm Y) \triangleq \mathrm{Var}(X) + \mathrm{Var}(Y)$, when X and Y are mutually independent, it immediately follows that $\mathrm{Var}[U_{\max} - U_{\min}] = \mathrm{Var}[U_{\max}] + \mathrm{Var}[U_{\min}]$, which yields

$$\sigma^2_{\max-\min} = 2\mathrm{Var}[U_{\max}] = \frac{\pi^2\beta^2}{3}, \tag{4.23}$$

and the scale parameter can be determined by

$$\beta = \sqrt{3\sigma^2_{U_{\max-\min}}}/\pi. \tag{4.24}$$

Using the already mentioned parameter representation of the Gumbel distribution with mean and variance values of U_k in (4.14) for the $\mathcal{H}_0$ hypothesis, one obtains

$$\begin{aligned} U_{\max-\min}|\mathcal{H}_0 &\sim \mathcal{Q}_{\mathcal{G}}\left(\alpha|_{\mathcal{H}_0}, \beta|_{\mathcal{H}_0}\right) \\ &\sim \mathcal{Q}_{\mathcal{G}}\left(\frac{\sigma^2_{w,k}}{2} + C\sqrt{\frac{6}{L_t}}\frac{\sigma^2_{w,k}}{\pi}, \sqrt{\frac{6}{L_t}}\frac{\sigma^2_{w,k}}{\pi}\right) \end{aligned} \tag{4.25}$$

where $\mathcal{Q}_{\mathcal{G}}(\alpha, \beta)$ denotes the Gumbel distribution. The standard Gumbel complementary distribution function is given by $\mathcal{G}\left(\frac{x-\alpha}{\beta}\right) = 1 - e^{-e^{-\frac{x-\alpha}{\beta}}}$ [34, 65].

In practical environment, noise uncertainty must be considered in the expressions of P_{FA} and P_D. It is recalled that the noise distribution can be summarized in the range by $\sigma^2_{w,k} \in [(1/\rho)\sigma^2_{n,k}, \rho\sigma^2_{n,k}]$, where ρ is the corresponding

noise uncertainty parameter. As a result, the worst-case false alarm probability is expressed as follows:

$$\begin{aligned} P_{FA} &= \max_{\sigma^2_{w,k}\in\left[\frac{1}{\rho}\sigma^2_{n,k},\rho\sigma^2_{n,k}\right]} \mathcal{G}\left(\frac{\gamma-\left(\frac{\sigma^2_{w,k}}{2}+C\sqrt{\frac{6}{L_t}}\frac{\sigma^2_{w,k}}{\pi}\right)}{\left(\frac{6}{L_t}\right)^{1/4}\frac{\sigma_{w,k}}{\sqrt{\pi}}}\right) \\ &= \mathcal{G}\left(\frac{\gamma-\left(\frac{\rho\sigma^2_{n,k}}{2}+C\sqrt{\frac{6}{L_t}}\frac{\rho\sigma^2_{n,k}}{\pi}\right)}{\left(\frac{6}{L_t}\right)^{1/4}\sqrt{\frac{\rho}{\pi}}\sigma_{n,k}}\right). \end{aligned} \tag{4.26}$$

Based on (4.26), the energy threshold can be determined by,

$$\gamma = \mathcal{G}^{-1}(P_{FA})\left(\frac{6}{L_t}\right)^{1/4}\sqrt{\frac{\rho}{\pi}}\sigma_{n,k}+\frac{\rho\sigma^2_{n,k}}{2}+C\sqrt{\frac{6}{L_t}}\frac{\rho\sigma^2_{n,k}}{\pi}. \tag{4.27}$$

4.5.2 Probability of Detection

Using the distribution parameters α and β with mean and variance values of U_k in (4.14) as in the case of P_{FA}, the $\mathcal{H}_1$ hypothesis can be expressed as:

$$\begin{aligned} U_{\max-\min}|\mathcal{H}_1 &\sim \mathcal{Q}_{\mathcal{G}}\left(\alpha|\mathcal{H}_1,\beta|\mathcal{H}_1\right) \\ &\sim \mathcal{Q}_{\mathcal{G}}\left(\frac{\kappa}{2}+C\sqrt{\frac{6}{L_t}}\frac{\kappa}{\pi},\sqrt{\frac{6}{L_t}}\frac{\kappa}{\pi}\right) \end{aligned} \tag{4.28}$$

where $\kappa = E_{\max}-E_{\min}+\sigma^2_{w,k}$, $E_{\max}=\max_k\left(|H_k|^2E_k\right)$, $E_{\min}=\min_k\left(|H_k|^2E_k\right)$, H_k is the PU channel gain in subband k, and E_k is PU signal energy in subband k. For analytical convenience/tractability and without loss of generality, the PU subband energies are assumed to be constant and independent of the transmitted symbol sequence. Then the worst case probability of detection with noise uncertainty can be expressed as:

$$\begin{aligned} P_D &= \min_{\sigma^2_{w,k}\in\left[\frac{1}{\rho}\sigma^2_{n,k},\rho\sigma^2_{n,k}\right]} \mathcal{G}\left(\frac{\gamma-\left(\frac{\kappa}{2}+C\sqrt{\frac{6}{L_t}}\frac{\kappa}{\pi}\right)}{\left(\frac{6}{L_t}\right)^{1/4}\sqrt{\frac{\kappa}{\pi}}}\right) \\ &= \mathcal{G}\left(\frac{\gamma-\left(\frac{\hat{\kappa}}{2}+C\sqrt{\frac{6}{L_t}}\frac{\hat{\kappa}}{\pi}\right)}{\left(\frac{6}{L_t}\right)^{1/4}\sqrt{\frac{\hat{\kappa}}{\pi}}}\right) \end{aligned} \tag{4.29}$$

where $\hat{\kappa} = E_{\max}-E_{\min}+\sigma^2_{n,k}/\rho$.

When the observed primary signal PSD is frequency dependent and the noise is additive white Gaussian, the proposed method can effectively remove the noise floor, resulting in the elimination of the noise uncertainty effects. Hence, under noise uncertainty the degradation of the detection performance is negligible in the proposed Max-Min ED compared to traditional ED. The performance of both traditional ED and simplified Max-Min ED is analyzed in Section 4.7.

To the best of our knowledge, equations (4.26), (4.27) and (4.29) have not been previously reported in the open technical literature. We have observed that this model provides clearly better match with the simulated sensing performance than the model presented in [25, 26]

Regarding the choice of the number of subbands in Max-Min ED, the following effects are essential:

- With fixed sample complexity and increasing number of subbands, the number of samples per subbands reduces. This increases the variance of the test statistic, thus degrading the sensing performance.
- With low number subbands, it may happen that (i) the subband reaching the maximum energy contains also frequency slots with relatively low PU PSD, and/or (ii) the minimum energy subband may partly overlap the PU transmission band.

Analytical characterization of this tradeoff remains as a topic for future studies.

4.6 Computational Complexity Evaluation

Computational complexity is a critical parameter in the spectrum sensing algorithms. Here computational complexity is defined as the number of real multiplications needed in the sensing process. The computational complexities of the proposed and the traditional spectrum sensing methods, shown in Table 4.2, are summarized now.

4.6.1 Complexity Analysis of EMaxE

Computational complexities of the traditional and the eigenvalue based spectrum sensing techniques are summarized for comparison as follows,

- Computational complexity of the calculation of the covariance matrix is MLN for both methods. The energy of the observation sequence is obtained as a by-product without additional computations.
- The main difference between the traditional and the modified eigenvalue based spectrum sensing methods is in the calculation of the eigenvalues. Complexity of maximum and minimum eigenvalues is $O(M^3L^3)$ on the traditional eigenvalue method, whereas the complexity of only maximum eigenvalue is $O(kML)$ on the eigenvalue method using the power iteration algorithm.
- The overall complexity can be decreased from $MLN+O(M^3L^3)$ to $MLN+O(kML)$ using the EMaxE algorithm compared to the traditional one.

4.6.2 Complexity Analysis of Max-Min ED

The major complexity of the proposed Max-Min ED scheme is due to the following elements:

- $N_{FFT}-$point FFT requires to $O(N_{FFT}\log(N_{FFT}))$ operations.
- $O(N_{FFT})$ complexity is required to find the required maximum and minimum energy values.

It is noted that the ordering and differentiation of N_{FFT} values require extra complexity of $O(N_{FFT})$ in the differential based approach.

4.7 Numerical Results

The performance of the traditional ED, the traditional Max/Min eigenvalue based detectors [P2] along with the modified EMaxE, Max-Min ED with differentiator, and the proposed simplified Max-Min ED are shown in this section. These methods are realized for three different signal cases, namely, non-oversampled, partially oversampled for observing the transition band during sensing, and 2x-oversampled. These scenarios are analyzed in the context of three different channel models: Indoor, ITU-R Vehicular A and SUI-1 frequency selective channels [79, 192]. The 1 dB noise uncertainty case is considered as the worst-case scenario in terms of noise variance estimation. Furthermore, the desired P_{FA} is chosen as $P_{FA} = 0.1$ in all addressed cases and the time record length is 10240 complex samples. 1000 Monte Carlo simulations are applied for reliable detection probability evaluation. Non-oversampled, partially oversampled (covering also the transition bands of the transmitted spectrum) and 2x-oversampled signal models are used under 20 MHz, 24 MHz and 40 MHz sensing bandwidths for quantifying the correlation effects in the eigenvalue based detector case, and the PSD variability in the Max-Min ED case. In the non-oversampled case, the correlations and PSD variability are introduced

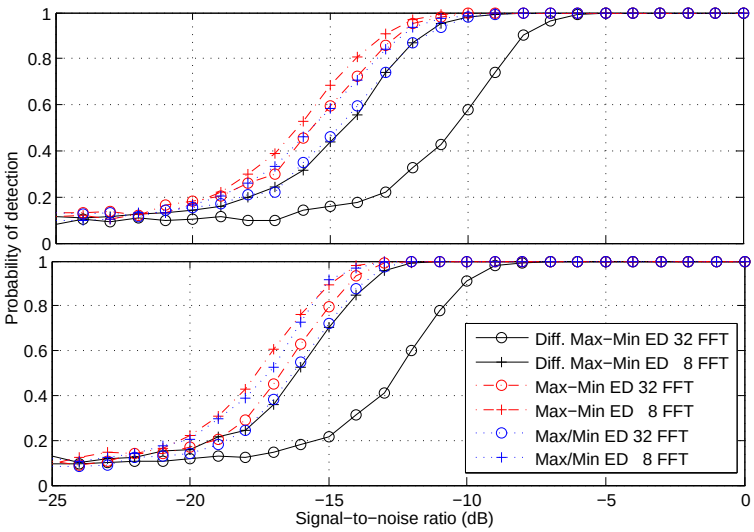

Figure 4.3: Simulated detection probabilities for differential Max-Min ED, Max-Min ED and Max/Min ED with $N = 10240$ under Indoor channel for QPSK signal.
a) Without oversampling (upper) b) 2x-oversampling (lower).

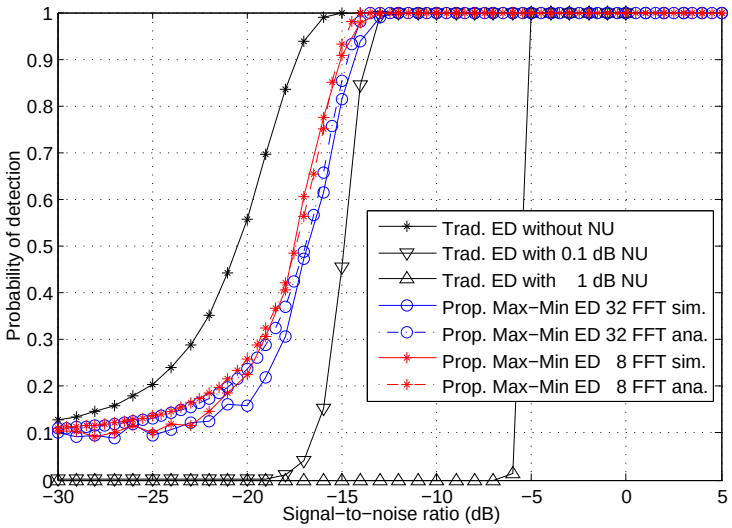

Figure 4.4: Analytical and simulated detection probabilities for traditional ED and Max-Min ED with 2x-oversampling $N = 10240$ under Indoor channel for QPSK signal.

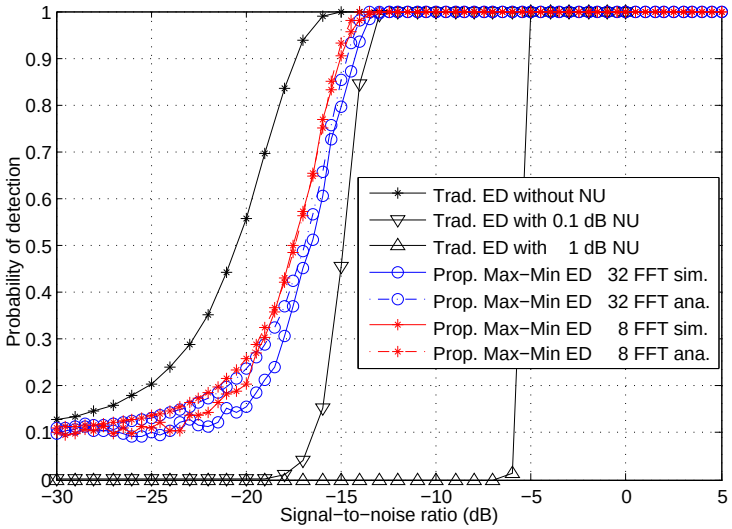

Figure 4.5: Analytical and simulated detection probabilities for traditional ED and Max-Min ED with 2x-oversampling N=10240 under Indoor channel for OFDM signal.

only by the multipath channel, whereas they are introduced both by the channel and the shape of the transmitted spectrum in the oversampling case. Single carrier waveform with quadrature phase shift keying (QPSK) with 22% roll off factor and OFDM signal with 64 subcarriers and QPSK subcarrier modulation are considered as PU signal models. Different FFT lengths have been tested for Max-Min ED and it was found that the two lengths of $N_{FFT} = \{8, 32\}$ illustrate well the performance-complexity trade-offs for this algorithm. For eigenvalue based approaches, the smoothing factor $L = 16$ was selected. Generally, while the performance would be slightly improved with higher smoothing factors, the complexity would grow quite significantly. In practice, also $L = 8$

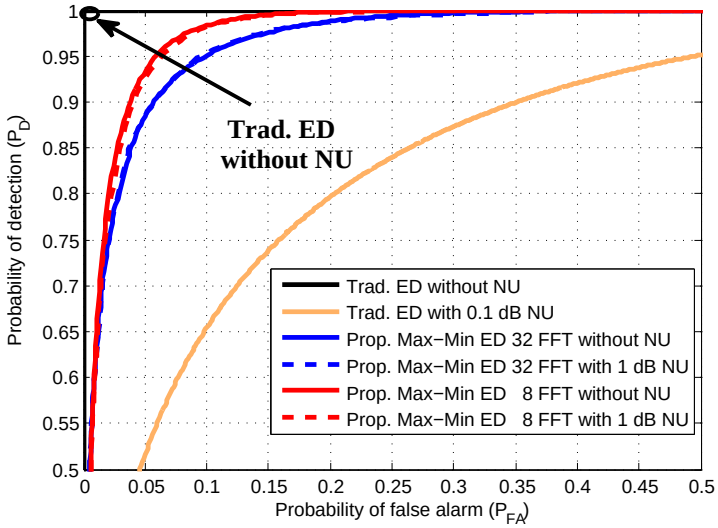

Figure 4.6: Receiver Operating Characteristics of traditional ED and Max-Min ED without oversampling under Indoor channel with QPSK signal, SNR=−12 dB, and $N = 10240$.

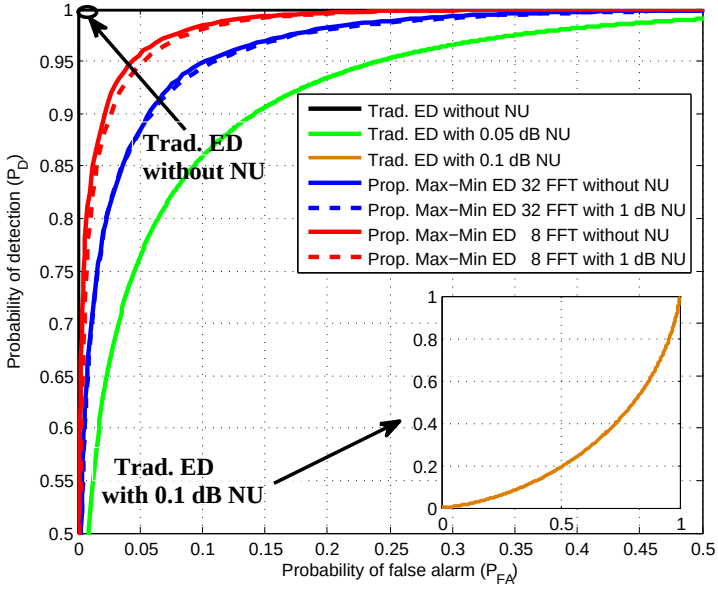

Figure 4.7: Receiver Operating Characteristics of traditional ED and Max-Min ED with 2x-oversampling under Indoor channel with OFDM signal, SNR=−14 dB, and $N = 10240$.

might provide interesting trade-off between complexity and performance. The choice of $L = 16$ means that the size of sample covariance matrix is 16×16 in the non-oversampled case whereas this size is 32×32 in the oversampled case [P2]. The optimum number of iterations k is chosen as 100 in the EMaxE method to obtain similar detection probability performance compared to the traditional eigenvalue based methods. Indoor channel model has 16 taps and

Table 4.1: Required SNR values for the detection probability of 90% and 99% with sample complexity of $N = 10240$ and $P_{FA} = 0.1$. QPSK PU signal and Indoor channel.

Required SNR values		N_{FFT}	***Non-oversampled***		***Partially oversampled***		***2x-oversampled***	
			$P_D = 0.9$	$P_D = 0.99$	$P_D = 0.9$	$P_D = 0.99$	$P_D = 0.9$	$P_D = 0.99$
Trad. Alg.	**Traditional ED ideal**	-	*-16 dB*	*-14 dB*	*-16 dB*	*-14 dB*	*-17 dB*	*-16 dB*
	Traditional ED with 0.1 dB NU		*-11.5 dB*	*-11 dB*	*-11.5 dB*	*-11 dB*	*-13 dB*	*-12.5 dB*
	Traditional ED with 1 dB NU	-	*-5 dB*	*-5 dB*	*-5 dB*	*-5 dB*	*-5 dB*	*-5 dB*
	Max/Min Eig. (*L=16*) (max. eig. / min eig.)	-	*-12 dB*	*-10 dB*	*-13 dB*	*-12 dB*	*-14.5 dB*	*-13.5 dB*
	EMaxE (*L=16*) Max eig. /average	-	*-11 dB*	*-9 dB*	*-12.5 dB*	*-10.5 dB*	*-14.5 dB*	*-13.5 dB*
Prop. Alg.	**Max-Min ED (max-min energy without diff.)**	***8***	*-13 dB*	*-11 dB*	*-14 dB*	*-12 dB*	*-15 dB*	*-13.5 dB*
		32	*-12.5 dB*	*-11 dB*	*-13 dB*	*-11.5 dB*	*-14 dB*	*-13 dB*

80 ns RMS delay spread whereas Vehicular A channel has 6 taps with about 2.5 μs maximum delay spread. SUI-1 channel model has 3 Ricean fading taps and 0.9 μs delay spread [79].

The simulated detection probabilities of differential Max-Min ED, Max-Min ED and Max/Min ED[1] based sensing methods which are applied for QPSK without oversampling and 2x-oversampling under $N_{FFT} = \{8, 32\}$ are shown

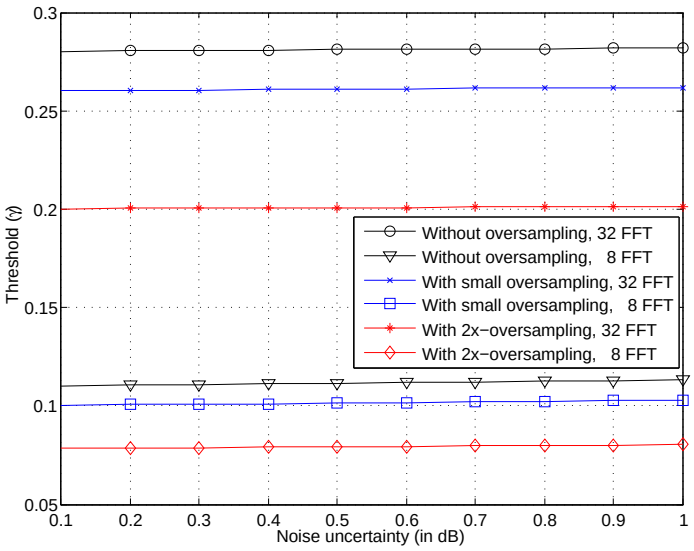

Figure 4.8: Variation of the threshold of the proposed Max-Min ED for different noise uncertainty values.

[1]This method uses the alternative test statistic as the ratio of the maximum and minimum subband energies instead of subband energy difference. This approach is difficult to treat analytically, and is considered only in this simulation study.

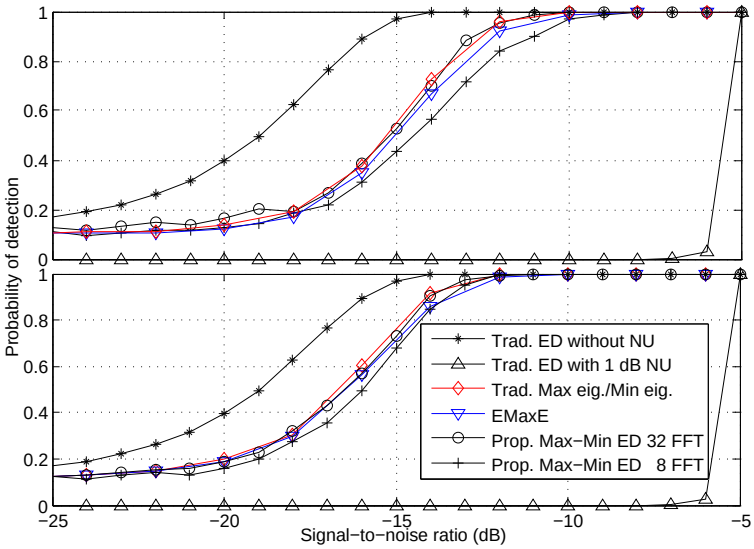

Figure 4.9: Detection probabilities using eigenvalue based an Max-Min energy based detectors without oversampling with $N = 10240$ under ITU-R Vehicular A channel. a) QPSK signal (upper) b) OFDM based signal (lower).

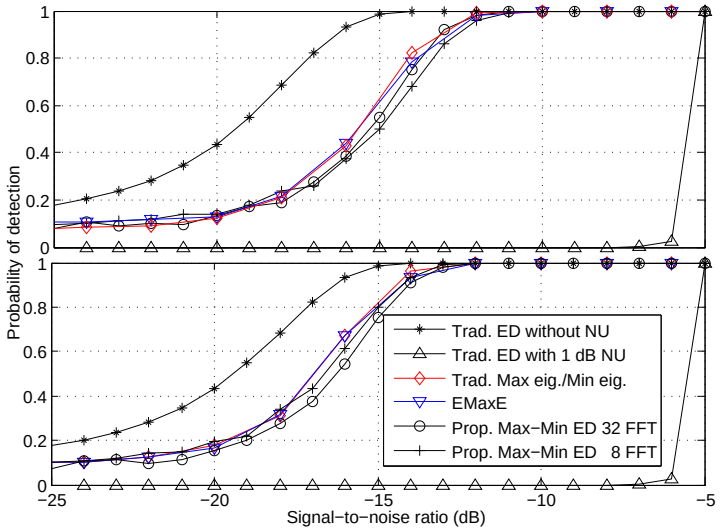

Figure 4.10: Detection probabilities using eigenvalue based an Max-Min energy based detectors with small oversampling (just passband and transition band) with $N = 10240$ under ITU-R Vehicular A channel. a) QPSK signal (upper) b) OFDM based signal (lower).

in Figure 4.3. In all the cases, the simplified Max-Min ED provides better sensing performance than both the differential Max-Min ED and Max/Min ED under Indoor channel.

The analytical and simulated detection probabilities of the sensing techniques are shown for QPSK and OFDM signals in Figure 4.4 and Figure 4.5, respectively. It can be seen from these figures that the simulation results match

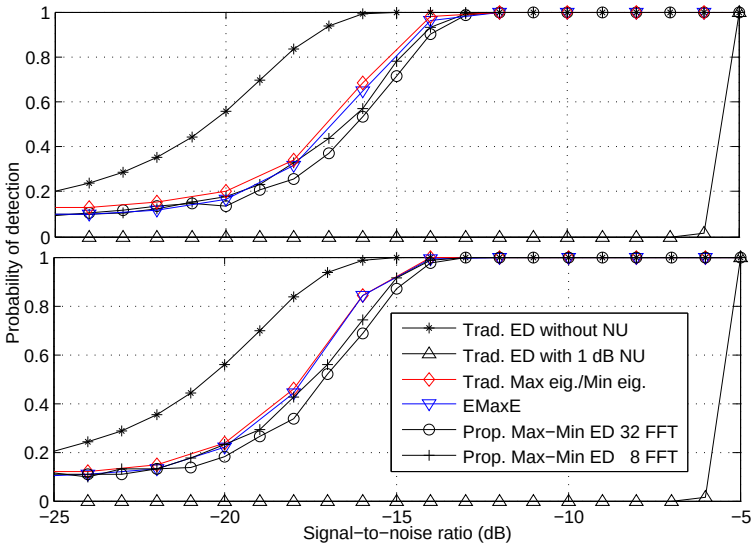

Figure 4.11: Detection probabilities using eigenvalue based an Max-Min energy based detectors with 2x-oversampling with $N = 10240$ under ITU-R Vehicular A channel. a) QPSK signal (upper) b) OFDM based signal (lower).

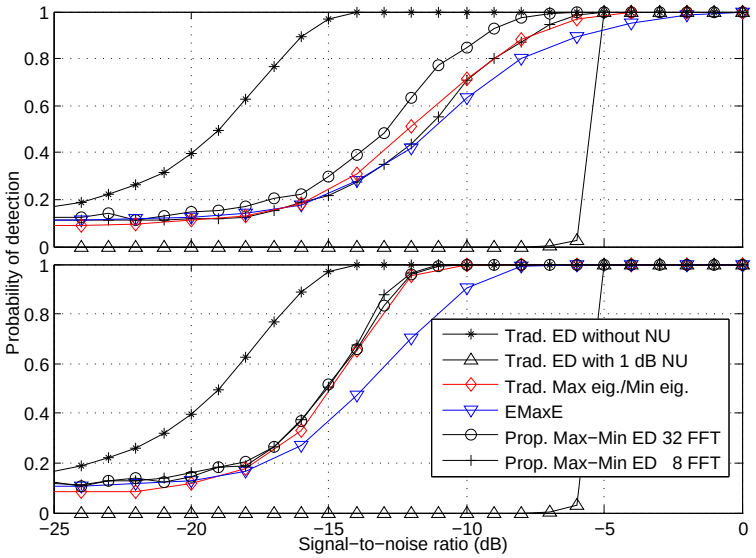

Figure 4.12: Detection probabilities using eigenvalue based an Max-Min energy based detectors without oversampling with $N = 10240$ under SUI-1 channel. a) QPSK signal (upper) b) OFDM based signal (lower).

well with the theoretical results. Two different noise uncertainty cases of 0.1 dB and 1 dB are considered in the traditional ED. Max-Min ED simulations were done with 1 dB noise uncertainty. In practice, when the PU power is fixed, noise uncertainty would have an effect on the SNR. However, in the following simulations it is assumed the PU SNR is fixed to the given value. The numerical results show that the Max-Min ED sensing techniques are able to overcome the noise uncertainty issues compared to the traditional ED based approach.

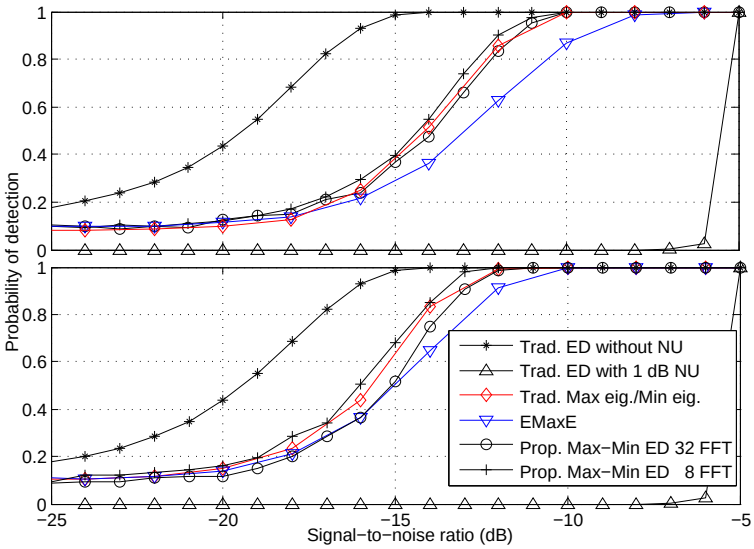

Figure 4.13: Detection probabilities using eigenvalue based an Max-Min energy based detectors with small oversampling (just passband and transition band) with $N = 10240$ under SUI-1 channel. a) QPSK signal (upper) b) OFDM based signal (lower).

Receiver Operating Characteristics curves for the proposed Max-Min ED and the traditional ED with/without noise uncertainty under -12 dB and -14 dB SNR values are shown in Figure 4.6 and Figure 4.7. These results reflect a fundamental tradeoff between P_{FA} and P_D. Small noise uncertainty, such as 0.1 dB effects the detection performance significantly in the traditional ED, whereas the proposed Max-Min ED based approach provides robust detection performance even under high noise uncertainty values, such as 1 dB.

Detailed comparison of the required SNR values of traditional and proposed spectrum sensing methods for the detection probability of 90% and 99% is given in Table 4.1. Proposed Max-Min ED and EMaxE algorithms provide significantly better performance under noise uncertainty than the traditional energy detector. While the detection performance of EMaxE almost reaches the performance of max/min eigenvalue detector (especially with oversampling), Max-Min ED slightly exceeds the performance of all eigenvalue based methods.

Figure 4.8 shows the variation of the threshold of the proposed Max-Min ED for non-oversampled, partially oversampled and 2x-oversampled cases under different noise uncertainty values between 0.1 dB and 1 dB. It is observed that the proposed Max-Min ED is robust to noise uncertainty challenges.

Figures 4.9−4.14 show the detection probabilities of the studied algorithms, with traditional eigenvalue based approach as a reference, under Vehicular A and SUI-1 channels for QPSK and OFDM signal models. While modified EMaxE performs adequately in all cases of oversampling under Vehicular and with 2x-oversampling case under SUI-1 channels, it is notable that EMaxE performs poorly in cases with no or small oversampling under SUI-1 channel. Furthermore, the detection performance of the Max-Min ED methods is rather similar to that of the Max/Min eigenvalue detector. It is also shown that 8 sub-

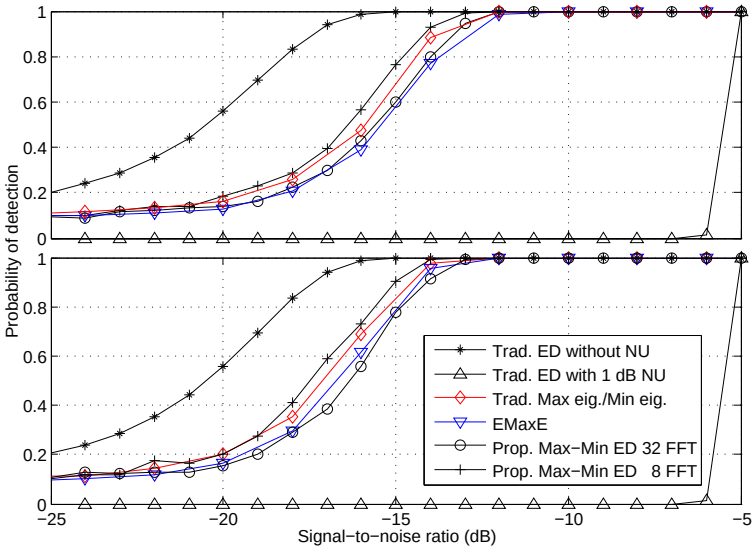

Figure 4.14: Detection probabilities using eigenvalue based an Max-Min energy based detectors with 2x-oversampling with $N = 10240$ under SUI-1 channel. a) QPSK signal (upper) b) OFDM based signal (lower).

channels (8-point FFT) is sufficient in all oversampled cases as well as in the non-oversampled ITU-R Vehicular A channel cases. It was additionally verified that employing 32 subbands constitutes an upper bound for the detection performance as increasing the number of subbands beyond that does not provide any performance improvements in any considered case.

The EMaxE based sensing technique is a rather promising alternative solution for the noise uncertainty challenge, requiring less computational complexity compared to the commonly used eigenvalue based sensing methods as seen in the figures. Small changes or uncertainty of noise variance have no effect on the sensing performance, because knowledge of the noise variance is not needed in the sensing process. The main drawback of this detector is its poor performance in cases with no or small oversampling and mildly frequency selective channel, like SUI-1. As an alternative solution, the proposed Max-Min ED using the order statistics exploits the frequency selectivity gain, which is naturally imposed over wireless channels during signal transmission. Furthermore, the proposed Max-Min ED method appears to provide similar performance as the best eigenvalue based methods and clearly better performance compared to traditional energy detector under noise uncertainty conditions.

Detailed comparison of the computational complexities of the Max/Min eigenvalue detector, modified EMaxE and the Max-Min ED variants is given in Table 4.2, Table 4.3 and Table 4.4. As Table 4.3 shows the computational complexity for the non-oversampled case, the corresponding complexity for the 2x-oversampled case is shown in Table 4.4. Depending on the values of L, M, N and N_{FFT}, significant reduction in the computational complexity is demonstrated. For instance, Table 4.4 indicates that when the number of samples is 10240 with $L = 16$ and $M = 2$, the overall computational complexity (number

of real multiplications) of the conventional max/min eigenvalue based algorithm is 360448, contrary to the 122880 and 81920 counterparts for the Max-Min ED with differentiation and without differentiation, respectively, for $N_{FFT} = 8$. Therefore, it is evident that using the Max-Min ED algorithm results in a complexity reduction by about 78%.

4.8 Chapter Summary

Proposed simplified Max-Min ED based spectrum sensing techniques were presented in this chapter. The proposed sensing methods are able to overcome the noise uncertainty problem in the case of channels with sufficient frequency selectivity. The performance of the Max-Min ED is shown to be comparable to the performance of the best eigenvalue based detectors. Additionally, the simplified Max-Min ED approach reaches or exceeds the performance of the differential Max-Min ED approach in all oversampled and non-oversampled cases with high frequency selectivity.

Even though the proposed simplified scheme is quite simple compared to the differential Max-Min ED approach, the computational complexities of these two methods are rather similar, and substantially smaller than the computational complexity of the eigenvalue based detector. Indicatively, the overall complexity can be decreased from $O((ML)^3) + MN(1 + L)$ to $O(N_{FFT} \log(N_{FFT})) + O(N_{FFT})$.

Table 4.2: Computational complexity of traditional and proposed energy and eigenvalue based spectrum sensing

ALGORITHMS		Eigenvalue Decomposition			Subband Energy Detection			*Total*
		Cov. matrix	max	min	DFT	Sort	Diff.	
Trad. Alg.	MaxMin Eig. (max. eig. / min. eig.)	MLN	$O(M^3L^3)$		-			$MLN + O(M^3L^3)$
	EMaxE (max. eig. / energy)	MLN	$O(kML)$	-				$MLN + O(kML)$
	Max-Min ED (max-min energy) with diff.	-	-	-	$O(N_{FFT}\log_2(N_{FFT}))$	$O(N_{FFT})$	$O(N_{FFT})$	$O(N_{FFT}\log(N_{FFT})) + 2O(N_{FFT})$
Prop Alg.	Max-Min ED (max-min energy) without diff.	-	-	-	$O(N_{FFT}\log_2(N_{FFT}))$	$O(N_{FFT})$	-	$O(N_{FFT}\log(N_{FFT})) + O(N_{FFT})$

Table 4.3: Some numerical values of computational complexities (number of real multiplications) for traditional and proposed sensing methods (Non-Oversampled)

ALGORITHMS		N_{FFT}	Number of samples (N)			
			512	*1024*	*4096*	*10240*
Trad. Alg.	MaxMin Eig. (max. eig. / min. eig.) L=16, M=1	-	12 288	20 480	69 632	167 936
	EMaxE (max eig. / average) L=16, M=1	-	9 792	17 984	67 136	165 440
	Max-Min ED (max-min energy) with differentiation	**8**	3 072	6 144	24 576	61 440
		16	3 584	7 168	28 672	71 680
		32	4 096	8 192	32 768	81 920
		64	4 608	9 216	36 864	92 160
Prop. Alg.	Max-Min ED (max-min energy) without differentiation	**8**	2 048	4 096	16 384	40 960
		16	2 560	5 120	20 480	51 200
		32	3 072	6 144	24 576	61 440
		64	3 584	7 168	28 672	71 680

Table 4.4: Some numerical values of computational complexities (number of real multiplications) for traditional and proposed sensing methods (2x-Oversampled)

ALGORITHMS		N_{FFT}	Number of samples (N)			
			512	*1024*	*4096*	*10240*
Trad. Alg.	MaxMin Eig. (max. eig. / min. eig.) L=16, M=2	-	49 152	65 536	163 840	360 448
	EMaxE (max eig. / average) L=16, M=2	-	19 656	35 968	134 272	330 880
	Max-Min ED (max-min energy) with differentiation	**8**	6 144	12 288	49 152	122 880
		16	7 168	14 336	57 344	143 360
		32	8 192	16 384	65 536	163 840
		64	9 216	18 432	73 728	184 320
Prop. Alg.	Max-Min ED (max-min energy) without differentiation	**8**	4 096	8 192	32 768	81 920
		16	5 120	10 240	40 960	102 400
		32	6 144	12 288	49 152	122 880
		64	7 168	14 336	57 344	143 360

CHAPTER 5

SPECTRUM SENSING AND RESOURCE ALLOCATION FOR MULTICARRIER COGNITIVE RADIO SYSTEMS

In this chapter, combined spectrum sensing and resource allocation approach for realistic multicarrier cognitive radio system under interference and power constraints is proposed [P3], [P4]. The main contributions of this chapter are summarized below.

- Various realistic multicarrier CR systems are considered in this study. Only CP-OFDM signal models have been considered as the PU and CR signal models for spectrum allocation algorithms in [7–9, 80, 96, 135, 150, 183, 200]. Likewise, FBMC has been considered for the CR only in [146, 147]. In our study, the 802.11g standard CP-OFDM, the E-OFDM [P4] and the 802.11g like FBMC [P3] with similar parameterization are considered as PU waveforms. Furthermore, most of the existing spectrum sensing studies ignore the impacts of RF imperfections, such as IQ-imbalance in the sensing receiver and PA nonlinearity of the PU transmitter. Energy detection and eigenvalue based spectrum sensing in both single-channel and multi-channel direct-conversion receiver scenarios impaired by IQ imbalance have also been analyzed in our previous studies [61–63]. In this study, a basic PA nonlinearity model, so-called Rapp PA model [137], is included in the PU signal model in order to obtain a realistic model for the PU spectrum. This aspect has not been considered earlier in the literature. This allows us to quantify the effects of the PU spectral characteristics on the SU capacity in more precise way then earlier. Furthermore, effects of frequency selectivity are also considered in terms of the performance of spectrum sensing and resource allocation

while the flat fading model has only been considered in the previous studies [7–9, 80, 96, 150, 183, 200].

- Combined spectrum sensing and resource allocation algorithms are considered for the CR transceiver. The sensing aspects have not been considered previously in the context of resource allocation and a constant number of available subbands has been assumed. Basically, a fixed predetermined width has been assumed for the spectrum hole so far. However, spectrum sensing plays a crucial and enabling role for the spectrum utilization process.

In this chapter, 802.11g standard CP-OFDM, E-OFDM and 802.11g like FBMC signal models are considered for PU and FBMC for CR in order to see the performance of the sensing and resource allocation during CR transmission.

5.1 Signal Models and Problem Definition

The PU and CR systems work in the same band of frequencies as seen in Figure 5.1. While PRTX and CRTX define the PU and CR transmitters, PRRX and CRRX are denoted as the PU and CR receivers, respectively. H_0, H_1, H_2 and H_3 are considered as frequency-selective channels between the PU and CR stations. It is assumed that the CR system is operating in a spectrum gap next to relatively strong on-going primary communications on either or both sides of the gap. Hence, interference is unavoidable between different PUs and CRs which are assumed to use the time-division multiplexing/duplexing (TDMA/TDD) principles. Detection of possible other transmissions or reappearing PUs within the spectrum gap is the main purpose of the spectrum sensing. One assumption is that the stations of the CR system have means to exchange control information with each other, e.g., using a cognitive control channel [155].

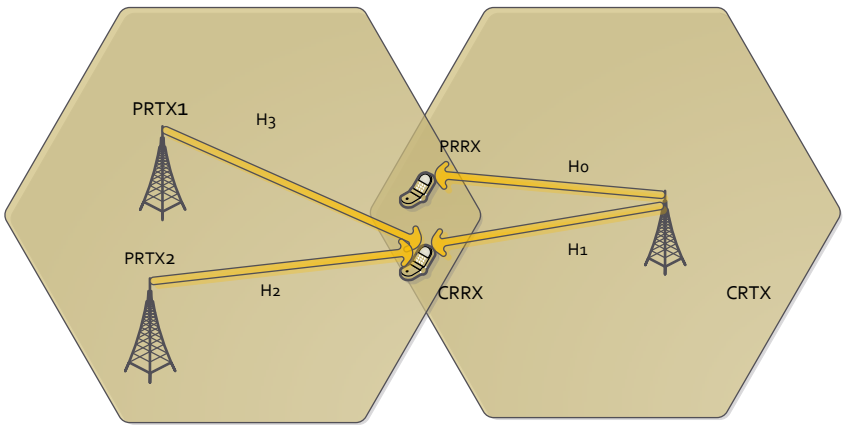

Figure 5.1: System model for spectrum sharing in CR.

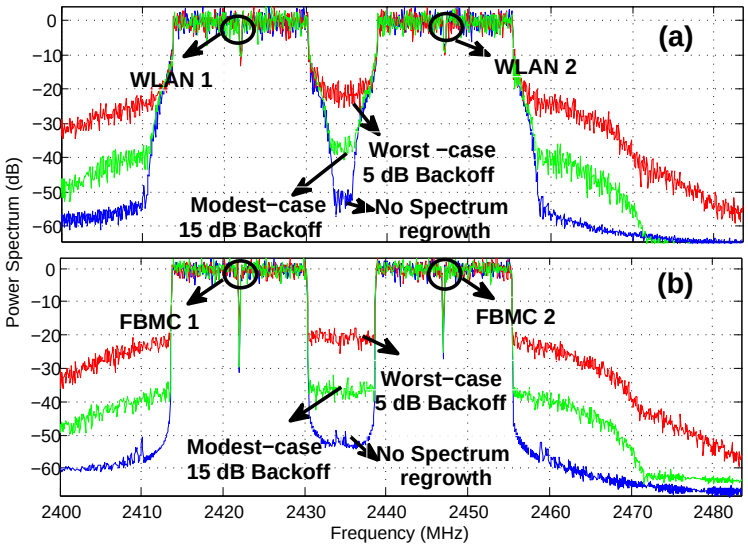

Figure 5.2: Effects of the Rapp Power Amplifier Model on (a) OFDM and (b) FBMC based primary users' spectra.

5.1.1 Signal Models for Primary Users

Two active primary radio systems which operate in the 2.4 GHz ISM band are considered in our scenario. 802.11g CP-OFDM based WLANs or 802.11g like FBMCs spectra both with the Rapp PA non-linearity model [137] are considered at 3rd and 8th channels, as illustrated in Figure 5.2. Between the active PU's there is a spectrum gap of 8 MHz nominal width.

The amplitude function at the PA output using the complex IQ baseband model is given as:

$$g_A = \frac{\kappa A}{\left(1 + [\kappa A / A_0]^{2p}\right)^{1/2p}} \tag{5.1}$$

where A is the input amplitude, κ is small signal gain, A_0 is the saturated amplitude and p is the amplitude smoothness factor. Figure 5.2 shows no regrowth (ideal case) and the Rapp PA non-linearity with two different back-off values of 15 dB (modest case) and 5 dB (worst case). Parameters of the Rapp model in [P3] are chosen according to the practical model for PU signals based on [48].

We have also considered a third alternative signal model for PUs, which is based on applying sidelobe suppression techniques for CP-OFDM. In particular, the combination of edge windowing [144, 145] and cancellation carrier scheme [16, 104, 105, 123, 188, 189] is applied to improve the spectrum localization of PU transmissions. With this approach, the cancellation carrier element targets to suppress the close spectrum sidelobes whereas edge windowing suppresses the far sidelobes. Detailed explanation of this enhanced OFDM (E-OFDM) scheme is given in [P4]. While the computational complexity of such E-OFDM schemes approaches or exceeds the complexity of FBMC, such approaches are interesting to consider due their high commonality/compatibility with existing CP-OFDM based systems.

5.1.2 Signal Model for Cognitive Radio

We consider a spectrally well-contained FBMC as the waveform for the CR systems, as well as an alternative waveform candidate for the future radio access techniques, which would be considered as PUs in the CR scenarios. In other words, the idea is to explore the possible gain in the efficiency of spectrum utilization, if also the PU waveforms were well-localized in spectrum. In FBMC, offset quadrature amplitude modulation (OQAM) needs to be used as subcarrier modulation to reach orthogonality [10, 77, 129]. The FBMC signal and system models are explained in more details in [P3].

In the system model of Figure 5.1, H_0 and H_1 are the channels from a CR transmitter to a PU receiver and a CR receiver, respectively. H_2 and H_3 are from two different PU transmitters to the CR receiver. H_1 is estimated by usual channel estimation procedure of the CR system whereas the knowledge of H_0 could be obtained through the channel reciprocity in time division duplexing (TDD) operation assumed for the PU system.

5.1.3 Definition of the Interference Problem

The CR and PU systems communicate in the same geographical location as seen in Figure 5.1, and cause interference to each other through spectrum leakage effects. The interference model is illustrated in Figure 5.3.

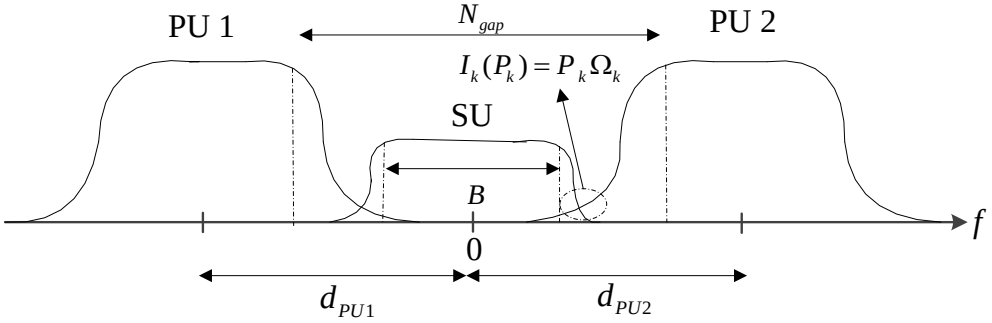

Figure 5.3: Interference model between primary and secondary users.

Even though FBMC based SU system is assumed in our specific studies, in our generic model, the secondary system operating in the spectrum hole may use any multicarrier transmission technique, with N_{gap} subcarriers and Δf as the subcarrier spacing. The effects of intercarrier interference (ICI) between subcarriers can be ignored due to the low mobility of the SU transmitter and the receiver. The interference from the CR to each of the primaries is required to be lower than the maximum tolerable interference by the primary, I_{th}. Fixing the origin of the frequency axis at the direct current subcarrier of the CR, the interference is given by:

$$I_k(P_k) = \int_{k\Delta f - B/2}^{k\Delta f + B/2} |H_0(f)|^2 P_k \Phi(f - k\Delta f)\Psi(f - d_{PU}) df = P_k \Omega_k. \quad (5.2)$$

Here, the spectral distance d_{PU} of a PU is defined as the frequency separation from the direct current subcarrier of the CR to the center frequency of the

PU. The interference to the primary transmission due to the k^{th} CR subcarrier depends on the CR subcarrier power P_k and d_{PU} [20]. $H_0(f)$ is the channel frequency response between the CR transmitter and a primary receiver. $\Phi(f)$ represents the subcarrier power spectral density of the underlying multicarrier technique employed by the CR. $\Psi(f)$ denotes the PU sensitivity mask characterizing the effects of the PU receiver filtering. B denotes the CR subcarrier bandwidth which is considered significant for the interference estimation. Finally, Ω_k represents the combined interference factor for the k^{th} CR subcarrier.

The other part of interference modeling is the interference from PU to SU. The signal-to-interference ratio (SINR) due to interference introduced by primary signal to the k^{th} subcarrier at the receiving CR is developed in similar manner in [P3].

5.2 Filter Bank Energy Detector Based Spectrum Sensing Algorithms

Subband based energy detector utilizing FFT or AFB for spectrum analysis is focused in this study. Figure 5.4 illustrates a block diagram of alternative FFT and AFB based spectrum sensing algorithms. The subband sampling rate is equal to the ADC sampling rate divided by the number of FFT/AFB frequency bins. As already discussed in Section 3.1, with subband-wise spectrum sensing method, the subband signals can be expressed as:

$$Y(m,k) = \left\{ \begin{array}{ll} W(m,k) & \mathcal{H}_0 \\ S(m,k)H_k + W(m,k) & \mathcal{H}_1 \end{array} \right\}, \tag{5.3}$$

where $S(m,k)$ is the transmitted OFDM, E-OFDM or FBMC based PU signal as seen in subband k during the m^{th} symbol interval, and assumed to have zero mean and variance $\sigma^2_{PU,k}$. Under hypothesis $\mathcal{H}_0$, the noise samples $W(m,k)$ are modeled as AWGN with zero-mean and variance σ^2_w, whereas under H_1, the signal can be modeled with zero-mean Gaussian distribution with variance $\sigma^2_{PU,k} + \sigma^2_w$.

The test statistics which can be obtained using time and frequency averaging [190] for more reliable detection performance can be obtained as follows,

$$\tilde{T}(m,k) = \frac{1}{L_t L_f} \sum_{l=k-\lfloor L_f/2 \rfloor}^{k+\lceil L_f/2 \rceil - 1} \sum_{u=m-L_t+1}^{m} \left| Y(u,l) \right|^2 \tag{5.4}$$

where L_f and L_t are the window lengths in frequency and time domains. The $\tilde{T}(m,k)$ is passed to a decision device to determine the possible occupancy of the corresponding frequency band at the corresponding time interval.

As $Y(m,k)$ has Gaussian distribution, the probability density function of $\tilde{T}(m,k)$ can be approximated as Gaussian distribution under both $\mathcal{H}_0$ and $\mathcal{H}_1$. With Gaussian approximation, the effects of the spectral leakage of PU transmitter are easily modeled on the actual false alarm probability $\tilde{P}_{FA}$ as:

$$\tilde{P}_{FA}(k) = Q\left(\frac{\lambda - (\sigma^2_w + I_{adj}(k))}{\sqrt{\frac{1}{L_t L_f}} (\sigma^2_w + I_{adj}(k))} \right). \tag{5.5}$$

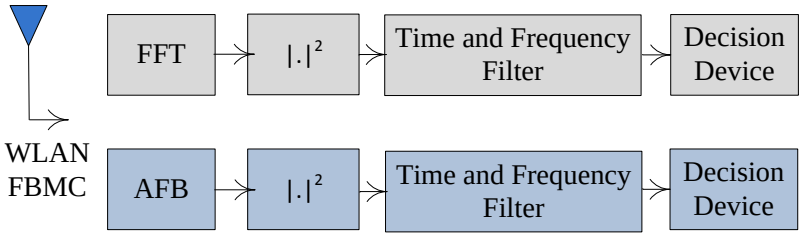

Figure 5.4: Block diagram of energy detector with AFB and FFT based spectrum analysis.

Here, the following expression:

$$I_{adj}(k) = \int_{f_1}^{f_2} |H_2(f)|^2 \psi_{PA}(f) df, \tag{5.6}$$

is the leakage power from the adjacent PU transmitter to the sensing frequency band between frequencies f_1 and f_2. $H_2(f)$ is the channel frequency response from a primary transmitter the CR receiver. Zero-mean circular Gaussian model is assumed for $I_{adj}(k)$. Then the threshold λ value can be obtain as follows,

$$\lambda = Q^{-1}\left(P_{FA}(k)\right) \sqrt{\frac{1}{L_t L_f}} (\sigma_w^2 + I_{adj}(k)) + (\sigma_w^2 + I_{adj}(k)). \tag{5.7}$$

The detection probability P_D can be expressed as follows,

$$P_D(k) = Q\left(\frac{\lambda - \left((\sigma_w^2 + I_{adj}(k)) + \sigma_{PU,k}^2\right)}{\sqrt{\frac{1}{L_t L_f}} \left((\sigma_w^2 + I_{adj}(k)) + \sigma_{PU,k}^2\right)} \right). \tag{5.8}$$

Due to the spectral leakage effects of PU and statistical nature of the spectrum sensing process, different number of empty subbands, N_{gap}, are detected under different SNR conditions, which is taken into consideration in resource allocation.

5.3 Resource Allocation

With the knowledge of non-active subbands in the spectral hole, which is obtained by the spectrum sensing part, resource allocation gains an important role for the overall efficiency of the CR transmission. The main functions of the resource allocation part are shown in Figure 5.5.

In the multicarrier case, the maximum rate at which transmission can take place is given by the Shannon capacity,

$$R_{\mathrm{CR}} = \sum_{k=1}^{N_{\mathrm{gap}}} \Delta f \cdot \log_2 \left(1 + \frac{P_k}{\sigma_k^2}\right). \tag{5.9}$$

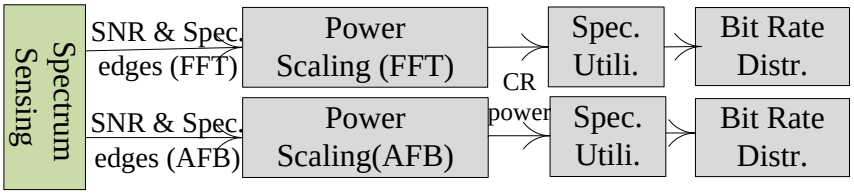

Figure 5.5: Block diagram of spectrum utilization with alternative AFB and FFT based spectrum analysis schemes.

Here, $\sigma_k^2 = \sigma_w^2 + \sum_{i=1}^{N_{PU}} J_{k,i}$ and $J_{k,i}$ is the effective interference power contributed by i^{th} primary to the k^{th} CR subcarrier. N_{PU} is the number of PUs contributing to the interference at the receiving CR station. In our case study, $N_{PU} = 2$, i.e., there is one adjacent PU to the lower and upper edges of the white space. In practice, the model could be simplified by assuming that these PUs affect only the lower and upper half of the subcarriers, respectively. P_k is the transmit power used by the CR for subcarrier k. It is assumed that the channel changes slowly so that the channel gains, and consequently $J_{k,i}$, will be approximately the same during each transmission frame. There is no ICI in the CR reception, due to low mobility, as mentioned before.

The main objective is to maximize the capacity as given in (5.9). Detailed derivation of the optimization problem is shown in [P3] and the final equations can be expressed as follows:

$$R_{\mathrm{CR}} = \max_{\{P_k\}} \sum_{k=1}^{N_{\mathrm{gap}}} \Delta f \log_2 \left(1 + \frac{P_k}{\sigma_k^2}\right), \tag{5.10}$$

subject to $\sum_{k=1}^{N_{\mathrm{gap}}} P_k \leq P_T$, $\sum_{k=1}^{N_{\mathrm{gap}}} P_k \Omega_k \leq I_{th}$ and $P_k \geq 0, \forall k \in \{1, 2, ..., N_{\mathrm{gap}}\}$. This is a convex optimization problem and the Lagrangian can be written as:

$$G_{snr} = \sum_{k=1}^{N_{gap}} \Delta f \log_2 \left(1 + \tfrac{P_k}{\sigma_k^2}\right) - \lambda_0 \sum_{k=1}^{N_{gap}} (P_k - P_T) - \lambda_1 (P_k \Omega_k - I_{th}) + \lambda_2 \sum_{k=1}^{N_{gap}} P_k. \tag{5.11}$$

With the Karush-Kuhn-Tucker (KKT) conditions, which are derived in details in [P3], the optimum solution can be written as:

$$P_k = \left[\frac{1}{\lambda_0 \Omega_k + \lambda_1} - \frac{\sigma_k^2}{|h_k|}\right]^+, \tag{5.12}$$

where $[y]^+ = \max(0, y)$. A lower complexity algorithm called the power interference (PI) divides the problem into stages [147]. Here, the PI algorithm is applied to find optimal solution with lower computational complexity. In the development of this algorithm, the interference constraint is first ignored keeping only the total power constraint, and this leads to the classical water filling

solution:

$$P_k = \left[\gamma - \frac{\sigma_k^2}{|h_k|}\right]^+, \tag{5.13}$$

where γ is the water filling level. When the total power is ignored the solution [147] becomes:

$$P_k = \left[\frac{1}{\lambda_0 \Omega_k} - \frac{\sigma_k^2}{|h_k|}\right]^+. \tag{5.14}$$

The value of $\lambda^{'}{}_0$ can be obtained by substituting (5.14) into the constraint $\sum_{k=1}^{N_{gap}} P_k{}^{'} \Omega_k = I_{th}$ to get:

$$\lambda_0 = \frac{|N_{gap,l}|}{I_{th}^{N_{gap}} + (\sum_i \Omega_k \sigma_k^2 / |h_k|^2)}. \tag{5.15}$$

Only when the total power is greater or equal to the power under the interference constraint, the above solution can be optimal. In practice, this condition is not true and this is the motivation for the PI algorithm which has four stages as maximum power determination, power constraint, power budget distribution and power level re-adjustment [147].

5.4 Numerical Results

In our test scenario, we assume that the spectrum sensing function of CR has determined a potential spectral hole between two relatively strong PUs, as seen in Figure 5.2. It is assumed that there is no additional signal in the spectral hole, but the spectrum sensing gives false alarms due to the spectral leakage of PA nonlinearity on PU. This effect is dependent upon the SNR values of the PUs. We use a smaller subband spacing of 81.5 kHz for the spectrum sensing and the CR transmissions, instead of the 325 kHz subcarrier spacing of WLAN, in order to reduce the effects of frequency selective channels. The required sample complexity is around 250 samples while targeting at -5 dB SNR with false alarm probability of 0.1 and detection probability of 90% in the sensing. The time and frequency averaging lengths are chosen as 50 and 5, respectively.

The actual false alarm probabilities in the spectral gap are shown as a function of the PU SNR for different levels of spectral regrowth in Figure 5.6. We consider the combinations of two PU waveforms, OFDM and FBMC based WLANs, as well as two spectrum sensing techniques, based on FFT or AFB. The CR waveform is always considered as FBMC.

Similarly, Figure 5.7 shows the false alarm probabilities for E-OFDM based PU. Similar performance can be seen with FBMC based PU. As expected, spectrally well-contained PU waveforms would make the CR system operation more effective.

A number of subbands, which is determined with FFT or AFB based spectrum sensing, are left empty in the spectrum utilization phase. The power of these occupied subchannels is reallocated to the other subbands that can be

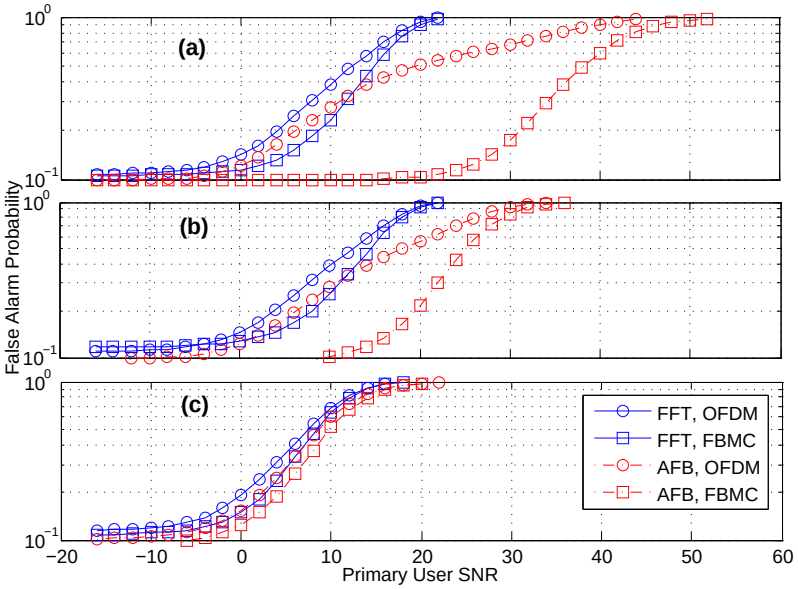

Figure 5.6: Actual P_{FA} for OFDM and FBMC primaries with target $P_{FA} = 0.1$, time record length of 50 and sensing bandwidth of 5 subbands under frequency selectivity for (a) ideal model, (b) Rapp PA with 15 dB backoff as modest case, (c) Rapp PA with 5 dB backoff as worst case.

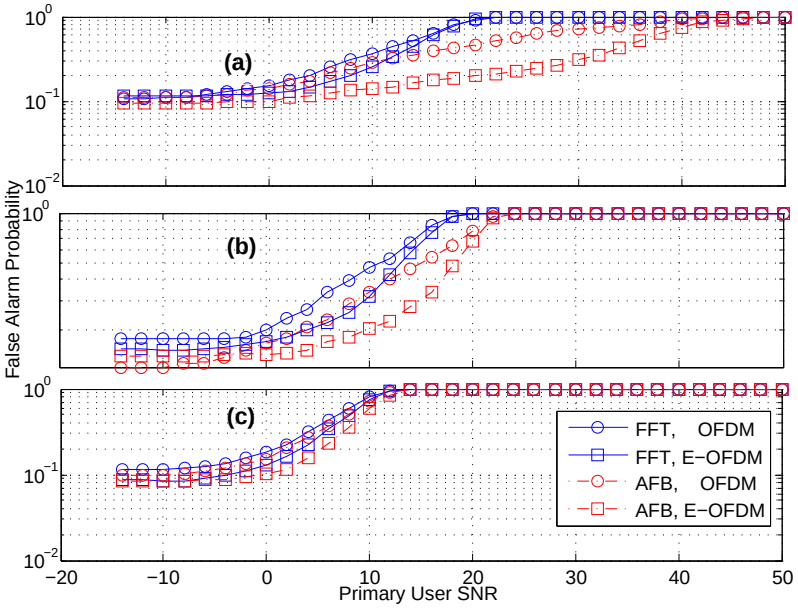

Figure 5.7: Actual P_{FA} for OFDM and E-OFDM primaries with target $P_{FA} = 0.1$, time record length of 50 and sensing bandwidth of 5 subbands under frequency selectivity for (a) ideal model, (b) Rapp PA with 15 dB backoff as modest case, (c) Rapp PA with 5 dB backoff as worst case.

used by the CR. The power allocation is done by utilizing the PI algorithm, and the resulting capacity, in terms of bits/s/Hz, is shown in Figure 5.8 for

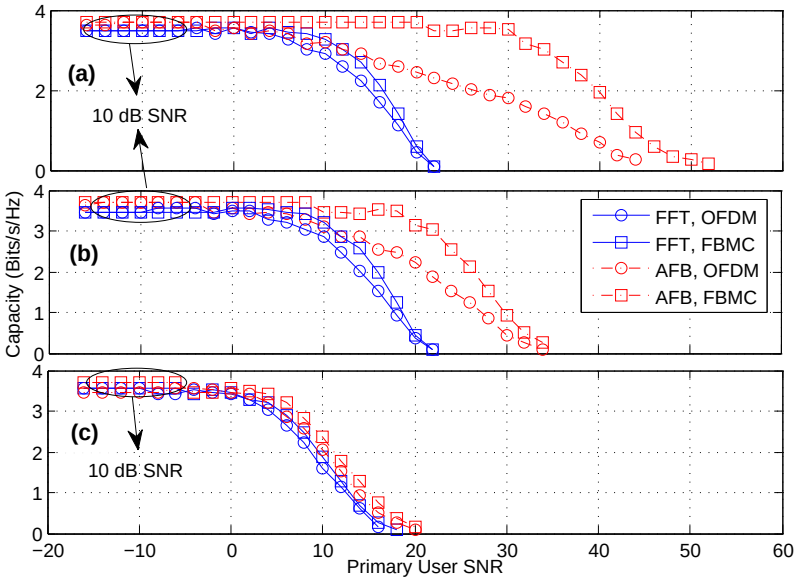

Figure 5.8: Capacity of a CR in a spectral gap between two OFDM or FBMC type PUs versus PU SNR when using PI algorithm for power allocation. The SNR of the CR is 10 dB. (a) Ideal model, (b) Rapp PA with 15 dB backoff as the modest case, (c) Rapp PA with 5 dB backoff as the worst case.

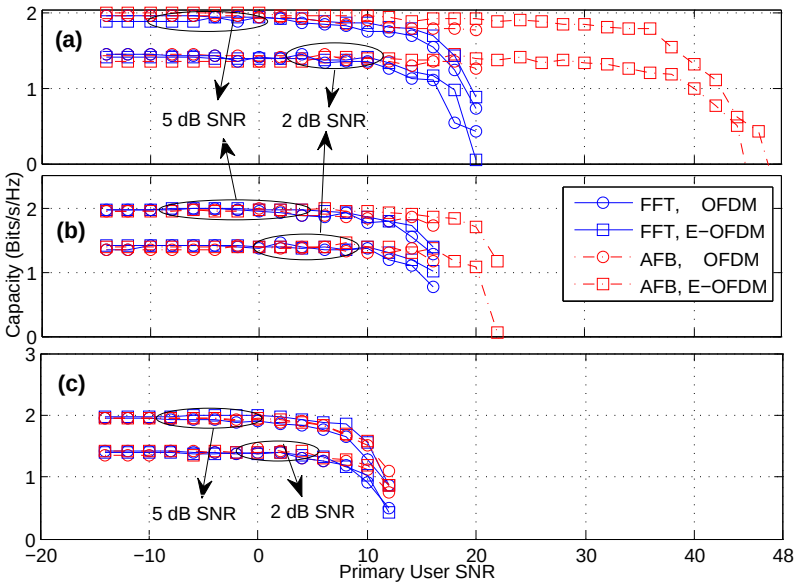

Figure 5.9: Capacity of a CR in a spectral gap between two OFDM or E-OFDM type PUs versus PU SNR when using water-filling algorithm for power allocation. The SNR of the CR is 2 dB or 5 dB. (a) Ideal model, (b) Rapp PA with 15 dB backoff as the modest case, (c) Rapp PA with 5 dB backoff as the worst case.

OFDM and FBMC primaries. The interference threshold is chosen to be 6 dB below the thermal noise level to get rid of significant performance loss in

case the primary receiver is operating close to the sensitivity level. Detailed information related to interference threshold value is given in [P3].

Similarly, the achievable data using water-filling algorithm in the spectral hole between two OFDM or E-OFDM type primary channels is shown in Figure 5.9. Detailed information related to parameters of water-filling algorithm is given in [P4].

Regarding the transmission waveform, FBMC and E-OFDM have clear benefit due to better spectral containment, if the effects of power amplifier nonlinearities can be kept at a modest level.

5.5 Chapter Summary

Combined spectrum sensing and utilization method with realistic signal model under frequency selective channel conditions was analyzed in this chapter. The FFT and AFB based sensing methods were evaluated for determining a spectral hole with OFDM, E-OFDM and FBMC based PU signal models. Then, water-filling or PI resource allocation methods were applied with available number of empty subbands, which were obtained from the spectrum sensing part.

In terms of the sensing performance, FFT and AFB based sensing performance depends greatly on the level of spectral regrowth due to the PA nonlinearity of PU. AFB has clear benefits due to much better spectral containment of the subbands. One important benefit of E-OFDM and FBMC as transmission techniques in CR systems is that these can utilize the narrow spectral gaps in an effective and flexible way, even in the presence of strong primaries at the adjacent spectral slots.

With water-filling and PI algorithms, the utilization of the sensed spectrum can be optimized. Water-filling algorithm is the simplest one and the PI algorithm improves the capacity of the CR system as compared to the simple water filling based spectrum allocation. According to the results of this study, the PI algorithm can be directly utilized with the developed highly enhanced and realistic CR system model. Due to the above features, E-OFDM and FBMC based CR systems achieve higher capacity in comparison to the traditional OFDM based systems.

CHAPTER 6

SUMMARY

In this thesis, we have dealt with enhanced spectrum sensing techniques to overcome low SNR and noise uncertainty challenges with low computational complexity. The study does not limit itself to any specific receiver architecture or communication waveform. The algorithms were applied to both single- and multi-carrier type of signals. On the waveform side, the main focus was on wideband multicarrier type OFDM, E-OFDM and FBMC signal models but also single-carrier waveforms were included in the study. There are various contributions in the studied areas which were presented in detail in [P1]-[P4] and shortly summarized below.

Chapter 3 summarized the studies of [P1] on novel, analytic techniques for various energy detection scenarios, that have not been sufficiently covered in the open literature. We investigated the effects of misaligned time frequency window on the test statistics. We proposed sliding window processing as a technique to find the best match in cases where the frequency range or burst timing of the PU signal is unknown to the sensing receiver. Additionally, the problem of known, non-flat PU spectrum was studied, considering Bluetooth as an example case. An expression of the optimum subband weights was derived for subband based sensing. An analytical model was developed for quantifying the effect of channel frequency selectivity on the sensing performance. The effect was found to be highly dependent upon the corresponding SNR level, and to have minor significance in low SNR scenarios. The AUC was employed as a single-valued performance metric for evaluating the different spectrum sensing algorithms in the different communications scenarios.

Chapter 4 reported our studies on spectrum sensing methods [P2], [41] which utilize the correlations of the received PU signal, or equivalently its non-flat power spectrum, which effects are due to the non-flat transmitted spectrum and/or the frequency selective channel. We presented the simplified Max-Min ED scheme, which is achieved by the replacement of the calculation process of covariance matrix and its eigenvalues by blockwise FFT processing. This scheme is conceptually quite simple compared to eigenvalue based approaches,

but was found to perform equally well. These sensing methods do not rely on knowledge of the noise power and, consequently, they are able to overcome the noise uncertainty problem under sufficient frequency selectivity of the PU signal.

Chapter 5 summarized the studies of [P3] and [P4] on combined spectrum sensing and resource allocation for FBMC or E-OFDM based CR with realistic signal models under frequency selective fading channel conditions. The performance of energy detection was analyzed using FFT and AFB based spectrum analysis methods with both OFDM and FBMC signal models for the PUs. Then, the utilization of dynamically identified spectral holes with spectrum allocation algorithms was investigated. This study highlighted the interdependence of spectrum sensing and resource allocation parts of CRs.

All the spectrum sensing techniques introduced in this thesis are applicable almost any type of realistic PU signal models, such as single carrier or multicarrier waveforms. On the other hand, our focus in this thesis is purely on single-antenna sensing due to less complex hardware implementation, but the results can be easily applied to multi-antenna sensing as well. They can also be extended to cooperative sensing scheme, which is an efficient method to ensure sensing robustness in realistic wireless communication environments.

Overall, the thesis contributes in various different areas of emerging radio communications disciplines which enables better understanding and handling of the spectrum sensing techniques in CR systems. These contributions are expected to provide a useful tools for the design and implementation of flexible, reconfigurable, power/size/cost efficient, and multi-standard capable modern CR transceivers.

APPENDIX A

APPENDIX: ANALYTICAL MODEL FOR MAXIMUM EIGENVALUE OVER ENERGY BASED DETECTOR

A.1 Probability of False Alarm and Threshold

The false alarm probability (P_{FA}) of the EMaxE detection can expressed as,

$$P_{FA} = P(\lambda_{\max} > \gamma T_y) = P\left(\frac{\sigma_w^2}{N}\lambda_{\max}(\tilde{\mathbf{R}}_{ww}) > \gamma T_y\right) \tag{A.1}$$

where $\tilde{\mathbf{R}}_{ww} = N\mathbf{R}_{ww}/\sigma_w^2$. Based on this, it immediately follows that,

$$\begin{aligned} P_{FA} &= P\left(\lambda_{\max}(\tilde{\mathbf{R}}_{ww}) > \gamma T_y \frac{N}{\sigma_w^2}\right) \\ &= P\left(\frac{\lambda_{\max}(\tilde{\mathbf{R}}_{ww}) - \mu}{\nu} > \frac{\gamma T_y N/\sigma_w^2 - \mu}{\nu}\right). \end{aligned} \tag{A.2}$$

With the aid of the Wishart random matrix theorem [162–164] one obtains,

$$\mu = \left(\sqrt{N-1} + \sqrt{M\,L}\right)^2 \tag{A.3}$$

and

$$\nu = \left(\sqrt{N-1} + \sqrt{M\,L}\right)\left(\frac{1}{\sqrt{N-1}} + \frac{1}{\sqrt{M\,L}}\right)^{1/3}. \tag{A.4}$$

Based on this, the corresponding P_{FA} is given as,

$$P_{FA} = 1 - F_1\left(\frac{\gamma T_y N/\sigma_w^2 - \mu}{\nu}\right) = 1 - F_1\left(\begin{array}{l}\left(\frac{\sqrt{ML}+\sqrt{N}}{\sqrt{MLN}}\right)^{-\frac{1}{3}} \times ... \\ \left[\frac{\gamma N}{\sqrt{N}+\sqrt{ML}} - \left(\sqrt{N}+\sqrt{ML}\right)\right]\end{array}\right) \tag{A.5}$$

where $F_1(\cdot)$ denotes the CDF of the Tracy-Widom distribution of order one [163]. It is recalled that the Tracy-Widom distribution has been used in numerous studies in wireless communications, and generally in natural sciences and engineering, [117, 130, 131, 176, 195] and is defined as,

$$F_1(t) = \exp\left(-\frac{1}{2}\int_t^\infty (q(u) + (u-t)q^2(u))du\right) \tag{A.6}$$

where $q(u)$ is the solution of the nonlinear Painleve II differential equation $q''(u) = uq(u) + 2q^3(u)$. It is noted that the proposed algorithm is very robust against noise uncertainty because it is not dependant upon knowledge of the noise variance. Based on this and using (A.5), the energy threshold is given by

$$\begin{aligned}\gamma &= \frac{{F_1}^{-1}(1-P_{FA})\nu\sigma_w^2 + \mu\sigma_w^2}{T(N)N} \\ &= 1 + \frac{(\sqrt{ML}+\sqrt{N})^{\frac{4}{3}}}{N^{\frac{7}{6}}(ML)^{\frac{1}{6}}}F_1^{-1}(1-P_{FA}) + 2\sqrt{\frac{ML}{N}} + \frac{ML}{N}\end{aligned} \tag{A.7}$$

which is seen to be a function of ML, N and P_{FA}.

A.2 Probability of Detection

When a signal is present, the sample covariance matrix $\mathbf{R}_{yy}$ is no longer a Wishart matrix [162–164]. As a consequence, the distributions of the eigenvalues of the sample covariance matrix become unknown and thus, it becomes analytically intractable to derive an exact closed-form expression for the corresponding P_D. As an effective alternative, we employ a tight empirical model that allows the derivation of a particularly accurate analytic expression for the P_D for the proposed algorithm. To this end, it is recalled that $\mathbf{R}_{ww}$ is accurately approximated by $\sigma_w^2 \mathrm{I}_{ML}$, yielding,

$$\lambda_{\max}(\mathbf{R}_{yy}) \approx \rho_1 + \lambda_{\max}(\mathbf{R}_{ww}). \tag{A.8}$$

Hence, the corresponding average energy can be expressed as,

$$T_y = \frac{\mathrm{Tr}(\mathbf{R}_{yy})}{ML} \approx \frac{\mathrm{Tr}(\mathbf{R}_{xx})}{ML} + \frac{\mathrm{Tr}(\mathbf{R}_{ww})}{ML}. \tag{A.9}$$

Based on (A.9), it follows that the P_D of the proposed algorithm is given as,

$$P_D = P(\lambda_{\max} > \gamma T_y) = P(\rho_1 + \lambda_{\max}(R_{ww}) > \gamma T_y) \tag{A.10}$$

which can be re-written as,

$$P_D = P\left(\frac{\lambda_{\max}(\tilde{\mathbf{R}}_{ww})\sigma_w^2}{N} > (\gamma T_y - \rho_1)\right). \tag{A.11}$$

After some algebraic manipulations, following closed-form expressions can be written as

$$P_D = P\left(\frac{\lambda_{\max}(\tilde{\mathbf{R}}_{ww}) - \mu}{\nu} > \frac{\left(\gamma\left(\frac{\mathrm{Tr}(\mathbf{R}_{xx}(\mathrm{N}))}{ML} + \frac{\mathrm{Tr}(\mathbf{R}_{ww}(\mathrm{N}))}{ML}\right) - \rho_1\right)\frac{N}{\sigma_w^2} - \mu}{\nu}\right) \tag{A.12}$$

and

$$P_D = 1 - F_1\left(\frac{N\gamma\frac{\mathrm{Tr}(\mathbf{R}_{xx})+\mathrm{Tr}(\mathbf{R}_{ww})}{\sigma_w^2 ML} - \frac{N\rho_1}{\sigma_w^2} - \mu}{\nu}\right). \tag{A.13}$$

APPENDIX: ANALYTICAL MODEL FOR MAXIMUM EIGENVALUE OVER ENERGY BASED DETECTOR

BIBLIOGRAPHY

[1] I. F. Akyildiz, W.-Y. Lee, M. C. Vuran, and S. Mohanty, "NeXt Generation/Dynamic spectrum Access/Cognitive radio wireless networks: A survey," *Comput. Netw.*, vol. 50, no. 13, pp. 2127–2159, Sep. 2006. [Online]. Available: http://dx.doi.org/10.1016/j.comnet.2006.05.001

[2] D. Ariananda, M. Lakshmanan, and H. Nikookar, "A survey on spectrum sensing techniques for cognitive radio," in *Second International Workshop on Cognitive Radio and Advanced Spectrum Management, 2009. CogART 2009*, May 2009, pp. 74–79.

[3] S. Atapattu, C. Tellambura, and H. Jiang, "Energy detection based cooperative spectrum sensing in cognitive radio networks," *IEEE Transactions on Wireless Communications*, vol. 10, no. 4, pp. 1232–1241, Apr. 2011.

[4] ——, "MGF based analysis of area under the ROC curve in energy detection," *IEEE Communications Letters*, vol. 15, no. 12, pp. 1301–1303, Dec. 2011.

[5] R. Bacchus, A. Fertner, C. Hood, and D. Roberson, "Long-term, wideband spectral monitoring in support of dynamic spectrum access networks at the IIT spectrum observatory," in *3rd IEEE Symposium on New Frontiers in Dynamic Spectrum Access Networks, 2008. DySPAN 2008*, Oct. 2008, pp. 1–10.

[6] A. Bagwari, G. Tomar, and S. Verma, "Cooperative spectrum sensing based on two-stage detectors with multiple energy detectors and adaptive double threshold in cognitive radio networks," *Canadian Journal of Electrical and Computer Engineering*, vol. 36, no. 4, 2013.

[7] G. Bansal, J. Hossain, and V. Bhargava, "Optimal and suboptimal power allocation schemes for OFDM-based cognitive radio systems," *IEEE Transactions on Wireless Communications*, vol. 7, no. 11, pp. 4710–4718, Nov. 2008.

[8] G. Bansal, M. Hossain, and V. Bhargava, "Adaptive power loading for OFDM-Based cognitive radio systems," in *IEEE International Conference on Communications, 2007. ICC '07*, Jun. 2007, pp. 5137–5142.

[9] ——, "Adaptive power loading for OFDM-Based cognitive radio systems with statistical interference constraint," *IEEE Transactions on Wireless Communications*, vol. 10, no. 9, pp. 2786–2791, Sep. 2011.

[10] M. Bellanger, T. Ihalainen, and M. Renfors, "Filter bank based cognitive radio physical layer," in *ICT 2009*, 2009, pp. 1–6.

[11] F. Benedetto, G. Giunta, E. Guzzon, and M. Renfors, "Effective monitoring of freeloading user in the presence of active user in cognitive radio networks," *IEEE Transactions on Vehicular Technology*, vol. 63, no. 5, pp. 2443–2450, Jun. 2014.

[12] U. Berthold, F. Fu, M. van der Schaar, and F. Jondral, "Detection of spectral resources in cognitive radios using reinforcement learning," in *3rd IEEE Symposium on New Frontiers in Dynamic Spectrum Access Networks, 2008. DySPAN 2008*, Oct. 2008, pp. 1–5.

[13] D. Bhargavi and C. Murthy, "Performance comparison of energy, matched-filter and cyclostationarity-based spectrum sensing," in *2010 IEEE Eleventh International Workshop on Signal Processing Advances in Wireless Communications (SPAWC)*, Jun. 2010.

[14] T. Bogale and L. Vandendorpe, "Moment based spectrum sensing algorithm for cognitive radio networks with noise variance uncertainty," in *2013 47th Annual Conference on Information Sciences and Systems (CISS)*, Mar. 2013, pp. 1–5.

[15] S. Bokharaiee, H. Nguyen, and E. Shwedyk, "Blind spectrum sensing for OFDM-based cognitive radio systems," *IEEE Transactions on Vehicular Technology*, vol. 60, no. 3, pp. 858–871, Mar. 2011.

[16] S. Brandes, I. Cosovic, and M. Schnell, "Sidelobe suppression in OFDM systems by insertion of cancellation carriers," in *Vehicular Technology Conference, 2005. VTC-2005-Fall. 2005 IEEE 62nd*, vol. 1, Sep. 2005, pp. 152–156.

[17] M. Buddhikot, P. Kolodzy, S. Miller, K. Ryan, and J. Evans, "DIMSUMnet: new directions in wireless networking using coordinated dynamic spectrum," in *World of Wireless Mobile and Multimedia Networks, 2005. WoWMoM 2005. Sixth IEEE International Symposium on a*, Jun. 2005, pp. 78–85.

[18] D. Cabric, S. Mishra, and R. Brodersen, "Implementation issues in spectrum sensing for cognitive radios," in *Conference Record of the Thirty-Eighth Asilomar Conference on Signals, Systems and Computers, 2004*, vol. 1, Nov. 2004, pp. 772–776 Vol.1.

[19] D. Cabric, A. Tkachenko, and R. Brodersen, "Spectrum sensing measurements of pilot, energy, and collaborative detection," in *IEEE Military Communications Conference, 2006. MILCOM 2006*, Oct. 2006, pp. 1–7.

[20] E. Candes and M. Wakin, "An introduction to compressive sampling," *IEEE Signal Processing Magazine*, vol. 25, no. 2, Mar. 2008.

[21] K. Cao and H. Shao, "Compressive wideband spectrum sensing using high-order statistics for cognitive radio," in *2013 IEEE Global High Tech Congress on Electronics (GHTCE)*, Nov. 2013, pp. 187–190.

[22] E. Castillo, *Extreme Value Theory in Engineering*. Academic Press, 1988.

[23] V. Cevher, R. Chellappa, and J. McClellan, "Gaussian approximations for energy-based detection and localization in sensor networks," in *IEEE/SP 14th Workshop on Statistical Signal Processing, 2007. SSP '07*, Aug. 2007, pp. 655–659.

[24] H.-S. Chen, W. Gao, and D. Daut, "Spectrum sensing for OFDM systems employing pilot tones," *IEEE Transactions on Wireless Communications*, vol. 8, no. 12, pp. 5862–5870, Dec. 2009.

[25] P. Cheraghi, Y. Ma, Z. Lu, and R. Tafazolli, "A novel low complexity differential energy detection for sensing OFDM sources in low SNR environment," in *2011 IEEE GLOBECOM Workshops (GC Wkshps)*, Dec. 2011, pp. 378–382.

[26] P. Cheraghi, Y. Ma, and R. Tafazolli, "Frequency-domain differential energy detection based on extreme statistics for OFDM source sensing," in *Vehicular Technology Conference (VTC Spring), 2011 IEEE 73rd*, May 2011, pp. 1–5.

[27] P. Cheraghi, Y. Ma, R. Tafazolli, and Z. Lu, "Cluster-based differential energy detection for spectrum sensing in multi-carrier systems," *IEEE Transactions on Signal Processing*, vol. 60, no. 12, pp. 6450–6464, Dec. 2012.

[28] C. Chiasserini and R. Rao, "Coexistence mechanisms for interference mitigation in the 2.4-GHz ISM band," *IEEE Transactions on Wireless Communications*, vol. 2, no. 5, pp. 964–975, Sep. 2003.

[29] Y.-J. Choi, W. Pak, Y. Xin, and S. Rangarajan, "Throughput analysis of cooperative spectrum sensing in rayleigh-faded cognitive radio systems," *IET Communications*, vol. 6, no. 9, Jun. 2012.

[30] S. Darak, J. Palicot, H. Zhang, V. Prasad, and C. Moy, "Reconfigurable filter bank with complete control over subband bandwidths for multi-standard wireless communication receivers," *IEEE Transactions on Very Large Scale Integration (VLSI) Systems*, vol. PP, no. 99, pp. 1–1, 2014.

[31] S. Darak, H. Zhang, J. Palicot, and A. Vinod, "Efficient spectrum sensing for green cognitive radio using low complexity reconfigurable fast filter bank," in *2013 International Conference on Advanced Technologies for Communications (ATC)*, Oct. 2013, pp. 318–322.

[32] D. Datla, R. Rajbanshi, A. M. Wyglinski, and G. Minden, "An adaptive spectrum sensing architecture for dynamic spectrum access networks," *IEEE Transactions on Wireless Communications*, vol. 8, no. 8, pp. 4211–4219, Aug. 2009.

[33] D. Datla, A. M. Wyglinski, and G. Minden, "A spectrum surveying framework for dynamic spectrum access networks," *IEEE Transactions on Vehicular Technology*, vol. 58, no. 8, pp. 4158–4168, Oct. 2009.

[34] H. A. David and H. N. Nagaraja, *Order Statistics*, 3rd ed. Hoboken, N.J: Wiley-Interscience, Aug. 2003.

[35] H. Dehner, H. Jakel, D. Burgkhardt, and F. Jondral, "The teager-kaiser energy operator in presence of multiple narrowband interference," *IEEE Communications Letters*, vol. 14, no. 8, pp. 716–718, Aug. 2010.

[36] R. Deng, J. Chen, C. Yuen, P. Cheng, and Y. Sun, "Energy-efficient cooperative spectrum sensing by optimal scheduling in sensor-aided cognitive radio networks," *IEEE Transactions on Vehicular Technology*, vol. 61, no. 2, Feb. 2012.

[37] F. Digham, M.-S. Alouini, and M. K. Simon, "On the energy detection of unknown signals over fading channels," *IEEE Transactions on Communications*, vol. 55, no. 1, pp. 21–24, Jan. 2007.

[38] S. Dikmese and M. Renfors, "Optimized FFT and filter bank based spectrum sensing for bluetooth signal," in *2012 IEEE Wireless Communications and Networking Conference (WCNC)*, Apr. 2012, pp. 792–797.

[39] S. Dikmese, M. Renfors, and H. Dincer, "FFT and filter bank based spectrum sensing for WLAN signals," in *2011 20th European Conference on Circuit Theory and Design (ECCTD)*, Aug. 2011, pp. 781–784.

[40] S. Dikmese, P. Sofotasios, M. Renfors, and M. Valkama, "Maximum-minimum energy based spectrum sensing under frequency selectivity for cognitive radios," in *2014 9th International Conference on Cognitive Radio Oriented Wireless Networks (CROWNCOM)*, 2014, pp. 61–67.

[41] ——, "Reduced complexity subband energy based spectrum sensing under noise uncertainty and frequency-selective spectral characteristics," *submitted to IEEE Transactions on Signal Processing*, 2015.

[42] S. Dikmese, S. Srinivasan, and M. Renfors, "FFT and filter bank based spectrum sensing and spectrum utilization for cogntive radios," in *2012 5th International Symposium on Communications Control and Signal Processing (ISCCSP)*, May 2012, pp. 1–5.

[43] S. Dikmese, J. L. Wong, A. Gokceoglu, E. Guzzon, M. Valkama, and M. Renfors, "Reducing computational complexity of eigenvalue based spectrum sensing for cognitive radio," in *2013 8th International Conference on Cognitive Radio Oriented Wireless Networks (CROWNCOM)*, Jul. 2013, pp. 61–67.

[44] S. Dikmese, A. Gokceoglu, M. Valkama, and M. Renfors, "Reduced complexity spectrum sensing based on maximum eigenvalue and energy," in *Proceedings of the Tenth International Symposium on Wireless Communication Systems (ISWCS 2013)*, Aug. 2013, pp. 1–5.

[45] S. Dikmese, T. Ihalainen, and M. Renfors, "Analysis and optimization of energy detection for non-flat spectral characteristics," in *Cognitive Communication and Cooperative HetNet Coexistence*, ser. Signals and Communication Technology, M.-G. D. Benedetto and F. Bader, Eds. Springer International Publishing, Jan. 2014, pp. 47–69. [Online]. Available: http://link.springer.com/chapter/10.1007/978-3-319-01402-9_3

[46] D. Dimitriadis, P. Maragos, and A. Potamianos, "On the effects of filterbank design and energy computation on robust speech recognition," *IEEE Transactions on Audio, Speech, and Language Processing*, vol. 19, no. 6, pp. 1504–1516, Aug. 2011.

[47] D. Dimitriadis, A. Potamianos, and P. Maragos, "A comparison of the squared energy and teager-kaiser operators for short-term energy estimation in additive noise," *IEEE Transactions on Signal Processing*, vol. 57, no. 7, pp. 2569–2581, Jul. 2009.

[48] A. Eltholth, A. Mekhail, A. Elshirbini, M. Desouki, and A. Aldelfattah, "Modeling the effect of clipping and power amplifier NonLinearities on OFDM systems," *Ubiquitous Comput. Commun. Journal*, vol. 1, no. 3, pp. 411–424, 2009.

[49] R. Fan and H. Jiang, "Optimal multi-channel cooperative sensing in cognitive radio networks," *IEEE Transactions on Wireless Communications*, vol. 9, no. 3, pp. 1128–1138, Mar. 2010.

[50] J. Fang, J. Li, Y. Shen, H. Li, and S. Li, "Super-resolution compressed sensing: An iterative reweighted algorithm for joint parameter learning and sparse signal recovery," *IEEE Signal Processing Letters*, vol. 21, no. 6, Jun. 2014.

[51] B. Farhang-Boroujeny, "Filter bank spectrum sensing for cognitive radios," *IEEE Transactions on Signal Processing*, vol. 56, no. 5, pp. 1801–1811, May 2008.

[52] B. Farhang-Boroujeny and R. Kempter, "Multicarrier communication techniques for spectrum sensing and communication in cognitive radios," *IEEE Communications Magazine*, vol. 46, no. 4, pp. 80–85, Apr. 2008.

[53] F. Fazel, M. Fazel, and M. Stojanovic, "Random access compressed sensing over fading and noisy communication channels," *IEEE Transactions on Wireless Communications*, vol. 12, no. 5, May 2013.

[54] FCC, "ET docket No 02-135 spectrum policy task force report," Nov. 2002.

[55] A. Fehske, J. Gaeddert, and J. Reed, "A new approach to signal classification using spectral correlation and neural networks," in *2005 First IEEE International Symposium on New Frontiers in Dynamic Spectrum Access Networks, 2005. DySPAN 2005*, Nov. 2005, pp. 144–150.

[56] W. Gardner, "Exploitation of spectral redundancy in cyclostationary signals," *IEEE Signal Processing Magazine*, vol. 8, no. 2, pp. 14–36, Apr. 1991.

[57] M. Gautier, V. Berg, and D. Noguet, "Wideband frequency domain detection using teager-kaiser energy operator," in *2012 7th International ICST Conference on Cognitive Radio Oriented Wireless Networks and Communications (CROWNCOM)*, Jun. 2012, pp. 332–337.

[58] M. Gautier, M. Laugeois, and D. Noguet, "Teager-kaiser energy detector for narrowband wireless microphone spectrum sensing," in *2010 Proceedings of the Fifth International Conference on Cognitive Radio Oriented Wireless Networks Communications (CROWNCOM)*, Jun. 2010, pp. 1–5.

[59] A. Ghasemi and E. Sousa, "Asymptotic performance of collaborative spectrum sensing under correlated log-normal shadowing," *IEEE Communications Letters*, vol. 11, no. 1, pp. 34–36, Jan. 2007.

[60] ——, "Spectrum sensing in cognitive radio networks: requirements, challenges and design trade-offs," *IEEE Communications Magazine*, vol. 46, no. 4, pp. 32–39, Apr. 2008.

[61] A. Gokceoglu, S. Dikmese, M. Valkama, and M. Renfors, "Analysis and mitigation of RF IQ imbalance in eigenvalue based multichannel spectrum sensing," in *2013 IEEE 24th International Symposium on Personal Indoor and Mobile Radio Communications (PIMRC)*, Sep. 2013, pp. 734–739.

[62] ——, "Enhanced energy detection for multi-band spectrum sensing under RF imperfections," in *2013 8th International Conference on Cognitive Radio Oriented Wireless Networks (CROWNCOM)*, Jul. 2013, pp. 55–60.

[63] ——, "Energy detection under IQ imbalance with single- and multi-channel direct-conversion receiver: Analysis and mitigation," *IEEE Journal on Selected Areas in Communications*, vol. 32, no. 3, pp. 411–424, Mar. 2014.

[64] R. M. Gray, "Toeplitz and circulant matrices: A review," Tech. Rep., 2001.

[65] E. J. Gumbel, *Statistical theory of extreme values and some practical applications: a series of lectures.* U. S. Govt. Print. Office, 1954.

[66] W. Han, J. Li, Z. Tian, and Y. Zhang, "Efficient cooperative spectrum sensing with minimum overhead in cognitive radio," *IEEE Transactions on Wireless Communications*, vol. 9, no. 10, pp. 3006–3011, Oct. 2010.

[67] X. Hao, M. H. Cheung, V. Wong, and V. Leung, "Hedonic coalition formation game for cooperative spectrum sensing and channel access in cognitive radio networks," *IEEE Transactions on Wireless Communications*, vol. 11, no. 11, Nov. 2012.

[68] A. G. Hawkes, "Statistical models in applied science, karl v. bury, wiley, london, 1975, no. of pages 625, ISBN 0-471-12590-3," *International Journal for Numerical Methods in Engineering*, vol. 12, no. 6, pp. 1054–1054, Jan. 1978. [Online]. Available: http://onlinelibrary.wiley.com/doi/10.1002/nme.1620120617/abstract

[69] S. Haykin, "Cognitive radio: brain-empowered wireless communications," *IEEE Journal on Selected Areas in Communications*, vol. 23, no. 2, pp. 201–220, Feb. 2005.

[70] S. S. Haykin, *Adaptive filter theory.* Prentice Hall, 2002.

[71] I. Held and A. Chen, "Channel estimation and equalization algorithms for long range bluetooth signal reception," in *Vehicular Technology Conference (VTC 2010-Spring), 2010 IEEE 71st*, May 2010, pp. 1–6.

[72] K. Hemachandra and N. Beaulieu, "Novel analysis for performance evaluation of energy detection of unknown deterministic signals using dual diversity," in *2011 IEEE Vehicular Technology Conference (VTC Fall)*, Sep. 2011, pp. 1–5.

[73] S. Herath, N. Rajatheva, and C. Tellambura, "Energy detection of unknown signals in fading and diversity reception," *IEEE Transactions on Communications*, vol. 59, no. 9, pp. 2443–2453, Sep. 2011.

[74] H.-y. Hsieh, H.-K. Chang, and M.-L. Ku, "Higher-order statistics based sequential spectrum sensing for cognitive radio," in *2011 11th International Conference on ITS Telecommunications (ITST)*, Aug. 2011, pp. 696–701.

[75] G. Huang and J. Tugnait, "On cyclostationarity based spectrum sensing under uncertain gaussian noise," *IEEE Transactions on Signal Processing*, vol. 61, no. 8, Apr. 2013.

[76] Y. Huang and X. Huang, "Detection of temporally correlated signals over multipath fading channels," *IEEE Transactions on Wireless Communications*, vol. 12, no. 3, pp. 1290–1299, Mar. 2013.

[77] T. Ihalainen, A. Viholainen, T. Stitz, and M. Renfors, "Spectrum monitoring scheme for filter bank based cognitive radios," in *Future Network and Mobile Summit, 2010*, Jun. 2010, pp. 1–9.

[78] M. Iqbal and A. Ghafoor, "Analysis of multiband joint detection framework for waveform-based sensing in cognitive radios," in *2012 IEEE Vehicular Technology Conference (VTC Fall)*, Sep. 2012, pp. 1–5.

[79] R. Jain, "Channel models: A tutorial," in *WiMAX Forum AATG*, 2007, pp. 1–6.

[80] J. Jang and K.-B. Lee, "Transmit power adaptation for multiuser OFDM systems," *IEEE Journal on Selected Areas in Communications*, vol. 21, no. 2, pp. 171–178, Feb. 2003.

[81] C. Jiang, Y. Li, W. Bai, Y. Yang, and J. Hu, "Statistical matched filter based robust spectrum sensing in noise uncertainty environment," in *2012 IEEE 14th International Conference on Communication Technology (ICCT)*, Nov. 2012.

[82] I. M. Johnstone, "On the distribution of the largest eigenvalue in principal components analysis," *The Annals of Statistics*, vol. 29, no. 2, pp. 295–327, Apr. 2001. [Online]. Available: http://projecteuclid.org/euclid.aos/1009210544

[83] F. K. Jondral, "Software-defined Radio-Basics and evolution to cognitive radio," *EURASIP Journal on Wireless Communications and Networking*, vol. 2005, no. 3, p. 652784, Aug. 2005. [Online]. Available: http://jwcn.eurasipjournals.com/content/2005/3/652784/abstract

[84] D. Kaiser and J. Kaiser, "Estimation of power systems amplitudes, frequencies, and phase characteristics using energy operators," in *2012 IEEE Energy Conversion Congress and Exposition (ECCE)*, Sep. 2012, pp. 930–937.

[85] J. Kaiser, "On a simple algorithm to calculate the 'energy' of a signal," in *, 1990 International Conference on Acoustics, Speech, and Signal Processing, 1990. ICASSP-90*, Apr. 1990, pp. 381–384 vol.1.

[86] M. Kaneko and K. Al Agha, "Compressed sensing based protocol for interfering data recovery in multi-hop sensor networks," *IEEE Communications Letters*, vol. 18, no. 1, Jan. 2014.

[87] S. Kapoor, S. V. R. K. Rao, and G. Singh, "Opportunistic spectrum sensing by employing matched filter in cognitive radio network," in *2011 International Conference on Communication Systems and Network Technologies (CSNT)*, Jun. 2011.

[88] S. M. Kay, *Fundamentals of Statistical Signal Processing: Detection theory.* Prentice-Hall PTR, 1998.

[89] Z. Khalaf, A. Nafkha, and J. Palicot, "Blind cyclostationary feature detector based on sparsity hypotheses for cognitive radio equipment," in *2011 IEEE 54th International Midwest Symposium on Circuits and Systems (MWSCAS)*, Aug. 2011, pp. 1–4.

[90] ——, "Enhanced hybrid spectrum sensing architecture for cognitive radio equipment," in *General Assembly and Scientific Symposium, 2011 XXXth URSI*, Aug. 2011, pp. 1–4.

[91] ——, "Blind spectrum detector for cognitive radio using compressed sensing and symmetry property of the second order cyclic autocorrelation," in *2012 7th International ICST Conference on Cognitive Radio Oriented Wireless Networks and Communications (CROWNCOM)*, Jun. 2012, pp. 291–296.

[92] Z. Khalaf, J. Palicot, A. Nafkha, and H. Zhang, "Blind free band detector based on the sparsity of the cyclic autocorrelation function," in *Signal Processing Conference (EUSIPCO), 2013 Proceedings of the 21st European*, Sep. 2013, pp. 1–5.

[93] H. Kim and K. Shin, "Fast discovery of spectrum opportunities in cognitive radio networks," in *3rd IEEE Symposium on New Frontiers in Dynamic Spectrum Access Networks, 2008. DySPAN 2008*, Oct. 2008, pp. 1–12.

[94] S.-J. Kim, E. Dall'Anese, and G. Giannakis, "Cooperative spectrum sensing for cognitive radios using kriged kalman filtering," *IEEE Journal of Selected Topics in Signal Processing*, vol. 5, no. 1, pp. 24–36, Feb. 2011.

[95] Y. Kim, M. Nadar, and A. Bilgin, "Wavelet-based compressed sensing using a gaussian scale mixture model," *IEEE Transactions on Image Processing*, vol. 21, no. 6, Jun. 2012.

[96] D. Kivanc, G. Li, and H. Liu, "Computationally efficient bandwidth allocation and power control for OFDMA," *IEEE Transactions on Wireless Communications*, vol. 2, no. 6, pp. 1150–1158, Nov. 2003.

[97] A. Kortun, T. Ratnarajah, M. Sellathurai, C. Zhong, and C. Papadias, "On the performance of eigenvalue-based cooperative spectrum sensing for cognitive radio," *IEEE Journal of Selected Topics in Signal Processing*, vol. 5, no. 1, pp. 49–55, Feb. 2011.

[98] V. Kostylev, "Energy detection of a signal with random amplitude," in *IEEE International Conference on Communications, 2002. ICC 2002*, vol. 3, 2002, pp. 1606–1610 vol.3.

[99] M. Kosunen, V. Turunen, K. Kokkinen, and J. Ryynanen, "Survey and analysis of cyclostationary signal detector implementations on FPGA," *IEEE Journal on Emerging and Selected Topics in Circuits and Systems*, vol. 3, no. 4, Dec. 2013.

[100] H. Li, C. Li, and H. Dai, "Quickest spectrum sensing in cognitive radio," in *42nd Annual Conference on Information Sciences and Systems, 2008. CISS 2008*, Mar. 2008, pp. 203–208.

[101] K. Li, L. Gan, and C. Ling, "Convolutional compressed sensing using deterministic sequences," *IEEE Transactions on Signal Processing*, vol. 61, no. 3, Feb. 2013.

[102] Y. Li and S. Jayaweera, "Dynamic spectrum tracking using energy and cyclostationarity-based multi-variate non-parametric quickest detection for cognitive radios," *IEEE Transactions on Wireless Communications*, vol. 12, no. 7, Jul. 2013.

[103] X. Liu and S. S. N., "Sensing-based opportunistic channel access," *Mob. Netw. Appl.*, vol. 11, no. 4, pp. 577–591, Aug. 2006. [Online]. Available: http://dx.doi.org/10.1007/s11036-006-7323-x

[104] A. Loulou, S. Gorgani, and M. Renfors, "Enhanced OFDM techniques for fragmented spectrum use," in *Future Network and Mobile Summit (FutureNetworkSummit), 2013*, Jul. 2013, pp. 1–10.

[105] A. Loulou and M. Renfors, "Effective schemes for OFDM sidelobe control in fragmented spectrum use," in *2013 IEEE 24th International Symposium on Personal Indoor and Mobile Radio Communications (PIMRC)*, Sep. 2013, pp. 471–475.

[106] L. Lu, X. Zhou, U. Onunkwo, and G. Y. Li, "Ten years of research in spectrum sensing and sharing in cognitive radio," *EURASIP Journal on Wireless Communications and Networking*, vol. 2012, no. 1, p. 28, Jan. 2012. [Online]. Available: http://jwcn.eurasipjournals.com/content/2012/1/28/abstract

[107] J. Lunden, V. Koivunen, A. Huttunen, and H. Poor, "Spectrum sensing in cognitive radios based on multiple cyclic frequencies," in *2nd International Conference on Cognitive Radio Oriented Wireless Networks and Communications, 2007. CrownCom 2007*, Aug. 2007, pp. 37–43.

[108] L. Ma, Y. Li, and A. Demir, "Matched filtering assisted energy detection for sensing weak primary user signals," in *2012 IEEE International Conference on Acoustics, Speech and Signal Processing (ICASSP)*, Mar. 2012.

[109] A. Madni, "A systems perspective on compressed sensing and its use in reconstructing sparse networks," *IEEE Systems Journal*, vol. 8, no. 1, Mar. 2014.

[110] R. Mahesh, A. Vinod, C. Moy, and J. Palicot, "A low complexity reconfigurable filter bank architecture for spectrum sensing in cognitive radios," in *3rd International Conference on Cognitive Radio Oriented Wireless Networks and Communications, 2008. CrownCom 2008*, May 2008, pp. 1–6.

[111] M. Malloy and R. Nowak, "Near-optimal adaptive compressed sensing," *IEEE Transactions on Information Theory*, vol. 60, no. 7, Jul. 2014.

[112] J. Meng, W. Yin, H. Li, E. Hossain, and Z. Han, "Collaborative spectrum sensing from sparse observations in cognitive radio networks," *IEEE Journal on Selected Areas in Communications*, vol. 29, no. 2, pp. 327–337, Feb. 2011.

[113] J. Mitola and J. Maguire, G.Q., "Cognitive radio: making software radios more personal," *IEEE Personal Communications*, vol. 6, no. 4, pp. 13–18, Aug. 1999.

[114] J. Mitola, "Cognitive radio — an integrated agent architecture for software defined radio," Ph.D. dissertation, Royal Institute of Technology (KTH), May 2000. [Online]. Available: http://web.it.kth.se/~maguire/jmitola/Mitola_Dissertation8_Integrated.pdf

[115] M. Mohamad, H. C. Wen, and M. Ismail, "Matched filter detection technique for GSM band," in *2012 International Symposium on Telecommunication Technologies (ISTT)*, Nov. 2012.

[116] H. Mu and J. Tugnait, "Joint soft-decision cooperative spectrum sensing and power control in multiband cognitive radios," *IEEE Transactions on Signal Processing*, vol. 60, no. 10, Oct. 2012.

[117] B. Nadler, "On the distribution of the ratio of the largest eigenvalue to the trace of a wishart matrix," *Journal of Multivariate Analysis*, vol. 102, no. 2, pp. 363–371, Feb. 2011. [Online]. Available: http://www.sciencedirect.com/science/article/pii/S0047259X10002113

[118] T. R. Newman, B. A. Barker, A. M. Wyglinski, A. Agah, J. B. Evans, and G. J. Minden, "Cognitive engine implementation for wireless multicarrier transceivers," *Wireless Communications and Mobile Computing*, vol. 7, no. 9, pp. 1129–1142, Nov. 2007. [Online]. Available: http://onlinelibrary.wiley.com/doi/10.1002/wcm.486/abstract

[119] A. O'Donnell, J. Wilson, D. Koltenuk, and R. Burkholder, "Compressed sensing for radar signature analysis," *IEEE Transactions on Aerospace and Electronic Systems*, vol. 49, no. 4, Oct. 2013.

[120] D.-C. Oh and Y.-H. Lee, "Low complexity FFT based spectrum sensing in bluetooth system," in *Vehicular Technology Conference, 2009. VTC Spring 2009. IEEE 69th*, Apr. 2009, pp. 1–5.

[121] M. Oner and F. Jondral, "Cyclostationarity based air interface recognition for software radio systems," in *2004 IEEE Radio and Wireless Conference*, Sep. 2004, pp. 263–266.

[122] ——, "Cyclostationarity-based methods for the extraction of the channel allocation information in a spectrum pooling system," in *2004 IEEE Radio and Wireless Conference*, Sep. 2004, pp. 279–282.

[123] S. Pagadarai, A. M. Wyglinski, and R. Rajbanshi, "A novel sidelobe suppression technique for OFDM-based cognitive radio transmission," in *3rd IEEE Symposium on New Frontiers in Dynamic Spectrum Access Networks, 2008. DySPAN 2008*, Oct. 2008, pp. 1–7.

[124] J. Palicot, *Radio Engineering: From Software Radio to Cognitive Radio*. John Wiley & Sons, Jan. 2013.

[125] J. Palicot, J. Mitola, Z. Z. Lei, and F. K. Jondral, "Special issue on 10 years of cognitive radio: state-of-the-art and perspectives," *EURASIP Journal on Wireless Communications and Networking*, vol. 2012, no. 1, p. 214, Jul. 2012. [Online]. Available: http://jwcn.eurasipjournals.com/content/2012/1/214/abstract

[126] P. Pawelczak, G. Janssen, and R. Venkatesha Prasad, "WLC10-4: performance measures of dynamic spectrum access networks," in *IEEE Global Telecommunications Conference, 2006. GLOBECOM '06*, Nov. 2006, pp. 1–6.

[127] E. Peh, Y.-C. Liang, Y. L. Guan, and Y. Zeng, "Cooperative spectrum sensing in cognitive radio networks with weighted decision fusion scheme," in *Vehicular Technology Conference (VTC 2010-Spring), 2010 IEEE 71st*, May 2010, pp. 1–5.

[128] J. Perez-Romero, O. Sallent, R. Agusti, and L. Giupponi, "A novel on-demand cognitive pilot channel enabling dynamic spectrum allocation," in *2nd IEEE International Symposium on New Frontiers in Dynamic Spectrum Access Networks, 2007. DySPAN 2007*, Apr. 2007, pp. 46–54.

[129] PHYDYAS, "Physical layer for dynamic spectrum access and cognitive radio," in *http://www.ict-phydyas.org/, Accessed*, Jun. 2013.

[130] N. Pillay and H. Xu, "Blind eigenvalue-based spectrum sensing for cognitive radio networks," *IET Communications*, vol. 6, no. 11, pp. 1388–1396, Jul. 2012.

[131] ——, "Eigenvalue-based spectrum sensing using the exact distribution of the maximum eigenvalue of a wishart matrix," *IET Signal Processing*, vol. 7, no. 9, pp. 833–842, Dec. 2013.

[132] H. V. Poor, *An Introduction to Signal Detection and Estimation*, 2nd ed. New York: Springer, Mar. 1998.

[133] J. Proakis and M. Salehi, *Digital Communications, 5th Edition*, 5th ed. Boston: McGraw-Hill Science/Engineering/Math, Nov. 2007.

[134] P. Qihang, Z. Kun, W. Jun, and L. Shaoqian, "A distributed spectrum sensing scheme based on credibility and evidence theory in cognitive radio context," in *2006 IEEE 17th International Symposium on Personal, Indoor and Mobile Radio Communications*, Sep. 2006, pp. 1–5.

[135] T. Qin and C. Leung, "Fair adaptive resource allocation for multiuser OFDM cognitive radio systems," in *Second International Conference on Communications and Networking in China, 2007. CHINACOM '07*, Aug. 2007, pp. 115–119.

[136] R. Rajbanshi, A. M. Wyglinski, and G. J. Minden, "OFDM-based cognitive radios for dynamic spectrum access networks," in *Cognitive Wireless Communication Networks*, E. Hossain and V. Bhargava, Eds. Springer US, Jan. 2007, pp. 165–188. [Online]. Available: http://link.springer.com/chapter/10.1007/978-0-387-68832-9_6

[137] C. Rapp, "Effects of HPA-Nonlinearity on a 4-DPSK/OFDM-Signal for a digital sound broadcasting system." pp. 179–184, 1991.

[138] M. Renfors, F. Bader, L. Baltar, D. Le Ruyet, D. Roviras, P. Mege, M. Haardt, and T. Hidalgo Stitz, "On the use of filter bank based multi-carrier modulation for professional mobile radio," in *Vehicular Technology Conference (VTC Spring), 2013 IEEE 77th*, Jun. 2013, pp. 1–5.

[139] J. Riba, J. Font-Segura, J. Villares, and G. Vazquez, "Frequency-domain GLR detection of a second-order cyclostationary signal over fading channels," *IEEE Transactions on Signal Processing*, vol. 62, no. 8, Apr. 2014.

[140] K. Ruttik, K. Koufos, and R. Jantti, "Detection of unknown signals in a fading environment," *IEEE Communications Letters*, vol. 13, no. 7, pp. 498–500, Jul. 2009.

[141] H. Sadeghi, P. Azmi, and H. Arezumand, "Cyclostationarity-based soft cooperative spectrum sensing for cognitive radio networks," *IET Communications*, vol. 6, no. 1, Jan. 2012.

[142] A. Sahai, N. Hoven, and R. Tandra, "Some fundamental limits on cognitive radio," in *in Forty-second Allerton Conference on Communication, Control, and Computing*, 2004.

[143] A. Sahai, R. Tandra, S. M. Mishra, and N. Hoven, "Fundamental design tradeoffs in cognitive radio systems," in *Proceedings of the First International Workshop on Technology and Policy for Accessing Spectrum*, ser. TAPAS '06. New York, NY, USA: ACM, 2006. [Online]. Available: http://doi.acm.org/10.1145/1234388.1234390

[144] A. Sahin and H. Arslan, "Edge windowing for OFDM based systems," *IEEE Communications Letters*, vol. 15, no. 11, pp. 1208–1211, Nov. 2011.

[145] ——, "The impact of scheduling on edge windowing," in *2011 IEEE Global Telecommunications Conference (GLOBECOM 2011)*, Dec. 2011, pp. 1–5.

[146] M. Shaat and F. Bader, "Power allocation with interference constraint in multicarrier based cognitive radio systems," in *Multi-Carrier Systems Solutions 2009, Proceedings from the 7th International Workshop on Multi-Carrier Systems Solutions, May 2009, Herrsching, Germany*, ser. Lecture Notes in Electrical Engineering, vol. 41. Springer, 2009, pp. 259–268.

[147] ——, "Computationally efficient power allocation algorithm in multicarrier-based cognitive radio networks: OFDM and FBMC systems," *EURASIP Journal on Advances in Signal Processing*, vol. 2010, no. 1, p. 528378, Feb. 2010. [Online]. Available: http://asp.eurasipjournals.com/content/2010/1/528378/abstract

[148] N. Shankar, C. Cordeiro, and K. Challapali, "Spectrum agile radios: utilization and sensing architectures," in *2005 First IEEE International Symposium on New Frontiers in Dynamic Spectrum Access Networks, 2005. DySPAN 2005*, Nov. 2005, pp. 160–169.

[149] J.-C. Shen and E. Alsusa, "An efficient multiple lags selection method for cyclostationary feature based spectrum-sensing," *IEEE Signal Processing Letters*, vol. 20, no. 2, Feb. 2013.

[150] Z. Shen, J. Andrews, and B. Evans, "Optimal power allocation in multiuser OFDM systems," in *IEEE Global Telecommunications Conference, 2003. GLOBECOM '03*, vol. 1, Dec. 2003, pp. 337–341 Vol.1.

[151] A. Singh, M. Bhatnagar, and R. Mallik, "Cooperative spectrum sensing in multiple antenna based cognitive radio network using an improved energy detector," *IEEE Communications Letters*, vol. 16, no. 1, Jan. 2012.

[152] P. Siohan, C. Siclet, and N. Lacaille, "Analysis and design of OFDM/OQAM systems based on filterbank theory," *IEEE Transactions on Signal Processing*, vol. 50, no. 5, pp. 1170–1183, May 2002.

[153] P. Sofotasios, E. Rebeiz, L. Zhang, T. Tsiftsis, D. Cabric, and S. Freear, "Energy detection based spectrum sensing over and extreme fading channels," *IEEE Transactions on Vehicular Technology*, vol. 62, no. 3, pp. 1031–1040, Mar. 2013.

[154] S. Srinivasan, S. Dikmese, and M. Renfors, "Spectrum sensing and spectrum utilization model for OFDM and FBMC based cognitive radios," in *2012 IEEE 13th International Workshop on Signal Processing Advances in Wireless Communications (SPAWC)*, Jun. 2012, pp. 139–143.

[155] V. Stavroulaki, K. Tsagkaris, P. Demestichas, J. Gebert, M. Mueck, A. Schmidt, R. Ferrus, O. Sallent, M. Filo, C. Mouton, and L. Rakotoharison, "Cognitive control channels: from concept to identification of implementation options," *IEEE Communications Magazine*, vol. 50, no. 7, pp. 96–108, Jul. 2012.

[156] A. Taherpour, M. Nasiri-Kenari, and S. Gazor, "Multiple antenna spectrum sensing in cognitive radios," *IEEE Transactions on Wireless Communications*, vol. 9, no. 2, pp. 814–823, Feb. 2010.

[157] R. Tandra and A. Sahai, "Fundamental limits on detection in low SNR under noise uncertainty," in *2005 International Conference on Wireless Networks, Communications and Mobile Computing*, vol. 1, Jun. 2005, pp. 464–469 vol.1.

[158] ——, "SNR walls for signal detection," *IEEE Journal of Selected Topics in Signal Processing*, vol. 2, no. 1, pp. 4–17, Feb. 2008.

[159] H. Tang, "Some physical layer issues of wide-band cognitive radio systems," in *2005 First IEEE International Symposium on New Frontiers in Dynamic Spectrum Access Networks, 2005. DySPAN 2005*, Nov. 2005, pp. 151–159.

[160] G. Taricco, "On the accuracy of the gaussian approximation with linear cooperative spectrum sensing over rician fading channels," *IEEE Signal Processing Letters*, vol. 17, no. 7, pp. 651–654, Jul. 2010.

[161] ——, "Optimization of linear cooperative spectrum sensing for cognitive radio networks," *IEEE Journal of Selected Topics in Signal Processing*, vol. 5, no. 1, pp. 77–86, Feb. 2011.

[162] C. A. Tracy and H. Widom, "On orthogonal and symplectic matrix ensembles," *Communications in Mathematical Physics*, vol. 177, no. 3, pp. 727–754, 1996. [Online]. Available: http://projecteuclid.org/euclid.cmp/1104286442

[163] ——, "The distribution of the largest eigenvalue in the gaussian ensembles," in *Calogero Moser Sutherland Models*, ser. CRM Series in Mathematical Physics, J. F. v. Diejen and L. Vinet, Eds. Springer New York, Jan. 2000, pp. 461–472. [Online]. Available: http://link.springer.com/chapter/10.1007/978-1-4612-1206-5_29

[164] A. M. Tulino and S. Verdu, "Random matrix theory and wireless communications," *Foundations and Trends in Communications and Information Theory*, vol. 1, no. 1, pp. 1–182, 2004. [Online]. Available: http://www.nowpublishers.com/articles/foundations-and-trends-in-communications-and-information-theory/CIT-001

[165] H. Urkowitz, "Energy detection of unknown deterministic signals," *Proceedings of the IEEE*, vol. 55, no. 4, pp. 523–531, Apr. 1967.

[166] P. Urriza, E. Rebeiz, and D. Cabric, "Multiple antenna cyclostationary spectrum sensing based on the cyclic correlation significance test," *IEEE Journal on Selected Areas in Communications*, vol. 31, no. 11, Nov. 2013.

[167] G. Vazquez-Vilar, R. Lopez-Valcarce, and J. Sala, "Multiantenna spectrum sensing exploiting spectral a priori information," *IEEE Transactions on Wireless Communications*, vol. 10, no. 12, pp. 4345–4355, Dec. 2011.

[168] H. Voss, "A symmetry exploiting lanczos method for symmetric toeplitz matrices," *Numerical Algorithms*, vol. 25, no. 1-4, pp. 377–385, Sep. 2000. [Online]. Available: http://link.springer.com/article/10.1023/A%3A1016665225002

[169] H. Vu-Van and I. Koo, "A sequential cooperative spectrum sensing scheme based on cognitive user reputation," *IEEE Transactions on Consumer Electronics*, vol. 58, no. 4, Nov. 2012.

[170] B. Wang and K. Liu, "Advances in cognitive radio networks: A survey," *IEEE Journal of Selected Topics in Signal Processing*, vol. 5, no. 1, pp. 5–23, Feb. 2011.

[171] X. Wang, P.-H. Ho, and A. Wong, "Towards efficient spectrum sensing for cognitive radio through knowledge-based reasoning," in *3rd IEEE Symposium on New Frontiers in Dynamic Spectrum Access Networks, 2008. DySPAN 2008*, Oct. 2008, pp. 1–8.

[172] L. Wei, P. Dharmawansa, and O. Tirkkonen, "Locally best invariant test for multiple primary user spectrum sensing," in *2012 7th International ICST Conference on Cognitive Radio Oriented Wireless Networks and Communications (CROWNCOM)*, Jun. 2012, pp. 367–372.

[173] ——, "Multiple primary user spectrum sensing in the low SNR regime," *IEEE Transactions on Communications*, vol. 61, no. 5, pp. 1720–1731, May 2013.

[174] L. Wei, M. McKay, and O. Tirkkonen, "Exact demmel condition number distribution of complex wishart matrices via the mellin transform," *IEEE Communications Letters*, vol. 15, no. 2, pp. 175–177, Feb. 2011.

[175] L. Wei and O. Tirkkonen, "Cooperative spectrum sensing of OFDM signals using largest eigenvalue distributions," in *2009 IEEE 20th International Symposium on Personal, Indoor and Mobile Radio Communications*, Sep. 2009, pp. 2295–2299.

[176] ——, "Analysis of scaled largest eigenvalue based detection for spectrum sensing," in *2011 IEEE International Conference on Communications (ICC)*, Jun. 2011, pp. 1–5.

[177] ——, "Approximate condition number distribution of complex non-central correlated wishart matrices," in *2011 IEEE International Conference on Communications (ICC)*, Jun. 2011, pp. 1–5.

[178] ——, "Spectrum sensing in the presence of multiple primary users," *IEEE Transactions on Communications*, vol. 60, no. 5, pp. 1268–1277, May 2012.

[179] L. Wei, O. Tirkkonen, and Y.-C. Liang, "Multi-source signal detection with arbitrary noise covariance," *IEEE Transactions on Signal Processing*, vol. 62, no. 22, pp. 5907–5918, Nov. 2014.

[180] L. Wei and O. Tirkkonen, "Multiple primary user spectrum sensing for unknown noise statistics," in *2013 IEEE 24th International Symposium on Personal Indoor and Mobile Radio Communications (PIMRC)*, Sep. 2013, pp. 871–875.

[181] B. Wild and K. Ramchandran, "Detecting primary receivers for cognitive radio applications," in *2005 First IEEE International Symposium on New Frontiers in Dynamic Spectrum Access Networks, 2005. DySPAN 2005*, Nov. 2005, pp. 124–130.

[182] D. Willkomm, S. Machiraju, J. Bolot, and A. Wolisz, "Primary users in cellular networks: A large-scale measurement study," in *3rd IEEE Symposium on New Frontiers in Dynamic Spectrum Access Networks, 2008. DySPAN 2008*, Oct. 2008, pp. 1–11.

[183] C. Y. Wong, R. Cheng, K. Lataief, and R. Murch, "Multiuser OFDM with adaptive subcarrier, bit, and power allocation," *IEEE Journal on Selected Areas in Communications*, vol. 17, no. 10, pp. 1747–1758, Oct. 1999.

[184] R. Woodings and M. Gerrior, "Avoiding interference in the 2.4-GHz ISM band," *Microwave Engineering*, Feb.2005.

[185] A. M. Wyglinski, M. Nekovee, and T. Hou, *Cognitive Radio Communications and Networks: Principles and Practice*. Academic Press, Nov. 2009.

[186] X. Yang, X. Tao, E. Dutkiewicz, X. Huang, Y. Guo, and Q. Cui, "Energy-efficient distributed data storage for wireless sensor networks based on compressed sensing and network coding," *IEEE Transactions on Wireless Communications*, vol. 12, no. 10, Oct. 2013.

[187] C.-M. Yu, S.-H. Hsieh, H.-W. Liang, C.-S. Lu, W.-H. Chung, S.-Y. Kuo, and S.-c. Pei, "Compressed sensing detector design for space shift keying in MIMO systems," *IEEE Communications Letters*, vol. 16, no. 10, Oct. 2012.

[188] Z. Yuan and A. M. Wyglinski, "Cognitive radio-based OFDM sidelobe suppression employing modulated filter banks and cancellation carriers," in *IEEE Military Communications Conference, 2009. MILCOM 2009*, Oct. 2009, pp. 1–5.

[189] ——, "On sidelobe suppression for multicarrier-based transmission in dynamic spectrum access networks," *IEEE Transactions on Vehicular Technology*, vol. 59, no. 4, pp. 1998–2006, May 2010.

[190] T. Yucek and H. Arslan, "Spectrum characterization for opportunistic cognitive radio systems," in *IEEE Military Communications Conference, 2006. MILCOM 2006*, Oct. 2006, pp. 1–6.

[191] ——, "A survey of spectrum sensing algorithms for cognitive radio applications," *IEEE Communications Surveys Tutorials*, vol. 11, no. 1, pp. 116–130, 2009.

[192] T. Yucek, "Channel, spectrum, and waveform awareness in OFDM-based cognitive radio systems," *Graduate School Theses and Dissertations, University of South Florida, USA*, Jan. 2007. [Online]. Available: http://scholarcommons.usf.edu/etd/2425

[193] H. J. M. Yuko Okamoto, "A novel algorithm for calculation of the extreme eigenvalues of large hermitian matrices," *Computer Physics Communications*, vol. 76, no. 2, pp. 191–202, 1993.

[194] S. Zahabi, A. Tadaion, and S. Aissa, "Neyman-pearson cooperative spectrum sensing for cognitive radio networks with fine quantization at local sensors," *IEEE Transactions on Communications*, vol. 60, no. 6, Jun. 2012.

[195] Y. Zeng, C. Koh, and Y.-C. Liang, "Maximum eigenvalue detection: Theory and application," in *IEEE International Conference on Communications, 2008. ICC '08*, May 2008, pp. 4160–4164.

[196] Y. Zeng and Y.-C. Liang, "Eigenvalue-based spectrum sensing algorithms for cognitive radio," *IEEE Transactions on Communications*, vol. 57, no. 6, pp. 1784–1793, Jun. 2009.

[197] ——, "Spectrum-sensing algorithms for cognitive radio based on statistical covariances," *IEEE Transactions on Vehicular Technology*, vol. 58, no. 4, pp. 1804–1815, May 2009.

[198] Y. Zeng, Y.-C. Liang, A. Hoang, and R. Zhang, "A review on spectrum sensing for cognitive radio: Challenges and solutions," *EURASIP Journal on Advances in Signal Processing*, vol. 2010, no. 1, p. 381465, Jan. 2010. [Online]. Available: http://asp.eurasipjournals.com/content/2010/1/381465/abstract

[199] Y. Zeng, Y.-C. Liang, and R. Zhang, "Blindly combined energy detection for spectrum sensing in cognitive radio," *IEEE Signal Processing Letters*, vol. 15, pp. 649–652, 2008, 00105.

[200] Y. Zhang, "Resource allocation for OFDM-based cognitive radio systems," 2008. [Online]. Available: http://circle.ubc.ca/handle/2429/2828

[201] Z. Zhang, Q. Yang, L. Wang, and X. Zhou, "A novel hybrid matched filter structure for IEEE 802.22 standard," in *2010 IEEE Asia Pacific Conference on Circuits and Systems (APCCAS)*, Dec. 2010.

[202] Q. Zou, S. Zheng, and A. Sayed, "Cooperative sensing via sequential detection," *IEEE Transactions on Signal Processing*, vol. 58, no. 12, pp. 6266–6283, Dec. 2010.

PUBLICATION 1

Sener Dikmese, Paschalis C. Sofotasios, Tero Ihalainen, Markku Renfors and Mikko Valkama, "Efficient Energy Detection Methods for Spectrum Sensing under Non-Flat Spectral Characteristics," *IEEE Journal on Selected Areas in Communications (JSAC)*, DOI:10.1109/JSAC.2014.236-1074, Oct. 2014.

Efficient Energy Detection Methods for Spectrum Sensing under Non-Flat Spectral Characteristics

Sener Dikmese, *Student Member, IEEE*, Paschalis C. Sofotasios, *Member, IEEE*, Tero Ihalainen, *Member, IEEE*, Markku Renfors, *Fellow, IEEE* and Mikko Valkama, *Member, IEEE*

***Abstract*—Cognitive radio is an emerging wireless technology that is capable of coordinating efficiently the use of the currently scarce spectrum resources and spectrum sensing constitutes its most crucial operation. The present work proposes wideband multichannel spectrum sensing methods utilizing fast Fourier transform or filter bank based methods for spectrum analysis. Fine-grained spectrum analysis facilitates optimal energy detection in practical scenarios where the transmitted signal, channel frequency response, and/or receiver frequency response do not follow the commonly assumed boxcar model which typically assumes, among others, narrowband communications with flat spectral characteristics. Such sensing schemes can be tuned to the spectral characteristics of the target primary user signals, allowing simultaneous sensing of multiple target primary signals with low additional complexity. This model is also extended for accounting for the specific scenario of detecting a reappearing primary user during secondary transmission, as well as in spectrum sensing scenarios where the frequency range of a primary user is unknown. Novel analytic expressions are derived for the corresponding probability of false alarm and probability of detection in each case while the useful concept of the area under the receiver operating characteristics curve is additionally introduced as a single scalar metric for evaluating the overall performance of the proposed spectrum sensing algorithms and scenarios. The derived expressions have a rather simple algebraic representation which renders them convenient to handle both analytically and numerically. The offered results are also validated extensively through comparisons with respective results from computer simulations and are subsequently employed in evaluating each technique analytically which provides meaningful insights that are anticipated to be useful in future deployments of cognitive radio systems.**

***Index Terms*—Cognitive radio, spectrum sensing, non-flat spectral characteristics, signal detection, radiometer, wideband communications, multichannel communications, AUC.**

Manuscript received January 5, 2014; revised May 15, 2014 and July 10, 2014. This work was supported in part by Tekniikan Edistamissaation (TES), GETA Graduate School, Tekes (the Finnish Funding Agency for Technology and Innovation) under the project ENCOR2 in the Trial Program, European Union FP7-ICT project EMPhAtiC under grant agreement no. 318362 and the Academy of Finland under the project 251138 "Digitally-Enhanced RF for Cognitive Radio Devices. Some elements of this paper were presented at CrownCom'10, Cannes, France and at IEEE WCNC'12, Paris, France.

S. Dikmese, M. Renfors and M. Valkama are with the Department of Electronics and Communications Engineering, Tampere University of Technology, FI-33101 Tampere, Finland (e-mail: {sener.dikmese; markku.renfors; mikko.e.valkama}@tut.fi)

P. C. Sofotasios was with the School of Electronic and Electrical Engineering, University of Leeds, LS2 9JT Leeds, UK. He is now with the Department of Electronics and Communications Engineering, Tampere University of Technology, 33101 Tampere, Finland and with the Department of Electrical and Computer Engineering, Aristotle University of Thessaloniki, 54124 Thessaloniki, Greece (e-mail: p.sofotasios@ieee.org).

T. Ihalainen is with Nokia Research, Nokia Technologies, FI-33720 Tampere, Finland (e-mail: tero.ihalainen@nokia.com)

Digital Object Identifier ...

I. Introduction

COGNITIVE radio (CR) is among the core prominent wireless technologies for the next generation of wireless communication systems namely, 5G. Its distinct feature is the capability to remarkably increase the utilization of the currently scarce spectrum resources by allowing unlicensed users to access unused licensed frequency bands opportunistically. This is achieved by identifying the presence or absence of unknown deterministic signals and deciding, accordingly, whether a primary licensed user (PU) is in active or idle state, respectively. Based on this decision, the corresponding secondary unlicensed user (SU) either remains silent, or proceeds in utilizing the unoccupied band [1], [2]. Therefore, it is evident that spectrum sensing (SS) constitutes the most critical operation in CR communications.

Energy detection (ED), also known as radiometry, has been the most popular SS method in both radar and CR systems thanks to its adequate performance and relatively simple practical realization [3], [4]. The majority of ED analyses typically employ simplistic scenarios and signal models where the entire frequency band under sensing contains either noise, or noise in addition with a PU information signal, both having constant power spectral density (PSD). Furthermore, ED is commonly formulated as a Neyman-Pearson type binary hypothesis testing problem, which is commonly modeled by the well-known chi-square, Gaussian or, in some cases, gamma type statistical distributions, see, e.g., [1]–[5] and the references therein.

It is widely known that the main limitation of basic ED is its inherent sensitivity to the knowledge of noise variance in the case of absent primary transmissions [6]. Multi-antenna sensing has been shown to provide robustness against noise uncertainty by exploiting the spatial correlation properties of the received energy [7], [8]. However, this approach has the drawback of increased hardware complexity and size, which often renders it impractical for several applications. Motivated by this, the present work focuses on proposing highly efficient SS techniques in the context of single-antenna sensing for ensuring that the involved complexity is kept at minimal level, thus achieving a rather adequate balance between performance and complexity. Furthermore, the offered results can be readily extended to cooperative sensing based applications, which is a highly effective method for ensuring acceptable SS performance and robustness in realistic wireless communication scenarios.

It is also recalled that several sensing methods which are shown to be robust against noise uncertainty effects, including

eigenvalue [9]–[13] and autocorrelation [8], [14] based methods, have substantially higher computational complexity and in most cases fail to reach the sensing performance of ED under moderate noise uncertainty and practical PU signal-to-noise ratio (SNR) levels [9]–[14]. Wideband multichannel sensing is capable of bringing various possibilities for calibrating the noise spectral density of the sensing receiver [15]–[19]. In this context, one obvious choice is to consider the spectral slot(s) with the lowest observed PSD as candidate(s) for white space, and use the corresponding PSD level as a reference for noise. This method can be generalized by searching for time-frequency zones with minimum PSD levels for using them as noise reference. For these reasons, we consider important to refine the analytical tools related to ED methods beyond the simplistic signal models and sensing scenarios that are commonly considered in the literature.

It is noted that receivers are commonly assumed to have an ideal frequency response while flat wireless channels are usually considered. Based on these models, numerous investigations have been reported in the context of additive-white-gaussian-noise (AWGN), fading channels, diversity techniques and collaborative detection, see, e.g., [20]–[34] and the references therein. Nevertheless, in realistic communication scenarios the sensing receiver has non-ideal frequency response, the transmitted PSD is not flat, the frequency-selective multipath channel has an effect on the received PU PSD and the sensing time window does not necessarily coincide with the frequency channel and time period of the PU transmission. Furthermore, it is often the case that a PU re-appears during SU transmission while the frequency range of a PU might be unknown. Motivated by these, the aim of the present work is to thoroughly investigate the aforementioned effects on the performance of energy detection and quantify the corresponding deviations from the ideal model. Specifically, the technical contributions of the paper are summarized below:

- We address the case where the sensing window in time-frequency domain contains both a zone where the PU signal is present and a zone where the PU signal is absent. This accounts for the critical scenarios where a PU re-appears and the analysis is performed by means of mixed test statistics which are subsequently employed in quantifying the corresponding effects in the detector's performance. Sliding window based SS is also addressed as an effective method for detecting a re-appearing PU. A semi-analytical performance analysis method for sliding window based ED is developed and the involved tradeoffs between sensing delay and sensitivity are highlighted.
- We analyze the case of non-flat PU spectrum focusing on a realistic Bluetooth based communication scenario as an indicative case study. Optimum weights are derived for fast Fourier transform (FFT) and filter bank based sensing where the PU signal band is divided into approximately flat subbands. Subsequent analysis reveals that using constant weights can practically achieve a similar performance when the subbands are selected optimally. In this context, we provide a simple numerical method for evaluating the performance of practical vs. optimum sensing filter. We also demonstrate how to utilize the developed analytical methods for evaluating and optimizing time-domain filters for SS relating applications.
- We quantify the effect of a stationary frequency selective channel. It is shown that in the low SNR regime, such as in the range between -5 dB and -15 dB, frequency selectivity creates a minor effect on the sensing performance, which is primarily dependent upon the temporal variations of the total received signal power. On the contrary, it is shown that for SNR values above 0 dB, the frequency selectivity characteristics play a non-negligible role in the performance of ED.
- We propose a useful single-parameter performance metric for evaluating the proposed SS algorithms based on the concept of the area under the receiver operating characteristics (ROC) curve (AUC) [25]. Novel analytical expressions for the AUC are derived for all considered spectrum sensing scenarios. These expressions are validated extensively through comparisons with respective results from computer simulations and have a tractable algebraic representation that renders them convenient to handle both analytically and numerically.

The aforementioned contributions are proposed in the context of wideband, multimode sensing employing FFT or filter bank methods for the required spectrum analysis procedures. This corresponds to wideband heterogeneous dynamic spectrum use scenarios, where different types of PUs may coexist. It is noted that the present work extends substantially earlier analyses in [35]–[37] by representing them in the context of a unified framework which consists of significant elaborations and strengthening by deriving novel closed-form expressions for the corresponding probabilities of false alarm (P_{FA}) and probabilities of detection (P_D). It is also noted that the proposed approach for analyzing the case of non-flat PU spectrum is based on the same foundations as the Spectral Feature Detector in [7], [38]. However, it is considered that the proposed model is relatively more straightforward and provides rather simple analytical expressions that relate the required sample complexity with the sensing performance parameters (P_{FA}, P_D) for optimal or suboptimal SS schemes. In addition, the autocorrelation based scheme of [8] is the time-domain equivalent of these methods and a remarkable benefit of frequency domain methods is their flexibility in sensing multiple PU types alternatingly, or simultaneously in the case of multiband sensing. On the contrary, time-domain methods require flexible channelization filtering schemes which in case of multiband sensing increases significantly the corresponding complexity. It is also noted that the required calculation of a sizeable sample covariance matrix for autocorrelation based methods has significant computational complexity, which tends to be rather high compared to the complexity involved in FFT or filter bank based processing in frequency domain methods. Therefore, the present work provides meaningful insights in ED based SS methods as well as useful enhancements in the form of easy-to-use analytical or semi-analytical expressions for straightforward analytic performance evaluation. Furthermore, the proposed contributions result to several worthwhile

performance gains in certain scenarios and they facilitate the comparison of suboptimal/simplified sensing schemes with respect to their optimal counterparts.

The remainder of the paper is organized as follows: Section II revisits the ED model and the foundations of wideband, multi-mode sensing utilizing FFT or analysis filter bank (AFB) for spectrum analysis. The effects of various forms of frequency dependency in ED based SS are analyzed in Section III where analytic expressions for the corresponding P_{FA} and P_D measures are derived in closed-form. The concept of AUC is introduced in Section IV as a useful analytical tool for evaluating the performance of each proposed SS method. Finally, numerical results and detailed discussions are provided in Section V while closing remarks are given in Section VI.

II. Basic Energy Detection Schemes

A. Analytical model

Spectrum sensing is typically formulated by the following binary hypothesis testing problem,

$$\begin{aligned} \mathcal{H}_0 &: \; y[n] = w[n] \\ \mathcal{H}_1 &: \; y[n] = \overbrace{s[n] \otimes h[n]}^{x[n]} + w[n] \end{aligned} \tag{1}$$

where $y[n]$ is the complex signal observed by the sensing receiver with $s[n]$, $h[n]$ and $w[n]$ denoting the PU information signal, the channel impulse response and the zero-mean, complex, circularly symmetric, wide-sense stationary white Gaussian noise, respectively [1]. Therefore, under hypothesis $\mathcal{H}_0$, the PU is considered absent and $y[n]$ consists only of $w[n]$. On the contrary, under hypothesis $\mathcal{H}_1$ the transmitted wireless signal $x[n]$ is also present along with $w[n]$. Based on this, the test statistic for the energy detector is expressed as,

$$T(y) = \frac{1}{N} \sum_{n=0}^{N-1} \left| y[n] \right|^2 \tag{2}$$

with N denoting the length of the observation sequence, which is also referred to as sample complexity.

The distribution of the test statistic can be modeled by the Gaussian distribution, which has been shown extensively to be a rather tractable and accurate approach [6], [39]–[41]. To this end, the following formulation is straightforwardly deduced,

$$T(y)|_{\mathcal{H}_0} \sim \mathcal{N}\left(\sigma_w^2, \frac{\sigma_w^4}{N}\right) \tag{3}$$

and

$$T(y)|_{\mathcal{H}_1} \sim \mathcal{N}\left(\sigma_x^2 + \sigma_w^2, \frac{(\sigma_x^2 + \sigma_w^2)^2}{N}\right) \tag{4}$$

where σ_x^2 and σ_w^2 denote the variance of the transmitted signal and AWGN process, respectively, which are assumed to be statistically independent. Based on this and given that the instantaneous SNR is $\gamma = \sigma_x^2/\sigma_w^2$, the corresponding false alarm probability P_{FA} and detection probability P_D measures can be expressed as follows:

$$P_{FA} = \Pr(T(y) > \lambda | \mathcal{H}_0) = Q\left(\frac{\lambda - \sigma_w^2}{\sigma_w^2/\sqrt{N}}\right) \tag{5}$$

and

$$P_D = \Pr(T(y) > \lambda | \mathcal{H}_1) = Q\left(\frac{\lambda - \sigma_w^2(1+\gamma)}{\sigma_w^2(1+\gamma)/\sqrt{N}}\right) \tag{6}$$

respectively, where $Q(\cdot)$ is the Gaussian Q−function and λ denotes the predefined energy threshold. The variance of the PU information signal is practically unknown and thus, the value of λ is determined by the assumed noise variance and targeted false alarm probability as follows,

$$\lambda = \sigma_w^2 \left(1 + \frac{Q^{-1}(P_{FA})}{\sqrt{N}}\right) \tag{7}$$

where $Q^{-1}(\cdot)$ denotes the inverse Gaussian Q−function [44]. Furthermore, the sample complexity N is determined under the constraint of acceptably low missed detection probability, $P_{MD} = 1 - P_D$, at the minimum PU power level. Based on this and after some algebraic manipulations, the required sensing time in samples can be expressed in terms of P_{FA}, $P_{MD} = 1 - P_D$ and γ, as [5],

$$\hat{N} = \frac{\left[Q^{-1}(P_{FA}) - Q^{-1}(P_D)(1+\gamma)\right]^2}{\gamma^2} \tag{8}$$

which is evaluated numerically rather straightforwardly.

B. FFT and filter bank based schemes for multiband sensing

It is recalled that the majority of SS methods are proposed assuming narrowband communication scenarios. Nevertheless, in realistic communication systems wireless channels are often wideband and this is particularly the case in emerging wireless technologies which are expected to satisfy substantially increased quality of service requirements. As a result, developing effective techniques for wideband SS scenarios is undoubtedly useful for future CR deployments and services. To this end, efficient and robust wideband multiband ED based methods are proposed in this sub-section as alternative solutions for effective SS in CR communications. Furthermore, it is shown that the proposed methods allow PU signals and multiple potential spectral gaps to be tested simultaneously in an efficient and flexible manner by averaging the output samples of an FFT or AFB based spectrum analyzer.

Most emerging broadband wireless technologies are based on multicarrier modulation such as, cyclic prefix based orthogonal frequency division multiplexing (CP-OFDM). Multicarrier techniques are characterized by the simplicity and robustness of the receiver signal processing functions. However, alternative multicarrier techniques have been considered increasingly in recent developments. In this context, filter bank multicarrier (FBMC) techniques have demonstrated various potential benefits particularly in the field of CR communications [42], [43]. One important feature of multicarrier systems is that existing signal processing blocks, i.e. the FFT of an OFDM receiver or the AFB of an FBMC receiver, can be also exploited for SS purposes. A block diagram for FFT or AFB based ED algorithms with weighting process is depicted in Fig. 1. It is also recalled that the main benefits of FBMC waveforms over OFDM are the good spectral localization of the transmitted signal spectrum and the high frequency

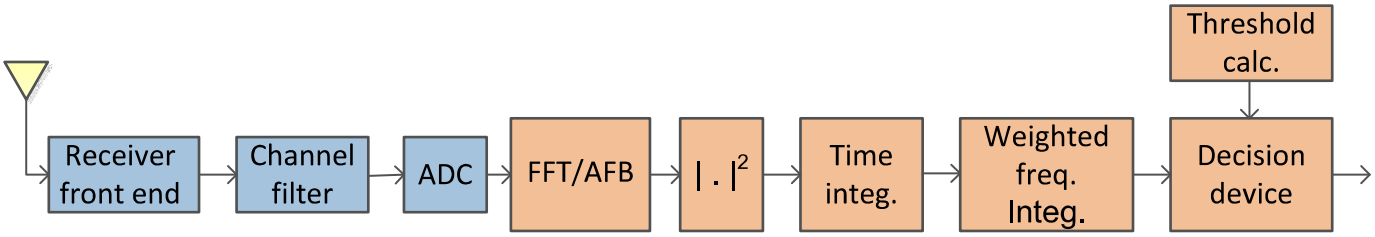

Fig. 1: Block diagram for energy detection with FFT/AFB based spectrum analysis.

selectivity of receiver signal processing. These features assist in improving the interference control, particularly in scenarios where users are not precisely synchronized to each other. In CR systems, the benefits of AFB are prominent in high-dynamic-range scenarios, such as in SS in the presence of strong transmissions at nearby frequencies. This is a critical scenario since the spectrum leakage of basic FFT processing appears to degrade significantly the sensing performance [35], [42], [43].

The present analysis focuses on SS in a wideband multichannel receiver, where ED is performed at subband level at the output of an FFT or AFB, which is used for splitting the received signal into relatively narrow signal bands. The output of these blocks is expressed as $y_k[m]$, where $k = 0, \ldots, K-1$ is the subband index and m is the subband sample index. Typically, the sampling rate of the subbands is equal to the analog-to-digital converter (ADC) sampling rate over the number of subbands in the filter bank, K. However, in FBMC/OQAM (offset quadrature amplitude modulation) systems, 2x oversampling of the subband signals is commonly considered [45], [46]. In the context of SS the subband signals can be expressed as follows,

$$y_k[m] = w_k[m] \qquad \mathcal{H}_0 \tag{9}$$

and

$$y_k[m] = x_k[m] + w_k[m] \qquad \mathcal{H}_1 \tag{10}$$

where $x_k(m) \cong H_k s_k(m)$ is the PU information signal at the m^{th} FFT or AFB output sample in subband k, H_k is the complex gain of subband k, and $w_k[m]$ is the corresponding noise sample. Furthermore, as in conventional ED, it is assumed that $w_k[m] \sim \mathcal{N}(0, \sigma^2_{w,k})$ and $x_k[m] \sim \mathcal{N}(0, \sigma^2_{x,k})$, with $\sigma^2_{x,k}$ denoting the PU signal variance in subband k. Thus, it follows that $\sigma^2_w/K \simeq \sigma^2_{w,k}$. The integrated test statistic over multiple subbands and over certain observation time is expressed as,

$$T(y_{m_0,k_0}) = \frac{1}{N_t N_f} \sum_{k=k_0-\lfloor N_f/2 \rfloor}^{k_0+\lceil N_f/2 \rceil - 1} \sum_{m=m_0-N_t+1}^{m_0} |y_k[m]|^2 \tag{11}$$

where N_f and N_t are the averaging filter lengths in frequency domain and time domain, respectively. According to Parseval's theorem, when a spectral component is entirely captured by the subband integration range, FFT based subband integration and full-band time-domain integration over the same time interval yield the same test statistics.

Assuming that the PU spectrum is flat over the sensing band, the corresponding probability distribution of the test statistic can be modeled as follows,

$$T(y_{m_0,k_0})|\mathcal{H}_0 \sim \mathcal{N}\left(\sigma^2_{w,k}, \frac{\sigma^4_{w,k}}{N_t N_f}\right) \tag{12}$$

and

$$T(y_{m_0,k_0})|\mathcal{H}_1 \sim \mathcal{N}\left(\sigma^2_{x,k} + \sigma^2_{w,k}, \frac{(\sigma^2_{x,k} + \sigma^2_{w,k})^2}{N_t N_f}\right) \tag{13}$$

which yields straightforwardly,

$$P_{FA} = \Pr(T(y) > \lambda | \mathcal{H}_0) = Q\left(\frac{\lambda - \sigma^2_{w,k}}{\sigma^2_{w,k}/\sqrt{N_f N_t}}\right) \tag{14}$$

and

$$P_D = \Pr(T(y) > \lambda | \mathcal{H}_1) = Q\left(\frac{\lambda - \sigma^2_{w,k}(1+\gamma_k)}{\sigma^2_{w,k}(1+\gamma_k)/\sqrt{N_f N_t}}\right) \tag{15}$$

respectively where,

$$\lambda = \sigma^2_{w,k}\left(1 + \frac{Q^{-1}(P_{FA})}{\sqrt{N_f N_t}}\right). \tag{16}$$

Furthermore, $\gamma_k = \sigma^2_{x,k}/\sigma^2_{w,k}$ denotes the subband-wise SNR. FFT/AFB processing allows tuning the sensing frequency band to the expected band of the PU signal, as well as sensing multiple PU bands simultaneously. It is subsequently shown that the subband integration process can be optimized to the PU characteristics. In addition, several candidate PU's, with different spectral characteristics and possibly overlapping spectra, can be optimally sensed simultaneously.

III. Energy Detection in the Presence of Frequency Variability

In CR based communications, SS is fundamentally performed for both assisting opportunistic access to SUs and monitoring the spectrum during SU operation for accounting robustly for a possible reappearance of a PU. In this context, multicarrier transmission techniques have a high degree of commonality between receiver processing and SS, since selected time-frequency zones can be dedicated to spectral monitoring purposes irrespectively of conventional data transmission [36].

However, in spite of its operational importance and performance effects, the specific case of a re-appearing PU has not been analyzed in the open technical literature. Motivated by this, this section first proposes band edge detection and transmission burst detection. In this context, we address the

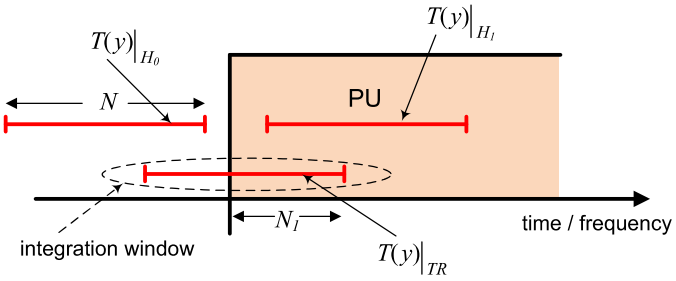

Fig. 2: Distribution analysis of the transient phase test statistic.

realistic mixed statistics case where the sensing window in time-frequency domain includes both a zone where the PU signal plus noise are present and a zone where only the noise is present. Then, sliding window based spectrum sensing (SW-ED) is proposed for handling such sensing situations effectively.

Furthermore, in this section we also develop novel generic tractable models for ED in cases where the PU information signal and/or noise are *non-white* within the sensing frequency band. More specifically, it is clear that the spectrum of a PU signal is affected by the spectrum of the transmitted waveform, channel frequency response and the sensing receiver filter, whereas the spectrum of the channel noise is only dependant upon the receiver filter frequency response.

A. Band Edge Detection and Transmission Burst Detection

It is recalled that a typical assumption in the vast majority of SS investigations is that the PU is strictly either absent or active during the sensing period and that the center frequency and bandwidth of the PU information signal are known. Nevertheless, in realistic communication scenarios it is often the case that either the PU re-activates during the measurement period or the sensing frequency band fails to match the band of the PU signal [47]. As a consequence, only a fraction of the integration window matches the time-frequency zone of the PU activity. Motivated by this, band edge detection and transmission burst detection is proposed as an effective method for detecting re-appearing PU signals. The corresponding analysis is performed by means of *mixed text statistics* which are subsequently employed in quantifying the corresponding effects in the performance of the energy detector.

The considered transient scenario, in time or frequency direction, is depicted in Fig. 2 along with the associated test statistic distributions [36]. The distribution of the transient phase test statistic can be obtained by virtually splitting the integration window into two distinct sub-windows; the one contains the observation samples corresponding to the idle state of the PU, $N - N_1$ samples, whereas the other contains the remaining N_1 samples. Based on this, the distributions of the corresponding sample subsets within these virtual sub-windows can be expressed as follows[1]

$$\mathcal{N}\left(\sigma_w^2, \frac{\sigma_w^4}{N-N_1}\right) \tag{17}$$

and

$$\mathcal{N}\left(\sigma_x^2+\sigma_w^2, \frac{(\sigma_x^2+\sigma_w^2)^2}{N_1}\right) \tag{18}$$

respectively. It is noted that the overall sequence of N samples can be interpreted as a linear combination of these independent normal random variables using relative weights of $(N - N_1)/N$ and N_1/N, respectively. Therefore, $X_1 \sim \mathcal{N}(\mu_1, \sigma_1^2)$ and $X_2 \sim \mathcal{N}(\mu_2, \sigma_2^2)$ and with the aid of the standard property of the normal distribution,

$$aX_1 + bX_2 \sim \mathcal{N}(a\mu_1 + b\mu_2, a^2\sigma_1^2 + b^2\sigma_2^2) \tag{19}$$

the following mixture-distribution is deduced,

$$T(y)\big|_{TR} \sim \mathcal{N}\left(\sigma_w^2 + \frac{N_1}{N}\sigma_x^2, \frac{N-N_1}{N^2\sigma_w^{-4}} + \frac{(\sigma_x^2+\sigma_w^2)^2}{N^2N_1^{-1}}\right). \tag{20}$$

The probability of detecting the presence of a PU signal during the transient phase is obtained by the tail probability towards $+\infty$ over the mixture distribution in (20), namely,

$$P_{D,TR} = Pr(T(y)|_{TR} > \lambda). \tag{21}$$

To this effect, the probability of false alarm and probability of detection can be expressed as

$$P_{FA} = Pr(T(y)|_{\mathcal{H}_0} > \lambda) \tag{22}$$

and

$$P_D = Pr(T(y)|_{\mathcal{H}_1} > \lambda) \tag{23}$$

respectively. Notably, after some algebraic manipulations the P_{FA} becomes identical to (5) whereas, the P_D is given by,

$$\begin{aligned} P_D &= \Pr(T(y)|_{\mathrm{TR}} > \lambda) \\ &= Q\left(\frac{\lambda N\sigma_w^{-2} - N - N_1\gamma}{\sqrt{N-N_1+N_1(1+\gamma)^2}}\right) \\ &= Q\left(\frac{\sqrt{N}Q^{-1}(P_{FA}) - \gamma N_1}{\sqrt{N-N_1+N_1(1+\gamma)^2}}\right). \end{aligned} \tag{24}$$

It is noted that $\gamma = \sigma_x^2/\sigma_w^2$ denotes the overall PU SNR and to the best of the Authors' knowledge (24) has not been previously reported in the open technical literature.

B. Sliding Window-Based Spectrum Sensing

This subsection is devoted to proposing SW-ED as an effective solution for detecting a re-appearing PU signal. To this end, a semi-analytical performance evaluation technique for SW-ED is developed along with a detailed analysis on the respective tradeoffs between detection delay and sensitivity.

For simplicity, it is assumed that the sensing receiver is capable of monitoring the target frequency channel continuously. This could be reached, for example, if the secondary system leaves a slot of the frequency channel unused for spectrum

[1]For the sake of notational simplicity, Sections III-A and III-B are formulated in a basic single-band energy detection setting.

sensing purposes [36]. It is recalled that SW-ED uses a sliding window of constant length N. Therefore, for a time instant $n+1$ the test statistic is obtained effectively as follows:

$$T_{n+1}(y) = T_n(y) + \frac{|y[n+1]|^2 - |y[n+1-N]|^2}{N}. \quad (25)$$

Figure 3 illustrates SW-ED in action. It is important to notice that even though the test statistic at any particular time instance follows the corresponding statistical model adequately, the probability of exceeding the decision threshold within a time interval grows with the length of the interval. Therefore,

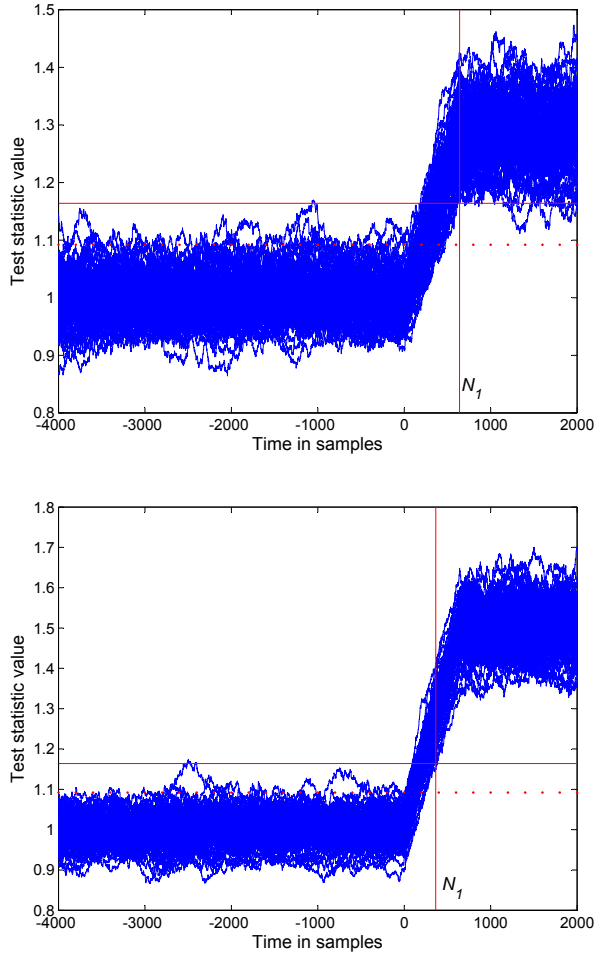

Fig. 3: Sliding window energy detection in action: 100 instances of SW processing with block length of $N = 640$ for -5.5 dB PU SNR (upper) and -3 dB SNR (lower). The horizontal lines indicate the thresholds for $P_{FA} = 0.01$ in basic single-shot ED (dotted) and in SW-ED with 12800 samples (solid). Time instant 0 corresponds to the beginning of the PU transmission and the vertical line indicates the first time instance (N_1) when $P_D = 0.99$ is reached.

the decision threshold has to be increased, in comparison to basic single-window sensing, in order to reach reasonable probability of false alarm. The special case of multiple (B) non-overlapping ED windows is rather convenient to handle, since the probability of not exceeding the threshold in any of the sensing windows can be expressed as,

$$\begin{aligned} 1 - P_{FA}^{(B)} &= \Pr\left(\max_{k=1}^{B} T^k(y) < \lambda\right) \\ &= \prod_{k=1}^{B} \Pr\left(T^{(k)}(y) < \lambda\right) \\ &= \left(1 - P_{FA}^{(1)}\right)^B. \end{aligned} \quad (26)$$

In SW-ED, consecutive outputs are strongly correlated, and to the best of the Authors' knowledge, no sufficient analytical models that address this scenario exist. Based on this, we present a numerical approach for analyzing the performance of this method by assuming the following simplistic scenario and sensing principles: (i) There are no on-going PU transmissions in the beginning of the sensing process; (ii) The channel is deemed to be occupied once the SW-ED output exceeds the threshold, even for a single sample; (iii) The detection delay is defined as the time duration from the beginning of the PU transmission to the time that the instantaneous detection probability exceeds the target value. An estimate for the sensing delay (N_1 in Fig. 3) for a given block length N and SNR γ is determined semi-analytically with the aid of (24) as follows:

- For a given P_{FA}, determine the threshold $\lambda_{N,B}$ so that the experimental probability of SW-ED exceeding the threshold over the whole frame of BN input samples equals the target P_{FA}.
- With $\lambda = \lambda_{N,B}$ in (24), find the minimum N_1 such that the target P_D is reached. This value of N_1, i.e. sensing delay, can be obtained form (24) as a root of a second order polynomial.

In Section V-B, it is shown that sliding window based SS is an effective method for detecting PUs with unknown time of appearance.

C. Effects of non-flat primary user spectrum

Novel optimum and constant weighting process based multi-band spectrum sensing techniques are proposed for reducing the involved complexity and required number of samples under non-flat spectral characteristics.

After the receiver front-end and ADC in the flexible multi-band sensing scheme of Fig. 1, FFT or AFB is performed for splitting the signal into relatively narrow subbands. Depending on the bandwidth of the candidate PU signal, a number of consecutive subbands is combined in the sensing process, typically after weighting, for optimizing the energy detection performance for non-flat PU signals. The weighting process can be performed in two manners: $i)$ Constant weights are optimal for a PU signal with flat power spectrum and upon effective selection of the number of subbands, they may also provide a good approximation for a non-flat spectrum. This is also the standard selection when no prior information of the PU spectrum is available; $ii)$ Optimized weights can be determined in case of prior knowledge of the PU power spectrum. Naturally, a frequency selective channel affects the spectrum of the received signal, but it is not realistic to assume knowledge of the channel characteristics. On the contrary, if

the wireless channel is assumed flat, the shape of the power spectrum of the received signal is identical to that of the transmitted signal and optimized weighting process can be considered realistically.

Under both $\mathcal{H}_0$ and $\mathcal{H}_1$, the test statistics are represented as a sum of independent Gaussian variables with different variances. Based on this, the probability distribution of the test statistic T_k for center frequency k and arbitrary weighting coefficients can be expressed as follows,

$$f(T_k)|_{\mathcal{H}_0} \sim \mathcal{N}\left(\sum_{\kappa=k-\overline{N_f}}^{k+\overline{N_f}} g_k\sigma_{w,k}^2, \sum_{\kappa=k-\overline{N_f}}^{k+\overline{N_f}} \frac{g_k^2\sigma_{w,k}^4}{N_tN_f}\right) \quad (27)$$

and

$$f(T_k)|_{\mathcal{H}_1} \sim \mathcal{N}\left(\sum_{\kappa=k-\overline{N_f}}^{k+\overline{N_f}} \frac{\sigma_{x,k}^2+\sigma_{w,k}^2}{g_k^{-1}}, \sum_{\kappa=k-\overline{N_f}}^{k+\overline{N_f}} \frac{(\sigma_{x,k}^2+\sigma_{w,k}^2)^2}{N_tN_fg_k^{-2}}\right) \quad (28)$$

where $N = N_tN_f$ is the overall sample complexity, as in Section II-B. For the sake of notational simplicity, we assume that the value of the window size in frequency domain is odd, i.e., $N_f = 2\overline{N_f}+1$. It is recalled here that the integration in frequency domain takes the weighted average of the time filter outputs, with g_k denoting the real-valued weight for subband k with PU signal power $\sigma_{x,k}^2$. In what follows, we address the problem of optimizing the subband weights.

For arbitrary weight values, the corresponding false alarm probability P_{FA} is given by [35],

$$P_{FA} = Q\left(\frac{\lambda - \sum_{\kappa=k-\overline{N_f}}^{k+\overline{N_f}} g_k\sigma_{w,k}^2}{\sqrt{\sum_{\kappa=k-\overline{N_f}}^{k+\overline{N_f}} \frac{g_k^2\sigma_{w,k}^4}{N}}}\right). \quad (29)$$

In the same context and recalling that $\gamma_k = \sigma_{x,k}^2/\sigma_{w,k}^2$, the probability of detection P_D with arbitrary weight values can be expressed as follows,

$$P_D = Q\left(\frac{\lambda - \sum_{\kappa=k-\overline{N_f}}^{k+\overline{N_f}} g_k\sigma_{w,k}^2(1+\gamma_k)}{\sqrt{\sum_{\kappa=k-\overline{N_f}}^{k+\overline{N_f}} \frac{g_k^2\sigma_{w,k}^4(1+\gamma_k)^2}{N}}}\right). \quad (30)$$

By equating λ in (29) and (30), the corresponding energy threshold λ can be determined by,

$$\lambda = Q^{-1}\Big(P_{FA}\Big)\sqrt{\sum_{\kappa=k-\overline{N_f}}^{k+\overline{N_f}} \frac{g_k^2\sigma_{w,k}^4}{N}} + \sum_{\kappa=k-\overline{N_f}}^{k+\overline{N_f}} g_k\sigma_{w,k}^2 \quad (31)$$

$$= Q^{-1}\Big(P_D\Big)\sqrt{\sum_{\kappa=k-\overline{N_f}}^{k+\overline{N_f}} \frac{g_k^2(1+\gamma_k)^2}{N\sigma_{w,k}^{-4}}} + \sum_{\kappa=k-\overline{N_f}}^{k+\overline{N_f}} \frac{1+\gamma_k}{g_k^{-1}\sigma_{w,k}^{-2}}.$$

Likewise, the minimum required sample complexity, $N = N_tN_f$, can be determined with the aid of (32) (top of the next page) which is expressed as a function of P_{FA}, P_D, w_k and γ_k.

It is noted that the required time record length N_t is determined according to the targeted minimum detectable PU power level. When employing optimum weighting coefficients, the frequency block length N_f should be selected to include all subbands that essentially contribute to the test statistics. Including extra subbands increases the involved complexity, yet it should not harm the sensing performance as the corresponding weights become rather small.

By also assuming that the weights are normalized for constant noise power level $\sum_i g_i = 1$, i.e., the first term is maximized by choosing

$$g_k = \frac{\sigma_{x,k}^2}{\sum_{\kappa=k-\overline{N_f}}^{k+\overline{N_f}} \sigma_{x,k}^2} = \frac{\sigma_{x,k}^2}{\sigma_x^2} = \frac{\gamma_k}{\gamma}. \quad (33)$$

In any realistic case, with $P_D > 0.5$ also the second term is positive and it is maximized by choosing

$$g_k = \frac{\gamma_k}{S(1+\gamma_k)^2} \quad (34)$$

where

$$S = \sum_{\kappa=k-\overline{N_f}}^{k+\overline{N_f}} \frac{\gamma_k}{(1+\gamma_k)^2} \quad (35)$$

denotes a normalization coefficient. The proofs are provided in Appendix I. Depending on the values of P_D and P_{FA}, the optimum weighting coefficients are between these two cases. For $P_{FA} << 1-P_D$ the first term dominates, whereas for $P_{FA} >> 1-P_D$ second term dominates. It can be numerically verified, that both (33) and (34) are very tight approximations for the optimum weights. Henceforth, equation (33) is used for simplicity. As an example, we consider the case of Raised Cosine and Square Root Raised Cosine filters, with different roll-off factors (10 % to 100 %), $P_D = 0.999$ and $P_{FA} = 0.1$, and PU SNR between 0 and -10 dB. In this case the right hand side term of (32) clearly dominates. Using weights based on (33), the required sample complexities obtained from (32) are no more than 3% higher than when using weights obtained from (34). Additional numerical results are presented subsequently for the Bluetooth scenario in Section V-D.

Evidently, the proposed expressions can be considered as approximations of matched filtering [48] in the sense that the squared magnitude response of the sensing filter is ideally the same as the transmitted power spectrum [5]. Alternatively, this can be viewed as maximum ratio combining of statistically independent variables since both models result to the maximization of the SNR in the presence of PU. This model is also consistent with the optimal spectral feature detection model in [38].

It is also meaningful to consider the resulting gain when using optimum weights instead of constant weights, which would be a conceptually simpler approach even though the difference in implementation complexity is minor. In case of constant weights, it is important to select the optimum number of subbands as subbands with small PU power affect the noise

$$\hat{N} = \frac{\left[Q^{-1}\left(P_{FA}\right)\sqrt{\sum_{\kappa=k-\overline{N_f}}^{k+\overline{N_f}} g_k^2} - Q^{-1}\left(P_D\right)\sqrt{\sum_{\kappa=k-\overline{N_f}}^{k+\overline{N_f}} g_k^2(1+\gamma_k)^2}\right]^2}{\left[\sum_{\kappa=k-\overline{N_f}}^{k+\overline{N_f}} g_k\gamma_k\right]^2}$$
$$= \left[Q^{-1}\left(P_{FA}\right)\sqrt{\frac{\sum_{\kappa=k-\overline{N_f}}^{k+\overline{N_f}} g_k^2}{\left(\sum_{\kappa=k-\overline{N_f}}^{k+\overline{N_f}} g_k\gamma_k\right)^2}} - Q^{-1}\left(P_D\right)\sqrt{\frac{\sum_{\kappa=k-\overline{N_f}}^{k+\overline{N_f}} g_k^2(1+\gamma_k)^2}{\left(\sum_{\kappa=k-\overline{N_f}}^{k+\overline{N_f}} g_k\gamma_k\right)^2}}\right]^2. \quad (32)$$

variance under $\mathcal{H}_0$, but can also decrease the SNR under $\mathcal{H}_1$ and thus, reduce the corresponding sensing performance. Given the PSD of the PU, the optimum number of subbands can be determined numerically with the aid of (32) for target values of P_{FA}, P_D, and PU SNR.

D. Frequency selectivity effects

It is widely known that the majority of SS techniques focus on the AWGN scenario assuming a flat wireless channel. Nevertheless, frequency selective channels are usually encountered in communication scenarios and thus, they need to be adequately considered. Based on this, novel analytical expressions are derived for multiband ED based SS techniques under frequency selective channels. Capitalizing on this, the frequency selectivity effects are subsequently quantified and the corresponding detection performance is evaluated in detail for different SNR values. To this end, it is firstly recalled that $\gamma = \sigma_x^2/\sigma_w^2$ and $\gamma_k = \sigma_{x,k}^2/\sigma_{w,k}^2$ denote the overall PU SNR and the subband-wise SNR's, respectively. Then, we assume that the channel amplitude responses of the subbands, F_k, satisfy the following relationship,

$$\sum_{k=1}^{N_f} F_k^2 = N_f \quad (36)$$

which basically indicates that the received PU signal power is assumed to be constant. Based on this and given that $\gamma_k = F_k\gamma$, the test statistics in (12) can be extended for the case of frequency selective channels, namely,

$$T(y)|_{\mathcal{H}_0} \sim \mathcal{N}\left(\sigma_w^2, \frac{\sigma_w^4}{N_t N_f}\right) \quad (37)$$

and

$$T(y)|_{\mathcal{H}_1} \sim \mathcal{N}\left(\sigma_s^2+\sigma_w^2, \frac{\beta_{ch}}{N_t N_f}(\sigma_s^2+\sigma_w^2)^2\right) \quad (38)$$

where,

$$\beta_{ch} = \frac{1}{N_f}\sum_{k=1}^{N_f}\frac{(\sigma_{x,k}^2+\sigma_{w,k}^2)^2}{(\sigma_x^2+\sigma_w^2)^2} = \frac{1}{N_f}\sum_{k=1}^{N_f}\frac{(1+F_k^2\cdot\gamma)^2}{K^2(1+\gamma)^2}. \quad (39)$$

The corresponding P_{FA} is identical to (14); likewise, the corresponding P_D is similar to (15) and can be straightforwardly deduced by making the necessary change of variables yielding,

$$\begin{aligned} P_D &= \Pr(T(y) > \lambda|\mathcal{H}_1) \\ &= Q\left(\frac{\sqrt{N_f N_t}\left[\lambda - \sigma_w^2(1+\gamma)\right]}{\sigma_w^2(1+\gamma)\sqrt{\beta_{ch}}}\right) \\ &= Q\left(\frac{Q^{-1}(P_{FA}) - \gamma\sqrt{N_t N_f}}{(1+\gamma)\sqrt{\beta_{ch}}}\right). \end{aligned} \quad (40)$$

Evidently, the channel frequency response affects only the variance of the test statistic under $\mathcal{H}_1$. Hence, when SS is performed in the low PU SNR regime, the effect of the frequency selectivity on the energy detection performance tends to be insignificant. However, equations (39) and (40) can assist in quantifying this and evaluate whether the effect is significant when operating with highly frequency selective channels at relatively high SNR levels. Numerical results that demonstrate this effect are presented in detail in Section V.

IV. Area Under the ROC Curve

The Area Under the ROC Curve (AUC) is an alternative measure for assessing the performance of a detector and it has been used extensively in various areas of natural sciences and engineering. Its usefulness over the P_{FA} and P_D is that it constitutes a single-parameter measure that provides a better view of the overall detector performance. Specifically, using the conventional approach, the performance of energy detector based spectrum sensing techniques depends on the value of the corresponding P_D and P_{FA}. Based on this, the most typical method to analyze the performance is to fix one of the two measures and vary the other one. This provides useful insights on the detectors performance which are, yet, specific and do not always extend readily to additionally account for the overall performance of the detector. On the contrary, in the case of AUC there is only one parameter involved, which provides a better insight on the overall performance of the detector. Ideally, AUC approaches the value of 1, in which case $P_D = 1$ for any given value of P_{FA}. Practically, the useful values of the AUC are those that are greater than 0.65 with those greater than 0.85 considered good/acceptable.

The AUC in the presence of AWGN is defined as [25],

$$\text{AUC} = A(\gamma) \triangleq -\int_0^{\infty} P_D(\gamma,\lambda)\frac{\partial P_{FA}(\lambda)}{\partial \lambda}d\lambda. \quad (41)$$

In what follows, we derive novel analytic expressions for the AUC of each proposed SS method.

A. AUC for the Conventional ED

It is firstly noticed that the algebraic representation of (5) and (6) is identical as they are both expressed in terms of the Gaussian $Q-$function with shifted arguments. Based on this, the corresponding AUC has the following algebraic form,

$$\text{AUC} = -\int_0^{\infty} Q(ax-b)\frac{\partial Q(cx-d)}{\partial x}dx \quad (42)$$

where a, b, c and d are arbitrary reals. The derivative in (42) can be determined with the aid of the standard properties of the Gaussian $Q-$function, namely,

$$\frac{\partial Q(cx-d)}{\partial x} = -\frac{ce^{-\frac{(cx-d)^2}{2}}}{\sqrt{2\pi}}. \quad (43)$$

Therefore, upon substituting accordingly in (42) one obtains the following generic expression,

$$\text{AUC} = \mathcal{I}(a,b,c,d) = \frac{c}{\sqrt{2\pi}}\int_0^{\infty} Q(ax-b)e^{-\frac{(cx-d)^2}{2}}dx. \quad (44)$$

Evidently, determining AUC is subject to analytic evaluation of the above integral. To this end, the analytic expression in (45) is deduced (top of the next page), where $x!$ is the increasing factorial whereas $\Gamma(x)$ and ${}_1F_1(a,b,x)$ denote the Euler gamma function and the Kummer's confluent hypergeometric function, respectively [44].

Proof. The proof is provided in Appendix II. □

As a result, by making the necessary variable transformation and substituting in (45), the AUC for the conventional ED can be expressed as follows,

$$\text{AUC}\,|_{ED} = \mathcal{I}\left(\frac{\sqrt{N}}{\sigma_w^2(1+\gamma)}, \sqrt{N}, \frac{\sqrt{N}}{\sigma_w^2}, \sqrt{N}\right) \quad (46)$$

which to the best of the Author's knowledge, it has not been previously reported in the open technical literature.

B. AUC for the Proposed ED Techniques

Starting with the FFT and filter bank ED methods for multiband channels, it is observed that the algebraic forms of (14) and (15) are similar to those of (5) and (6), respectively. Hence, an analytic expression for the corresponding AUC can be readily obtained by setting $N = N_f N_t$ in (46), yielding,

$$\text{AUC}\,|_{WB} = \mathcal{I}\left(\frac{\sqrt{N_f N_t}}{\sigma_w^2(1+\gamma)}, \sqrt{N_f N_t}, \frac{\sqrt{N_f N_t}}{\sigma_w^2}, \sqrt{N_f N_t}\right). \quad (47)$$

Likewise, for the specific scenario of a re-appearing PU, the AUC can be deduced for

$$a = \frac{N}{\sigma_w^2\sqrt{N - N_1 + N_1(1+\gamma)^2}} \quad (48)$$

and

$$b = \frac{N + N_1\gamma}{\sqrt{N - N_1 + N_1(1+\gamma)^2}} \quad (49)$$

as well as $c = \sqrt{N}/\sigma_w^2$ and $d = \sqrt{N}$, which yields (50), at the top of the next page.

In the same context, by following the same procedure, the corresponding AUC for the ED in (29) and (30) is given by (51) (at the top of the next page). For the case of frequency selective channels, the following expression is deduced,

$$\text{AUC}\,|_{sel} = \mathcal{I}\left(\frac{\sqrt{N_t N_f}\sigma_w^{-2}}{\sqrt{\beta_{ch}}(1+\gamma)}, \sqrt{\frac{N_t N_f}{\beta_{ch}}}, \frac{\sqrt{N_t N_f}}{\sigma_w^2}, \sqrt{N_t N_f}\right). \quad (52)$$

To the best of the Authors' knowledge, the proposed expressions are novel.

V. Numerical Results

A. Basic Energy Detection

This Section is devoted to the analysis of the behavior and performance of the proposed ED methods starting with basic single-band AWGN scenario. To this end, Fig. 4 illustrates the AUC for a conventional ED under different values of the sample complexity N. It is shown that AUC is rather sensitive to variations of N while, as expected, the performance of the ED improves substantially as N increases. In the same context, the behavior of the multiband ED techniques is depicted in Fig. 5 and Fig. 6 in terms of the ROC and AUC measures, respectively. In the former, it is observed that the behavior of the ED is significantly dependent upon N_t and particularly by N_f. In the latter, it is noticed that the overall performance of the multiband ED is quite adequate in the positive and near-positive SNR regimes; yet, substantial increase of N_f and N_t is required, as expected, for achieving a similar result at moderately low SNR values. In all these comparisons, the analytical results match very well the simulations.

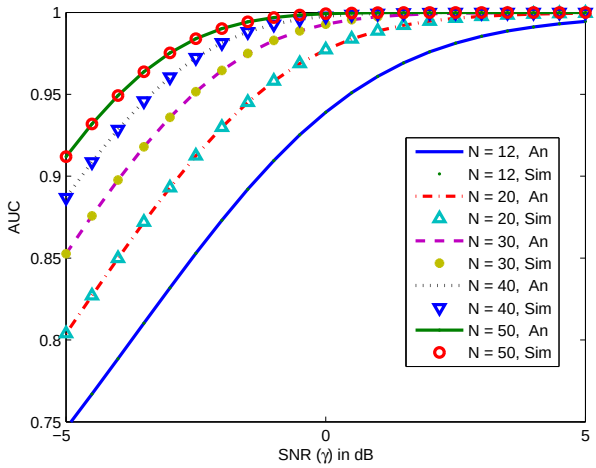

Fig. 4: Analytical and simulated AUC for the conventional ED for different values of sample complexity N.

$$\mathcal{I}(a,b,c,d)=\frac{Q(-d)}{2}-\sum_{l=0}^{\infty}\sum_{i=0}^{2l+1}\frac{(-1)^{3l-i+1}(2l)!b^{2l+1}a^{i}\left[d\Gamma\left(1+\frac{i}{2}\right)\,{}_1F_1\left(1+\frac{i}{2},\frac{3}{2},\frac{d^2}{2}\right)+\frac{\Gamma\left(\frac{i+1}{2}\right)}{\sqrt{2}}\,{}_1F_1\left(\frac{i+1}{2},\frac{1}{2},\frac{d^2}{2}\right)\right]}{2^{l-\frac{i}{2}+1}\pi l!i!b^{i}(2l-i+1)!c^{i}e^{\frac{d^2}{2}}}. \quad (45)$$

$$\text{AUC}\,|_{TR}=\mathcal{I}\left(\frac{N}{\sigma_w^2\sqrt{N-N_1+N_1(1+\gamma)^2}},\frac{N+N_1\gamma}{\sqrt{N-N_1+N_1(1+\gamma)^2}},\frac{\sqrt{N}}{\sigma_w^2},\sqrt{N}\right). \quad (50)$$

$$\text{AUC}\,|_{weights}=\mathcal{I}\left(\frac{\sqrt{N}}{\sqrt{\sum_{k=\kappa-\overline{N_f}}^{\kappa+\overline{N_f}}g_k^4\sigma_{w,k}^4\left(1+\gamma_k\right)^2}},\frac{\sqrt{N}\sum_{k=\kappa-\overline{N_f}}^{\kappa+\overline{N_f}}g_k^2\left(1+\gamma_k\right)}{\sqrt{\sum_{k=\kappa-\overline{N_f}}^{\kappa+\overline{N_f}}g_k^4\left(1+\gamma_k\right)^2}},\frac{\sqrt{N}}{\sqrt{\sum_{k=\kappa-\overline{N_f}}^{\kappa+\overline{N_f}}g_k^4\sigma_{w,k}^4}},\frac{\sqrt{N}\sum_{k=\kappa-\overline{N_f}}^{\kappa+\overline{N_f}}g_k^2}{\sqrt{\sum_{k=\kappa-\overline{N_f}}^{\kappa+\overline{N_f}}g_k^4}}\right). \quad (51)$$

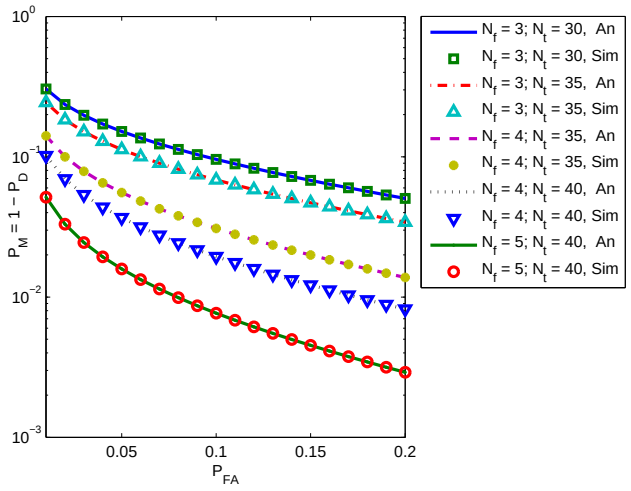

Fig. 5: Multiband ED ROC for $\gamma = -5$ dB and different values of N_f and N_t.

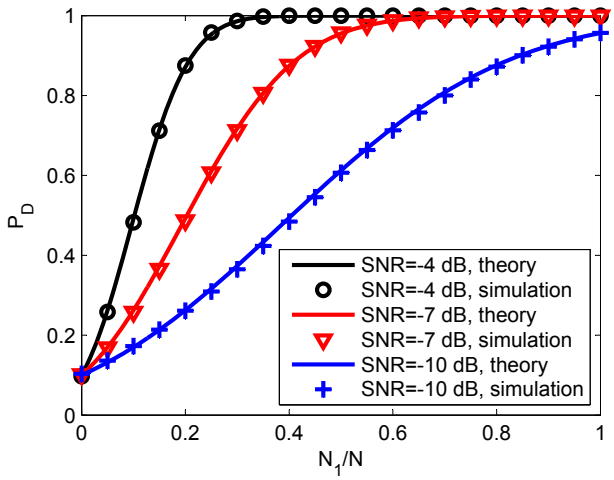

Fig. 7: Analytic and experimental transient phase detection for $P_{FA} = 0.1$, $N = 1000$ and 10000 independent trials.

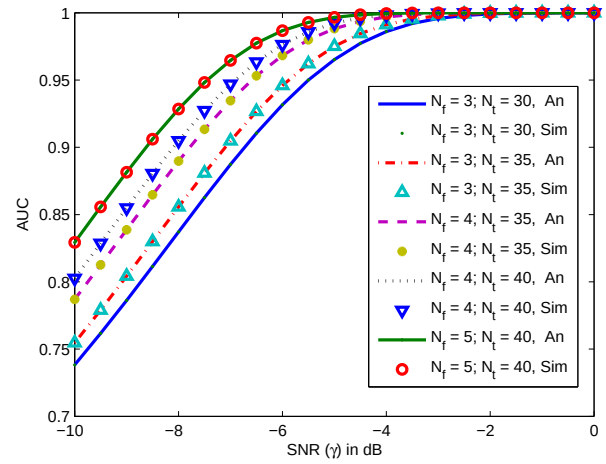

Fig. 6: Multiband ED AUC for different values of N_f and N_t.

B. Re-Appearing PU Case

The ED behavior in the case of a re-appearing PU and AWGN channel is demonstrated in Fig. 7 where it is shown that the proposed statistical model is in excellent agreement with the experimental transient phase ED performance. Evidently, the overall performance of the ED appears to reduce dramatically as the ratio N_1/N decreases and particularly in the case that $N_1/N < 0.5$. On the contrary, when $N_1/N > 0.75$, the performance of the ED is in general quite acceptable. The overall ED performance for this specific scenario is also illustrated in Fig. 8 and Fig. 9 in terms of the corresponding ROC and AUC, respectively, for $N = 1000$. Particularly the latter indicates that ED can achieve robust performance in the re-appearing PU scenario at non-negative SNR values as its value is higher than 0.95 as N_1 increases. Since N is common in all considered scenarios, Fig. 8 and Fig. 9 provide an indicative connection on the behavior between P_D and AUC. By recalling that AUC is a single-parameter performance

measure, its usefulness is inherently in the areas of values approaching unity as this provides an overall performance of the detector, for various SNR levels, regardless of the value of P_{FA}. As a result, it is evident that such transient situations,

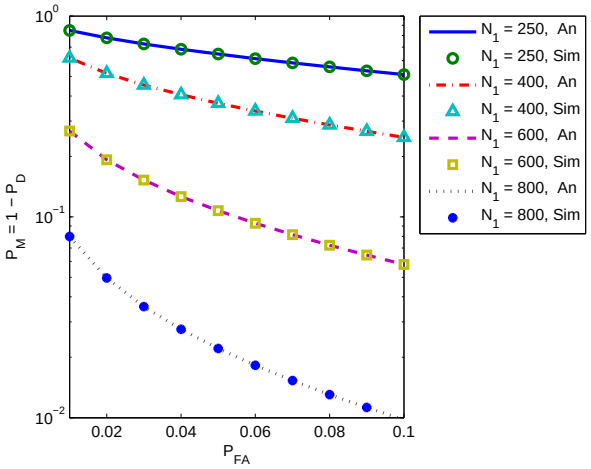

Fig. 8: ROC for the transient phase ED with $\gamma = -8$ dB, $N = 1000$ and different values of N_1.

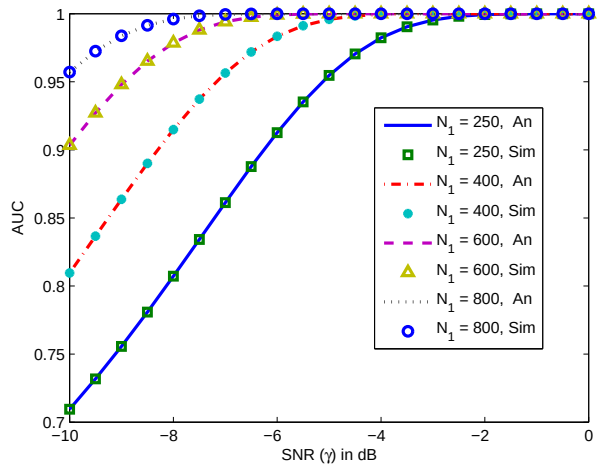

Fig. 9: AUC for the transient phase ED with $N = 1000$ and different values of N_1.

i.e., unknown PU channel band edges and/or transmission burst timing, can be handled effectively with the aid of the sliding window processing. In FFT or AFB based ED, sliding window processing can be performed in time and/or frequency domain so that the PU transmission is located in terms of time or frequency measures, respectively.

In the case of sliding window based energy detection, Fig. 10 demonstrates the detection delay as a function of the PU SNR for different ED block lengths. Here the target values are: $P_D = 0.99$ and $P_{FA} = 0.01$ for the frame length of 12800 samples. The performance of ED with repeated overlapping windows (denoted as NO-ED), following (26) is also shown for comparison. For this scheme, the worst case sensing delay is considered; this approaches $2N$ when the SNR approaches the sensitivity limit and N at high SNR values. Basic ED, using a single sensing window, is also illustrated for reference. Depending on the used window length, there is a clear tradeoff between the sensing delay and sensitivity of the sensing process. The SW-ED approach allows to rapidly detect PUs with power levels above the targeted detection sensitivity. Compared to the non-overlapping ED scheme with the same block length, SW-ED appears to have a sensitivity loss, but no more than 1 dB in this example case.

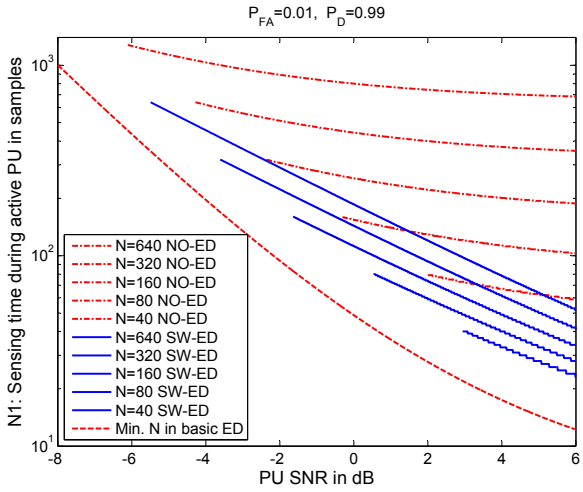

Fig. 10: Detection delay in sliding window energy detection (SW-ED) and non-overlapping repeated energy detection (NO-ED) as a function of SNR for different block lengths N. Target $P_{FA} = 0.01$ and $P_D = 0.99$. Also the minimum block length for these target values in basic (single-shot) ED is shown, but this is applicable only if the time of possible reappearance of PU is predetermined.

C. Effect of Frequency Selectivity

The numerical results are also extended for calculating the β_{ch}-values in (39) for the ITU-R Vehicular A channel. It was found that the theoretical β-values are in the range $[1.13, 2.47]$ for the noise-free case, whereas the corresponding range of β_{ch}-values is $[1.03, 1.37]$ for 0 dB SNR and $[1.01, 1.06]$ for -6 dB SNR. In the same context, a more generic scenario is depicted in Fig. 11 with respect to ROC and AUC curves. For both cases we assume a moderate SNR value of $\gamma = 0$ dB, i.e., $\beta_{ch} \in \{1.03, 1.20, 1.37\}$. Furthermore, for the ROC case we assume $N_t = 20$ and $N_f = 2$, while the AUC is illustrated as a function of $N = N_t N_f$. It is evident that in this scenario the effect of frequency selectivity on the performance of the ED is significant. Importantly, regarding the commonly considered low SNR regime (e.g., $\gamma < -3$ dB), one can safely conclude that the performance of ED based SS is not affected by frequency selectivity and the performance is determined by the temporal variations of the received PU signal power [21]. It also follows that in ED analysis over fading channels, it is sufficient to model the total received power, while the multipath effects on frequency selectivity are not essential in the low SNR regime [21]–[23]. This is in contrast to certain

other SS techniques, such as the eigenvalue based methods, that exploit the non-whiteness of the received power spectrum, which may be due to the transmitted spectrum and/or channel.

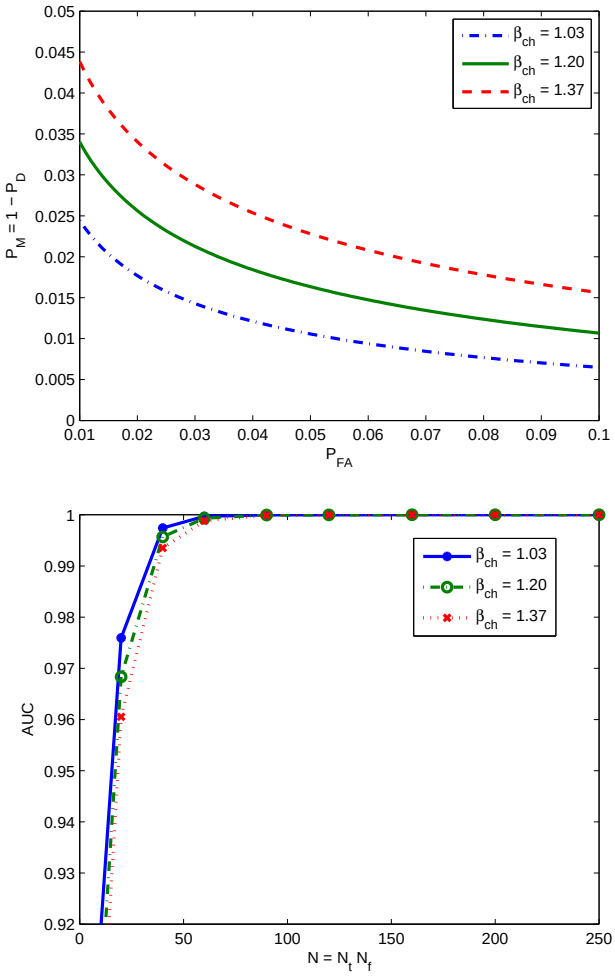

Fig. 11: ROC and AUC curves for frequency selective channels at $\gamma = 0$ dB, for different values of β_{ch} and $N_t N_f = 20 \times 2$ for the ROC case.

D. The Bluetooth Test Case

In the majority of practical telecommunication scenarios, wireless channels are frequency selective and thus, one can not realistically assume knowledge of the received PU signal power spectrum. However, for certain short-range and/or narrowband cases, channel models are commonly assumed to be flat and the Bluetooth (BT) wireless technology constitutes a notable example of such systems [49]. The ISM band around 2.4 GHz is an unlicensed frequency band which is utilized by various applications, including IEEE 802.15 based BT wireless devices, cordless phones, WLAN signals and even microwave ovens, which can introduce interference within this frequency band. The frequency hopped frequency shift keying (FH-FSK) based IEEE 802.15 BT signal has 79 different frequency channels at center frequencies spanning between 2.402 GHz and 2.480 GHz with 1 MHz spacing. The nominal bandwidth of BT signal is 1 MHz whereas the corresponding hopping rate is 1600 hops per second.

In the present analysis, we firstly consider a simplified scheme with continuous BT signal at the 33^{rd} channel with the corresponding signal spectrum illustrated in Fig. 12. Subsequently, we analyze the performance of the multiband spectrum sensing scheme with weighting process in sensing a BT information signal and the corresponding spectral holes. Since we consider scenarios with small dynamic range, in the absence of strong PUs at adjacent frequencies, the differences between filter bank and FFT based sensing are insignificant. Therefore, the present analysis is limited to analyzing the corresponding results only for the FFT case. To this end, we assume 83.5 MHz sampling rate and that the ISM band consists of 1024 subbands. Furthermore, each 1 MHz sensing bandwidth of the BT signal, the sensing window comprises 11 subbands. In the present scenario, SS is performed assuming $\gamma = -5$ dB with $P_{FA} = 0.1$ and $P_D = 0.9$. With a simplified, non-frequency-selective model, the required sample complexity for the target SNR, P_D and P_{FA} is determined with the aid of (8) as $\hat{N} = 89$. If the BT power was equally distributed among the 11 subbands, 8 samples from each of these subbands would be sufficient for reaching the target requirements. Also, when sensing is performed only by utilizing the center subband, $\hat{N} = 89$ is a lower bound for the time record length. Fig. 13 depicts the number of required subband samples needed with the BT signal for different sensing bandwidths and with optimized and constant weights. For instance, when the optimum weight values are used for all 11 subbands of the BT signal, the required number of subband samples is 45, which corresponds to a lower time record length than the respective 50 samples hoping interval. It is also recalled here that most of the BT energy is concentrated on the center subbands; therefore, only 3 or 5 subbands with 0.25 MHz or 0.42 MHz bandwidth, respectively, are sufficient for sensing. The corresponding results are depicted in Fig. 13 both for optimum weighting and for constant weights and different SNR values.

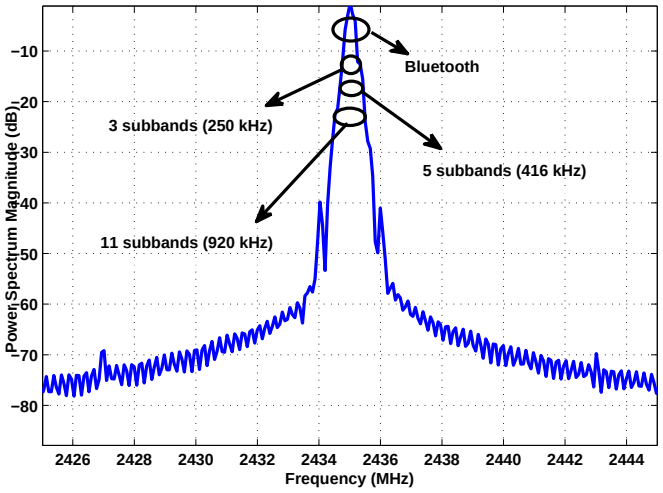

Fig. 12: Bluetooth signal spectrum in 2.4 GHz ISM band.

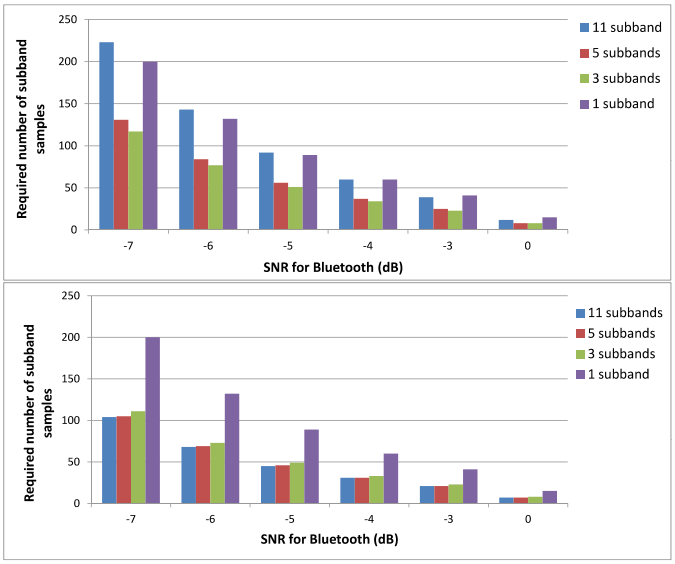

Fig. 13: Required time record length in subband samples for different weighting schemes in Bluetooth sensing for constant weights (upper) and optimum weights (lower).

It can also be observed that almost the same time record length can be used when sensing a single subband at the BT center frequency as when sensing the entire 1 MHz BT band with constant weights. For the case of constant weights, 3 subbands constitutes the optimum choice for all considered SNR values. On the contrary, using optimum weights reduces the sensing time by about 10%. In the same context, Fig. 14 (a) shows the P_D with constant and optimum weight values as a function of the active BT SNR with AWGN based on simulations. The time record length is 50 samples, and the constant weight case uses 3 subbands. In the case of optimum weight values using 11 subbands, highest detection probability

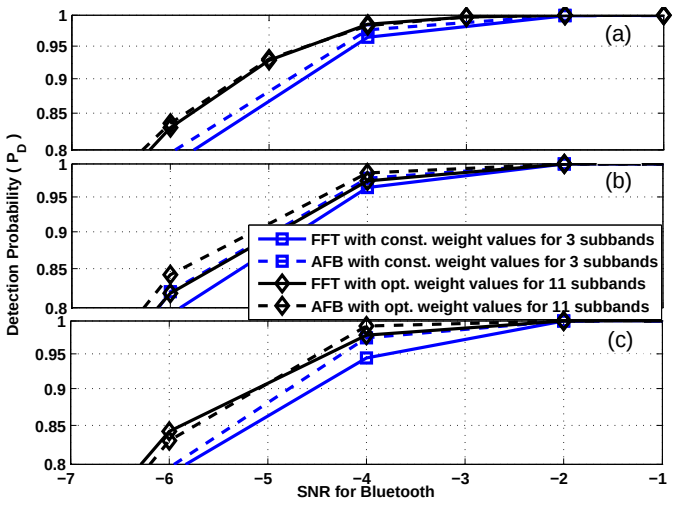

Fig. 14: Detection probability of Bluetooth signal with $P_{FA} = 0.1$ using time record length of 50 for constant and optimum weight values under (a) AWGN, (b) ITU-R Vehicular A channel, (c) Indoor channel including FFT and AFB based sensing.

performance is again achieved but the benefit over the constant weight case is marginal. Hence, it is evident that in this low dynamic range case the P_D is not substantially different between FFT and AFB[2]. Fig. 14 (b) and Fig. 14 (c) show the corresponding results for the ITU-R Vehicular A channel and Indoor channel cases, respectively [50]. The Vehicular A channel has 6 taps and its maximum delay spread is about 2.5 μs. 16-tap model with 80 ns rms delay spread is also applied for realistic Indoor channel model as second channel model [50], [51]. We can see that the optimum weighting scheme derived for the flat-fading model gives the best results. The difference is most noticeable with the ITU-R Vehicular A channel. However, the benefits over constant weights with 3 subbands are marginal.

E. The TETRA Case

The developments of Section III-C, and (32) in particular, can be used also for analyzing and optimizing traditional time-domain filters for spectrum sensing purposes. The example case considered here is the Terrestrial Trunked Radio (TETRA) waveform used in Professional Mobile Radio (PMR) context by safety and security personnel. The basic TETRA waveform uses differential BPSK or QPSK modulation with the roll-off factor $\beta = 0.35$, 18 kHz symbol rate, and 25 kHz bandwidth. When developing a coexisting broadband PMR system, utilizing the same frequency band for broadband data communications, it is important to be able to detect the possible presence of legacy TETRA signals [52], [53].

Based on the results of Section III-D, a root raised cosine (RRC) filter with $\beta = 0.35$ is the optimum choice for ED based sensing. However, there are meaningful reasons for considering other filter designs for the sensing task. As an example, we consider sensing a TETRA signal with -10 dB SNR using RRC filters and raised cosine (RC) filters with different roll-off factors, assuming frequency flat channels. The standard ED model indicates that for a coherent matched filter solution, the required time record length is $\tilde{N}$ =1475 symbol intervals. However, this assumes synchronization, which is not feasible in the spectrum sensing context. Based on (32), it is easily found out that with 2x oversampled RRC filters, the required values are $\tilde{N}$ =1600 with $\beta = 0.35$ and $\tilde{N}$ =1664 with $\beta = 1$. The corresponding values for 2x oversampled RC filters are $\tilde{N}$ =1632 with $\beta = 0.35$ and $\tilde{N}$ =1710 with $\beta = 1$. Due to 2x oversampling, the actual sample complexities are $N = 2\tilde{N}$. However, the differences between the required sensing times with these solutions are rather small. Yet, a filter with $\beta = 1$ is much easier to implement than a filter with $\beta = 0.35$ and it may provide a significantly better stopband attenuation, which is important in case of high dynamic range scenarios. It is also well known that, in comparison to RRC filters, RC filters of the same order provide clearly better stopband attenuation. Thus, it is evident that is reasonable to

[2]The previous discussion did not consider the frequency hopping characteristic of the BT system. A critical issue is that if the time record for calculating the test statistics is not aligned with the received BT burst, the detection performance degrades significantly, as discussed in Section III-A. Notably, this issue can be ultimately avoided by determining the test statistics with the aid of the sliding window approach.

consider sensing filter designs which are different from the filters used for data reception and (32) provides an easy-to-use tool for evaluating the sensing performance of different filter designs.

VI. Closing Remarks

We explored the effects of different forms of frequency selectivity on energy detection performance. We also considered the effect of misaligned time-frequency window on the test statistics in a generic way by means of a mixed statistical model based on Gaussian approximation. Then, we proposed sliding window processing as a method to search for the best match in cases where the frequency range or burst timing of the PU signal is unknown to the sensing receiver. We analyzed numerically the specific case of a re-appearing PU detection using the sliding window approach, indicating significantly reduced detection delay compared to existing methods. The analytical elaboration of the sliding window approach remains as a subject to future work.

Furthermore, we addressed the problem of known, non-flat PU spectrum, considering Bluetooth as an example case. Optimum weights were derived for FFT or filter bank based sensing where the PU signal band is divided into approximately flat subbands. An analytical model was developed for quantifying the effect of channel frequency selectivity on the sensing performance, which is shown to be highly dependent upon the corresponding SNR levels. It was also concluded that, in the low SNR regime, the channel frequency selectivity has a minor effect on the sensing performance, but at around 0 dB SNR the effect becomes significant enough to be taken into consideration.

A central tool in our discussions has been the possibility to split a wideband, multichannel signal into relatively narrow subbands and then recombining subband samples within a proper time-frequency zone with optimized weighting as a test statistic. The required subband filtering can be realized using plain FFT, windowed FFT, or analysis filter bank with the latter providing the best possibilities to control the spectral leakage between subbands. There is no major difference between FFT and AFB based spectrum sensing with small spectral dynamic range. However, when trying to identify spectral gaps between strong and spectrally well-contained PU signals, the AFB based algorithm provides clearly better performance, as demonstrated in [35].

Finally, novel analytic methods were developed for the proposed energy detection scenarios, that have not been sufficiently covered in the open literature. The offered results were subsequently employed in analyzing the corresponding detectors' performance. This was also the case for the concept of the area under the receiver operating characteristics curve (AUC), which was employed as an effective single-valued performance metric for evaluating different SS algorithms in different communication scenarios.

Appendix I
Derivation of Eq. (33) and Eq. (34)

(i) First term: Based on Schwartz inequality we obtain,

$$\left(\sum_{\kappa=k-\overline{N_f}}^{k+\overline{N_f}} g_k\gamma_k\right)^2 \leq \sum_{\kappa=k-\overline{N_f}}^{k+\overline{N_f}} g_k^2 \sum_{\kappa=k-\overline{N_f}}^{k+\overline{N_f}} \gamma_k^2. \tag{53}$$

Based on this, it follows that

$$\frac{\sum_{\kappa=k-\overline{N_f}}^{k+\overline{N_f}} g_k^2}{\left(\sum_{\kappa=k-\overline{N_f}}^{k+\overline{N_f}} g_k\gamma_k\right)^2} \geq \frac{\sum_{\kappa=k-\overline{N_f}}^{k+\overline{N_f}} g_k^2}{\sum_{\kappa=k-\overline{N_f}}^{k+\overline{N_f}} g_k^2 \sum_{\kappa=k-\overline{N_f}}^{k+\overline{N_f}} \gamma_k^2} = \frac{1}{\sum_{\kappa=k-\overline{N_f}}^{k+\overline{N_f}} \gamma_k^2}. \tag{54}$$

However, by choosing $g_k = \gamma_k/\gamma$ we obtain this minimum.

(ii) Second term: By replacing

$$\hat{g}_k = g_k(1-\gamma_k) \tag{55}$$

the second term can take the same form as the first one. Based on the above, (34) is deduced. It is also noted that the minimum can be reached for,

$$\hat{g}_k = \frac{\gamma_k}{1-\gamma_k} \tag{56}$$

or

$$g_k = \frac{\gamma_k}{(1-\gamma_k)^2} \tag{57}$$

which completes the proof.

Appendix II
Derivation of Eq. (45)

The $Q(x)$ function is mathematically linked to the complementary error function by the identity $Q(x) \triangleq \frac{1}{2}\mathrm{erfc}(x/\sqrt{2})$, where $\mathrm{erfc}(x) \triangleq 1-\mathrm{erf}(x)$. Thus, (44) can be re-written as,

$$\begin{aligned}\mathcal{I}(a,b,c,d) = &\frac{c}{2\sqrt{2\pi}}\int_0^\infty e^{-\frac{(cx-d)^2}{2}}dx \\ &- \frac{c}{2\sqrt{2\pi}}\int_0^\infty \mathrm{erf}\left(\frac{ax-b}{\sqrt{2}}\right)e^{-\frac{(cx-d)^2}{2}}dx.\end{aligned} \tag{58}$$

By expanding the $(cx-d)^2$ term and with the aid of [44, eq. (8.253.1)] one obtains,

$$\begin{aligned}\mathcal{I}(a,b,c,d) = &\frac{ce^{-\frac{d^2}{2}}}{2\sqrt{2\pi}}\int_0^\infty e^{-\frac{c^2x^2}{2}}e^{cdx}dx \\ &- \frac{ce^{-\frac{d^2}{2}}}{2\sqrt{2\pi}}\sum_{l=0}^{\infty}\int_0^\infty \frac{(-1)^l(ax-b)^{1+2l}e^{-\frac{c^2x^2}{2}}}{l!\sqrt{\pi}(2l+1)2^{l+\frac{1}{2}}e^{-cdx}}dx.\end{aligned} \tag{59}$$

Importantly, since $1+2l \in \mathbb{N}$, the $(ax-b)^{1+2l}$ term can be expanded according to [44, eq. (1.111)] yielding,

$$\mathcal{I}(a,b,c,d) = \frac{ce^{-\frac{d^2}{2}}}{2\sqrt{2\pi}}\overbrace{\int_0^\infty e^{-\frac{c^2x^2}{2}}e^{cdx}dx}^{\mathcal{T}_1} - \tag{60}$$

$$\frac{ce^{-\frac{d^2}{2}}}{2\sqrt{2\pi}}\sum_{l=0}^{\infty}\sum_{i=0}^{1+2l}\binom{1+2l}{i}\frac{(-1)^{1-i+3l}b^{1+2l-i}a^i}{l!\sqrt{\pi}(2l+1)2^{l+\frac{1}{2}}}\underbrace{\int_0^{\infty}\frac{x^i e^{cdx}}{e^{\frac{c^2x^2}{2}}}dx}_{\mathcal{T}_2}$$

where $\binom{b}{a} \triangleq \frac{b!}{a!(b-a)!}$ denotes the binomial coefficient [44]. Importantly, the $\mathcal{T}_1$ integral can be expressed in closed-form according to [44, eq. (3.322)]. Likewise, the $\mathcal{T}_2$ integral can be expressed in closed-form in terms of the parabolic cylinder function in [44, eq. (3.462)] which can be subsequently expressed in terms of the Kummer's hypergeometric function with the aid of [44, eq. (9.240)]. Hence, after the necessary variable transformation and substituting in (60) yields (45), which completes the proof.

REFERENCES

[1] H. Urkowitz, "Energy detection of unknown deterministic signals," *Proc. IEEE*, vol. 55, no. 4, pp. 523−531, Apr. 1967.

[2] H. Poor, "An Introduction to signal detection and estimation," *2nd ed. Berlin, Germany: Springer-Verlag,* 1994.

[3] S. Haykin, "Cognitive radio: Brain-empowered wireless communications," *IEEE J. Select. Areas Commun.* vol. 23, no. 2, pp. 201−220, Feb. 2005.

[4] T. Yucek and H.Arslan "A survey of spectrum sensing algorithms for cognitive radio applications," *IEEE J. Comm. Survey & Tut.* vol. 11, no. 1, pp. 116−130, Feb. 2009.

[5] D. Cabric, A. Tkachenko, and R. Brodersen, "Spectrum sensing measurements of pilot, energy, and collaborative detection," in *proc. IEEE MILCOM 2006*, Washington, DC, pp. 1−7.

[6] R. Tandra, and A. Sahai, "SNR walls for signal detection," *IEEE J. Sel. Topics Signal Process.*, vol. 2, no. 1, pp. 4−17, Feb. 2008.

[7] G. V. Vilar, R. L. Valcarce, and J. Sala, "Multiantenna spectrum sensing exploiting spectral a priori information," *IEEE Trans. Wireless Commun.*, vol. 10, no. 12, pp. 4345−4355, Dec. 2011.

[8] Y. Huang and X. Huang, "Detection of temporally correlated signals over multipath fading channels," *IEEE Trans. Wireless Commun.*, vol. 12, no. 3, pp. 1290−1299, Mar. 2013.

[9] Y. Zeng and Y. C. Liang, "Eigenvalue-based spectrum sensing algorithms for cognitive radio," *IEEE Trans. Commun.*, vol. 57, no. 6, pp. 1784−1793, June 2009.

[10] A. Kortun, T. Ratnarajah, M. Sellathurai, C. Zhong and C.B. Papadias, "On the performance of eigenvalue-based cooperative spectrum sensing for cognitive radio," *IEEE Journal of Selected Topics in Sign. Proc.*, vol.5, no.1, pp.49−55, Feb. 2011.

[11] S. Dikmese and M. Renfors "Performance analysis of eigenvalue based spectrum sensing under frequency selective channels," in *Proc. 7th IEEE CROWNCOM'12*, Stocholm, Sweden, pp. 356−361.

[12] S. Dikmese, J. L. Wong, A. Gokceoglu, E. Guzzon, M. Valkama and M. Renfors "Reducing computational complexity of eigenvalue based spectrum sensing for cognitive radio," in *Proc. 8th IEEE CROWNCOM'13*, Washington DC, USA, pp. 61−67.

[13] S. Dikmese, A. Gokceoglu, M. Valkama and M. Renfors "Reduced complexity spectrum sensing based on maximum eigenvalue and energy," in *Proc. ISWCS 2013*, Ilmenau, Germany, pp. 1−5.

[14] Y. Zeng and Y. C. Liang, "Spectrum sensing algorithms for cognitive radio based on statistical covariance," *IEEE Trans. Veh. Technol.* vol. 58, no. 4, pp. 1804−1815, May 2009.

[15] S. Dikmese, M. Renfors and H. Dincer "FFT and filter bank based spectrum sensing for WLAN signals," *in Proc. ECCTD*, pp. 781−784, Linkoping, Sweden, Aug. 2011.

[16] S. Dikmese, S. Srinivasan and M. Renfors "FFT and filter bank based spectrum sensing and spectrum utilization for cogntive radios," *in Proc. ISCCSP*, pp. 1−5, Rome, Italy, May. 2012.

[17] S. Srinivasan, S.Dikmese and M. Renfors "Spectrum sensing and spectrum utilization model for OFDM and FBMC based cognitive radios," *in Proc. SPAWC*, pp. 139−143, Cesme, Turkey, June 2012.

[18] S. Dikmese, A. Loulou, S. Srinivasan and M. Renfors, "Spectrum sensing and resource allocation models for enhanced OFDM based cognitive radio," in *Proc. 9th IEEE CROWNCOM'14*, Oulu, Finland, June 2014.

[19] S. Dikmese, S. Srinivasan, M. Shaat, F. Bader and M. Renfors "Spectrum sensing and spectrum allocation for multicarrier cognitive radios under interference and power constraints," *EURASIP Journal on Advances in Signal Processing*, DOI: 10.1186/1687-6180-2014-68, May 2014.

[20] V. I. Kostylev, "Energy detection of signal with random amplitude," *in Proc. IEEE Int. Conf. on Comm. (ICC '02)*, pp. 1606−1610, May 2002.

[21] F. Digham, M. S. Alouini, and M. K. Simon, "On energy detection of unknown signals over fading channels," *IEEE Trans. Commun.*, vol. 55, no. 1, pp. 21−24, Jan. 2007.

[22] K. Ruttik, K. Koufos and R. Jantti, "Detection of unknown signals in a fading environment," *IEEE Comm. Lett.*, vol. 13, no. 7, pp. 498−500, July 2009.

[23] P. C. Sofotasios, E. Rebeiz, Li Zhang, T. A. Tsiftsis, D. Cabric, and S. Freear, "Energy detection-based spectrum sensing over κ-μ and κ-μ extreme fading channels," *IEEE Trans. Veh. Technol.*, vol. 62, no.3, pp.1031−1040, March 2013.

[24] K. Ho-Van, P. C. Sofotasios, "Outage behaviour of cooperative underlay cognitive networks with inaccurate channel estimation," *in Proc. IEEE ICUFN '13*, pp. 501−505, Da Nang, Vietnam, July 2013.

[25] S. Atapattu, C. Tellambura, and H. Jiang, "MGF based analysis of area under the ROC curve in energy detection," *IEEE Comm. Lett.*, vol. 15, no. 12, Dec. 2011.

[26] S. P. Herath, N. Rajatheva and C. Tellambura, "Energy detection of unknown signals in fading and diversity reception," *IEEE Trans. Commun.*, vol. 59, no. 9, pp. 2443−2453, Sep. 2011.

[27] K. Ho-Van, P. C. Sofotasios, "Bit error rate of underlay multi-hop cognitive networks in the presence of multipath fading," *in IEEE ICUFN '13*, pp. 620−624, Da Nang, Vietnam, July 2013.

[28] K. T. Hemachandra, N. C. Beaulieu, "Novel analysis for performance evaluation of energy detection of unknown deterministic signals using dual diversity," *in Proc. IEEE VTC-Fall '11,*, pp. 1−5, Sep. 2011.

[29] P. C. Sofotasios, M. K. Fikadu, K. Ho-Van, M. Valkama, "Energy detection sensing of unknown signals over Weibull fading channels," *in Proc. IEEE Int. Conf. on Advanced Technol. for Commun. (ATC '13)*, pp. 414−419, HoChiMing City, Vietnam, Oct. 2013.

[30] A. Ghasemi, E. S. Sousa, "Spectrum sensing in cognitive radio networks: Requirements, challenges and design trade-offs," *IEEE Commun. Mag.*, pp. 32−39, Apr. 2008.

[31] K. Ho-Van, P. C. Sofotasios, "Exact bit-error-rate analysis of underlay decode-and-forward multi-hop cognitive networks with estimation errors," *IET Communications*, vol. 7, no. 18, pp. 2122−2132, Dec. 2013.

[32] A. Ghasemi, E.S. Sousa, "Asymptotic performance of collaborative spectrum sensing under correlated Log-normal shadowing," *IEEE Comm. Lett.,* vol. 11, no. 1, pp. 34−36, Jan. 2007.

[33] P. C. Sofotasios, M. Valkama, T. A. Tsiftsis, Yu. A. Brychkov, S. Freear, G. K. Karagiannidis, "Analytic solutions to a Marcum Q−function-based integral and application in energy detection of unknown signals over multipath fading channels," *in Proc. of 9*$^{\text{th}}$ *CROWNCOM '14*, pp. 260−265, Oulu, Finland, 2-4 June, 2014.

[34] S. Atapattu, C. Tellambura, H. Jiang, "Energy detection based cooperative spectrum sensing in cognitive radio networks," *IEEE Trans. Wireless Commun.*, vol. 10, no. 4, pp. 1232−1241, Apr. 2011.

[35] S. Dikmese, and M. Renfors, "Optimized FFT and filter bank based spectrum sensing for Bluetooth signal," in *Proc. of IEEE WCNC'12*, Paris, France, pp. 792−797.

[36] T. Ihalainen, A. Viholainen, T. Hidalgo Stitz, and M. Renfors, "Reappearing primary user detection in FBMC/OQAM cognitive radio," in *Proc. CROWNCOM 2010*, Cannes, France, pp. 411−416.

[37] S. Dikmese, T. Ihalainen and M. Renfors, "Analysis and optimization of energy detection for non-flat spectral characteristics," Chapter 3 in M.-G. Di Benedetto and F. Bader (Eds.), *Cognitive Communication and Cooperative HetNet Coexistence*, Springer 2014.

[38] Z. Quan, W. Zhang, S.J. Shellhammer and A.H.Sayed, "Optimal spectral feature detection for spectrum sensing at very low SNR," *IEEE Trans. Commun.*, vol. 59, no. 1, pp. 201−212, Jan. 2011.

[39] V. Cevher, R. Chellappa, and J. McClellan, "Gaussian approximation for energy-based detection and localization in sensor networks," in *Proc. IEEE SSP 2007*, Madison, WI, USA, pp. 655−659.

[40] G. Taricco, "On the accuracy of the Gaussian approximation with linear cooperative spectrum sensing over Rician fading channels," *IEEE Signal Process. Lett.*, vol. 17, no. 7, pp. 651−654, Jul. 2010.

[41] G. Taricco, "Optimization of linear cooperative spectrum sensing for cognitive radio physical layer," *IEEE J. Sel. Topics Signal Process.*, vol. 5, no. 1, pp. 77−86, Feb. 2011.

[42] M. Bellanger, T. Ihalainen, and M. Renfors, "Filter bank based cognitive radio physical layer," in *Proc. ICT*, Santander, Spain, June 2009.

[43] B. Ferhang-Boroujeny, and R. Kempter, "Multicarrier communication techniques for spectrum sensing and communication in cognitive radios," *IEEE Commun. Mag.*, vol. 46, no. 4, pp. 80−85, Apr. 2008.
[44] I. S. Gradshteyn and I. M. Ryzhik, "Table of integrals, series, and products," *in* 7^{th} *ed. Academic*, New York, 2007.
[45] INFO-ICT-211887 Project PHYDYAS, Deliverable 5.1 prototype filter and structure optimization, 2009, *http://www.ict-phydyas.org/userfiles/file/PHYDYASD5-1.pdf* [Online].
[46] P. Siohan, C. Siclet, and N. Lacaille, "Analysis and design of OFDM-OQAM systems based on filterbank theory," *IEEE Trans. Signal Process.*, vol. 50, no. 5, pp. 1770−1183, May 2002.
[47] F. Penna, C. Pastrone, M. Spirito, and Garello, "Energy detection spectrum sensing with discontinuous primary user signal," in *Proc. IEEE ICC 2009*, Dresden, Germany, pp. 1−5.
[48] J. Barry, E. Lee, and D. Messerschmitt, *Digital Communications*, 3rd ed. Kluwer, 2004.
[49] I. Held, and A. Chen, "Channel estimation and equalization algorithms for long range Bluetooth signal reception," in *Proc. IEEE VTC-Spring 2010*, Taipei, Taiwan, pp. 1−7.
[50] R. Jain, "Channel models: A tutorial," *WiMAX Forum AATG*, Feb., 2007.
[51] T. Yucek, "Channel, spectrum, and waveform awareness in OFDM-based cognitive radio systems," *PhD thesis*, USF, FL, USA, 2007.
[52] M. Renfors, F. Bader, L. Baltar, D. Le Ruyet, D. Roviras, P. Mege, M. Haardt and T. Hidalgo Stitz, "On the use of filter bank based multicarrier modulation for professional mobile radio," in *Proc. IEEE VTC-Spring 2013*, Dresden, Germany, pp.1−5.
[53] J. Yli-Kaakinen and M. Renfors, "Multi-mode filter bank solution for broadband PMR coexistence with TETRA," in *Proc. EuCNC 2014*, Bologna, Italy, June 2014.

Sener Dikmese was born in Edirne, Turkey, in 1983. He received the B.Sc. and M.Sc. degrees from the Department of Electronics and Communications Engineering, Kocaeli University, Turkey, in 2005 and 2007, respectively. He worked as a research assistant at the Department of Computer Engineering, Kocaeli University, Turkey between 2005 and 2009. He was as a visiting researcher at Wireless Communications and Signal Processing (WCSP) Group, University of South Florida, USA in 2007. He is currently studying towards the doctoral degree at the Department of Electronics and Communications Engineering, Tampere University of Technology, Finland. He is working as a researcher at the same department and at the EU 7th Framework Programme project EMPhAtiC. He worked as a visiting researcher at CTTC, Barcelona, Spain in 2012 and at SUPELEC, Rennes, France in 2013, respectively. Among his research topics are digital signal processing, cognitive radios, spectrum sensing, and resource allocation.

Paschalis C. Sofotasios was born in Volos, Greece in 1978. He received the MEng degree from the University of Newcastle upon Tyne, UK, in 2004, the MSc degree from the University of Surrey, UK, in 2006, and the PhD degree from the University of Leeds, UK, in 2011. His Master's studies were funded by a scholarship from UK-EPSRC and his Doctoral studies were sponsored by UK-EPSRC and Pace plc. He was a Post-Doctoral Researcher at the University of Leeds until August 2013 and he has been a Visiting Researcher at the University of California, Los Angeles, USA, Aristotle University of Thessaloniki, Greece and Tampere University of Technology, Finland. Since Fall 2013, he is a Post-Doctoral Research Fellow at the Department of Electronic and Communications Engineering of Tampere University of Technology and at the Wireless Communications Systems Group of Aristotle University of Thessaloniki. His research interests are in the areas of fading channel characterisation and modelling, cognitive radio, cooperative communications, optical wireless communications as well as in the theory of special functions and statistical distributions. He received a 2012 Exemplary Reviewer award by IEEE Communication Letters and the best paper award at IEEE ATC '13.

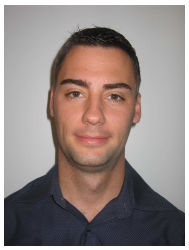

Tero Ihalainen (S'07) received the M.Sc. degree in electrical engineering and the D.Tech. degree in communications engineering from Tampere University of Technology (TUT), Tampere, Finland, in 2005 and 2011, respectively. From 2005 to 2010, he was a Researcher with the Department of Communications Engineering, TUT. He actively participated in the European Union 7th Framework Programme project Physical Layer for Dynamic Access and Cognitive Radio, where multirate filter banks were considered in the context of cognitive radio and developed for dynamic spectrum access applications. From April 2011 to April 2014, he was with Nokia Research Center, Finland. Currently, he is with Nokia Research / Nokia Technologies, Finland. His research interests include different potential technology components for the future 5G communications system, interference cancellation/suppression techniques for advanced UE receivers, as well as signal processing algorithms for multicarrier and frequency-domain-equalized single-carrier communications systems, with emphasis on filter bank based techniques.

Markku Renfors (S'77-M'82-SM'90-F'08) received the Dr.Tech. degree from Tampere University of Technology (TUT), Tampere, Finland, in 1982. Since 1992, he has been a Professor with the Department of Electronics and Communications Engineering, TUT, where he was the Head from 1992 to 2010.

His research interests include advanced multicarrier systems and signal processing algorithms for flexible communications receivers and transmitters, with emphasis on filter bank based signal processing. He is the Technical manager of the European Union 7th Framework Programme project Enhanced Multicarrier Techniques for Professional Ad-Hoc and Cell-Based Communications (EMPhAtiC) developing advanced filter bank based waveforms and signal processing techniques for dynamic spectrum access and heterogenous radio environments.

Mikko Valkama was born in Pirkkala, Finland, on November 27, 1975. He received the M.Sc .and Ph.D. Degrees (both with honours) in electrical engineering (EE) from Tampere University of Technology (TUT), Finland, in 2000 and 2001, respectively. In 2002, he received the Best Ph.D. Thesis -award by the Finnish Academy of Science and Letters for his dissertation entitled "Advanced I/Q signal processing for wideband receivers: Models and algorithms". In 2003, he was working as a visiting researcher with the Communications Systems and Signal Processing Institute at SDSU, San Diego, CA. Currently, he is a Full Professor and Department Vice-Head at the Department of Electronics and Communications Engineering at TUT, Finland. He has been involved in organizing conferences, like the IEEE SPAWC'07 (Publications Chair) held in Helsinki, Finland. His general research interests include communications signal processing, estimation and detection techniques, signal processing algorithms for software defined flexible radios, cognitive radio, radio localization, 5G mobile cellular radio, digital transmission techniques such as different variants of multicarrier modulation methods and OFDM, and radio resource management for ad-hoc and mobile networks.

PUBLICATION 2

Sener Dikmese and Markku Renfors, "Performance Analysis of Eigenvalue Based Spectrum Sensing under Frequency Selective Channels," in *Proceedings of 7th International Conference on Cognitive Radio Oriented Wireless Networks (CROWNCOM)*, Stocholm, Sweden, June 2012.

Performance Analysis of Eigenvalue Based Spectrum Sensing under Frequency Selective Channels

Sener Dikmese and Markku Renfors
Department of Communications Engineering
Tampere University of Technology
Tampere, Finland
sener.dikmese@tut.fi and markku.renfors@tut.fi

***Abstract*— Detecting primary signals with very low Signal-to-Noise Ratio (SNR) is a very important problem in cognitive radio (CR) systems. Small parameter uncertainties are unavoidable in any practical system, and especially the noise variance uncertainty has great effect on the performance of the most basic spectrum sensing method, energy detection. This has motivated the need for advanced spectrum sensing algorithms, like eigenvalue based spectrum sensing, which can be used to overcome the effects of parameter uncertainty in very low SNR cases. In this paper we study the effects of channel frequency selectivity, in combination with noise uncertainty, in case of energy detector and eigenvalue based spectrum sensing. It is demonstrated that channel frequency selectivity significantly enhances the performance of eigenvalue based spectrum sensing techniques.**

Keywords-component; Energy detector based spectrum sensing, eigenvalue based spectrum sensing, AWGN, frequency selective channel and noise uncertainty

I. INTRODUCTION

Increasing traffic rates, limited system capacity and inefficient spectrum utilization are very important challenges in the future development of wireless communications [1]. In solving these challenges, cognitive radio (CR) and advanced signal processing techniques have recently been studied extensively [2, 3, 4, 5, 6]. Spectrum sensing is a fundamental component of CR systems. Hence, different spectrum sensing algorithms have been developed with different characteristics regarding detection sensitivity and tolerance against various imperfections which are unavoidable in practical sensing devices.

There are many problems which affect the performance of spectrum sensing in practice. The first problem is that reliable sensing has to be achieved with very low signal-to-noise ratio (SNR). Secondly, the multipath fading and shadowing cause power fluctuation of the received signal [7]. Variation and unpredictability of the precise noise level at the sensing device is another critical issue, which is called "noise uncertainty". In many studies, the noise variance is assumed to be exactly known according to previous measurements [8], but in practice it is often very difficult to estimate the noise level accurately. Especially, the performance of the traditional energy detector based spectrum sensing methods significantly decreases under noise uncertainty [7].

Alternative spectrum sensing methods have been investigated to overcome these challenges. Eigenvalue and covariance based spectrum sensing techniques are very interesting alternative solutions for the noise uncertainty case, in spite of relatively high computational complexity. While the noise variance knowledge is not required for eigenvalue and covariance based spectrum sensing techniques, small changes or uncertainty on noise variance have no effect on the spectrum sensing performance [9,10].

So far, most of the spectrum sensing studies have focused on the AWGN channel model. While most of CR systems work under frequency selective channel, investigation of frequency selective channel effects on spectrum sensing algorithms is a very important topic.

The goal of this paper is to investigate the effects of frequency selective channel, considering also the noise uncertainty effects, using traditional energy detector and eigenvalue based spectrum sensing. We consider a simplified signal scenario, where only Gaussian signal model is used under Indoor, SUI-1 and ITU-R Vehicular A multipath delay profiles [11]. The applications of cooperative sensing approaches, which are very essential for reliable overall spectrum sensing schemes, are left as topics for future studies.

The rest of the paper is organized as follows. In Section 2, signal models are given for different frequency selective channels and analysis of energy detector and eigenvalue based spectrum sensing are summarized. Section 3 gives simulation results for the channel models considered, and finally, some concluding remarks are given about the performance of these methods and about the effects of channel frequency selectivity on the performance of eigenvalue based spectrum sensing

II. SPECTRUM SENSING TECHNIQUES

A. Energy detector based spectrum sensing with noise uncertainty

The analysis of energy detector based spectrum sensing, considering also the effects of noise uncertainty, is given in this section based on [7]. The two hypotheses regarding the absence or presence of a primary transmission in the received signal, can be expressed as

$$H0: y(n) = w(n) \sim N(0, \sigma_w^2)$$
$$H1: y(n) = \overbrace{s(n) \otimes c(n)}^{x(n)} + w(n) \sim N(0, \sigma_x^2 + \sigma_w^2) \quad (1)$$

When the AWGN only is present, the white noise is modeled as a zero-mean Gaussian random variable with variance σ_w^2, i.e., $w = N(0, \sigma_w^2)$. Signal can also be modeled as a zero-mean Gaussian variable $x = N(0, \sigma_x^2)$ where, σ_x^2 is the variance (power) of the received primary user signal, including the effects of the channel fading and frequency selectivity.

For this case, the decision statistics can be obtained as [3]

$$T_y = \frac{1}{N} \sum_{n=0}^{N-1} |y[n]|^2 \quad (2)$$

As y has complex Gaussian distribution, the probability distribution functions (PDF) of the outputs of test statistic T_y can be approximated as Gaussian distributions under H_0 and H_1 [7]. Hence, the probability distribution of test statistic T_y can be modeled as

$$T_y|_{H0} \sim N(\sigma_w^2, \frac{1}{N}\sigma_w^4)$$
$$T_y|_{H1} \sim N(\sigma_x^2 + \sigma_w^2, \frac{1}{N}(\sigma_x^2 + \sigma_w^2)^2) \quad (3)$$

There are two vital probabilities, the probability of detection P_D and probability of false alarm P_{FA}. When there is a signal in the sensing spectrum interested, P_D is considered and it can be defined as

$$P_D = P(T_y > \gamma \mid H_1) \quad (4)$$

where λ is the threshold value for detection. The false alarm probability P_{FA} gives the probability for the event that the primary signal is absent, but the decision device decides incorrectly that there is a signal. It can be formulated as [3]

$$P_{FA} = P(T_y > \gamma \mid H_0) \quad (5)$$

The threshold value can be obtained according to the target false alarm probability and noise variance assumed. The threshold value and the actual false alarm and detection probabilities can be expressed as follows

$$\gamma = Q^{-1}(P_{FA}) \sqrt{\frac{1}{N}\sigma_w^4} + \sigma_w^2 \quad (6)$$

$$P_{FA} = P(T_y > \gamma \mid H_0) = Q((\gamma - \sigma_w^2)/\sqrt{\frac{1}{N}\sigma_w^4}) \quad (7)$$

$$P_D = P(T_y > \gamma \mid H_1) = Q(\frac{\gamma - (\sigma_x^2 + \sigma_w^2)}{\sqrt{\frac{1}{N}(\sigma_x^2 + \sigma_w^2)^2}}) \quad (8)$$

The optimum threshold value λ is calculated according to the noise and primary signal variances information. It is very difficult to actually know the signal variance due to the channel environment characteristics. Hence, threshold value always is calculated from the noise variance which is assumed to be known according to the previous measurements or special noise calibration techniques possibly applied in the receiver. In practice, the estimation of exact noise variance is not possible. The detection and false alarm probabilities as functions of the SNR depend critically on the accuracy of noise variance estimate. In practice, the noise variance can be expected to be in the range $\sigma_w^2 \in [(1/\rho)\sigma_w^2, \rho\sigma_w^2]$ where $\rho > 1$ is a parameter that quantizes the size of the uncertainty. The noise uncertainty is usually expressed in dB units as $x = 10\log_{10}\rho$. In the presence of noise uncertainty, the expressions for P_{FA} and P_D are modified as follows [7]

$$P_{FA} = \max_{\sigma^2 \in \left[\frac{1}{\rho}\sigma_w^2, \rho\sigma_w^2\right]} Q((\gamma - \sigma^2)/\sqrt{\frac{1}{N}(\sigma^2)^2}) = Q((\gamma - \rho\sigma_w^2)/\sqrt{\frac{1}{N}(\rho\sigma_w^2)^2}) \quad (9)$$

$$P_D = \min_{\sigma^2 \in \left[\frac{1}{\rho}\sigma_w^2, \rho\sigma_w^2\right]} Q((\gamma - (\sigma_x^2 + \sigma^2))/\sqrt{\frac{1}{N}(\sigma_x^2 + \sigma^2)^2}) = Q(\frac{\gamma - (\sigma_x^2 + (1/\rho)\sigma_w^2)}{\sqrt{\frac{1}{N}(\sigma_x^2 + (1/\rho)\sigma_w^2)^2}}) \quad (10)$$

The noise uncertainty introduces the so-called SNR wall: with a given uncertainty ρ there is a minimum SNR value under which a primary signal cannot be reliably detected, no matter how long time record is used.

B. Eigenvalue based spectrum sensing

Eigenvalue based spectrum sensing algorithms can be applied for different kind of signals without noise variance knowledge. Hence, these algorithms are very robust, overcoming the noise uncertainty problem, and can even perform better than energy detection when the signals to be detected are highly correlated. In the following we review the eigenvalue based algorithms based on [9,10].

The signal model of eq. (1) is valid also in this case. We considering L consecutive symbol intervals with M samples within each interval. Within each symbol interval, the signal is highly correlated. M is called the oversampling factor. Now the sequences of received signal, primary signal, and noise are defined as

$$\hat{\mathbf{y}} = [y(n)\ \ y(n-1)\ y(n-2)...y(n-ML+1)]^T,$$
$$\hat{\mathbf{s}} = [s(n)\ \ s(n-1)\ s(n-2)...s(n-ML+1)]^T, \quad (11)$$
$$\hat{\mathbf{w}} = [w(n)\ \ w(n-1)\ w(n-2)...w(n-ML+1)]^T$$

The statistical covariance matrices of the signal and noise are defined as

$$\mathbf{R}_{yy} = E(\hat{\mathbf{y}}\hat{\mathbf{y}}^\dagger)$$
$$\mathbf{R}_{ss} = E(\hat{\mathbf{s}}\hat{\mathbf{s}}^\dagger)$$
$$\mathbf{R}_{ww} = E(\hat{\mathbf{w}}\hat{\mathbf{w}}^\dagger) \quad (12)$$
$$\mathbf{R}_{yy} = \mathbf{H}\mathbf{R}_{ss}\mathbf{H}^\dagger + \mathbf{R}_{ww}$$

Eigenvalues of $\mathbf{R}_{yy}$ and $\mathbf{H}\mathbf{R}_{ss}\mathbf{H}^\dagger$ are defined as $\lambda_1 \geq \lambda_2 \geq ... \geq \lambda_{ML}$ and $\rho_1 \geq \rho_2 \geq ... \geq \rho_{ML}$, respectively.

1) Algorithm 1: Max-Min eigenvalue based sensing (MME)

Compute the maximum and minimum eigenvalues $(\lambda_{max}, \lambda_{min})$ of the covariance matrix $\mathbf{R}_{yy}(N)$. The covariance matrix is obtained by averaging N sample covariance matrices (here n indicates the first sample used in the calculation of each covariance estimate)

$$\mathbf{R}_{yy}(N) = \frac{1}{N}\sum_{n=ML-1}^{L-2+N} \hat{\mathbf{y}}(n)\hat{\mathbf{y}}(n)^{\dagger} \tag{13}$$

The ratio of $\lambda_{max}, \lambda_{min}$ is compared with the threshold γ_1 which is calculated according to the distribution of covariance matrix of noise, when the signal is absent

$$\mathbf{R}_{ww}(N) = \frac{1}{N}\sum_{n=ML-1}^{L-2+N} \hat{\mathbf{w}}(n)\hat{\mathbf{w}}(n)^{\dagger} \tag{14}$$

$\mathbf{R}_{ww}(N)$ is nearly a Wishart random matrix [12]. The distribution of the eigenvalues has been investigated to define the threshold value. In [13, 14] the Tracy-Widom distributions were studied and F_1, the cumulative distribution function (CDF) of the Tracy-Widom distribution of order 1 was derived to get closed form expression

$$F_1 = \exp\left(-\frac{1}{2}\int_t^{\infty}(q(u)+(u-t)q^2(u))du\right) \tag{15}$$

where $q(u)$ is the solution of the nonlinear Painleve II differential equation

$$q''(u) = uq(u) + 2q^3(u) \tag{16}$$

Table 1 gives the values of F_1 at some points. Also F_1^{-1} can calculated using same table

TABLE I

NUMERICAL TABLE FOR THE TRACY-WIDOM DIST. OF ORDER 1

t	-3.90	-3.18	-2.78	-1.91	-1.27	-0.59	0.45	0.98	2.02
$F_1(t)$	0.01	0.05	0.10	0.30	0.50	0.70	0.90	0.95	0.99

Utilizing the table or numerical method for calculating the values for F_1^{-1}, together with values of N and L, the threshold γ_1 can be formulated as

$$\gamma_1 = \frac{(\sqrt{N}+\sqrt{ML})^2}{(\sqrt{N}-\sqrt{ML})^2}\cdot\left(1+\frac{(\sqrt{N}+\sqrt{ML})^{-2/3}}{(NML)^{1/6}}F^{-1}(1-P_{FA})\right) \tag{17}$$

When $(\lambda_{max}/\lambda_{min}) > \gamma_1$, the primary signal is deemed to be present, otherwise it is assumed that there is no signal in the band of interest.

It is very intractable mathematically to get theoretical detection probabilities for the max/min eigenvalue based spectrum sensing algorithm. Hence, approximated value has been obtained using an empirical mode [9]. This approximation is given for Algorithm1 as follows

$$\mathbf{R}_{yy} = \mathbf{H}\mathbf{R}_{ss}\mathbf{H}^{\dagger} + \mathbf{R}_{ww} = \mathbf{H}\mathbf{R}_{ss}\mathbf{H}^{\dagger} + \sigma_w^2\mathbf{I} \tag{18}$$

$$\begin{aligned}
&\lambda_{max}(\mathbf{R}_{xx}(N)) \approx \rho_1 + \lambda_{max}(\mathbf{R}_{ww}(N)) \\
&\lambda_{min}(\mathbf{R}_{xx}(N)) \approx \rho_{ML} + \sigma_w^2 \\
&P_d = P(\lambda_{max}(\mathbf{R}_{xx}(N)) > \gamma_1\lambda_{min}(\mathbf{R}_{xx}(N))) \\
&\quad \approx P(\lambda_{max}(\mathbf{R}_{ww}(N)) > \gamma_1(\rho_{ML}+\sigma_w^2) - \rho_1 \\
&\quad = 1 - F_1\left(\frac{\gamma_1 N + N(\gamma_1\rho_{ML} - \rho_1)/\sigma_w^2 - \mu}{v}\right)
\end{aligned} \tag{19}$$

In equation (20), according to the random matrix theorem [12], μ and v are calculated as $(\sqrt{N-1}+\sqrt{ML})^2$ and $\left(\sqrt{N-1}+\sqrt{ML}\right)\left((1/\sqrt{N-1})+(1/\sqrt{ML})\right)^{1/3}$.

2) Algorithm 2: Energy with min eigenvalue based sensing (EME)

Compute the minimum eigenvalue λ_{min} of the covariance matrix $\mathbf{R}_{yy}(N)$ in the same way with Algorithm 1. Then, compute average power of the received signal as

$$T(N) = \frac{1}{MN}\sum_{n=0}^{NM-1}|y(n)|^2 \tag{20}$$

Threshold value γ_2 is calculated with the inverse q-function Q^{-1} as follows

$$\gamma_2 = \left(\sqrt{\frac{1}{MN}}Q^{-1}(P_{FA})+1\right)\frac{N}{(\sqrt{N}-\sqrt{ML})^2} \tag{21}$$

When $(T(N)/\lambda_{min}) > \gamma_2$, the signal is assumed to be present, otherwise it is expected that there is no signal in the band of interest.

While the thresholds can be pre-computed based only on N, L and P_{FA}, there is no need to estimate noise variance according to the previous measurements. Hence, it can be seen that these two algorithms are very robust to noise uncertainty.

Similar theoretical difficulties are encountered when calculating the probability of detection for Algorithm 2. However, the following numerical expression has been established [9]

$$\begin{aligned}
&P_d = P(T(N) > \gamma_2\lambda_{min}(\mathbf{R}_{xx}(N))) \\
&\approx P\left(\frac{Tr(\mathbf{R}_{ww}(N))}{ML} > \gamma_2\left(\rho_{ML}+\frac{\sigma_w^2}{\sqrt{N}}\left(\sqrt{N}-\sqrt{ML}\right)\right) - \left(\frac{Tr(\mathbf{H}\mathbf{R}_{ss}\mathbf{H}^{\dagger})}{ML}\right)\right) \\
&= Q\left(\frac{\gamma_2\left(\rho_{ML}+\frac{\sigma_w^2}{\sqrt{N}}\left(\sqrt{N}-\sqrt{ML}\right)\right) - \left(\frac{Tr(\mathbf{H}\mathbf{R}_{ss}\mathbf{H}^{\dagger})}{ML}\right) - \sigma_w^2}{\sqrt{\frac{1}{MN}}\sigma_w^2}\right)
\end{aligned} \tag{22}$$

Due to the approximation, there are some differences between theoretical and simulation results of the two algorithms.

The effects of channel frequency selectivity appear into the detection probability expressions (20) and (23) through the eigenvalues. The eigenvalue spread is a metric for the correlatedness of the sample sequence used in detection. Naturally, flat signal or noise spectra correspond to uncorrelated sample sequences, in which case the covariance matrix approaches a scaled unit matrix and the eigenvalues are

identical. Correlations are introduced to the possible primary signal spectrum through the characteristics of the transmitted waveform, e.g., by pulse shaping or channelization filtering. Additionally, frequency selective channel introduces correlations (i.e., a non-flat power spectrum) to the received sample sequence. With non-oversampled signal model, the waveform generation related correlations disappear if the signal spectrum is flat within the used signal band. Still the channel frequency selectivity based correlations may be sufficient for detecting the primary signal. This idea is tested in the following through numerical examples.

III. SIMULATION RESULTS

Simple Gaussian signal models which includes both non-oversampled and 2x-oversampled signal are shown as seen figure 1. In this figure, the signals are shown for the ITU-R Vehicular A channel case [11]. In our signal model, the bandwidth is chosen as 20 MHz. The Vehicular A channel model has 6 taps the maximum delay spreads is about 2.5 μs.

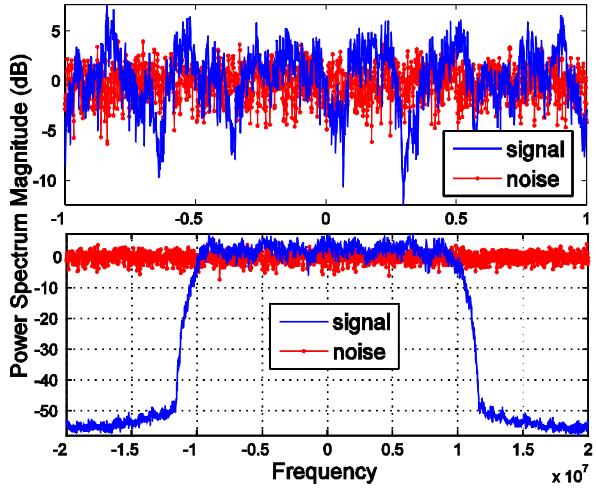

Figure 1. Examples non-oversampled and 2x-oversampled spectral models under Vehicular A channel and AWGN noise.

For realistic Indoor channel model, we use the 16-tap model with 80 ns rms delay spread such as from [15]. The third channel model used in this study is the SUI-1 model [11]. This model has 3 Ricean fading taps and 0.9 μs delay spread, and it is clearly less frequency selective than the other two. These different cases are presented in the following subsections. Theoretical results with channel effects are obtained using the model of eqs. (9) and (10) for energy detection with noise uncertainty and eqs. (20) and (23) for eigenvalue based spectrum sensing. The simulation results, as well as theoretical results are averaged over 1000 channel instances.

A. Indoor channel case for both non-oversampled and oversampled Gaussian signal model

Figure 2 shows detection probabilities of traditional energy detector and eigenvalue based spectrum sensing with Indoor channel [15] in the non-oversampled case. The 1 dB noise uncertainty case is considered as the worst-case scenario in terms of channel noise variance estimation. The time record length is 10000 complex samples. With this number of samples and 1 dB noise uncertainty, eigenvalue based spectrum sensing has still better performance compared to the energy detector based spectrum sensing with frequency selective channel. Similar results are shown for 2x -over-sampled signal using the same channel instances as in figure 3.

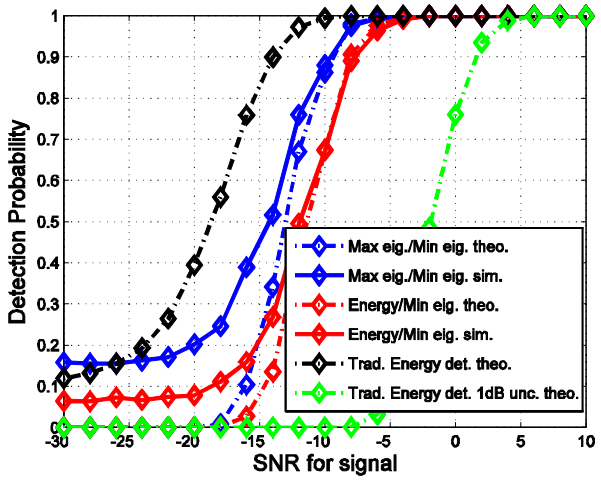

Figure 2. Detection probability of energy detector and eigenvalue based spectrum sensing under 1 dB uncertainty using Indoor channel with non-oversampled signal.

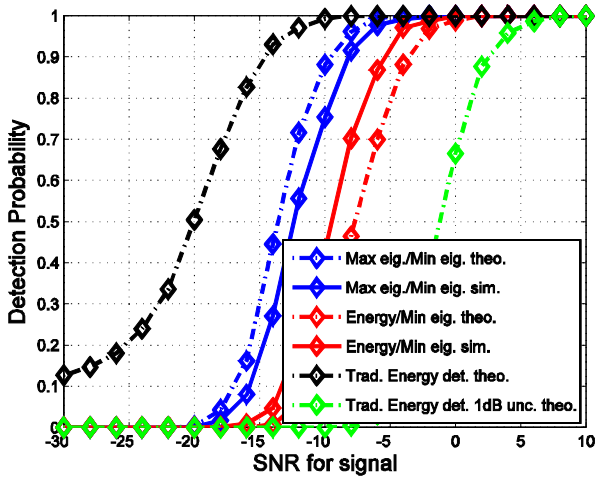

Figure 3. Detection probability of tenergy detector and eigenvalue based spectrum sensing under 1 dB uncertainty using Indoor channel with 2x-oversampled signal.

The actual false alarm probabilities of eigenvalue based spectrum sensing for both non-oversampled and oversampled signals are given in figure 4. We notice that the false alarm probability is independent of SNR, as expected [9, 10]. While the simulated false alarm probability in the non-oversampled signal case becomes quite significant, the actual false alarm probability under oversampled signal model becomes very

small. Very similar performance is obtained also for SUI-1 and Vehicular A channel cases, as can be seen from the 'floors' of the detection performance curves. Thus the actual false alarm probability is not related to channel effects in eigenvalue based spectrum sensing. The same detection threshold is used in non-oversampled and oversampled cases. Based on these results, there is the possibility to reduce the detection threshold in the oversampled case to improve the detection performance, while maintaining a realistic false alarm probability.

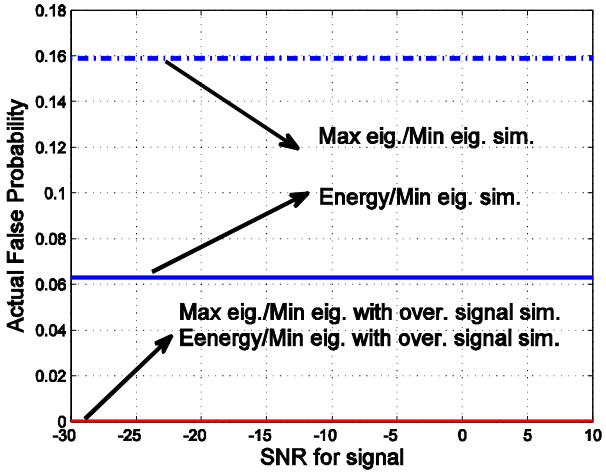

Figure 4. Actual false alarm probability of eigenvalue based spectrum sensing techniques.

B. Vehicular A channel case for both non-oversampled and oversampled Gaussian signal model

Vehicular A channel model [11] is applied for both non-oversampled and oversampled signal models in figure 5 and figure 6, respectively. The same signal parameters are used as in the Indoor channel case. Significant performance differences can be seen due to the difference of channel models.

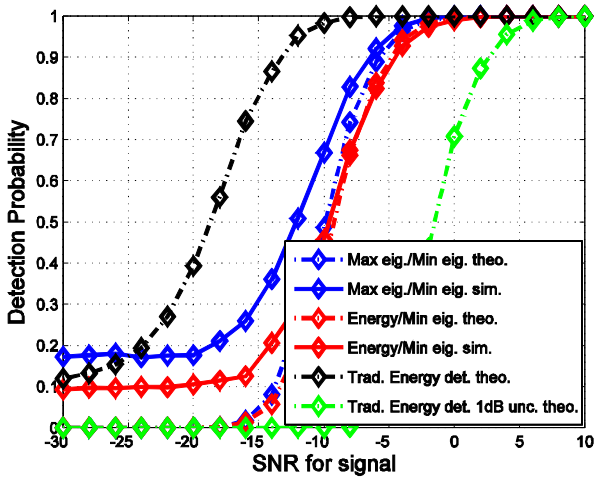

Figure 5. Detection probability of energy detector and eigenvalue based spectrum sensing under 1 dB uncertainty using Vehicular A channel with non-oversampled signal.

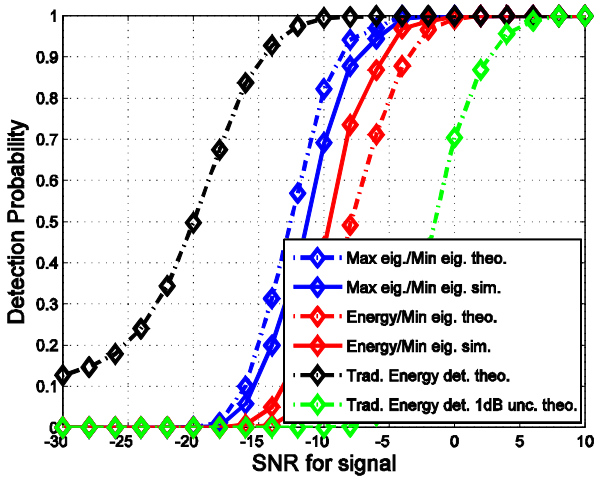

Figure 6. Detection probability of energy detector and eigenvalue based spectrum sensing under 1 dB uncertainty using Vehicular A channel with oversampled signal.

C. SUI-1 channel case for both non-oversampled and oversampled Gaussian signal model

In figures 7 and 8, the channel model is chosen as SUI-1 [11] for both non-oversampled and oversampled signal models, respectively. Comparing the results of non-oversampled and oversampled signal cases, significant difference of detection probability can be seen with eigenvalue based spectrum sensing. In the oversampled signal case, the correlation between consecutive samples is increased. In case of traditional energy detector, the detection performance is somewhat reduced with oversampling due to increased noise bandwidth.

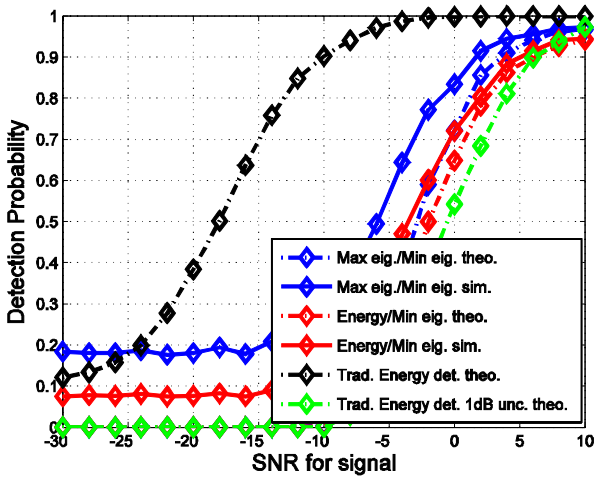

Figure 7. Detection probability of energy detector and eigenvalue based spectrum sensing under 1 dB uncertainty using SUI-1 channel with non-oversampled signal.

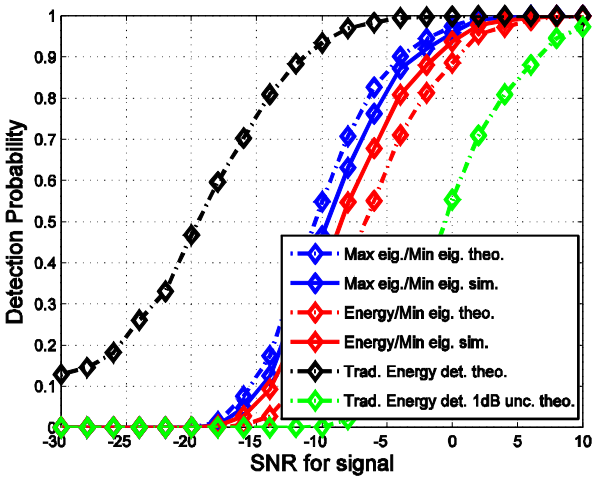

Figure 8. Detection probability of energy detector and eigenvalue based spectrum sensing under 1 dB uncertainty using SUI-1 channel with oversampled signal.

IV. CONCLUSIONS

We have analyzed the performance of the traditional energy detector and eigenvalue based spectrum sensing techniques under different frequency selective channels, the Indoor, ITU-R Vehicular A and SUI-1 channel models in particular. Actually, the frequency selective channel can help to increase detection probability when using eigenvalue or covariance based spectrum sensing algorithms.

It was seen that max/min eigenvalue approach gives consistently better detection performance that energy/min eigenvalue approach. Especially, in simulation based results with oversampling the difference is significant.

We have seen that eigenvalue based spectrum sensing clearly exceeds the performance of energy detector with 1 dB noise uncertainty with Indoor and Vehicular-A channel models, whereas with SUI-1, the difference is rather small. Using oversampled signal model in detection clearly reduces the false alarm probability with eigenvalue based sensing. With SUI-1, also the detection performance is significantly improved when oversampled signal is used in eigenvalue based detection, whereas with Indoor and Vehicular-A channel models, the detection performance is slightly degraded in the oversampled case.

The above observations are explained by the fact that SUI-1 is much less frequency selective than the other channel models used. Thus in this case the channel creates less correlations to the received signal, and the correlations due to the spectral shaping of the transmitted signal are much more important in the eigenvalue based detection than in the more frequency selective cases.

One related general aspect regarding spectrum sensing is the following: When the sensing station has a line-of sight (LOS) connection, the channel can be expected to be mildly frequency selective, but also the power level is high due to lower path loss. When the sensing station does not have a LOS connection, the signal level is lower, but also the channel can be expected to be highly frequency selective. Thus, in case of shadowing, the PU signal can be detected using the eigenvalue based approach without essential limitations due to noise uncertainty. In case of LOS channel, simple energy detection based approach might be sufficient.

While Gaussian signal model is used in this study, similar techniques and similar conclusions can be also applied for spectrum sensing with other primary systems. In the future work, to complete the picture, we will consider the effects of the spectrum sensing using real-life signal models such as WLAN and Bluetooth. It would be interesting also to quantify analytically the correlations introduced by the waveform and channel in different scenarios. Another topic is to apply low-complexity covariance matrix based methods, instead of the relatively complicated eigenvalue based approaches.

ACKNOWLEDGMENT

This work was partially supported by Tekniikan Edistämissäätiön (TES), GETA Graduate School and Tekes (the Finnish Funding Agency for Technology and Innovation) under the project ENCOR in the Trial Program.

REFERENCES

[1] I. Mitola, J. and J. Maguire, G. Q., "Cognitive radio: making software radios more personal," IEEE Personal Commun. Mag., vol. 6, no. 4, pp. 13–18, Aug. 1999.

[2] Y. Zeng, Y.C. Liang, A. T. Hoang, and R. Zhang, "A Review on Spectrum Sensing for Cognitive Radio: Challenges and Solutions," EURASIP Jor. on Ad. in Sig. Proc, vol. 2010, pp. 1-15, Jan. 2010.

[3] T. Yucek and H. Arslan, "A survey of spectrum sensing algorithms for cognitive radio applications," IEEE Communications Surveys & Tutorials, vol. 11, no. 1, pp. 116–130, March 2009.

[4] S. Dikmese, M. Renfors and H. Dincer, "FFT and Filter Bank Based Spectrum Sensing for WLAN Signals," in Proc. ECCTD2011 conf., Linkoping, Sweden, August 2011.

[5] S. Dikmese and M. Renfors, "Optimized FFT and Filter Bank Based Spectrum Sensing for Bluetooth Signal" in Proc. WCNC2012, Paris, France, April 2012.

[6] S. Dikmese and S. Srinivasan and M. Renfors, "FFT and Filter Bank Based Spectrum Sensing and Spectrum Utilization for Cognitive Radios" in Proc. Int. Symposium on Comm., Cont. and Sig. Proc. (ISCCSP 2012), Rome, Italy.

[7] R.Tandra and A. Sahai, "SNR walls for signal detection," IEEE J. Selected Topics Signal Processing, vol. 2, pp. 4-17, February 2008.

[8] S. Geirhofer, L. Tong, and B. Sadler, "A measurement-based model for dynamic spectrum access in WLAN channels," in Proc. IEEE MilitaryCommun. Conf., Washington, D.C., USA, Oct. 2006.

[9] Y. H. Zeng and Y.-C. Liang, "Eigenvalue-based spectrum sensing algorithms for cognitive radio," IEEE Transactions on Communications, vol. 57, no. 6, pp. 1784–1793, 2009.

[10] Y. H. Zeng and Y.-C. Liang, "Spectrum-sensing algorithms for cognitive radio based on statistical covariances," IEEE Transactions on Vehicular Technology, vol. 58, no. 4, pp. 1804–1815, 2009.

[11] R. Jain, "Channel Models: A Tutorial," WiMAX Forum AATG, February 2007.

[12] A. M. Tulino and S. Verdu, "Random Matrix Theory and Wireless Communications" Now Publishers Inc., 2004.

[13] C. A. Tracy and H. Widom, "On orthogonal and symplectic matrix ensembles, " Commun. Math. Phys., vol.177, pp. 727-754, 1996.

[14] C. A. Tracy and H. Widom, "The distribution of the largest eigenvalue in the gaussian ensembles," in Calogero-Moser-Sutherland Models, J. van Diejen and L. Vinet, eds., pp. 461-472. Newyork: Springer, 2000.

[15] T.Yucek, "Channel, Spectrum, and Waveform Awareness in OFDM-Based Cognitive Radio Systems" Ph.D. thesis, Tampa, 2007

PUBLICATION 3

Sener Dikmese, Sudharsan Srinivasan, Musbah Shaat, Faouzi Bader and Markku Renfors, "Spectrum Sensing and Spectrum Allocation for Multicarrier Cognitive Radios under Interference and Power Constraints," *EURASIP Journal on Advances in Signal Processing* DOI: 10.1186/1687-6180-2014-68, May 2014.

EURASIP Journal on Advances in Signal Processing
a SpringerOpen Journal

RESEARCH Open Access

Spectrum sensing and resource allocation for multicarrier cognitive radio systems under interference and power constraints

Sener Dikmese[1*], Sudharsan Srinivasan[1], Musbah Shaat[2], Faouzi Bader[3] and Markku Renfors[1]

Abstract

Multicarrier waveforms have been commonly recognized as strong candidates for cognitive radio. In this paper, we study the dynamics of spectrum sensing and spectrum allocation functions in cognitive radio context using very practical signal models for the primary users (PUs), including the effects of power amplifier nonlinearities. We start by sensing the spectrum with energy detection-based wideband multichannel spectrum sensing algorithm and continue by investigating optimal resource allocation methods. Along the way, we examine the effects of spectral regrowth due to the inevitable power amplifier nonlinearities of the PU transmitters. The signal model includes frequency selective block-fading channel models for both secondary and primary transmissions. Filter bank-based wideband spectrum sensing techniques are applied for detecting spectral holes and filter bank-based multicarrier (FBMC) modulation is selected for transmission as an alternative multicarrier waveform to avoid the disadvantage of limited spectral containment of orthogonal frequency-division multiplexing (OFDM)-based multicarrier systems. The optimization technique used for the resource allocation approach considered in this study utilizes the information obtained through spectrum sensing and knowledge of spectrum leakage effects of the underlying waveforms, including a practical power amplifier model for the PU transmitter. This study utilizes a computationally efficient algorithm to maximize the SU link capacity with power and interference constraints. It is seen that the SU transmission capacity depends critically on the spectral containment of the PU waveform, and these effects are quantified in a case study using an 802.11-g WLAN scenario.

Keywords: CR; OFDM; FBMC; Filter bank; Spectrum sensing; Energy detector; Spectrum utilization; Loading algorithms; Multicarrier

1 Introduction

One of the major challenges in cognitive radio (CR) operation is to utilize the available whitespace with minimal interference to the primary or prioritized secondary transmission systems [1]. Several spectrum sensing techniques have been proposed, e.g., in [2-5] to facilitate CR operation. Especially, energy detector-based spectrum sensing algorithms have been widely considered due to low computational complexity. On the other hand, the fading channel capacity has already been studied from an information theoretic perspective, e.g., in [6,7] in terms of resource allocation. Recently, the secondary user (SU) capacity has been widely studied. The SU channel capacity for additive white Gaussian noise (AWGN) channels under different power constraint is studied in [8]. The effect of various types of fading channels on the CR capacity has been studied in [9] under optimal power allocation strategy for the CR and subjected to an interference power constraint at the coexisting primary. Further, [10] discusses the effects of peak power and average interference power constraints on the outage capacity. In [11], the ergodic capacity, the delay-limited capacity, and the outage capacity of the CR in block-fading channels under spectrum sharing are discussed.

In this paper, we investigate two important features of the cognitive radio. We begin with the spectrum sensing function and later study the spectrum utilization

* Correspondence: sener.dikmese@tut.fi
[1]Department of Electronics and Communications Engineering, Tampere University of Technology, P.O. Box 692, Tampere 33101, Finland
Full list of author information is available at the end of the article

function implementing optimized resource allocation under power and interference constraints. Instead of elaborate spectrum sensing techniques, such as cyclostationary and eigenvalue-based methods [2,3], energy detector-based spectrum sensing is utilized. This is motivated by subband-based energy detector's capability to implement the needed spectrum analysis functions for identifying the available spectral slots and for estimating the signal-to-interference-plus-noise (SINR) ratios at subcarrier level for resource allocation purposes.

For a CR system, multicarrier modulation techniques are generally better suited as they are spectrally more efficient than single carrier systems and have the flexibility to allocate resources to the available spectral gaps and among different users to maximize system throughput. There are various ways of improving the spectral containment of multicarrier waveforms, including methods to suppress the strong side lobes of the orthogonal frequency-division multiplexing (OFDM) spectrum [12-14]. Filter bank multicarrier (FBMC) is another multicarrier modulation scheme which has significantly reduced spectrum leakage compared to the cyclic prefix-based OFDM systems [15]. Also, the analysis filter bank (AFB) module of an FBMC receiver can be easily used for spectrum analysis purposes [15-22].

This paper includes a brief summary of our earlier studies concerning simple energy detection-based wideband multichannel spectrum sensing techniques for identifying the spectrum holes, considering the 2.4-GHz ISM band as a case study. We apply an AFB-based energy detector, which averages the subband sample energies. By this way, multiple center frequencies, bandwidths, and multiple spectral gaps can be identified rapidly, efficiently, and flexibly for potential use by the CR. A similar fast Fourier transform (FFT)-based scheme is considered as a reference.

At the resource allocation stage, the transmit power of the subcarriers must be adjusted according to the channel state information (CSI) and the location of subcarriers with respect to the primary user's (PU) spectrum. In [23], an optimal and two sub-optimal power loading algorithms are developed. These algorithms use Lagrange formulation which maximizes the downlink capacity of the CR keeping the interference to the primary transmission below a threshold, without considering the total power constraint. In [23,24], the spectral hole and the signal-to-noise (SNR) are fixed to simplify the model. In [25], a low-complexity suboptimal algorithm is proposed. The algorithm gives maximum power to each subcarrier based on the results from conventional water filling and then modifies these values by applying power reduction algorithm in such a way that the interference constraint is satisfied. In [23,25], the used signal models are closer to the ideal signal model, e.g., assuming fixed spectral hole bandwidth, instead of a realistic system model. In reality, the spectral hole bandwidth varies with the SNR. A proper system model should include also a practical power amplifier model. Our study focuses on the missing aspects of these studies.

The optimal solution which maximizes the CR link capacity under both transmission power and interference constraints requires high computational complexity, and it is unsuitable for the practical applications. Low complexity algorithms are proposed in [25,26]. However, in these methods, the interfered subcarriers are deactivated without considering optimized power and bit loading based on each subcarrier's SINR. Such optimization can be carried out using the power interference (PI) algorithm [27,28]. The resource allocation method utilizes the results of spectrum sensing in an efficient way, so there is interdependence between the spectrum sensing and spectrum allocation functions, which has not been addressed in earlier work. We study this interdependence, focusing on its effects on efficient utilization of the sensed spectrum.

The main contributions of this study are listed as follows:

- We have generalized the study for realistic signal models which can be applied to any multicarrier CR system.
  Until now, simplistic CP-OFDM signal models have been used as the PU and CR signal models for spectrum allocation algorithms [23-26,29-32]. Except for [27,28], CP-OFDM has also been used for the CR. The primary knowledge we assume about the PU waveform is its transmitted power spectral density (PSD) and the receiver selectivity mask; otherwise, there are no limitations regarding the PU signal model. In our case study, we select the PU waveform either as CP-OFDM following the 802.11-g standard or an FBMC waveform with similar parameterization. Furthermore, a nonlinear transmitter power amplifier model (the so-called Rapp model [33]) is used for the PU system in order to obtain a realistic model for the PU spectrum. To the best of our knowledge, this aspect has not been considered in earlier work. In this way, we are able to quantify the effects of the PU spectral characteristics on the SU capacity. It is seen that the nonlinear power amplifier-induced spectral leakage (regrowth) effect, which is present in any radio communication system, has a significant impact on the SU capacity. As for the SU waveform, we have chosen the FBMC scheme for the case study because it has the sharpest spectrum, reaching the maximum spectral containment among the alternatives.
  However, generic multicarrier model is included in the overall system model, and the analysis and

optimization methods are readily applicable for any multicarrier waveform for the CR.
Furthermore, previous studies on CR resource allocation in [23-25,27-32] consider only flat fading channel models. However, the performance of spectrum sensing and resource allocation is affected significantly when frequency-selective fading channel is assumed. In our study, all the links within/between PU and SU systems associated with spectrum estimation and spectrum utilization are modeled as frequency selective block fading channels.

- Combined spectrum sensing and resource allocation algorithms for cognitive radios.
There has been no previous work addressing the combined spectrum sensing and resource allocation algorithm in the literature. Especially, different types of spectrum sensing algorithms have been applied without considering any particular spectrum utilization techniques to make efficient use of the available spectral holes [1-5]. Similarly, resource allocation algorithms have only been applied without any spectrum sensing information so far [27-32,34,35]. Constant number of available subbands has been considered in the spectral hole. However, the variation of the PUs' power level affects the actual number of available subbands, and this depends critically on the spectral characteristics of the PUs. Hence, spectrum sensing plays a crucial and enabling role for spectrum utilization process. The sensing function identifies the frequency band which is considered for allocation, but it is also needed for detecting possible other PU's starting to operate in the spectral gap during the SU operation. For this purpose, we assume that there are gaps in the CR transmission. In our study, efficient spectrum utilization methods are investigated and applied for maximizing the cognitive radio's throughput based on robust spectrum sensing results. It turns out that the PI algorithm is applicable in our scenario, with all the mentioned generalizations of the system model. The main contribution of this study is evaluating the SU performance with the combination of energy detection-based wideband sensing algorithm and the PI algorithm for spectrum utilization in a realistic cognitive radio scenario.

The rest of this paper is organized as follows. In Section 2, the signal models for the CR and the primary transmission system, along with the mutual interference model between the CR and primary are explained. The problem definition for this study is given in the same section. In Section 3, FFT- and AFB-based wideband spectrum sensing is reviewed considering the spectrum analysis aspects related to the multicarrier techniques. Section 4 develops the algorithms for spectrum allocation. Section 5 gives the numeric and graphic results obtained through simulations. Finally, some concluding remarks are given about the performance of these methods, along with discussion of possible further studies in this area.

2 Signal models and problem definition

As shown in Figure 1, the CR system works in the same band of frequencies with PU networks. Hence, there will be some interference between different PUs and CRs. The PU and CR systems are assumed to use the time-division multiplexing/duplexing (TDMA/TDD) principles, i.e., each system is using a fixed frequency slot for communications between all the stations. While the CR system has the capability to operate in other parts of the ISM band, we focus on the situation where the CR

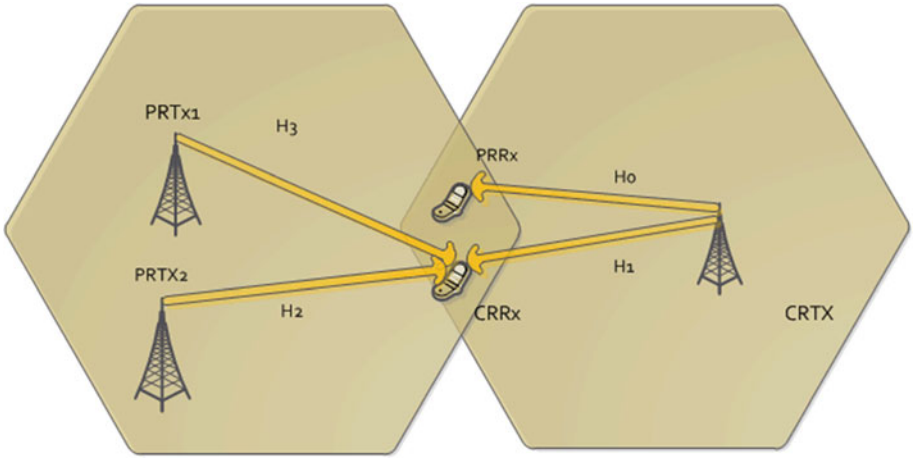

Figure 1 System model for spectrum sharing in CR.

system has identified a spectrum opportunity in the mentioned frequency slot and is initiating communications in it. The primary purpose of the spectrum sensing function is to detect possible other transmissions or reappearing PUs in the spectrum gap. It is also assumed that the stations of the CR systems have means to exchange control information with each other, e.g., using a cognitive control channel [36].

2.1 Signal model for PU

In this study, we focus on a specific spectrum use scenario with two active primary radio systems which are operating in the 2.4-GHz ISM band, using either as 802.11 g-based WLAN waveforms or 802.11 g-like FBMC signals. The WLAN and FBMC spectra considered here use third and eighth channels as illustrated in Figure 2. The signals do not overlap each other, and an 8-MHz spectral hole is available between the two PU spectra. Both active signals are assumed to have the same power level, normalized to 0 dB in our scenario. This means that the spectrum leakage effects on both edges of the white space are equally critical for the CR system performance.

The Rapp power amplifier (PA) nonlinearity model [33] is considered as seen in Figure 2. Using the complex I/Q baseband model, the amplitude function at the PA output is given as follows:

$$g_A = \frac{\kappa A}{\left(1 + [\kappa A / A_0]^{2p}\right)^{1/2p}} \quad (1)$$

where A is the input amplitude, κ is the small signal gain, A_0 is the saturated amplitude, and p is the amplitude smoothness factor of the transition from linear to saturated amplitude range. Three cases with respect to the PA nonlinearity are considered in this study. *No regrowth* is the ideal case, and the Rapp PA nonlinearity with two different back-off values of 15 dB (*modest case*) and 5 dB (*worst case*) is illustrated in Figure 2. Parameters of the Rapp model have been chosen according to the practical model for PU signals based on [37]. In our study, we use $\kappa = 1$, $p = 3$, and $A_0 = 1$ as Rapp model simulation parameters.

The 802.11-g-based WLAN signal specifications allow the spectral regrowth in this scenario to be at the level of about −20 dB, i.e., close to the worst case model. We investigate how the CR system performance is affected by improved spectral containment of the PU signal through enhanced multicarrier waveform and/or improved power amplifier linearity. These effects for both sensing and utilization functions will be addressed in the study.

2.2 Signal model for cognitive radio

In this work, the CR waveform is chosen as FBMC due to its high spectral containment. Offset quadrature amplitude modulation (OQAM) is used for FBMC-based CRs to achieve orthogonality of subcarriers, as discussed in [18,19,38]. In Figure 1, the channels h_0 and h_1 are the channels from a cognitive transmitter to a primary receiver and a cognitive receiver, respectively. Channels h_2 and h_3 are from two different primary transmitters to the cognitive radio receiver. The channel estimate for h_1 is made available by usual channel estimation procedure of the CR system. The knowledge about channel h_0 can be obtained through the channel reciprocity in TDD

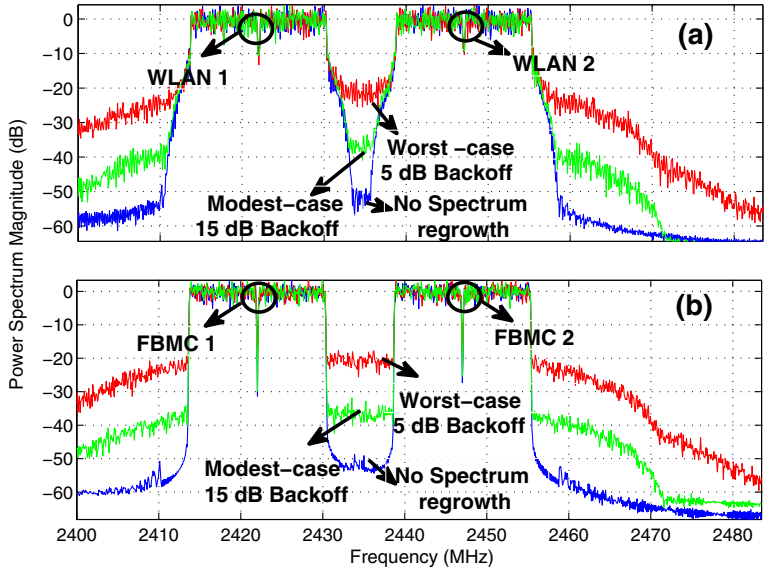

Figure 2 Effects of the Rapp power amplifier model on (a) OFDM- and (b) FBMC-based primary users' spectra.

operation. Here, the channel amplitude response is sufficient and the phase response is irrelevant. The amplitude responses of channels h_2 and h_3 are first obtained through the spectrum sensing function of the CR device and later on, during secondary transmission, through the SINR estimation function of the CR device. The effects of primary spectral dynamics at the edges of the white space play an important role both in spectrum sensing and in spectrum allocation. This dependency is captured by the analytical models and revealed by the simulations to be presented later.

For FBMC/OQAM, a signal model with real valued symbol sequence at twice the QAM symbol rate is applied, instead of complex symbols. The synthesis filter bank (SFB) for transmitter and AFB for receiver is designed with this idea in mind. The FBMC-based transmitted signal can be expressed mathematically as

$$s(n) = \sum_{k} \sum_{l \in Z} a_{k,l} g(n - l\tau_0) e^{j2\pi(k/N)n} e^{j\phi_{k,l}} \tag{2}$$

where $\{k\}$ is the set of active subbands, l is the symbol index belonging to the set of integers, g is the pulse shape (prototype filter impulse response), and $\phi_{k,l}$ is a phase term. The real symbol values, obtained alternatingly as real and imaginary parts of complex QAM symbols, are denoted as $a_{k,l}$ and τ_0, respectively, is the corresponding half-symbol duration. Both the real and imaginary parts of the QAM sequence have zero mean and equal variances $\sigma_r^2 = \sigma_I^2 = \sigma_s^2/2$. The PSD of the FBMC based CR waveform can be written as

$$\phi_{\mathrm{FBMC}}(f) = \frac{\sigma_r^2}{\tau_0} \sum_{k} \left| G\left(f - \frac{k}{N}\right) \right|^2 \tag{3}$$

where G is the frequency response of the prototype filter with impulse response $g(n)$ with $n = 0, 1 \ldots, L - 1$. Here, $L = KN$ is the prototype filter length and K is the overlapping factor (length of each polyphase component) while N is the number of subbands. The prototype coefficients have even symmetry around the $(KN/2)$th coefficient, and the first coefficient is zero [13]. In our study, the prototype filter of the FBMC-based CR is designed according to the PHYDYAS model [38], with $K = 4$. Then its frequency response can then be expressed as

$$|G(f)| = g[L/2] + 2 \sum_{r=1}^{L/2-1} g[L/2 - r] \cos(2\pi f r) \tag{4}$$

Also, the nonlinear PA model can be straightforwardly included in the CR signal model and the interference models developed below. However, in the numerical studies of this paper, we consider an ideal FBMC waveform for the CR as the focus is on the SU capacity and its dependency on the PU waveform characteristics. Generally, good spectral containment is regarded as one of the key requirements for the CR transmitter. Detailed evaluation of the performance-complexity tradeoffs for the CR implementation, including the PA linearity requirements, is a rather complicated issue and is left as a topic for future studies.

2.3 Definition of the interference problem

According to the above scenario, the CR system coexists with the primary transmission system in the same geographical location. The CR transmitter causes some interference to the primary transmission system, and similarly, the secondary transmission between two active PU spectra is exposed to some interference due to the PUs. The secondary transmission system uses multicarrier transmission technique. There are N_{gap} subcarriers in the sensed spectrum hole and the subcarrier spacing is Δf. Since the transmitter and receiver are assumed to be static or slowly moving, the effect of inter-carrier interference (ICI) between subcarriers can be ignored. The primary and secondary transmission systems occupy contiguous frequency slots. The interference that the CR produces to each of the primaries is required to be is less than the maximum interference that can be tolerated by the primary, Ith. The spectral distance d_{PU} of a PU is defined as the frequency separation from the DC subcarrier of the CR to the center frequency of the PU (positive for a PU above the upper edge of the gap, negative for a PU below the gap). The interference to the primary transmission due to the kth CR subcarrier depends on the CR subcarrier powers P_k and d_{PU} [20]. Fixing the origin of the frequency axis at the DC subcarrier of the CR, the interference is given by the equation

$$I_k(P_k) = \int_{k\Delta f - B/2}^{k\Delta f + B/2} |H_0(f)|^2 P_k \Phi(f - k\Delta f) \Psi(f - d_{\mathrm{PU}}) df = P_k \Omega_k \tag{5}$$

Here, $H_0(f)$ is the channel frequency response between the CR transmitter and a primary receiver. $\Phi(f)$ represents the subcarrier power spectral density of the underlying multicarrier technique employed by the CR. $\Psi(f)$ denotes the PU sensitivity mask characterizing the effects of the PU receiver filtering. B denotes the CR subcarrier bandwidth which is considered significant for the interference estimation. Finally, Ω_k represents the combined interference factor for the kth CR subcarrier.

The signal-to-interference-plus-noise ratio due to interference introduced by primary signal to the kth subcarrier at the receiving CR is given by

$$\mathrm{SINR}_k = \frac{P_k |H_{1,k}|^2}{\sigma_w^2 + \int_{k\Delta f - B/2}^{k\Delta f + B/2} |H_2(f)|^2 \Phi(f - k\Delta f)\psi_{\mathrm{PA}}(f - d_{\mathrm{PU}})df} = \frac{P_k}{\sigma_w^2 + J_k} \tag{6}$$

where $H_2(f)$ is the channel frequency response between the primary transmitter and CR receiver. $H_{1,k}$ is the channel gain between the CR transmitter and the CR receiver at the frequency of kth subcarrier. This channel can be assumed to be flat-fading at the subcarrier level. $\Psi_{\mathrm{PA}}(f)$ is the power spectral density as seen at the output of the PU's transmitter antenna. This depends on the PU transmission power and its subcarrier spectrum, as well as on the spectral regrowth due to the PU power amplifier. $\Phi(f)$ is the CR receiver sensitivity mask characterizing the CR receiver subband filtering effects. σ_w^2 is the variance of the additive white Gaussian noise.

The power amplifier effects of the secondary transmission are not considered in our numerical study as they play no role in the spectrum sensing part and the effect of PA-related spectrum leakage on the interference to the PUs is expected to be relatively small. For this reason, the same $\Phi(f)$ function can be used in (5) for the CR subcarrier spectrum and in (6) for the CR receiver sensitivity mask. However, the developed generic signal model allows to include also the CR transmitter PA effects by using different CR-related spectral functions in (5) and (6).

The interference models of (5) and (6) assume certain knowledge about PU characteristics and the channels between PUs and CRs. Regarding the interference from an active PU transmitter to a CR receiver in (6), the joint effect of transmitter power spectrum and the transmission channel can be estimated by the receiving CR station by utilizing the spectrum sensing function. This information can be communicated through the control channel to the transmitting CR station for optimizing the spectrum utilization. Regarding the channel from the CR transmitter to PU receiver, the knowledge would be available in a TDMA/TDD-based PU system (like a WLAN) based on channel reciprocity, if the PU transmission power is known. Of course, for a PU station which is in idle mode over long periods, such information is not available.

3 Filter bank energy detector-based spectrum sensing algorithms

Energy detector, which is also known as radiometer, is the most common method of spectrum sensing due to its low computational and implementation complexity [2-5]. Furthermore, it is more generic compared to most of the other methods as it does not need any information about the PU waveform. Subband-based energy detection, using FFT or AFB for spectrum analysis, is in the focus of this study. Basically, the energy of the received signal is compared with a threshold value which is calculated according to noise variance and desired false alarm probability in detecting spectral holes.

A block diagram of alternative FFT- and AFB-based spectrum sensing algorithms is shown in Figure 3. The subband sampling rate is equal to the ADC sampling rate divided by the number of FFT/AFB frequency bins. With subband-wise spectrum sensing method, the subband signals can be expressed as [3]

$$Y(m,k) = \begin{cases} W(m,k) & \mathcal{H}_0 \\ S(m,k)H_k + W(m,k) & \mathcal{H}_1 \end{cases} \tag{7}$$

where $S(m, k)$ is the transmitted WLAN or FBMC based PU signals as seen in subband k during the mth symbol interval with zero mean and variance σ_{PU}^2. When there are no PU signals (hypothesis $\mathcal{H}_0$), the noise samples $W(m, k)$ are modeled as AWGN with zero-mean and variance σ_w^2. When a PU signal is present (hypothesis $\mathcal{H}_1$), the WLAN- and FBMC-based PU signals can also be modeled as zero-mean Gaussian distribution with variance $\sigma_{\mathrm{PU},k}^2 + \sigma_w^2$.

Time and frequency averaging techniques can be applied to obtain more reliable decision statistic [3]. The decision statistics at different frequencies can be obtained with this idea as follows in [39]:

$$\tilde{T}(m,k) = \frac{1}{L_t L_f} \sum_{l=k-\lfloor L_f/2 \rfloor}^{k+\lceil L_f/2 \rceil - 1} \sum_{u=m-L_t+1}^{m} |Y(u,l)|^2 \tag{8}$$

In this formula, L_f and L_t are the window lengths in frequency and time domain averaging, respectively. The output of $\tilde{T}(m,k)$ is passed to a decision device to determine the possible occupancy of the corresponding frequency band at the corresponding time interval. The window length in frequency direction is selected based on the expected minimum bandwidth of the PU signal or spectrum hole, and then the required time domain window length can be calculated from the target false

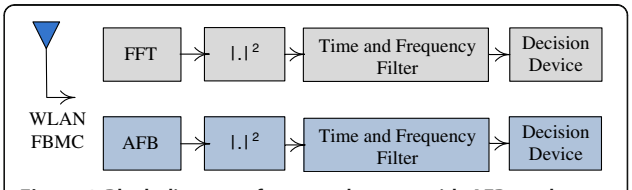

Figure 3 Block diagram of energy detector with AFB- and FFT-based spectrum analysis.

alarm and missed detection probabilities. The basic approach would be to calculate (8) for a nonoverlapping set of windows. However, using a sliding window in frequency and/or time direction can also be done with relatively small addition to complexity. Time-domain sliding window helps to detect rapidly re-appearing PU [4,5] whereas sliding window in the frequency direction helps to locate spectrum gaps with unknown center frequencies. Due to the Gaussian distribution of $Y(m, k)$, the probability distribution function (PDF) of $\tilde{T}(m,k)$ becomes approximately Gaussian under $\mathcal{H}_0$ and $\mathcal{H}_1$. [3].

Using Gaussian approximation, it is straightforward to model the effect of PU transmitter's spectral leakage on the actual false alarm probability $\tilde{P}_{\mathrm{FA}}$ as

$$\tilde{P}_{\mathrm{FA}}(k) = Q\left(\frac{\lambda - \left(\sigma_w^2 + I_{\mathrm{adj}}(k)\right)}{\sqrt{\frac{1}{L_t L_f}\left(\sigma_w^2 + I_{\mathrm{adj}}(k)\right)}}\right) \tag{9}$$

Here,

$$I_{\mathrm{adj}}(k) = \int_{f_1}^{f_2} |H_2(f)|^2 \psi_{\mathrm{PA}}(f) df \tag{10}$$

is the leakage power from the adjacent PU transmitter to the sensing frequency band between frequencies f_1 and f_2. $H_2(f)$ is the channel frequency response from a primary transmitter the CR receiver. In (9), λ is the decision threshold value which is calculated using a well-known analytical model from the noise variance estimate and target false alarm probability P_{FA}.

The detection probability P_D and threshold value λ can also be expressed as follows:

$$P_D(k) = Q\left(\frac{\lambda - \left(\left(\sigma_w^2 + I_{\mathrm{adj}}(k)\right) + \sigma_{\mathrm{PU},k}^2\right)}{\sqrt{\frac{1}{L_t L_f}\left(\left(\sigma_w^2 + I_{\mathrm{adj}}(k)\right) + \sigma_{\mathrm{PU},k}^2\right)}}\right) \tag{11}$$

$$\lambda = Q^{-1}(P_{\mathrm{FA}}(k))\sqrt{\frac{1}{L_t L_f}\left(\sigma_w^2 + I_{\mathrm{adj}}(k)\right)} + \left(\sigma_w^2 + I_{\mathrm{adj}}(k)\right) \tag{12}$$

In principle, if there is a reliable estimate of the PU transmission power and reliable knowledge about its spectrum shape, then the above analysis could be used for improving the spectrum sensing at the frequencies affected by the spectrum leakage. However, this would be very challenging in practice due to the unpredictability of the PA characteristics, and the above model is used only for the purpose of performance analysis.

For different PU SNR values, different number of empty subbands, N_{gap}, will be detected due to the PU spectral leakage effects and statistical nature of the spectrum sensing process. The expression (9) can be used for evaluating the false alarm probability for different sensing bandwidths in different parts of the spectrum gap.

The spectrum sensing function identifies groups of L_f subbands which are deemed to be available for secondary transmissions. In the following stage, the spectrum utilization function is employed to perform power and bit allocation to those subcarriers.

4 Spectrum utilization

After nonactive spectrum has been identified, spectrum utilization becomes an important consideration, when considering the overall efficiency of the CR system. The number of available nonactive subbands is the output of the sensing algorithm, along with information about the nonactive band edges.

In the multicarrier case, the rate at which transmission can take place is given by Shannon's capacity

$$R_{\mathrm{CR}} = \sum_{k=1}^{N_{\mathrm{gap}}} \Delta f \log_2\left(1 + \frac{P_k}{\sigma_k^2}\right) \tag{13}$$

$$\sigma_k^2 = \sigma_w^2 + \sum_{i=1}^{N_{\mathrm{PU}}} J_{k,i} \tag{14}$$

where $J_{k,i}$ is the effective interference power contributed by ith primary to the kth CR subcarrier as given by (6). N_{PU} is the number of PU's contributing to the interference at the receiving CR station. In our case study, $N_{\mathrm{PU}} = 2$, i.e., there is one PU adjacent to the lower and upper edges of the white space. The model could be simplified by assuming that these PUs affect only the lower and upper half of the subcarriers, respectively. P_k is the transmit power used by the CR for subcarrier k. It is assumed that the channel changes slowly so that the channel gains, and consequently $J_{k,i}$, will be approximately the same during each transmission frame. Further, there is no ICI in the CR reception due to low mobility. The main objective here is to maximize the capacity as given in (13).

The block diagram of spectrum utilization is shown in Figure 4. As seen in this block diagram, knowledge which comes from sensing part is passed to spectrum utilization part to obtain better capacity.

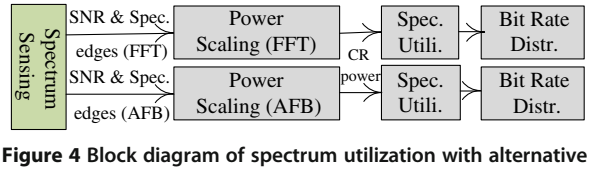

Figure 4 Block diagram of spectrum utilization with alternative AFB- and FFT-based spectrum analysis schemes.

The optimization problem can be formulated as follows [27]:

$$R_{\mathrm{CR}} = \max_{\{P_k\}} \sum_{k=1}^{N_{\mathrm{gap}}} \Delta f \log_2\left(1+\frac{P_k}{\sigma_k^2}\right) \tag{15}$$

Subject to

$$\sum_{k=1}^{N_{\mathrm{gap}}} P_k \le P_T \tag{16}$$

$$\sum_{k=1}^{N_{\mathrm{gap}}} P_k \Omega_k \le I_{th} \tag{17}$$

$$P_k \ge 0, \forall k \in \{1,2,\ldots,N_{\mathrm{gap}}\} \tag{18}$$

This is a convex optimization problem, and the Lagrangian can be written as

$$\begin{aligned} G_{\mathrm{snr}} &= \sum_{k=1}^{N_{\mathrm{gap}}} \Delta f \log_2\left(1+\frac{P_k}{\sigma_k^2}\right) \\ &-\lambda_0 \sum_{k=1}^{N_{\mathrm{gap}}} (P_k - P_T) - \lambda_1 (P_k \Omega_k - I_{\mathrm{th}}) + \lambda_2 \sum_{k=1}^{N_{\mathrm{gap}}} P_k \end{aligned} \tag{19}$$

The Karush-Kuhn-Tucker (KKT) conditions [27] can be written as

$$P_k \ge 0, \forall k \in \{1,2,\ldots,N_{\mathrm{gap}}\}, \tag{20}$$

$$\lambda_j \ge 0, \forall j \in \{0,1,2\} \tag{21}$$

$$\sum_{k=1}^{N_{\mathrm{gap}}} (P_k - P_T) \ge 0 \tag{22}$$

$$\lambda_1 (P_k \Omega_k - I_{\mathrm{th}}) \ge 0 \tag{23}$$

$$\lambda_2 \sum_{k=1}^{N_{\mathrm{gap}}} P_k \ge 0 \tag{24}$$

The optimal solution to the problem above as given in [27] is as follows:

$$P_k = \left[\frac{1}{\lambda_0 \Omega_k + \lambda_1} - \frac{\sigma_k^2}{|h_k|}\right]^+ \tag{25}$$

where $[y]^+ = \max(0, y)$. The optimal solution has high computationally complexity; hence, a lower complexity algorithm called the PI algorithm which divides the problem into stages has been developed [27]. First, the interference constraint is ignored, keeping only the total power constraint and this leads to the classical water filling solution

$$P_k' = \left[\gamma - \frac{\sigma_k^2}{|h_k|}\right]^+ \tag{26}$$

where γ is the water filling level. When the total power is ignored the solution [27] becomes

$$P_k' = \left[\frac{1}{\lambda'_0 \Omega_k} - \frac{\sigma_k^2}{|h_k|}\right]^+ \tag{27}$$

The value of λ'_0 can be obtained by substituting (27) into the constraint $\sum_{k=1}^{N_{\mathrm{gap}}} P_k' \Omega_k = I_{\mathrm{th}}$ to get

$$\lambda'_0 = \frac{|N_{\mathrm{gap},I}|}{I_{\mathrm{th}}^{N_{\mathrm{gap}}} + \left(\sum_i \Omega_k \sigma_k^2 / |h_k|^2\right)} \tag{28}$$

The above solution is optimal only when the total power is greater than or equal to the power under the interference constraint. Mostly, in practice, this condition is not true and this is the motivation for the PI algorithm. Detailed discussion and its comparison to various other algorithms for spectrum utilization are available in [27].

In this study, the PI algorithm is found to be directly applicable in case of the developed greatly enhanced system model for the secondary usage scenario. PI algorithm has four stages: maximum power determination, power constraint, power budget distribution, and power level re-adjustment [27].

5 Simulation results

In our test scenario, the CR's spectrum sensing function has identified a potential spectral gap between two relatively strong PUs, as illustrated in Figure 2. We should also consider the possibility that there is another, relatively weak PU signal, using one of the WLAN channels 4...7, and fully or partly occupying the gap between channels 3 and 8. Thus, one purpose of spectrum sensing is to secure that there are no other PUs active in the considered gap. We assume that there are no additional signals within the spectral gap, but the spectrum sensing makes anyway false alarms. Especially close to the edges of the gap, the spectrum leakage from the PUs raises the false alarm probability. This effect depends on the power level (SNR) of the PUs. In our case study, the spectrum sensing and CR transmissions use a smaller subband spacing of 81.5 kHz, instead of the 325-kHz subcarrier spacing of WLANs, in order to reduce the effects of frequency selective channels. Targeting at −5 dB SNR in spectrum sensing, false alarm probability of 0.1, and detection probability of 90%, the required sample complexity is around 250 complex samples. The time and frequency averaging lengths are chosen as 50 and 5, respectively. The spectral hole starts from the side lobes of WLAN 1 signal and ends at the side lobes of WLAN 2 spectrum. The available number of subbands/bandwidth

of the spectrum is obtained after subband-based energy detection, using FFT or AFB for spectrum analysis. Then, the initial SINR estimation and spectrum allocation is done based on the sensing results. Later on, the SINR estimates are updated during SU system operation to track the changing radio environment under frequency-selective fading channel conditions. It is assumed that the spectrum sensing is done in regular intervals during gaps in the CR transmission and this helps in detecting reappearing PU signals in the spectral gap.

It should be noticed that in the considered scenario, there is no way for the CR system to determine the useful received power level at the PU receiver. Therefore, we choose the interference threshold to be 6 dB below the thermal noise level, in order not to introduce significant performance loss in case the primary receiver is operating close to the sensitivity level (i.e., minimum received power level expected to be detectable). To determine the threshold value, we assume a simplified scenario, where the path losses of channels h_0 and h_1 are normalized to 1, i.e., the average power gains of channels h_0 and h_1, denoted as G_0 and G_1, are equal to one. Further, we assume that the average SNR of the CR receiver is 10 dB. Then, the interference threshold is −16 dB in reference to the total CR transmission power P_T, or $I_{\text{th}} = P_T/40$. More generally, relaxing the normalization of h_0 and h_1, this can be expressed as $I_{\text{th}} = G_1 P_T/(40G_0)$.

The bandwidth of the detected spectral hole is shown in Figure 5 as a function of the average PU SNR at the CR RX. The spectral leakage due to primary users' PA nonlinearity is affecting significantly on the width of the detected hole. In this respect, we consider three different cases, as explained in Subsection 2.1: ideal PA, modest PA nonlinearity with 15 dB back-off, and worst case nonlinearity with 5 dB back-off. All PU and CR channels h_0, h_1, h_2, and h_3 use frequency-selective channel models with 90 ns delay spread and 16 taps [40]. We consider the combinations of two PU waveforms, CP-OFDM- and FBMC-based WLANs, as well as two spectrum sensing techniques, based on FFT or AFB. The CR waveform is always FBMC.

From Figure 5, it can be easily seen that AFB-based spectrum sensing is able to detect the unoccupied spectrum close to strong primary users much better than FFT-based sensing. FBMC-based transmission results in much better spectral containment, which can be effectively utilized by AFB-based sensing. However, even with relatively modest power amplifier nonlinearity, this benefit of FBMC waveform is compromised.

In Figure 6, the actual false alarm probability within the spectral hole is shown as a function of the active PU's SNR for different levels of spectral regrowth. The results indicate the probability of the 5 subband groups to be detected to be occupied.

The efficiency of the utilization of the 8-MHz white space by SU in between two active PUs is shown in Figure 7 versus the PU SNR. In this figure, perfect CSI is considered for the CR channel, both for CR channel h_1

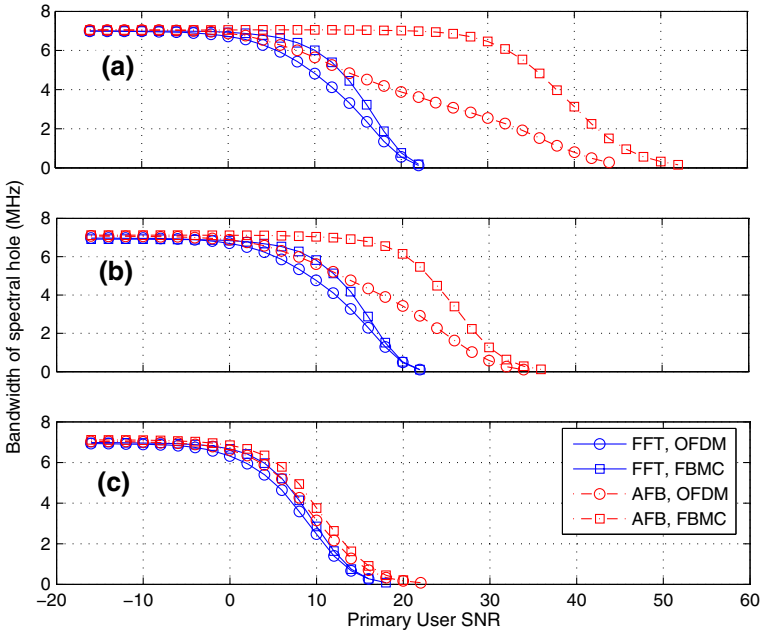

Figure 5 Average bandwidth of the detected spectral hole with target $P_{FA} = 0.1$. Using sample complexity of 250 samples under frequency-selective channel model for **(a)** ideal model, **(b)** Rapp PA with 15 dB back-off as the modest case, **(c)** Rapp PA with 5 dB back-off as the worst case. Different combinations of FFT/AFB-based sensing and OFDM/FBMC based PU waveforms.

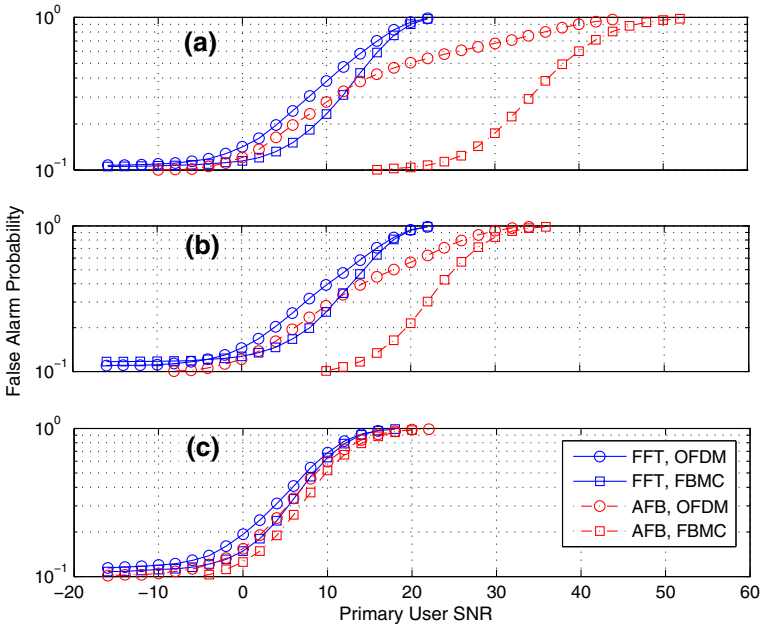

Figure 6 Actual false alarm probability for target $P_{FA} = 0.1$. Time record length of 50 and sensing bandwidth of 5 subbands under frequency selective channel model for **(a)** ideal model, **(b)** Rapp PA with 15 dB backoff as modest case, **(c)** Rapp PA with 5 dB backoff as worst case. Different combinations of FFT/AFB based sensing and OFDM/FBMC based PU waveforms.

equalization and in the PI algorithm for resource allocation. Perfect knowledge of the amplitude response of channel h_0 is also assumed, while channels h_2 and h_3 are known from spectrum sensing results. The subband-wise noise + interference estimates are obtained using time filtering length of 50. According to FFT- or AFB-based spectrum sensing results, a number of subbands are left empty in the spectrum utilization phase. The power of these occupied subchannels is reallocated to the other subbands that can be used by the CR. The

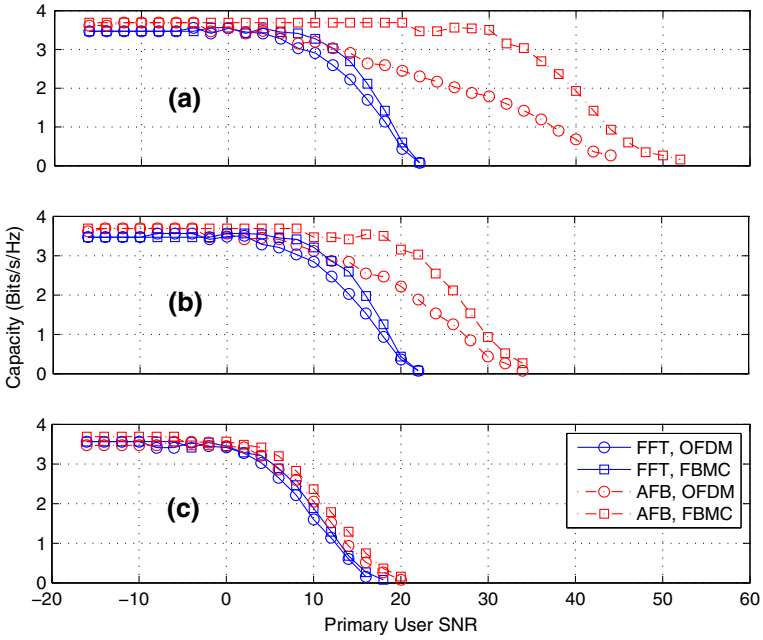

Figure 7 Capacity of a CR in a spectral gap between two PUs versus PU SNR. PI algorithm used for power allocation **(a)** Ideal model, **(b)** Rapp PA with 15 dB backoff as the modest case, **(c)** Rapp PA with 5 dB backoff as the worst case. Different combinations of FFT/AFB-based sensing and OFDM/FBMC-based PU waveforms.

power allocation is done utilizing the PI algorithm, and the resulting capacity, in terms of bits/s/Hz, is shown in Figure 7. The limitations of FFT-based spectrum sensing can again be clearly seen from the results, whereas AFB-based sensing is able to identify gaps between relatively strong PU signals. Regarding the transmission waveform, FBMC has clear benefit due to better spectral containment, if the effects of power amplifier nonlinearities can be kept at a modest level. As expected, the capacity is proportional to the available bandwidth in the gap, i.e., there is a clear connection between the results of Figures 5 and 6. The resource allocation algorithm (i) optimizes the performance with frequency selective channels in the presence of spectral leakage from the strong PUs and (ii) secures that the interference leakage from the CR transmission to the primaries is at an acceptable level.

6 Conclusions

We have studied the effects of combined spectrum sensing and spectrum utilization for FBMC-based cognitive radios with realistic signal model under frequency-selective fading channel conditions. Firstly, the performance of energy detection-based spectrum sensing technique was analyzed using both the FFT and filter bank-based spectrum analysis methods for both WLAN and FBMC signal models. Then, the utilization of dynamically identified spectral holes with spectrum allocation algorithms, subject to power and interference constraints, was investigated. Through this study, the effect of PU waveform's spectral containment on the CR transmission capacity was revealed. Here, we considered the choice between OFDM and FBMC primaries, together with the effect of spectral regrowth due to power amplifier nonlinearity.

In terms of the spectrum sensing performance, AFB has clear benefits due to much better spectral containment of the subbands. One important benefit of FBMC as a transmission technique in CR systems is that it can utilize narrow spectral gaps in an effective and flexible way, even in the presence of strong primaries at the adjacent spectral slots. This is due to the excellent spectral containment properties of the FBMC system. Additionally, an FBMC receiver can use the AFB for high-performance spectrum sensing with no additional complexity.

The utilization of the sensed spectrum can be optimized by using proper spectrum allocation algorithms. The PI algorithm has relatively low complexity, and it improves the capacity of the CR system as compared to the simple water filling-based spectrum allocation. One of the main observations of this work was that the PI algorithm can be directly utilized with the developed highly enhanced and realistic CR system model. The system model accommodates frequency-selective channel models for all the associated transmission links between PUs and SUs, as well as arbitrary transmitted power spectra and receiver frequency responses. Because of the above features, a FBMC-based CR system achieves higher capacity in comparison with traditional WLAN-based system. This increase in capacity can be attributed to the efficient use of the available spectrum and very small interference introduced to the primary transmissions at adjacent frequencies.

One of the important aims of this study was to understand the interdependence of the spectrum sensing and the spectrum utilization parts. It can be seen that increased false alarm probability has a direct effect on the available spectrum, and hence, it heavily influences the spectrum utilization. The PU power amplifier nonlinearity influences the sensed secondary spectrum introducing false alarms, hence lowering the CR system's spectrum utilization. It was demonstrated that, with heavy power amplifier nonlinearity, the FBMC-based primary is no better than the OFDM primary in what comes to the available capacity for secondary usage in the nearby frequencies.

In the numerical studies of this paper, we considered an ideal FBMC waveform for the CR, without considering the PA nonlinearity effects, since the focus is on the SU capacity and it dependency on the PU signal characteristics. Generally, good spectral containment is regarded as one of the key requirements for the CR transmitter. Also, the nonlinear PA model can be straightforwardly included in the developed interference models. Detailed evaluation of the performance-complexity tradeoffs for the CR implementation, including the PA linearity requirements, is a rather complicated issue and is left as a topic for future studies.

Competing interests

The authors declare that they have no competing interests.

Acknowledgements

This work was partially supported by Tekniikan Edistämissäätiö (TES), GETA Graduate School, the European Commission under Project EMPhAtiC (FP7-ICT-2012-09-318362), COST Action IC0902, Tekes (the Finnish Funding Agency for Technology and Innovation) under the project ENCOR in the Trial Program.

Author details

[1]Department of Electronics and Communications Engineering, Tampere University of Technology, P.O. Box 692, Tampere 33101, Finland. [2]Centre Tecnològic de Telecomunicacions de Catalunya (CTTC), Parc Mediterrani de la Tecnología (PMT), Avenida Carl Friedrich Gauss 7, 08860 Barcelona, Spain. [3]Signal, Communication & Embedded Electronics Research Group, Ecole Supérieur D'Électricité –SUPELEC University, F-35576 Cesson-Sévigné Cedex, Gif-sur-Yvette C.S. 47601, France.

Received: 10 December 2013 Accepted: 15 April 2014
Published: 12 May 2014

References

1. J Mitola, JGQ Maguire, Cognitive radio: making software radios more personal. IEEE Pers Commun Mag **6**(4), 13–18 (1999)

2. Y Zeng, YC Liang, AT Hoang, R Zhang, A review on spectrum sensing for cognitive radio: challenges and solutions. EURASIP J Adv Signal Process **2010**, 1–15 (2010)
3. T Yucek, H Arslan, A survey of spectrum sensing algorithms for cognitive radio applications. IEEE Commun Surv Tutorials **11**(1), 116–130 (2009)
4. S. Dikmese, M. Renfors, H. Dincer, *FFT and filter bank based spectrum sensing for WLAN signals, in Proc (European Conference on Circuit Theory and Design (ECCTD'11)* (Linkoping, Sweden, 2011)
5. S Dikmese, M Renfors, *Optimized FFT and filter bank based spectrum sensing for bluetooth signal, in Proc (Wireless Communications and Networking Conference (WCNC'12)* (France, Paris, 2012)
6. AJ Goldsmith, PP Varaiya, Capacity of fading channels with channel side information. IEEE Trans Inf Theory **43**(6), 1986–1992 (1997)
7. E Biglieri, J Proakis, S Shamai, Fading channels: information-theoretic and communications aspects. IEEE Trans Inf Theory **44**(6), (1998)
8. M Gastpar, *On capacity under received-signal constraints, in Proc (42nd Annual Allerton Conference Communication* (Control Comput, Monticello, USA, 2004)
9. A Ghasemi, E Sousa, Fundamental limits of spectrum-sharing in fading environments. IEEE Trans Wirel Commun **6**(2), 649–658 (2007)
10. L Musavian, S Aissa, *Ergodic and outage capacities of spectrum-sharing systems in fading channels, in Proc (IEEE Global Telecommunications Conference (GLOBECOM'07), Washington* (DC, USA, 2007)
11. X Kang, YC Liang, A Nallanathan, HK Garg, R Zhang, Optimal power allocation for fading channels in cognitive radio networks: ergodic capacity and outage capacity. IEEE Trans Wirel Commun **8**(2), 940–950 (2009)
12. A Sahin, H Arslan, Edge windowing for OFDM based systems. Commun Lett IEEE **15**(11), 1208–1211 (2011)
13. S Brandes, I Cosovic, M Schnell, *Sidelobe suppression in OFDM systems by insertion of cancellation carriers,' in Proc (Vehicular Technology Conference, (VTC'05-Fall)* (Dallas, USA, 2005)
14. A Loulou, M Renfors, *'Effective schemes for OFDM sidelobe control in fragmented spectrum use, in Proc (IEEE 24th International Symposium on Personal, Indoor and Mobile Radio Communications (PIMR'13)* (United Kingdom, London, 2013)
15. BF Boroujeny, R Kempter, Multicarrier communication techniques for spectrum sensing and communication in cognitive radios. IEEE Commun Mag (Spec Issue Cogn Radios Dynamic Spectr Access) **48**(4), 80–85 (2008)
16. A Amini, R Kempter, L Lin, B Farhang-Boroujeny, *Filter bank multitone: a candidate for physical layer of cognitive radio, in Proc (Software Defined Radio Technical Conference and Product Exhibition (SDR '05)* (Orange County, USA, 2005)
17. A Amini, R Kempter, B Farhang-Boroujeny, *A comparison of alternative filterbank multicarrier methods in cognitive radios, in Proc (Software Defined Radio Technical Conference and Product Exhibition (SDR '06)* (Orlando, USA, 2006)
18. M Bellanger, T Ihalainen, M Renfors, *Filter bank based cognitive radio physical layer, in Proc* (Future Network & Mobile Summit, Santander, Spain, 2009)
19. T Ihalainen, A Viholainen, *TH Stitz, M Renfors, Spectrum monitoring scheme for filter bank based cognitive radios, in Proc* (Future Network & Mobile Summit, Florence, Italy, 2010)
20. S Srinivasan, S Dikmese, M Renfors, *Spectrum sensing and spectrum utilization model for OFDM and FBMC based cognitive radios, in Proc (Signal Processing Advances in Wireless Communications (SPAWC'12)* (Cesme, Turkey, 2012)
21. V Ringset, H Rustad, F Schaich, J Vandermot, M Najar, *Performance of a filterbank multicarrier (FBMC) physical layer in the WiMAX context, in Proc* (Future Network & Mobile Summit, Florence, Italy, 2010)
22. S Dikmese, S Srinivasan, M Renfors, *FFT and filter bank based spectrum sensing and spectrum utilization for cognitive radios, in Proc (International Symposium on Communications, Control, and Signal Processing (ISCCSP'12)* (Rome, Italy, 2012)
23. G Bansal, MJ Hossain, VK Bhargava, *Adaptive power loading for OFDM-based cognitive radio systems, in Proc (IEEE International Conference on Communications (ICC '07)* (Glasgow, UK, 2007)
24. G Bansal, MJ Hossain, VK Bhargava, Optimal and suboptimal power allocation schemes for OFDM-based cognitive radio systems. IEEE Trans Wirel Commun **7**(11), 4710–4718 (2008)
25. T Qin, C Leung, *Fair adaptive resource allocation for multiuser OFDM cognitive radio systems, in Proc (2nd International Conference on Communications and Networking in China (ChinaCom '07)* (Shanghai, China, 2007)
26. Y Zhang, *Resource allocation for OFDM-based cognitive radio systems* (University of British Columbia, Vancouver, Canada, 2008). Dec, Ph.D. dissertation
27. M Shaat, F Bader, Computationally efficient power allocation algorithm in multicarrier-based cognitive radio networks: OFDM and FBMC systems. EURASIP J Adv Signal Process **13**, (2010). doi:Article ID 528378
28. M Shaat, F Bader, *Power allocation with interference constraint in multicarrier based cognitive radio systems, in Proc (7th International Workshop on Multi-Carrier Systems and Solutions (MCSS '09)* (Herrsching, Germany, 2009)
29. J Jang, KB Lee, Transmit power adaptation for multiuser OFDM systems. IEEE J Selected Areas Commun **21**(2), 171–178 (2003)
30. D Kivanc, G Li, H Liu, Computationally efficient bandwidth allocation and power control for OFDMA. IEEE Trans Wirel Commun **2**(6), 1150–1158 (2003)
31. Z Shen, JG Andrews, BL Evans, *Optimal power allocation in multiuser OFDM systems, in Proc (IEEE Global Telecommunications Conference (GLOBECOM '03)* (San Francisco, USA, 2003)
32. CY Wong, RS Cheng, KB Letaief, RD Murch, Multiuser OFDM with adaptive subcarrier, bit, and power allocation. IEEE J Selected Areas Commun **17**(10), 1747–1758 (1999)
33. C Rapp, Effects of the HPA-nonlinearity on 4-DPSK OFDM signal for a digital sound broadcasting system, in *Proc Conf. Rec. ECSC'91* (Luettich, Germany, 1991)
34. J Cioffi, *Digital Communication: Signal Processing* (Standford, California, USA, 2000)
35. Q Lu, T Peng, W Wang, Efficient multiuser water-filling algorithm under interference temperature constraints in OFDMA-based cognitive radio networks, in *Proc IEEE International Symposium Microwave, Antenna, Propagation, and EMC Technologies for Wireless Communications* (MAPE'07, Hangzhou, China, 2007)
36. V Stavroulaki, K Tsagkaris, P Demestichas, J Gebert, M Mueck, A Schmidt, R Ferrus, O Sallent, M Filo, C Mouton, L Rakotoharison, Cognitive control channels: from concept to identification of implementation options. IEEE Commun Mag **50**(7), 96–108 (2012)
37. AA Eltholth, AR Mekhail, A Elshirbini, MI Dessouki, AI Abdelfattah, Modeling the effect of clipping and power amplifier non-linearities on OFDM systems. Ubiquitous Comput Commun J **3**(1), 54–59 (2009)
38. PHYDYAS, Physical layer for dynamic spectrum access and cognitive radio. http://www.ict-phydyas.org/. Accessed 5 June 2013
39. T Yucek, H Arslan, *Spectrum characterization for opportunistic cognitive radio systems, in Proc* (IEEE Military Communication Conference, Washington, D.C., USA, 2006)
40. R Jain, Channel Models, A Tutorial (2007). http://www.cse.wustl.edu/~jain/cse574-08/ftp/channel_model_tutorial.pdf. Accessed 5 July 2013

doi:10.1186/1687-6180-2014-68
Cite this article as: Dikmese *et al.*: **Spectrum sensing and resource allocation for multicarrier cognitive radio systems under interference and power constraints.** *EURASIP Journal on Advances in Signal Processing* 2014 **2014**:68.

PUBLICATION 4

Sener Dikmese, AlaaEddin Loulou, Sudharsan Srinivasan and Markku Renfors, "Spectrum Sensing and Resource Allocation Models for Enhanced OFDM Based Cognitive Radio," in *Proceedings of 9th International Conference on Cognitive Radio Oriented Wireless Networks (CROWNCOM)*, Oulu, Finland, June 2014.

Spectrum Sensing and Resource Allocation Models for Enhanced OFDM Based Cognitive Radio

Sener Dikmese, AlaaEddin Loulou, Sudharsan Srinivasan and Markku Renfors

Department of Electronics and Communications Engineering
Tampere University of Technology
Tampere, Finland

{sener.dikmese, alaa.loulou, sudharsan.srinivasan, markku.renfors}@tut.fi

Abstract—Multicarrier waveforms have been commonly proposed as strong candidates for cognitive radio (CR) due to their high spectrum efficiency, flexibility in resource allocation and commonality of signal processing for spectrum sensing and spectrum utilization. OFDM based 802.11 Wireless Local Area Network (WLAN) technologies are good candidates as CR waveforms. However, the OFDM based systems have significant limitations as CR due to their limited spectral containment, which degrades the performance in determining the free spaces and in coordinating the spectrum usage. Therefore, methods for suppressing the spectral sidelobes of OFDM are considered in this study. In particular, a combination of edge windowing and cancellation carrier techniques is applied for sidelobe suppression. In this study, such an enhanced OFDM scheme is compared with traditional OFDM and filter bank based schemes in spectrum sensing and spectrum allocation, considering also the spectral leakage effects appearing in practical WLAN devices due to power amplifier nonlinearity.

Index Terms— cognitive radio, FFT, filter bank, enhanced OFDM, edge windowing, cancellation carrier, spectrum sensing, spectrum utilization, loading algorithms.

I. INTRODUCTION

The usage of wireless communication devices is growing exponentially and they are widely produced all around the world. One of the important challenges in maximizing the efficiency of the spectrum use is to improve the interference control between different systems/users [1] . Especially, the 2.4 GHz ISM band is freely available and hence used by various kinds of wireless systems due to the global availability. To reduce interference and better utilize the spectrum, cognitive radio (CR) and advanced signal processing techniques for efficient spectrum use have been studied extensively [2], [3], [4] and [5].

Spectrum sensing is an important part of CR applications. It is used for identifying spectrum holes in an efficient way. With reliable spectrum information, a CR can provide a non-interfered reliable communication. Repeated monitoring and cooperation with other users is necessary to obtain reliable spectrum information due to varying channel conditions and radio scene [6].

Most of the recent wireless communication standards have preferred to use cyclic prefix based CP-OFDM techniques due to its reliable and robust performance and simplicity of the signal processing functions on the transmitter and receiver sides. CP-OFDM is the most well-known multicarrier technology, since it is adopted in many popular standards, e.g., WiMAX, 3GPP LTE, 802.11a/g/n, and DVB. However, also alternative multicarrier techniques have been studied increasingly in the literature to get rid of spectral leakage which comes from the sidelobes. Especially, enhanced OFDM based techniques have been realized to have various potential benefits in the CR context. Hence, various enhancements are suggested in the literature improving the spectral efficiency of OFDM scheme. An interesting enhancement for OFDM model is the combination of edge windowing technique and cancellation carrier techniques [7], [8], [9], [10] and [11].

Wideband energy detector based multichannel spectrum sensing techniques are considered in this paper. By averaging the output samples of a filter bank based spectrum analyzer simultaneously for multiple center frequencies and bandwidths, multiple spectral gaps can be tested and identified rapidly in an efficient and flexible way.

As a second step, efficient spectrum utilization is important in maximizing the cognitive radio's throughput after the spectrum sensing process. The performance of the spectrum utilization can be improved with proper loading algorithms [12], [13] and [14]. Loading algorithms require knowledge of the channel. The channel state information (CSI) gives this information to the transmitter when there is a feedback from the receiver. The transmit power and/or the data rate can be adapted at the transmitter according to the CSI. The adaptation algorithms use commonly the water-filling principle. The water-filling solution can be thought of as the curve of inverted channel signal to noise ratio (SNR) being filled with energy to a constant line. There are two different variations of these algorithms, rate adaptive and margin adaptive [15]. While using these algorithms, it is common to assume that the channel is quasi-static. Therefore once the allocation of bits and energy is done at the beginning

of the transmission, it can be maintained until a new set of CSI is made available.

Here, we consider maximizing the data rate of a CR operating in a spectral hole. The secondary transmission power is controlled adaptively. Hence, the interference towards the primary is kept to minimum. To meet this goal, we choose the rate adaptive algorithm in this study. The total data rate of the CR is maximized when the achievable rate for each subband is maximized constraint on the total energy that is allowed for the CR transmission symbols without causing any substantial increase in the interference [15].

In Section 2, traditional and Enhanced OFDM based WLAN signal models are given. FFT and analysis filter bank (AFB) based spectrum sensing is reviewed, considering the spectrum analysis aspects related to the multicarrier techniques in Section 3. An efficient spectrum utilization model will be presented in Section 4. Section 5 presents the simulation results for the considered radio scene. Finally, some concluding remarks are presented about the performance of these methods.

II. TRADITIONAL AND ENHANCED OFDM BASED WLAN SIGNAL MODELS

Even though CP-OFDM is the most well-known multicarrier technology, enhanced OFDM based WLAN signal model can be used to overcome the spectral leakage problems. Basically, each OFDM subcarrier is expressed mathematically by a sinc function due to the rectangular shape of the CP-OFDM symbol in time domain. Accordingly, the spectrum of the OFDM symbol can be expressed as follows

$$S(f) = T_s \sum_{k=0}^{N_{IFFT}-1} x_k \text{sinc}\left[T_s\left(f - \frac{k}{T_u}\right)\right] \quad (1)$$

where $\{x_0, x_1, \ldots x_{N_{IFFT}-1}\}$ are the input samples to the IFFT with the block of size N_{IFFT}, T_u is the useful symbol duration, T_s is the total CP-OFDM symbol duration and $\text{sinc}=\sin(\pi x)/\pi x$.

To improve the spectral efficiency of OFDM scheme, a combination of two techniques is used. The combination utilizes the edge windowing scheme, which is a special form of time domain windowing [8]. Edge windowing divides the subcarriers in several groups, usually two: edge group and inner group. The edge group contains the subcarriers around the edges where long window and short CP are utilized. Other subcarriers are contained in the inner group, where short window and long CP are applied. This technique introduces a controllable Intercarrier Interference/Intersymbol Interference (ICI/ISI), while providing efficient sidelobes suppression. Edge windowing can be combined with the partial transmit sequence (PTS) for peak to average power ratio (PAPR) mitigation in computationally efficient way [11]. However, time domain windowing technique has insufficient suppression performance on sidelobes close to active subcarriers [7]. Hence, a simplified version of the cancellation carrier scheme is used in the combination since cancellation carrier technique has effective suppression performance on sidelobes near the edges [9]. The simplified cancellation carrier model reduces the computational complexity significantly compared to the common cancellation carrier scheme, especially in non-contiguous scenarios and power limited cases [10]. The reduction in complexity is produced by optimizing each edge separately. If the number of used cancellation carrier on each edge is V and the number of optimization points is U, the optimization problem is expressed in the following way

$$\min_z \|\mathbf{Q} + \mathbf{C}\mathbf{z}\| \quad (2)$$

where $\mathbf{Q} = [Q_1, Q_2, ..., Q_U]^T$ the sidelobes values at the chosen optimization points and $\mathbf{C} = [C_1, C_2, ..., C_V]$ contains the sidelobes values of the inserted cancellation carriers in the optimization points. Moreover, the column vector $\mathbf{C}_1 = [C_{11}, C_{21}, ..., C_{U1}]^T$ represents the sidelobes values of the un-weighted cancellation carrier at the optimization points, and $\mathbf{z} = [z_1, z_2, ..., z_V]^T$ are the cancellation carriers' weights. The solution of the problem in (2) is then [16]

$$\mathbf{z} = -\mathbf{C}^{\dagger}\mathbf{P} \quad (3)$$

where $\mathbf{C}^{\dagger} = (\mathbf{C}^{\mathrm{T}}\mathbf{C})^{-1}\mathbf{C}^{\mathrm{T}}$ is the pseudo-inverse of the matrix $\mathbf{C}$. In figure 1, the implementation of the combination is illustrated. The first block of the implementation evaluates the weight vector $\mathbf{z}$. It is critical to consider the edge windowing effect in the evaluation of the matrices $\mathbf{P}$ and $\mathbf{C}$. Otherwise, the cancellation carrier technique will be inefficient. Regarding edge windowing, two IFFTs and two CP&window blocks are required. The division allows applying different CP and window lengths on the two groups. The sum of the edge group branch and the inner group branches results in the required enhanced CP-OFDM signal.

The combination results in strong suppression of the sidelobes since the cancellation carrier targets the close subcarriers and edge windowing suppresses the farther subcarriers. Nevertheless, the combination needs an extension to CP-OFDM symbol in order to apply time windowing. To reach sufficient sidelobe suppression performance, we use two cancellation carriers at both edges, increasing the total number of transmitted subcarriers by four.

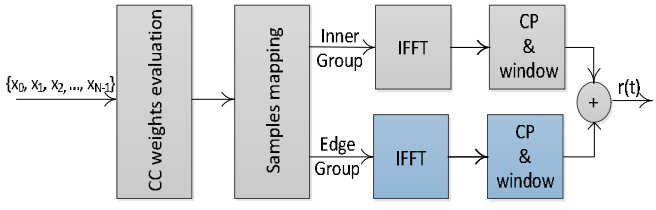

Figure 1. Block diagram of enhanced OFDM signal

In our numerical studies, we consider a scenario with two active 802.11g type traditional or enhanced OFDM based WLANs signals with similar parameters, as shown in figure 2. The two channels are assumed to have the same power level, normalized to 0 dB. In this case, the traditional and enhanced OFDM based WLAN1 and WLAN2 signals use the channels 3 and 8, out of the entire 11 different channels. The channels don't overlap and there is 8 MHz spectrum hole available in this scenario. Due to the transmitter power amplifier (PA) non-linearity, spectral regrowth gets introduced, raising the spectral density in the nearby frequencies. Considering the worst case situation allowed by the 802.11g specifications, the power spectrum density in the gap between the two channels can be at about -20 dBr (20 dB below the pass-band level) [4]. For realistic model of the power amplifier effects, we use the Rapp model [17]. The mentioned worst-case situation corresponds to 5 dB back-off. We consider also 15 dB back-off for modest spectrum regrowth, and also the ideal power amplifier case is included as a reference. The specific enhanced OFDM based WLAN design has at least 40 dB stop band attenuation. However, depending on the linearity of the PA, some spectrum leakage would be present also in the enhanced OFDM based WLAN case.

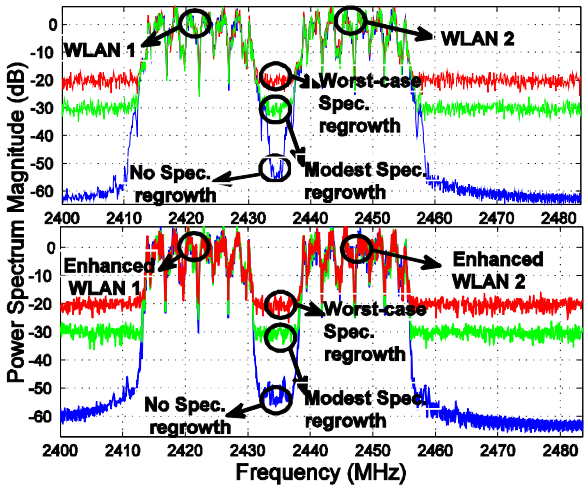

Figure 2. Two traditional and enhanced WLAN signals using 3rd and 8th WLAN channels in the 2.4 GHz ISM band.

III. FFT AND AFB BASED SPECTRUM SENSING

The schemes of alternative FFT and AFB based spectrum sensing algorithms are illustrated in figure 3.

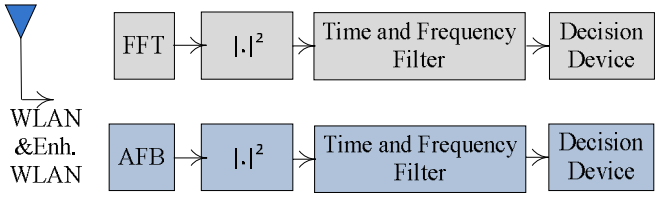

Figure 3. Scheme of energy detector with AFB and FFT based spectrum analysis

In the following analysis, it is assumed that the subband sampling rate is equal to the ADC sampling rate divided by the number of FFT/AFB frequency bins. With subband-wise spectrum sensing, the subband signals can be expressed as [3]

$$Y(m,k)=\begin{cases} W(m,k) & H_0 \\ S(m,k)H_k+W(m,k) & H_1 \end{cases} \quad (4)$$

where $W(m,k)$ is the channel noise, $S(m,k)$ is the transmitted primary user (PU) signal which is seen in subband k of the m^{th} FFT or AFB output block, and H_0 and H_1 denote the absent hypothesis and present hypothesis of a PU, respectively. When only AWGN noise is present, it can be modeled as a zero-mean white Gaussian random variable with variance σ_w^2, i.e., $W(m,k)=N(0,\sigma_w^2)$. The traditional or enhanced WLAN signals can also be modeled with a zero-mean Gaussian variable $S(m,k)=N(0,\sigma_k^2)$ and σ_k^2 is the variance (power) at subband k.

The test statistic, which is calculated as the absolute square of the FFT or AFB output $|Y(m,k)|^2$ is compared with a threshold value to decide between H_0 and H_1. The threshold is calculated from the noise variance, which is assumed to be known based on previous measurements, and target false alarm probability. Time and/or frequency averaging of the observed $|Y(m,k)|^2$ values are necessary to get more reliable decision statistic [3]. Decision statistics at different frequencies can then be calculated as

$$\tilde{Y}(m,k)=\frac{1}{L_tL_f}\sum_{l=k-\lfloor L_f/2\rfloor}^{k+\lceil L_f/2\rceil-1}\sum_{u=m-L_t+1}^{m}|Y(u,l)|^2 \quad (5)$$

where L_f and L_t are the filter lengths in frequency and time, respectively. The output of $\tilde{Y}(m,k)$ is passed to threshold function for determining the possible occupancy of the corresponding frequency band at the corresponding time interval. Later on, the sensing time index m is dropped and we use $\tilde{Y}_k$ instead of $\tilde{Y}(m,k)$ to simplify the notations.

The probability distribution functions (PDF) of the time filter outputs $\tilde{Y}_k$ can be approximated as Gaussian distributions under H_0 and H_1 [3]. The threshold value λ can be calculated from the target false alarm probability and estimated noise variance. The false alarm probability P_{FA} and detection probability P_D can be obtained as follows

$$P_D=\Pr(\tilde{Y}_k>\lambda\mid H_1)=Q\left(\frac{\lambda-(\sigma_n^2+\sigma_k^2)}{\sqrt{(\sigma_n^2+\sigma_k^2)^2/L_tL_f}}\right) \quad (6)$$

$$P_{FA}=\Pr(\tilde{Y}_k>\lambda\mid H_0)=Q\left(\frac{\lambda-\sigma_n^2}{\sqrt{\sigma_n^4/L_tL_f}}\right) \quad (7)$$

IV. SPECTRUM UTILIZATION

Figure 4 shows spectrum utilization process. Proper loading of each subband maximizes the spectrum utilization by a CR. As discussed earlier in the introduction part, rate adaptive loading algorithms are better suited as they offer better control of the interference from a CR to the PU receivers. By fixing the energy constraint to a constant, the rate adaptive loading algorithm maximizes the number of bits per symbol [15]. In the following, $1/T$ is the symbol rate, b_n is the number of bits in subcarrier n, and e_n is the nth subcarrier energy. Then the total number of bits in the available set of N parallel subcarrier symbols is $b = \sum_n b_n$. The overall data rate is $R = b/T$ and the total energy of the N parallel subcarrier symbols is constraint to $\sum_{n=1}^{N} e_n = N\bar{e}_n$ where $N\bar{e}_n$ is the total energy allowed in the system under consideration.

The largest data rate is achieved by maximizing the sum

$$b = \frac{1}{2}\sum_{n=1}^{N} \log_2\left(\frac{1+e_n * g_n}{\Gamma}\right) \tag{8}$$

where $g_n = |H_n|^2 / (\sigma_n{}^2)$ is the subband SNR per unit energy from the transmitter, $|H_n|^2$ is the channel gain of the nth subband and Γ is the gap formulation as given in [15]. $\sigma_n{}^2$ is the noise and interference variance in subband n, i.e., it contains both the channel white noise and spectrum leakage from the WLAN channels.

The optimum loading can be formulated as

$$\max_{e_n} b = \frac{1}{2}\sum_{n=1}^{N} \log_2\left(\frac{1+e_n * g_n}{\Gamma}\right)$$
$$subject: N\bar{e}_x = \sum_{n=1}^{N} e_n \tag{9}$$

The solution to this optimization problem leads to the water filling constant K given below [15].

Spectrum Utilization Algorithm

The rate maximization algorithm from [15], which is used in this work, is given below

1. Sort the sub-channels based on their gains $g_1 > g_2 > g_3 > \ldots > g_N$
2. Find the largest i for which $e_{N-i} = K - \Gamma / g_{N-i} \leq 0$ with

$$K = \frac{1}{N-i}\left[Ne_n + \Gamma \cdot \sum_{n=1}^{N-i} \frac{1}{g_n}\right] \tag{10}$$

3. Eliminate the negative energies $e_n < 0$ and set $e_n = 0$ and $b_n = 0$ for those subcarriers. Set $N^* = N - i$, where i is the number of subcarriers with negative energies, $e_i = K - \Gamma / g_i \leq 0$. The filling constant is also recalculated for the new N^*.
4. Compute the water-filling energies $e_n = K - \Gamma / g_n$ where $n = 1, 2 \cdots, N^*$
5. Calculate the data rate for unsorted sub-channels $b_n = \log_2(1 + e_n \cdot g_n)/2 \quad \forall n = 1, 2, \cdots, N^*$

The algorithm needs the channel estimate, in the form of subband gains H_n, as well as estimates of the noise and interference powers $\sigma_n{}^2$ of the subbands. The estimates are done using subcarrier wise FFT based energy metric, i.e., using (5) with $L_f = 1$.

The most important issue in our discussion is the effect of the spectral leakage in OFDM on the throughput of the CR utilizing the spectral hole. Due to the good spectral containment of the subbands in the enhanced OFDM method proposed here, we expect the spectral leakage to be less critical in this case.

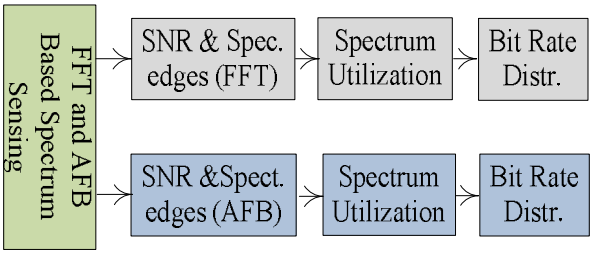

Figure 4. Block diagram of spectrum utilization with water filling after spectrum analysis

V. SIMULATION RESULTS

The enhanced WLAN model uses 802.11g parameters. However, some modifications are needed to apply the enhanced scheme. Hence, enhanced OFDM appends additional 0.8 µs to 802.11g symbol duration for applying the time windowing. 10 subcarriers per edge are contained in the edge group. In each edge group, the CP and window duration are 0.4 µs and 1.2 µs, respectively. In inner group, CP and window durations are 1.2 µs and 0.4 µs, respectively. Regarding the simplified cancellation carrier part, two cancellation carriers and two optimization points are used on each edge. Optimization points are located at the first sidelobes next to cancellation carriers.

In figure 2, we consider a worst-case situation for secondary transmissions using the spectral hole between the two WLAN channels which are at equal power levels. Otherwise the spectral leakage effects would be less critical on the side of the weaker WLAN channel. Traditional and enhanced WLAN systems are based on the 802.11g OFDM standarts. We assume that the spectrum sensing and CR

transmissions use smaller subchannel bandwidth of 81.5 kHz. The time and frequency filtering lengths are chosen as 50 and 5, respectively, in order to be able to detect other narrowband systems, like Bluetooth [5] in the spectrum sensing part. For the power amplifier, the Rapp model [17] is used with different back-offs. Three cases are considered: no spectral regrowth due to the PA, modest regrowth at the level of -30 dBr and worst-case regrowth at -20 dBr.

The number of empty subbands both for traditional and enhanced OFDM based PUs are shown in figure 5 with different levels of spectral regrowth. P_{FA}=0.1 is chosen as the target false alarm probability in the scenario. The ITU-R Vehicular A channel model is applied for the PU signals. Enhanced OFDM based PU's would allow a clearly higher number of subchannels to be used by the CR system compared to traditional OFDM-based WLAN, especially in the no-regrowth and modest regrowth cases. Morever, AFB finds higher number of empty subbands compared to FFT, in reliable way due to the sharp subchannel filtering. With the worst-case regrowth allowed by 802.11g, these differences dissappear.

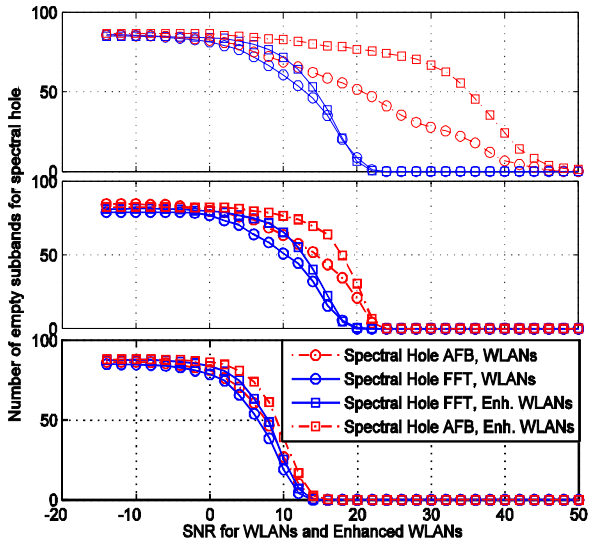

Figure 5. Number of empty subbands in the spectral hole between traditional and enhanced WLANs with target $P_{FA}=0.1$, time record length of 50, sensing bandwidth of 5 subbands for (a) no spectrum regrowth, (b) modest-case spectrum regrowth, and (c) worst-case spectrum regrowth

The actual false alarm probabilities versus the active primary systems' SNR are illustrated in figure 6. This is actually the probability that a group of 5 subchannels in the center of the gap would be detected to be occupied due to spectral leakage.

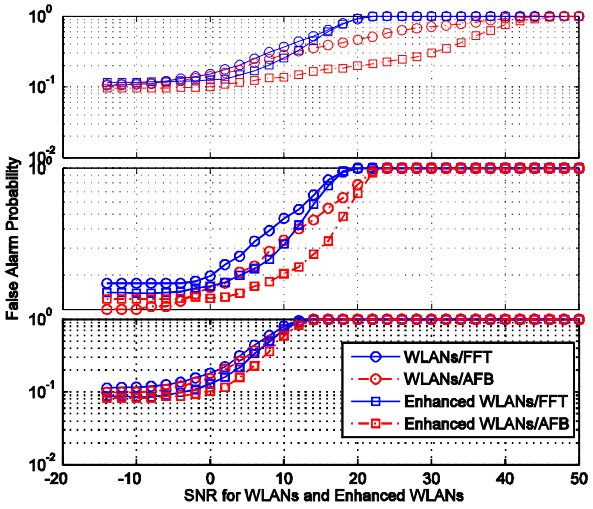

Figure 6. Actual false alarm probability with target $P_{FA}=0.1$ with (a) no spectrum regrowth, (b) modest-case spectrum regrowth, and (c) worst-case spectrum regrowth

The achievable data rate in the spectral hole between two active primary channels is seen in figure 7. The model gives the theoretical maximum data rate, assuming ideal multicarrier operation for the secondary user (SU) transmission. The subband-wise signal to interference plus noise ratio (SINR) estimates are obtained using time filtering length of 50 samples.

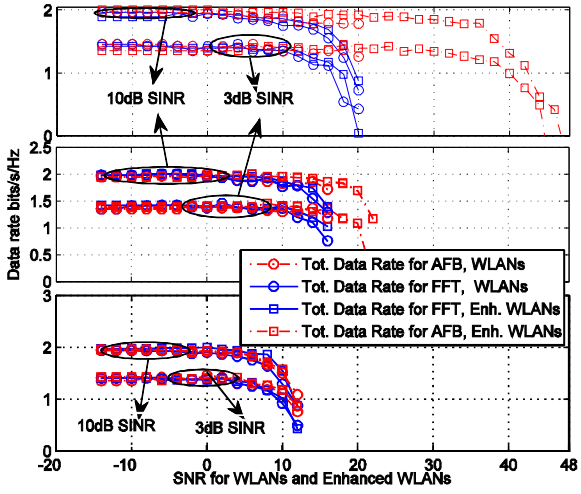

Figure 7. Available data rate as a function of the PU SNR with 10 dB and 3 dB SNR for the CR with (a) no spectrum regrowth, (b) modest-case spectrum regrowth, and (c) worst-case spectrum regrowth.

It can be seen that under the high SNR case, the number of subbands that can be used by the CR reduces in the traditional OFDM case due to the spectral leakage. An enhanced OFDM based primary with AFB based spectrum sensing at the CR would maximize the CR system performance, while AFB based sensing in the traditional OFDM case shows significant benefit with low or modest spectral regrowth.

The benefits of enhanced OFDM based WLAN and AFB disappear under the worst case spectral regrowth. It can also be seen that with the used parameters, the spectrum sensing algorithm and the rate adaptive bit loading algorithm (which can be applied after the spectrum has first been detected to be available) end up in using about the same number of sub bands.

VI. CONCLUSION

The performance of energy detection based spectrum sensing techniques using either FFT or filter bank based spectrum analysis methods for both traditional and enhanced OFDM based WLAN signal models were considered in this study. Furthermore, utilizing the detected spectral holes with water filling algorithms were analyzed in both scenarios.

The enhanced OFDM waveforms provide effective suppression to the spectral sidelobes, which makes it possible for opportunistic users to make use of the nearby frequencies, enhancing the effeciency of the overall spectrum usage. However, a prerequisite for this is improved linearity of the transmitter power amplifier to reduce the spectral regrowth effects. Naturally, the same approach allows independent SU systems to operate side-by-side with minimized guardbands.

The used simplistic SU system model gives the theoretical maximum data rate, assuming ideal multicarrier operation for the SU transmission. This model is justified, e.g., for scenarios where the SU system is used for low-power short range communication with power levels well below the WLANs at reasonable distances from the operating SUs. In this case it can be safely assumed that the SU's don't introduce interference significantly harming the PU operation, and the exact SU system model is not critical. More generally, also the interference introduced by the SU's towards the primary receivers should be taken into consideration in the power allocation context. This is one important topic for future studies.

In practice, also the SU's are preferred to use waveforms with well-contained spectrum, like enhanced OFDM or filter bank based multicarrier (FBMC) [14]. In general, the enhanced OFDM techniques result in certain losses of the spectral efficiency, e.g., due to increased guard interval length in case of time-domain windowing methods. FBMC schemes provide spectrally well-contained waveforms with minimimum overheads from the spectrum efficiency point of view. However, an important benefit of enhanced OFDM schemes, in comparison to FBMC, is high level of compatibility with the existing OFDM based systems. In fact, while the proposed spectrum sensing and allocation scheme is completely independent of the actual waveforms of the primaries, it makes it possible for the opportunistic users to effectively exploit the enhanced spectral containment of the on-going transmissions.

ACKNOWLEDGMENT

This work was partially supported by Tekniikan Edistamissaation (TES), FP7-ICT project EMPhAtiC under grant no.318362, GETA Graduate School and the Finnish Funding Agency for Technology and Innovation (Tekes) under the project "Enabling Methods for Dynamic Spectrum Access and Cognitive Radio (ENCOR2)" in the TRIAL Program.

REFERENCES

[1] I. Mitola, J. and J. Maguire, G. Q., "Cognitive radio: making software radios more personal," IEEE Personal Commun. Mag., vol. 6, no. 4, pp. 13–18, Aug. 1999.

[2] Y. Zeng, Y.C. Liang, A. T. Hoang, and R. Zhang, "A Review on Spectrum Sensing for Cognitive Radio: Challenges and Solutions," EURASIP Journal. on Advances. in Sig. Proc, vol. 2010, pp. 1-15, Jan. 2010.

[3] T. Yucek and H. Arslan, "A survey of spectrum sensing algorithms for cognitive radio applications," IEEE Communications Surveys & Tutorials, vol. 11, no. 1, pp. 116–130, March 2009.

[4] S. Dikmese, M. Renfors and H. Dincer, "FFT and Filter Bank Based Spectrum Sensing for WLAN Signals," in Proc. ECCTD2011 conf., Linkoping, Sweden, August 2011.

[5] S. Dikmese and M. Renfors, "Optimized FFT and Filter Bank Based Spectrum Sensing for Bluetooth Signal" in Proc. Wireless Communications and Networking Conference (WCNC 2012), Paris, France.

[6] S. M. Mishra, A. Sahai, and R. W. Broderson, "Cooperative sensing among cognitive radios," in Proc. ICC, Istanbul, Turkey, Jun.11–15, 2006.

[7] T. Weiss, J. Hillenbrand, A. Krohn, and F. Jondral, "Mutual interference in OFDM-based spectrum pooling systems" in Proc. (VTC 2004), May 2004.

[8] A. Sahin and H. Arslan, "Edge Windowing for OFDM Based Systems" Communications Letters, IEEE, vol. 15, no. 11, pp. 1208-1211, 2011.

[9] S. Brandes, I. Cosovic, and M. Schnell, "Sidelobe suppression in OFDM systems by insertion of cancellation carriers" in Proc. (VTC 2005), September, 2005

[10] A. Loulou and M. Renfors, "Effective Schemes for OFDM Sidelobe Control in Fragmented Spectrum Use" in Proc. (PIMRC 2013, London, UK, Sep. 2013.

[11] A. Loulou, S. Afrasiabi Gorgani, and M. Renfors, "Enhanced OFDM Techniques for Fragmented Spectrum Use" in Future Netw., Lisbon. Portugal, July, 2013.

[12] J. Cioffi, "Digital Communication: Signal Processing" at Standford University, Standford, California, USA, 2000.

[13] S. Dikmese, S. Srinivasan and M. Renfors, "FFT and Filter Bank Based Spectrum Sensing and Spectrum Utilization for Cognitive Radios" in Proc. (ISCCSP 2012), Rome, Italy, May 2012.

[14] S. Srinivasan, S. Dikmese and M. Renfors, "Spectrum Sensing and Spectrum Utilization Model for OFDM and FBMC Based Cognitive Radios" in Proc. (SPAWC 2012), Izmir, Turkey, June 2012.

[15] K. Baamrani, A. Ouahmana, and S. Allakib, "Rate adaptive resource allocation for OFDM downlink transmission" AEU – Int. Jour. of Elec.and Comm.Vo. 61, Issue 1, 2 Jan. 2007.

[16] G. H. Golub and C. F. Van Loan , "Matrix computations (3rd ed.)". The Johns Hopkins University Press, 1996.

[17] C.Rapp "Effects of the HPA nonlinearity on 4-DPSK OFDM signal for a digital sound broadcasting system" in Proc.Conf. Rec. ECSC'91 Luettich Oct 1991.

Tampereen teknillinen yliopisto
PL 527
33101 Tampere

Tampere University of Technology
P.O.B. 527
FI-33101 Tampere, Finland

ISBN 978-952-15-3454-6
ISSN 1459-2045